Investigating the roles of phosphorylation in modulating Argonaute 2 activity and localization

by

Joaquin Lopez-Orozco

A thesis submitted in partial fulfillment of the requirements for the degree of

Doctor of Philosophy

Department of Cell Biology
University of Alberta

Abstract

RNA interference (RNAi) has enabled the study of gene function with unprecedented specificity and reliability. Almost twenty years after the discovery of RNAi, we now know that this process is carried out by a set of evolutionarily conserved proteins. In mammals, these proteins form part of the miRNA pathway that controls the expression of most protein-encoding genes. At the core of the miRNA pathway are Argonaute proteins, which are guided by miRNAs to downregulate the expression of more than 50% of all mRNAs. While there is a vast literature describing how miRNAs regulate numerous cellular pathways, comparatively less is known about how miRNA pathways are modulated. Because of their role in gene expression on a global level, miRNA pathways must clearly be subjected to extensive regulation. Recent findings indicate that post-transcriptional modifications of Argonaute proteins are important for this process. Human Argonaute 2 is phosphorylated on at least seven amino acid residues but we know very little about the function consequences of these modifications. Furthermore, very little is known about the kinases and phosphatases that catalyze these modifications.

One unexpected finding in my thesis research is that changes in phosphorylation can lead to profound changes in the localization of Argonaute proteins without dramatically affecting their gene-silencing functions. Using a screen biased to detect kinases that regulate the late stages of RNAi, I identified a large number of kinases that decrease or increased RNAi activity. Few kinases were found to inhibit RNAi activity, but interestingly, the majority were tyrosine kinases. Among this group, FGFR3 was further examined and its effects on RNAi activity were studied in detail. Of note, I showed that stimulation of multiple FGFR family members inhibit RNAi, likely through phosphorylation of Argonaute

proteins. Finally, I showed that Argonaute 2 interacts with the serine/threonine phosphatase PP1 and that elevated expression of PP1 inhibits RNAi activity.

Preface

A version of Chapter 3 of this thesis has been previously published as “LOPEZ-OROZCO J., PARE J.M., HOLME A.L., CHAULK S.G., FAHLMAN R.P., and HOBMAN T.C. (2015) Functional analyses of phosphorylation events in human Argonaute 2. *RNA* **21**:1–9”. I was responsible for data collection and analyses, figure preparation and composition of the manuscript. Dr. Pare and Dr. Hobman helped in the design of experiments and manuscript edits. Dr. Holme helped with data collection and analyses resulting in figures 3.2 and 3.3. Dr. Chaulk and Dr. Fahlman helped in data collection that resulted in figures 3.7 and 3.11.

Work presented in Chapters 4 and 5 of this thesis have not been published. I was responsible for experimental design, data acquisition, data analyses and preparation of figures. Min Hsuan Wu assisted in performing replicates that resulted in figures 5.1 and 5.2. as part of an undergraduate project under my supervision. Robert Maranchuk provided technical assistance that resulted in figures 4.1 and 5.3. And, Dr. Pare and Dr. Hobman played a role in the design and planning of experiments and data analysis.

All other components presented in this thesis are my original work under the supervision of Dr. Hobman.

Dedication

I dedicate this thesis to my family. Because you were, you are, and you will be my motivation to wake up every day.

Acknowledgements

I want to thank first and the most my supervisor Dr. Tom Hobman. Because he gave me the best opportunity of my life, and because his patient mentorship was the major determinant in my development as a scientist.

My friends and lab mates Dr. Justin Pare, Dr. Henry Parker and Dr. Matt Urbanowski, I am truly grateful that such intelligent and talented people were all together in my lab. You provided a nurturing environment that helped in no small measurement during my PhD.

My supervisors Dr. Paul LaPointe and Dr. Edan Foley, thanks for being there for me all these years. I appreciate you taking the time to read all those meeting reports and for the wonderful suggestions and ideas that helped shape my research into this interesting thesis.

Dr. Andrew Simmons and Dr. Craig McCormick thank you for taking the time to carefully read, correct and suggest ideas for this thesis and future research topics. This required a great deal of work, and I really appreciate your input.

I would also like to thank Dr. Andrea Holme, Dr. Steven Ogg and Robert Maranchuk for technical advice and instructing me on how to use advanced research instruments.

And to my family, which even though you were far away during my PhD, you kept me sane and gave me the strength to keep going until I succeeded in this, the greatest journey yet of my life.

Table of contents

List of Tables

List of Figures

Chapter 1

Introduction

1.1. RNA interference

1.1.1. Overview

The influence of small double stranded RNA (dsRNA) on protein expression through its interaction with messenger RNA (mRNA) has been studied since the late 1990s (Fire et al. 1998). Since the discovery of RNA interference (RNAi) by Fire *et al*, a variety of tools have been developed that allow investigators to “knock down” the expression of virtually any protein by utilizing small interfering RNAs (siRNAs). A second type of small RNA that also confers specificity in RNAi pathways, microRNAs, are encoded by most eukaryotic genomes, and were discovered in 1993 (Lee, Feinbaum and Ambros 1993). The fact that small RNA-dependent silencing is widely conserved implies that RNAi is critical for regulating gene expression in eukaryotes. Indeed, at least half of all mammalian genes are thought to be regulated by miRNAs (Friedman et al. 2009).

Comprehensive investigation has shed light on the mechanisms by which small RNAs influence protein expression (Reinhart et al. 2000, Olsen and Ambros 1999, Wightman, Ha and Ruvkun 1993). A complex comprised of the cytoplasmic RNAse-III Dicer, HIV-1 TAR RNA-Binding Protein (TRBP) and/or Protein ACTivator of the interferon-induced protein kinase (PACT), is responsible for cleaving dsRNA precursors to produce siRNAs or miRNAs that are 19-22 nt in length (Haase et al. 2005, Provost et al. 2002, Zhang et al. 2002). The small RNAs are then loaded onto an Argonaute (Ago) protein to form the RNA-Induced Silencing Complex (RISC). The specificity of this complex is provided by the sequence of the small RNA, which guides the RISC complex to a target

mRNA (Liu et al. 2005a). Once bound to the targeted mRNA, the Ago component of RISC silences the expression of that mRNA through endonucleolytic cleavage or recruitment of additional protein factors that mediate suppression of translation (Wee et al. 2012). The extent of complementarity between the 'guide' small RNA and the target mRNA determines the mechanism of silencing (Figure 1.1).

Figure 1.1 small RNA pathways. A) siRNA pathway. Long double strand RNA or hairpin RNA precursors from endogenous or exogenous sources are processed into RNAs ~22 nucleotides (nt) in length by Dicer, and loaded onto Ago proteins. mRNAs that are perfectly complementary to the siRNAs are cleaved by the endonuclease activity of Ago. **B) miRNA pathway.** Primary miRNAs are transcribed in the nucleus and then undergo consecutive processing by the RNAses Drosha and Dicer to produce ~22 nt mature miRNAs. Once loaded onto Ago proteins the miRNA-Ago complex, or miRISC represses translation of the targeted mRNAs. **C) Drosha-independent miRNAs.** Splicing of mRNA introns by the spliceosome machinery can produce RNAs with intramolecular complementarity that are structurally similar to miRNA precursors. These RNA species are substrates for Dicer. **D) Dicer-independent miRNAs.** The precursor of miR451 is transcribed from DNA, processed by Drosha and then transported to the cytoplasm where its pre-miRNA is processed by Ago2-mediated endonucleolityc cleavage to the mature miRNA form.

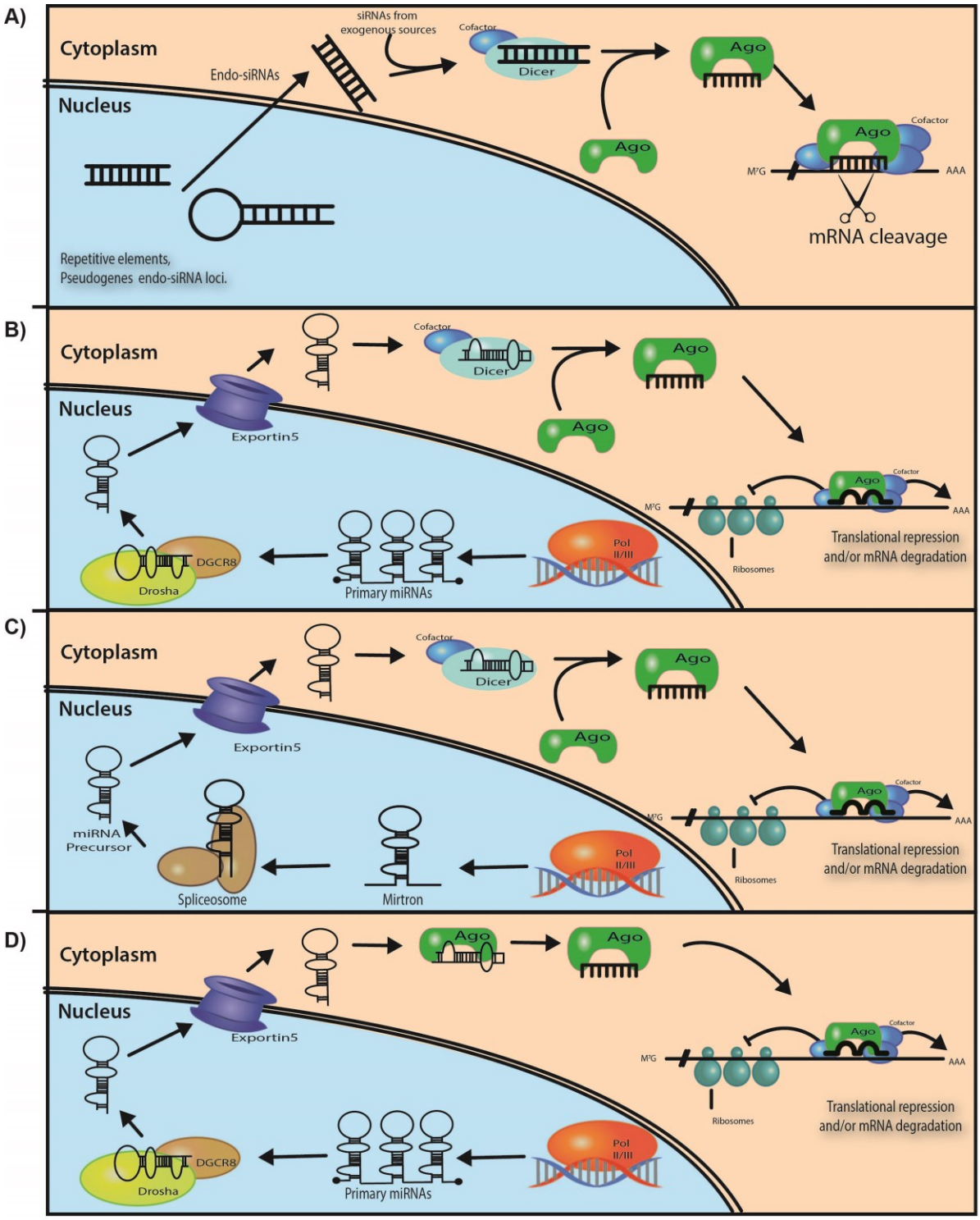
A)
Cytoplasm
Nucleus
siRNAs from exogenous sources
Endo-siRNAs
Cofactor
Dicer
Ago
Ago
Cofactor
M⁷G
AAA
mRNA cleavage
Repetitive elements, Pseudogenes endo-siRNA loci.
B)
Cytoplasm
Nucleus
Cofactor
Dicer
Ago
Ago
Exportin5
Cofactor
Ago
M⁷G
AAA
Translational repression and/or mRNA degradation
Ribosomes
Pol II/III
DGCR8
Drosha
Primary miRNAs
C)
Cytoplasm
Nucleus
Cofactor
Dicer
Ago
Ago
Exportin5
Cofactor
Ago
M⁷G
AAA
Translational repression and/or mRNA degradation
Ribosomes
miRNA Precursor
Spliceosome
Mirtron
Pol II/III
D)
Cytoplasm
Nucleus
Ago
Ago
Exportin5
Cofactor
Ago
M⁷G
AAA
Translational repression and/or mRNA degradation
Ribosomes
Pol II/III
DGCR8
Drosha
Primary miRNAs

Figure 1.1

1.1.2 Classes of Small RNAs

Small RNAs that function in RNAi are between 21-32 nt in length and are categorized by the type of Ago protein on to which they are loaded.

1.1.2.1. Piwi-interacting RNA (piRNA)

P-element induced wimpy testis (Piwi)-interacting RNAs or piRNAs are 24-32 nt in length (Perkel 2013). They are bound by Piwi subfamily of Ago proteins and differ from other small RNAs with respect to origin and chemical modifications (Aravin et al. 2006, Girard et al. 2006, Thomson and Lin 2009). piRNAs are derived from single-stranded RNAs, and their biogenesis is independent of Dicer processing (Saito et al. 2006, Grivna et al. 2006). They usually have a uracil residue on their 5' end and are methylated on the 3' end (Kirino and Mourelatos 2007a, Kirino and Mourelatos 2007b, Kirino and Mourelatos 2007c, Kirino et al. 2009). piRNAs have by far the largest sequence diversity of all small RNAs. In fact, there are more piRNAs than all other small RNAs combined (Thomson and Lin 2009).

The best-characterized function of piRNAs is repression of mobile genetic elements known as transposons (Saito et al. 2006, Carmell et al. 2007). They are also involved in epigenetic regulation through heterochromatin assembly, histone methylation, and double stranded DNA breaks reparation (Klattenhoff et al. 2007, Shirayama et al. 2012, Ashe et al. 2012). Some evidence suggests that they are involved in posttranscriptional control of genes too (Malone et al. 2009). piRNA-mediated gene silencing is well documented in *C. elegans*, and there are reports that in *M. musculus*,

piRNA target non-transposon genes to control cell shape in the hippocampus (Houwing et al. 2007, van Wolfswinkel 2014, Lee et al. 2011).

As discussed above, piRNAs are distinct from other small RNAs used in the RNAi pathway because they are produced without Dicer (Vagin et al. 2006, Brennecke et al. 2007). Mature piRNAs are produced from single strand RNAs by two different mechanisms, the primary pathway and the secondary or “ping-pong” pathway (Saito et al. 2010, Pane, Wehr and Schüpbach 2007). In *M. musculus*, the primary pathway produces piRNAs for the “ping-pong” stage. piRNAs precursors are first produced as long antisense transcripts from specific loci, then transported to the cytoplasm where they are cleaved by the endonuclease Mitochondrial Phospholipase D (MitoPLD) into smaller sizes (Huang et al. 2011). RNAs with uracil on the 5’ends are selectively loaded onto Mili/Miwi proteins. At this point, piRNAs are longer than the final 24-32 nt, but their size is reduced by an unknown 3’ to 5’ exonuclease to the mature size. Finally, HEN1 Methyltransferase Homolog 1 (HENMT1) methylates the piRNA 3’ end to complete the maturation process. In *M. musculus*, the primary pathway primes the “ping-pong” pathway (Kirino and Mourelatos 2007a, Kirino and Mourelatos 2007b, Kirino and Mourelatos 2007c). Mili proteins loaded with piRNAs by the primary pathway, target and cleave transposon-specific transcripts. The sense-strand cleavage products are loaded onto Miwi2 in order to target the antisense transposon. The Miwi2-loaded piRNAs are shortened and methylated to finalize their maturation. Through a homologous process, Miwi2 can drive the loading of Mili with new piRNAs. This cycle of cleavage-loading between the Piwi proteins Mili and Miwi2 is known as the ping-pong cycle (Grentzinger et

al. 2012). The ping-pong cycle carried in the cytoplasm explains the origin of the enormous diversity of piRNAs and how they repress transposons.

1.1.2.2. Short interfering RNAs (siRNAs)

The first report that protein expression can be potently and specifically suppressed by long dsRNA perfectly complementary to the targeted mRNA was Andrew Fire's and Craig Mello's ground breaking work performed in *C. elegans (*Fire et al. 1998). They were later awarded the Nobel Prize in 2006 for this work.

This process, now known as RNAi, has been described in organisms across all eukaryotes, and has been developed into a powerful tool that has revolutionized the study of gene function in eukaryotes (Carmichael et al. 2006, Liu et al. 2004b, Morita et al. 2007, Baillat and Shiekhattar 2009, Chapman and Carrington 2007, El-Shami et al. 2007, Emery et al. 2003, Eulalio et al. 2007c, Förstemann et al. 2005, Fortin, Nicholson and Nicholson 2002, Ghildiyal et al. 2008, Bohmert et al. 1998, Chen et al. 2009b, Kawamura et al. 2008, Drinnenberg et al. 2009). The dsRNA mediators of the sequence specific down regulation of the target mRNA are 21-23 nt dsRNAs now universally known as siRNAs (Elbashir et al. 2001b, Elbashir, Lendeckel and Tuschl 2001a). siRNAs pair with the complementary sequence within the target mRNA, stimulating cleavage of the mRNA by the endonuclease activity of the Ago protein at the core of RISC (Elbashir et al. 2001a, Wee et al. 2012).

At first, siRNAs were best known as tools for controlling gene expression, however, they have been reported to be part of the innate antiviral activity against virus infection in plants and insects (Swarts et al. 2014, Mallory and Vaucheret 2010). When RNA viruses

infect their hosts, long dsRNA molecules are generated. Dicer processes these long dsRNAs into siRNAs that are loaded onto Ago proteins that target the viral RNA for cleavage (Wang et al. 2006). In this regard, RNAi may have evolved as a primitive immune system (Kemp and Imler 2009, Kemp et al. 2013). Although this mechanism to control viral infections is still present in fungi, plants, and invertebrates, more complex animals, such as vertebrates, lack some of the proteins involved in this process, and it is generally accepted that this process no longer plays a major role in fighting viral infections.

1.1.2.3. Endogenous siRNAs (endo-siRNAs)

In many organisms, long dsRNAs are transcribed and then processed to generate endogenous-siRNAs (endo-siRNAs). This is in contrast to the production of canonical siRNAs where the siRNAs are generally produced from exogenous dsRNA (Ender and Meister 2010, Kawamura et al. 2008). Endo-siRNA transcripts have hairpin structures with extensive intramolecular pairings and their processing is dependent on Dicer (Czech et al. 2008). To date, endo-siRNAs have been reported in *D. melanogaster*, plants, *C. elegans* and vertebrates such as *D. rerio* and *M. musculus* (Chapman and Carrington 2007, Piatek and Werner 2014).

Endo-siRNAs are thought to act primarily as repressors of transposable elements in fungi, plants, and nematodes (Czech et al. 2008). Their effectiveness relies on the activity of RNA-dependant RNA polymerase (RdRP), which acts as an amplifier of long single stranded RNA for the otherwise low levels of endo-siRNAs (Okamura and Lai 2008). Insects and vertebrates do not encode RdRPs, and therefore the copy numbers

of endo-siRNAs in *D. melanogaster* and *M. musculus* are relatively very low. Regardless of the low concentration of endo-siRNAs in these organisms, the RISC-associated endo-siRNAs map to repetitive sequences in the genome that are reminiscent of transposons, thereby suggesting a conserved function (Ghildiyal et al. 2008).

1.1.2.4. MicroRNAs (miRNAs)

miRNAs were discovered in *C.elegans* and were first known as temporal RNAs (Lee et al. 1993). Lin-4 was the first named miRNA and was found to control expression of protein encoding genes (Olsen and Ambros 1999, Reinhart et al. 2000). The known roles of miRNAs in cellular activity have been vastly expanded since they were first discovered. Some of those roles include developmental timing, metabolism, differentiation, proliferation and even metastasis (Brennecke et al. 2003, Chen 2004, Chen et al. 2004, Morita et al. 2007, Emery et al. 2003, Johnston and Hobert 2003, Palatnik et al. 2003, Sun et al. 2011, Xu et al. 2003, Aukerman and Sakai 2003).

miRNAs are processed from primary miRNAs (pri-miRNAs) that are transcribed in the nucleus by RNA polymerases II and III. Pri-miRNAs are cleaved by the RNAse III type enzyme, Drosha, and its cofactor DGCR8 (DiGeorge syndrome Critical Region 8) into ~70 nt long RNAs called precursor miRNAs (pre-miRNAs) (Kim 2005, Han et al. 2006). Exportin5 transports pre-miRNAs to the cytoplasm, where they are further processed by another RNAse III type enzyme, Dicer, in combination with its cofactors TRBP and/or PACT. Dicer cleavage of pre-miRNA yields a partially dsRNA duplex of 21-24 nt that is loaded onto an Ago protein (Lund et al. 2004, Provost et al. 2002, Kawamata and Tomari 2010). Once the Ago protein/RNA duplex is formed, the miRNA duplex is unwound and

in most cases, the “guide” strand remains associated with the Ago protein forming the miRNA Induced Silencing Complex (miRISC).

The vast majority of known miRNAs are produced by the canonical miRNA biogenesis pathway described above. However, some miRNAs are produced independently of Drosha and/or Dicer. The Drosha-independent pathway uses introns removed from mRNA by the spliceosome machinery (Okamura et al. 2007, Berezikov et al. 2007, Ender and Meister 2010). These introns have a structure similar to pre-miRNAs and are transported to the cytoplasm following the same pathway (Berezikov et al. 2007, Okamura et al. 2007). Dicer-independent miRNAs are produced and processed in the nucleus, transported to the cytoplasm as pre-miRNAs, but instead of being processed by Dicer, the maturation of these miRNAs requires the endonuclease activity of an Ago protein (Cheloufi et al. 2010). Dicer-independent miRNAs are the newest reported class of miRNAs and the least studied. miRNAs produced by these non-canonical pathways constitute only a small fraction of the total cellular miRNA pool, however, they still play important roles in the cell. For example, the Dicer-independent *M. musculus* miRNA, miR451, is essential for viability in *M. musculus* and Drosha-independent miRNAs function in the elimination of unspliced mRNAs that are transported to the cytoplasm (Cheloufi et al. 2010, Liu et al. 2015).

Repression of protein translation by miRNAs is not fully understood, but the process involves binding of miRNAs to the 3’UTRs of mRNAs. The miRNA-binding sites in mRNAs are perfectly complementary sites to the “Seed domains” (nt 2-8) of miRNAs (Lewis et al. 2003, Brennecke et al. 2005). Structural analyses of human Ago2 complexed with a miRNA revealed that the seed domain of the miRNA is exposed, presumably to

allow scanning for complementary sites on mRNAs (Schirle and MacRae 2012). As indicated above, perfect base pairing between the remaining sequence of the miRNA and the mRNA is not required for efficient downregulation of translation (Clancy et al. 2011, Lytle, Yario and Steitz 2007, Pillai et al. 2005). In fact, most miRNA binding sites on mRNAs are poorly conserved outside of the section complementary to the miRNA seed region. Some Ago proteins have endonuclease activity (*i.e.* hAgo2, dmAgo2, etc.) and can cleave or "slice" mRNA resulting in enhanced down regulation of translation (Liu et al. 2004b, Ender and Meister 2010). However, for Agos to use endonuclease activity for slicing mRNAs, extensive sequence complementarity between the miRNA and mRNA is required, especially at positions 10-12, where the mRNA cleavage occurs. In most cases however, miRNA down regulate translation of mRNAs through translational repression rather than endonucleolityc cleavage (Ameres and Zamore 2013, Hendrickson et al. 2009, Guo et al. 2010, Eichhorn et al. 2014). Translational repression of mRNAs by miRISC requires the GW family of proteins (TNRC6 in humans) (Rehwinkel et al. 2005, Behm-Ansmant et al. 2006). Ago-miRNA complexes recruit GW proteins to the 3'UTRs of targeted mRNAs by direct protein-protein interaction. Subsequently, GW proteins recruit additional factors that inhibit translation of the mRNA by a combination of two mechanisms. 1) The first and most prevalent mechanism is mRNA destabilization. Once a GW protein binds to Ago, it decircularizes actively translating mRNA and then recruits deadenylases and decapping enzymes that will further destabilize mRNA (Eulalio et al. 2007c, Chen et al. 2009b). 2) Stopping the formation of the ribosome pre-initiation complex. This mechanism is not well characterized nor is it known to what extent or at what point in the repression process this "interruption" is implemented. However,

evidence suggests that miRISC stops the start-codon scanning process by the small ribosomal subunit through either binding or displacing the helicase eukaryotic initiation factor-4A (EIF4A). It is not clear if miRISC requires GW proteins for this function though (Kuzuoğlu-Öztürk et al. 2016).

1.1.3 Protein components of RNA-mediated silencing

1.1.3.1. RNAse III enzymes

Biogenesis of small RNAs that function in RNA-mediated silencing requires the activities of the type III RNAses Drosha and Dicer, in the nucleus and the cytoplasm, respectively (Kim 2005). These RNAses are large (>200 kDa) multidomain proteins that cleave dsRNA and produce a characteristic 2nt overhang on the 3' end (Bernstein et al. 2001). Although Drosha and Dicer can cleave dsRNAs *in vitro* without any co-factors, in cells they associate with other proteins that modulate their enzymatic activities, contribute to substrate selection, and direct cleavage specificity (Förstemann et al. 2005, Chendrimada et al. 2005). Drosha and Dicer are required for production of the vast majority of the 29,000 known miRNAs in different eukaryotes (Kwon et al. 2016, Burger and Gullerova 2015).

1.1.3.1.1 Drosha

Drosha proteins contain N-terminal proline-rich (P-rich) and an Arginine/Serine-rich (R/S-rich) regions, a platform region, a Piwi-Ago-Zwille (PAZ) -like domain, and two RNAse III domains and, a dsRNA binding domain (dsRBD) in the C-terminal region (Filippov et al. 2000, Wu et al. 2000). The proline- and R/S-rich domains are thought to

be important for protein-protein interactions (Wu et al. 2000, Fortin et al. 2002). Human Drosha was recently crystalized and it was revealed that the platform region separates the PAZ-like domain and the two RNAse III domains by ~35 nt of a dsRNA (Kwon et al. 2016). This explains the ~70 nt length of the pre-miRNA produced by Drosha cleavage of pri-miRNAs. The dsRBD at the C-terminus acts as a substrate-binding regulator (Kwon et al. 2016).

Drosha is localized predominantly in the nucleus and is an essential enzyme, as it is required for production of ribosomal RNA precursors (Wu et al. 2000). It functions upstream of Dicer in miRNA biogenesis pathways as part of a complex known as microprocessor (Lee et al. 2003). The other main component of the microprocessor complex is DGRC8, a dsRNA-binding protein (Denli et al. 2004). DGRC8 first binds pri-miRNAs and delivers them to Drosha for trimming (Kwon et al. 2016, Han et al. 2006).

Figure 1.2 Core protein components of the mammalian RNAi pathway. A. Schematic representation of human Drosha, Dicer, GW182 and Ago2. The most pertinent domains of each protein are indicated. **B.** The crystal structure of hAgo2 complexed to a small RNA (Red). Tryptophan bound to hydrophobic pockets in PIWI domain are depicted in orange. The crystal structure of hAgo2 was cropped from (Elkayam et al. 2012).

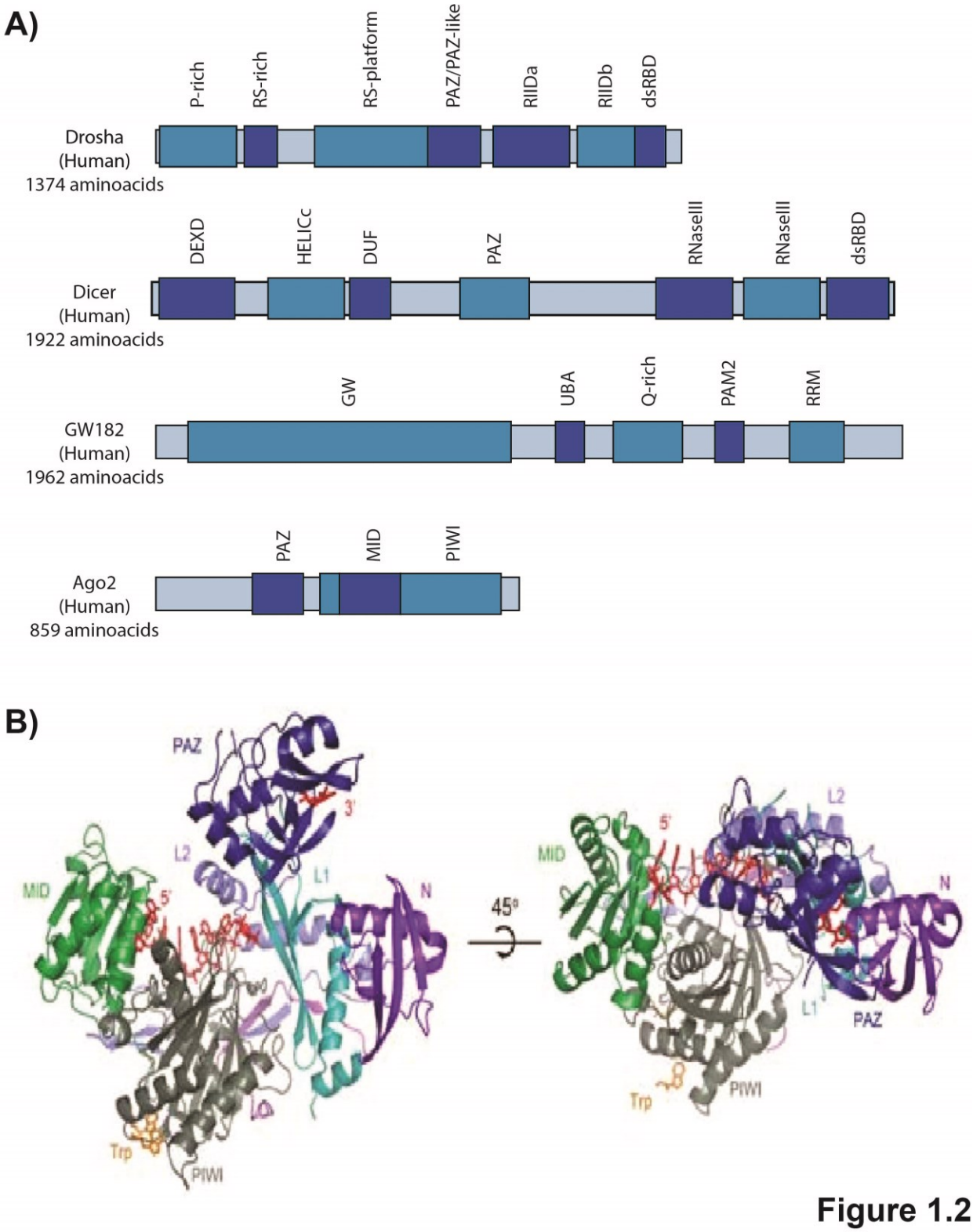
A)
P-rich
RS-rich
RS-platform
PAZ/PAZ-like
RIIDa
RIIDb
dsRBD
Drosha
(Human)
1374 aminoacids
DEXD
HELICc
DUF
PAZ
RNaseIII
RNaseIII
dsRBD
Dicer
(Human)
1922 aminoacids
GW
UBA
Q-rich
PAM2
RRM
GW182
(Human)
1962 aminoacids
PAZ
MID
PIWI
Ago2
(Human)
859 aminoacids
B)
PAZ
3'
L2
L1
MID
5'
N
Trp
PIWI
45°
L2
5'
MID
N
L1
PAZ
Trp
PIWI

Figure 1.2

1.1.3.1.2 Dicer

The crystal structure of the complete human Dicer protein has yet to be resolved, but a low-resolution cryoelectron microscopy (Cryo-EM) image coupled with crystal structures of individual Dicer domains have enabled the computational construction of a model (Ma et al. 2008, Macrae et al. 2006b, Macrae et al. 2006a). Although Dicer and Drosha have very low sequence similarity, their 3D structures are very similar (Kwon et al. 2016, Li and Patel 2016). Similar to Drosha, Dicer contains two RNAse III domains at the C-terminus that confer its catalytic activity (Figure 1.2). It also has a PAZ domain separated from the C-terminal catalytic domain by a platform region (Wang et al. 2009). In the N-terminal region, Dicer contains a complex helicase structure that is important for its regulation, and this is distinct from Drosha (Li and Patel 2016).

Dicer was first identified in *D. melanogaster* as the protein that mediated the processing of long dsRNA to 22 nt siRNAs (Bernstein et al. 2001). Humans express one Dicer protein that has evolved to primarily process pre-miRNAs generated by Drosha, into miRNAs (Jaskiewicz and Filipowicz 2008). The PAZ domain is an oligonucleotide-binding domain that prefers 2 nt 3' overhangs of dsRNA. Ago proteins also contain PAZ domain, but they are not identical to those found in Dicer (Macrae et al. 2006b, Song et al. 2003). The PAZ domains of Dicer and Ago proteins contain different regulatory loops that may account for the transfer of newly generated miRNA from Dicer to Agos (Cerutti, Mian and Bateman 2000). Pre-miRNAs are bound and positioned by the PAZ domain of Dicer, while cleavage is mediated by the intramolecular dimer formed by the two RNAse III domains (Macrae et al. 2006b). The platform region that separates PAZ from the catalytic center acts as a "molecular ruler" to generate products of ~22 nt length. The bias

toward pre-miRNAs instead of long dsRNA in human Dicer is provided by the helicase domain in the C-terminus (Macrae et al. 2006b).

In cells, Dicer functions with protein cofactors that deliver the substrate RNA and stimulate its function. Two Dicer cofactors, have being identified in mammals, TRBP and PACT (Chendrimada et al. 2005, Haase et al. 2005). They are structurally similar and contain two active dsRNA binding domains in their N-termini, which are involved in binding pre-miRNAs (Kok et al. 2007). Their C-termini contain inactive RNA-binding domains that are important for regulating binding of TRBP-PACT homo- or heterodimers to Dicer (Daniels et al. 2009). The lack of either TRBP or PACT does not significantly reduce the total amount of miRNAs produced in a cell, however they both contribute to substrate specificity and cleavage fidelity at the pre-miRNA to miRNA step (Heyam, Lagos and Plevin 2015). For example, while both TRBP and PACT bind to pre-miRNAs, PACT blocks Dicer activity on pre-miRNAs with high intramolecular complementarity, while TRBP activates Dicer activity regardless of the degree of complementarity in a pre-miRNA (Daniels et al. 2009, Heyam et al. 2015). Also, Dicer can generate different 5' ends from the same substrate pre-miRNA depending on binding to TRBP or PACT (Lee et al. 2013). The 5' end cleavage of miRNAs is crucial because it can change the miRNA seed domain, and therefore change their target mRNA (Friedman et al. 2009, Wee et al. 2012).

1.1.3.2 TNRC6

TNRC6 also known as GW182 is essential for miRNA-mediated translational repression of mRNAs. It was first identified using antibodies from sera of a patient with

neuropathy (Eystathioy et al. 2002). The protein contains Glycine-Tryptophan (GW) rich regions and had an apparent molecular mass of 182 kDa size, hence the name, GW182 (Figure 1.2). GW proteins are not present in all organisms, but they are found in vertebrates and invertebrates. There are three GW182 paralogs in humans (TNRC6A, TNRC6B, and TNRC6C), one in *D. melanogaster* and two in *C. elegans (Eulalio, Tritschler and Izaurralde 2009b)*.

The most distinctive feature of GW proteins is the N-terminal GW-rich domain that is responsible for interaction with Ago proteins (El-Shami et al. 2007, Eulalio et al. 2009b, Takimoto, Wakiyama and Yokoyama 2009). The GW region contains multiple “Ago hooks”, which are pairs of tryptophan residues spaced by 8-14 amino acid residues that directly interact with hydrophobic pockets in Ago proteins (Eulalio et al. 2009a, Baillat and Shiekhattar 2009, Zipprich et al. 2009, Till et al. 2007, Takimoto et al. 2009, Lazzaretti, Tournier and Izaurralde 2009). These interactions are critical for miRNA-mediated silencing. While the GW-rich domain is important for Ago interaction, domains in the C-termini are important for inhibiting protein translation. When the C-terminal domain of GW182 is artificially tethered to an mRNA, it can silence the mRNA expression independently of Ago2 and, hence, is called the silencing domain of GW proteins (Lazzaretti et al. 2009). GW proteins first interact with Ago proteins bound to mRNAs through miRNA-mRNA pairing. Then, the silencing domains block translation by disrupting the interaction between Poly(A)-binding-protein I (PABP-I) and EIF4G, which leads to the decircularizing of the mRNAs (Chen et al. 2009b). To further destabilize mRNA, the silencing domain can also recruit the deadenylases, PAN2-PAN3 and CCR4-NOT, which shorten the mRNA 3’ poly(A) tail (Behm-Ansmant et al. 2006). Recruitment

of the decapping proteins Dcp1 and Dcp2 results in removal of the 7-Methylguanosine (m7G) cap at the 5' end of the mRNA (Rehwinkel et al. 2005). After these steps, the exonuclease XRN1 rapidly degrades the de-capped and de-tailed mRNA (Ingelfinger et al. 2002). It remains to be determined what factors further contribute to mRNA destabilization or which ones promote dissociation of miRISC from mRNAs.

GW proteins localize to the cytoplasm and are major components of RNA granules known as processing-bodies (P-bodies), also known as GW-bodies. These granules are involved in mRNA degradation and contain protein components mRNA decay pathways as well as miRISC components (Ago proteins and miRNAs). This will be further discussed in section 1.2.1. (Jakymiw et al. 2005, Yang et al. 2004).

1.1.3.3 Ago superfamily

Ago proteins were discovered in *Arabidopsis thaliana* and are named after the mutant phenotype leaves, which resemble a small squid, caused by the pleiotropic effects of the deletion of AtAgo1 (Bohmert et al. 1998). They are essential for all aspects of the RNAi pathway as they bind small RNAs and form the protein core of RISC. The Ago family is subdivided into two subfamilies: Piwi and Ago. The Ago subfamily is broadly expressed in all cells and throughout all stages of development. Conversely, the Piwi subfamily members are expressed during gametogenesis and the germline development (Ender and Meister 2010).

1.1.3.3.1 Piwi subfamily

Piwi proteins were first described in *D. melanogaster* and are named after the phenotype produced by mutations in these genes that manifest during the gonadal development (Cox et al. 1998). Expression of Piwi proteins is transient during early developmental stages and gametogenesis, where they bind to piRNAs and function silencing of transposons. Only multicellular eukaryotes encode Piwi proteins. Humans encode four Piwi proteins (HIWI, HIWI2, HIWI3, and HILI) while *M. musculus* and *D. melanogaster* each encode three (Ender and Meister 2010). Much of what we know about human Piwi protein function is inferred from studies in *M. musculus* and *D. melanogaster (Gunawardane et al. 2007)*. The expression of Piwi proteins in *M. musculus* is restricted to early stages of development and spermatogenesis and is coordinated with the production of piRNAs. In fact, Piwi proteins are essential for the production of piRNAs. Loss of Piwi protein function results in meiotic arrest in *D. melanogaster, C. elegans*, *D. rerio* and *M. musculus* leading to male sterility (Wang and Reinke 2008, Houwing et al. 2007, Houwing, Berezikov and Ketting 2008).

Piwi proteins are di-methylated on arginines in their C-termini, a process that is catalyzed by the protein arginine methyltransferase 5 (PRMT5) (Nishida et al. 2009, Chen et al. 2009a). Methylation of Piwi proteins is important for their interaction with the Tudor-domain-containing proteins (TDRDs), which are essential for most Piwi protein functions. TDRDs regulate Piwi proteins localization in the cytoplasm and translocation to the nucleus, piRNA loading and ultimately their activity in transposon silencing (Boswell and Mahowald 1985, Meister et al. 2001). In *D. melanogaster*, there are at least a dozen

TDRDs that interact with Piwi proteins, all of which have one or more homologs in mammals (Nishida et al. 2009).

1.1.3.3.2 Ago subfamily

All multicellular and many unicellular eukaryotes express Ago proteins through all stages of development and in all cell types. They are not required for cell viability, but are essential for development of higher eukaryotes. The number of Ago proteins expressed in a cell varies widely among organisms from one in *S. pombe* to 25 in *C. elegans*. Humans encode four Ago isoforms (Ago1, Ago2, Ago3, and Ago4), all of which are expressed all cells and can bind siRNAs and miRNAs (Yigit et al. 2006, Ender and Meister 2010, Swarts et al. 2014).

Ago proteins (~100 kDa) contain three conserved domains: PAZ, MID and PIWI. The PAZ domain, as mentioned above is also present on Dicer proteins, binds to Drosha and Dicer cleavage products; small dsRNAs with 2nt, 3' overhangs. The MID domain contains a positively charged pocket that resembles a Rossman-like fold that binds the 5' ends of small RNAs in a sequence-independent manner (Boland et al. 2010). The PIWI domains of some Ago proteins have RNAse H activity that cleaves si/miRNA-mRNA complexes with extensive base pairing (Liu et al. 2004b). Of the four human Agos, only Ago2 has endonucleolytic activity (Liu et al. 2004b). Four essential amino acid residues form the catalytic site of the PIWI domain, but their presence does not confer nuclease activity in all cases (Nowotny et al. 2005). For example, introduction of nuclease activity in human Ago1 requires the catalytic tetrad in the PIWI domain as well as the N-terminal domain of hAgo2 (Faehnle et al. 2013).

The crystal structure of human Ago2 bound to miRNA has been resolved (Schirle and MacRae 2012, Elkayam et al. 2012). The structure is similar to the previously reported crystal structure of *P. furiosus* Ago (Song et al. 2004). hAgo2 is bi-lobular, with the PAZ domain and N-region in one lobe and the MID and PIWI domain in the opposite lobe (Figure 1.2 B). The domains are separated by flexible linkers that allow intramolecular movement of the domains. The interaction between the MID domain and the miRNA is entirely based on the phosphate backbone of the miRNA, explaining the sequence-independent nature of this interaction. The 5' end of a miRNA interacts with amino acid residues of the MID domain, exposing nt 2-8 of the seed region outward (Schirle and MacRae 2012). This positioning likely facilitates mRNA target scanning, which is why the seed region plays such an important role in target mRNA recognition. The four 3' nt of the miRNA interact with the PAZ domain through the phosphate backbone (Figure 1.2 B).

Ago-miRNA complexes regulate most human genes at the transcriptional level, a process that must be highly regulated. Post-translational modification of Ago proteins is likely a faster way of modulating RNAi than reprogramming of RISC with new miRNAs. Indeed, multiple post-translational modifications of Ago proteins have been reported but in many cases, their effects on Ago function are not well understood (Qi et al. 2008, Rüdel et al. 2011, Leung et al. 2011, Horman et al. 2013, Sahin et al. 2014, Shen et al. 2013).

In humans, Ago2 is arguably the important isoform and most of the information available on post-transcriptional regulation of Ago proteins is from the study of this protein. Hydroxylation of hAgo2 at P-700 is reported to be important for stability, whereas sumoylation at K-402 promotes degradation (Qi et al. 2008, Sahin et al. 2014). Ribosylation of hAgo2, which can occur during viral infection, inhibits its activity. Lastly,

hAgo2 is phosphorylated on at least seven amino acid residues, but effect of phosphorylation of only three residues has been investigated in significant detail (Rüdel et al. 2011). Phosphorylation of hAgo2 at S-387 is reported to be important but not essential, for targeting to P-bodies, and to switch off Ago2 endonucleolytic activity (Horman et al. 2013, Zeng et al. 2008, Lopez-Orozco et al. 2015). Phosphorylation at Y-393 blocks Dicer loading of long-loop-miRNAs, providing a mechanism for biasing the type of miRNAs that get incorporated into RISC (Shen et al. 2013). Finally, phosphorylation of Y-529 blocks small RNA binding to hAgo2 and consequently inhibits RNAi (Rüdel et al. 2011, Mazumder et al. 2013).

1.2 RNA Granules

1.2.1 Overview

mRNA translation is a complex process that is subject to multiple layers of regulation. Translation rates are affected by cis-elements mRNAs, such as strong or weak start codon strength (Fasken and Corbett 2005, Gebauer, Preiss and Hentze 2012, Muhlrad, Decker and Parker 1995, Muckenthaler et al. 1997). Secondary structures and/or regulatory sequences at the 3'UTR also play a role in determining translation rates. Trans-acting elements (*i.e.* RNA binding proteins) also modulate mRNA stability ultimately determining their fate (Schwartz and Parker 1999). The two major stability determinants of mRNAs are the poly(A) tail with bound Poly(A)-binding protein-1 (PABP-1) at the 3' end, and the 7-Methylguanosine (m7G) structure that associates with the cap-binding

proteins (Yamashita et al. 2005). It is well established that mRNAs engaged in rounds of translation exist in a “circularized” form, where PABP-1 at one end interacts with proteins associated with the M7G cap at the other end (*i.e.* translation initiation factors) (Tucker et al. 2002, Behm-Ansmant et al. 2006). This ensures that only intact mRNAs are translated, and also protects mRNA ends from exonuclease degradation. The initial hypotheses for regulation of mRNA expression were simplistic; mRNA engaged in translation is protected from degradation while mRNAs not being actively translated are not protected from degradation. It is now known that mRNA regulation is actually much more complex (Yamashita et al. 2005). mRNAs exist in dynamic states with competing factors that either stall or initiate translation. If translation of a particular mRNA stalls, that mRNA can continue to be displaced from active ribosomes by additional inhibition factors. Subsequently, the mRNA can be destabilized by shortening of the poly(A) tail. mRNAs become committed for degradation only after their poly(A) tails are too short to bind PABP-1 or if the 5’ cap structure is removed (Chen and Shyu 2011).

mRNAs can be re-routed to active polysomes, or targeted to RNA granules in the cytoplasm (Knowles et al. 1996). There are different types of RNA granules: P-bodies, stress granules, neuronal granules, germline granules, etc. RNA granules are non-membranous organelles composed of protein-RNA aggregates that are involved in storage, spatial localization, and/or decay of RNA (Bashkirov et al. 1997, Kedersha et al. 1999). Disruption of neuronal granules is reported to affect neuronal function, but the specific functions involving this and other RNA granules are still under investigation. P-bodies and stress granules are the only RNA granules that are present in all cells, whereas all other RNA granules are cell line specific (*i.e.* neuronal granules are only

present in polarized neurons) (Savas et al. 2010). Significantly, both P-bodies and stress granules are associated with Ago proteins and other proteins that function in RNAi pathways (Leung, Calabrese and Sharp 2006, Liu et al. 2005a)(Figure 1.3).

Figure 1.3 RNA granules. De-circularization of mRNA causes cessation of translation. mRNAs in early stages of inhibition can be further de-stabilized and targeted to P-bodies for degradation or they can be transported to stress granules. Stress granules and P-bodies can dock and exchange mRNA and proteins. Adapted from (Decker and Parker 2012).

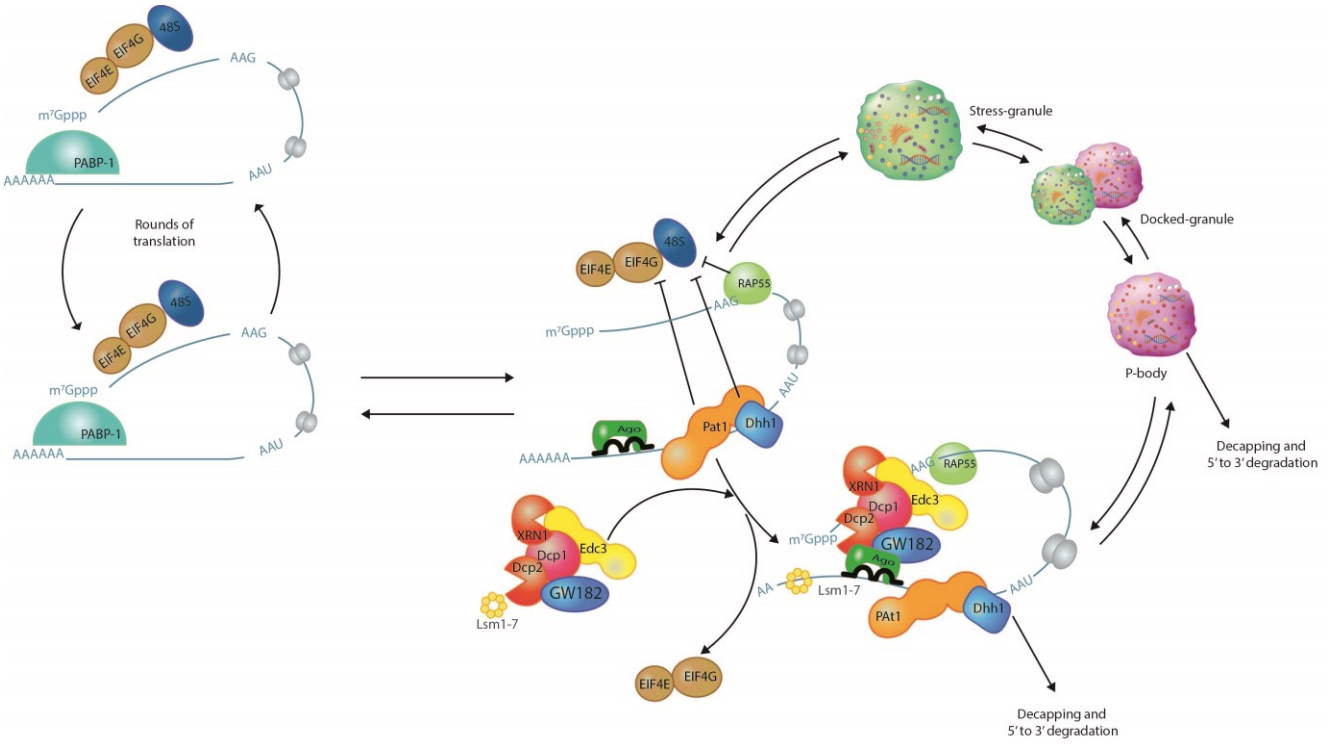
40S
EIF4E
EIF4G
AAG
m7Gppp
PABP-1
AAAAAA
AAU
Rounds of translation
Stress-granule
Docked-granule
P-body
RAP55
Ago
Pat1
Dhh1
XRN1
Dcp1
Edc3
Dcp2
GW182
Lsm1-7
AA
PAt1
Decapping and 5'to 3'degradation

Figure 1.3

1.2.2 Processing Bodies

P-bodies were initially described as cytoplasmic foci enriched in the exonuclease XRN1 (Bashkirov et al. 1997). It was speculated that these foci were centers for mRNA decay. Indeed, what at the time were called XRN1 granules, and are now known as P-bodies, contain deadenylated mRNA and are enriched with enzymes involved in mRNA decay. P-bodies contain: Deadenylases and related factors (*i.e.* CCR4, NOT 1/2/3/4/5, PAN2/3, TOB2, etc.), decapping and related factors (*i.e.* Dcp1/Dcp2, Edc, Lsm 1 – 7, Pat1, etc.), exonuclease XRN1, Nonsense-mediated decay (*i.e.* UPf1 – 3, SMG 5 – 7, etc.) among others. In total, there are more than 100 proteins that are known to associate with P-bodies (Andrei et al. 2005, Yang et al. 2004, Liu et al. 2005a, Wilczynska et al. 2005). Even though P-bodies are thought to function in degradation of mRNA, this process occurs when microscopically visible P-bodies (150 to 350 nm in diameter) are absent from cells (Eulalio et al. 2007b, Cougot et al. 2012).

P-bodies are dynamic structures and their numbers and composition varies according to the cell cycle and cellular stress (Moser et al. 2007). They actively exchange proteins with the cytoplasm and rely on the microtubule network for this process as well as motility (Aizer et al. 2008, Carmichael et al. 2006). Biogenesis of P-bodies is not completely understood, but glutamine/asparagine-rich (Q/N) motifs on numerous P-body proteins are known to be important for assembly of these structures (Decker, Teixeira and Parker 2007, Mazzoni, D'Addario and Falcone 2007). Formation of P-bodies in yeast is thought to occur as follows: (i) mRNAs with shortened poly(A) tails form closed-loop mRNA through interaction with translation inhibitors at both ends; (ii) once there is a large number of closed-loop mRNAs, they aggregate via protein-protein interactions of their

Q/N-rich motifs (Reijns et al. 2008). It is still a matter of debate what the function of microscopically visible P-bodies is, and how proteins with Q/N-rich domains are prevented from spontaneously aggregating. However, it has been speculated that Q/N motifs are disorganized and only aggregate after conformational changes brought on by protein-RNA interactions. This implies that P-bodies form as a consequence of mRNA decay (Eulalio et al. 2007b).

GW and Ago proteins localize to P-bodies but the role of P-bodies in RNA silencing is still controversial. Analyses suggest that less than 10% of the Ago protein pool resides in P-bodies (Leung and Sharp 2013). One study reported that association of Ago2 with P-bodies is stimulated by phosphorylation of S-387 (Zeng et al. 2008). This was interpreted as increased RNA silencing activity, but definitive evidence for this is lacking. Finally, P-bodies have been linked to storage of selected mRNAs and may be sites where ribonucleoprotein complexes are modified by exchange of RNA binding proteins (Savas et al. 2010).

1.2.3. Stress Granules

Stress granules were first described in cells from *Lycopersicon peruvianum* (tomato) where it was observed that specific mRNAs accumulated in cytoplasmic regions after heat stress (Nover, Scharf and Neumann 1989). We know now that in addition to heat, oxidative, translation and metabolic stress trigger formation of stress granules (Kedersha et al. 1999, Kedersha et al. 2002, Barber 2005, Wek, Jiang and Anthony 2006, Kaufman 2004).

Stress granules, like P-bodies, are non-membranous protein-RNA aggregates localized in the cytoplasm. However, they are only observed during or shortly after cellular stress, unlike P-bodies which are constitutively present. Formation of these structures may aid survival under stress by sequestering mRNAs that encode non-essential proteins from the translating pool. In doing so, translation of mRNAs encoding proteins that are required for responding to stress response is prioritized, while allowing the cell to conserve energy (Stöhr et al. 2006). The mechanism for excluding mRNAs from stress granules is not well understood, but mRNAs of stress response genes have Internal Ribosomal Entry Sites (IRES) sequences in their 5'UTRs allowing for translation in a cap-binding-protein independent manner (Stöhr et al. 2006, Kedersha and Anderson 2002).

Stress granules share some components with P-bodies, but overall, their composition is quite different. The mRNAs that accumulate in stress granules are capped and polyadenylated, and the proteins present are associated with mRNAs sequestered from the translation initiation process, such as PABP, translation factors, ataxin, and DDX3 and small ribosomal units (Krishnamoorthy et al. 2001, Ohn et al. 2008). Other stress granule resident proteins include kinases (FAK and FAST) and O-linked β-N-acetylglucosamine (O-GlcNAc) transferases (Ohn et al. 2008, Kedersha et al. 2005). Altogether, there are more than 100 proteins components that associate with stress granules. They form rapidly upon cell stress and dissociate after removal of the stress, a process that is likely facilitated by rapid exchange rate of resident proteins with the cytoplasmic pool (Kedersha et al. 1999, Kedersha et al. 2002, Kedersha and Anderson 2002, Gilks et al. 2004). Stress granules also dock with P-bodies and exchange mRNAs and resident proteins (Stoecklin and Kedersha 2013, Kedersha et al. 2005).

Biogenesis of stress granules is primarily driven by the accumulation of stalled ribosomal pre-initiation complexes (48S). Phosphorylation of EIF2α at S-51 stops EIF2α from recruiting the essential tRNAMet to the translation initiation complex; a preeminent block to initiation of translation that accounts for a fast accumulation of stalled pre-initiation complexes (Dever 2002, Kimball 2001). After this initial stalling step, the prion-like proteins TIA, TIA-R and G3BP1 aggregate via interactions of their Q/N-rich domains to nucleate the formation of stress granules (Tourrière et al. 2003, Gilks et al. 2004, Kedersha et al. 1999, Kedersha et al. 2002). These nucleation factors are essential for the biogenesis of stress granules and their depletion impairs stress granule formation. Conversely, overexpression of these proteins can trigger stress granule formation in the absence of cellular stress (Anderson, Kedersha and Ivanov 2015). Formation of stress granules is dependent on a functional microtubule network and drugs (*i.e.* nocodazole) that inhibit microtubule depolymerisation prevent the formation of stress granules (Fujimura et al. 2009, Kolobova et al. 2009).

While the timing of stress granule formation and the molecular composition of these granules point to a function in inhibition of mRNA translation, protein synthesis can be blocked without these granules. This is analogous to what is observed for P-bodies, which are not necessary for RNAi (Eulalio et al. 2007b), but form when RNAi activity is increased.

Recruitment of Ago proteins to stress granules is dependent on miRNAs and Ago mutants that cannot bind miRNAs do not localize to stress granules (or P-bodies) (Pare, López-Orozco and Hobman 2011b). Conversely, GW proteins are residents of P-bodies but do not localize to stress granules. A model to explain these observations is that Ago

proteins that associate with RNA granules do so because of their interaction with small RNAs (Huntzinger and Izaurralde 2011). Pools of Ago that associate with stress granules are thought to move en bloc to these granules in complex with miRNAs and targeted mRNAs (Eulalio, Behm-Ansmant and Izaurralde 2007a). In contrast, Agos are targeted to P-bodies together with GW proteins following miRNA-dependent interaction with mRNAs in the late stages of degradation (Liu et al. 2005a). Association of Ago-miRNA complexes with RNA granules is likely influenced by other factors. However, very little is known about this process other than phosphorylation of Ago2 at S-387 is reported to increase the association of Agos with P-bodies during stress (Zeng et al. 2008). Given the importance of mRNA regulation by RNAi and other mechanisms, more research in this area is warranted.

1.3. Kinases

1.3.1. Overview

Phosphorylation of proteins by kinases is a common and pervasive mechanism used to reversibly alter their activities and/or intracellular localizations (Hunter 2000, Knowles 1980). The human genome encodes 518 protein kinases that play roles in virtually every cellular process including cell cycle, cell differentiation, intracellular communication, cytoskeletal rearrangement, motility, and apoptosis (Manning et al. 2002, Domenicali Pfister et al. 2006, Tudzarova et al. 2016, Harashima et al. 2016).

Protein kinases catalyze the transfer of phosphate (PO_4^{-3}) onto hydroxyl groups of serine, threonine and tyrosine residues (Adams 2001). The primary phosphate donor for

this reaction is ATP, but a few kinases (*i.e.* casein kinase 2) can use GTP (Li and Roux 1992). The replacement of a mildly negative hydroxyl group with a bulky PO_4^{-3} group changes not only the overall charge of proteins, but often their conformations (Knowles 1980). The latter can alter protein-protein interactions and/or the affinities of enzymes for substrates. Because it is a reversible modification, phosphorylation is a dynamic and effective way to modulate protein function (Figure 1.3). Dephosphorylation results in restoration of the OH^- group and release of PO_4^{-3} and is catalyzed by protein phosphatases (described further in section 1.1.6.2). Kinases can be organized into nine groups based on sequence similarities (Manning et al. 2002).

Table 1.1 Kinase groups.

Group	Number of members
Protein Kinase A, G, and C (AGC)	63
Calmodulin/Calcium regulated kinases (CAMK)	74
Casein Kinase 1 (CK1)	12
CDK, MAPK, GSK3 and CLK (CMGC)	61
Homologs of the yeast STE7, STE11 and STE20 genes (STE)	47
Tyrosine Kinase (TK)	90
Tyrosine Kinase-like (TKL)	43
Receptor Guanylate Cyclases (RGC)	5
Other	123

The vast majority of human protein kinases catalyze transfer of phosphates to serine or threonine residues exclusively. Conversely, there are approximately 90 tyrosine kinases that phosphorylate tyrosine residues but not serine or threonine residues

(Manning et al. 2002). Finally, Tyrosine Kinase- Like (TKL) kinases (~43 in humans) can phosphorylate serine/threonine residues was well as tyrosine residues. For this reason they are also known as dual-specificity kinases. Regardless of the group classification, kinases share multiple similarities including a highly conserved catalytic core domain whose activity is modulated by heterogenous regulatory domains (Manning et al. 2002, Lemmon and Schlessinger 2010). The catalytic domains of kinases from archaea to higher eukaryotes share a highly conserved structure that includes: 1) A glycine-rich region that binds and positions ATP for donation of its gamma phosphate; 2) A regulation loop that separates ATP from the substrate thus preventing indiscriminate phosphorylation activity; and 3) A core catalytic triad consisting of a lysine and two aspartic acid residues (Knighton et al. 1991). All three amino acid residues are critical for activity. Interestingly, approximately 10% of all human kinases lack one or more of these residues, known as pseudokinases (Manning et al. 2002, Parang et al. 2001). These pseudokinases are catalytically inactive but can act as decoys and are crucial for the negative regulation of other kinases. The kinase variable regulatory regions are very diverse in structure and function to control subcellular localization, binding partners and substrate selection. Examples of regulatory domain types include: hydrophobic domains to interact with membranes, immunoglobulin/fibronectin-like domains for extracellular interactions, and adaptor and other protein-protein interaction domains (Manning G. et al, 2002).

Figure 1.4 The phosphorylation cycle. Phosphorylation is a reversible post-translational modification. Kinases catalyze the addition of phosphate groups to proteins whereas phosphatases catalyze the removal of these groups. In the example provided, phosphorylation activates the protein, but in some cases, phosphorylation does the opposite. The outcome of phosphorylation varies according to the kinase and substrate.

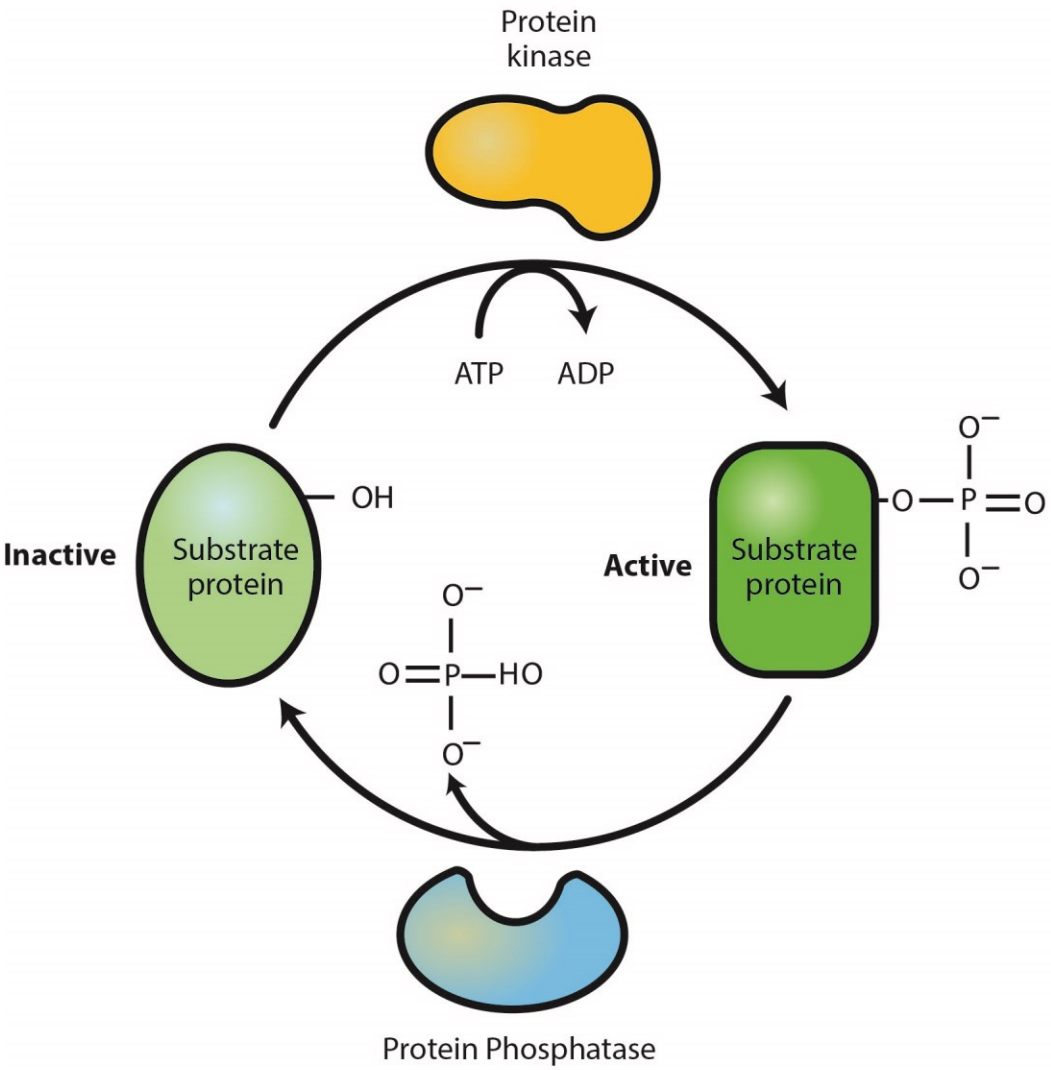
Protein
kinase
ATP
ADP
Inactive
Substrate
protein
OH
Active
Substrate
protein
O⁻
O—P═O
O⁻
O⁻
O═P—HO
O⁻
Protein Phosphatase

Figure 1.4

1.3.2 Kinase-substrate interaction

Evidence suggests that a large fraction of human proteins are regulated by phosphorylation (Sharma et al. 2014). Ultradeep phosphoproteome analysis revealed that at least 75% of human proteins are phosphorylated (Sharma et al. 2014). Kinases typically bind consensus sequences or motifs around the target residue in the substrate protein. In doing so, kinase catalytic domain is brought in close proximity to the target residue and the donor phosphate. The phosphate transfer is achieved by conformational changes induced as a result of the kinase binding (Wang and Cole 2014, Hari, Merritt and Maly 2013).

Phosphorylated amino acid residues are generally found on the surface of proteins where they are accessible to kinases (Ubersax and Ferrell 2007). However, by working with chaperones, kinases can gain access to otherwise unavailable target sites on some proteins. Kinases may also employ scaffold proteins to select protein targets (Sacks 2006, Zheng et al. 2013). The scaffold itself is not phosphorylated, but helps to optimally position substrates for phosphorylation (Good et al. 2009). In the absence of the necessary chaperone, scaffolds, target proteins may not be phosphorylated, thereby adding another regulatory layer. The kinase-substrate interaction is often transient, but has lasting effects once the target is phosphorylated.

1.3.3. Kinase Networks

In many cases interaction between kinases is critical for proliferation and propagation of signalling events. For example, many kinases work together in a hierarchical manner (Ruhe et al. 2006, Wu, Chen and Ullrich 2003, Katoh 2006). In this

scheme, an upstream kinase phosphorylates downstream kinases, leading to their activation and subsequent amplification of the signal, which in many cases leads to activation of transcription factors. This results in changes to protein expression within the cell (Nazarov et al. 2013). In addition, crosstalk between kinase networks can activate multiple pathways and trigger a broader response to a specific stimulus. Because of the robust signal amplification that often follows kinase activation, negative feedback mechanisms are required to limit uncontrolled signalling. For example, activation of fibroblast growth factor receptor (FGFR), a transmembrane kinase, eventually induces the transcription of proteins that inactivate its signalling pathway (Kunii et al. 2008, Cabrita and Christofori 2008)(Figure 1.5).

Figure 1.5 The Fibroblast Growth Factor (FGF) pathway. Binding of the FGF ligand to FGFR promotes formation of the ternary complex FGFR-FGF- heparin sulphate proteoglycan (HPSG) (Purple). This activates the intracellular tyrosine kinase domains of FGFRs, which then cross-phosphorylate each triggering recruitment and activation of other kinases. Four main downstream pathways can be activated by activated FGFR. These include RAS - mitogen-activated protein kinases (MAPKs), PI3K-AKT, PLCγ and STAT. Depicted in red are the main negative regulators of the FGF pathway (Modified from (Ornitz and Itoh 2015))

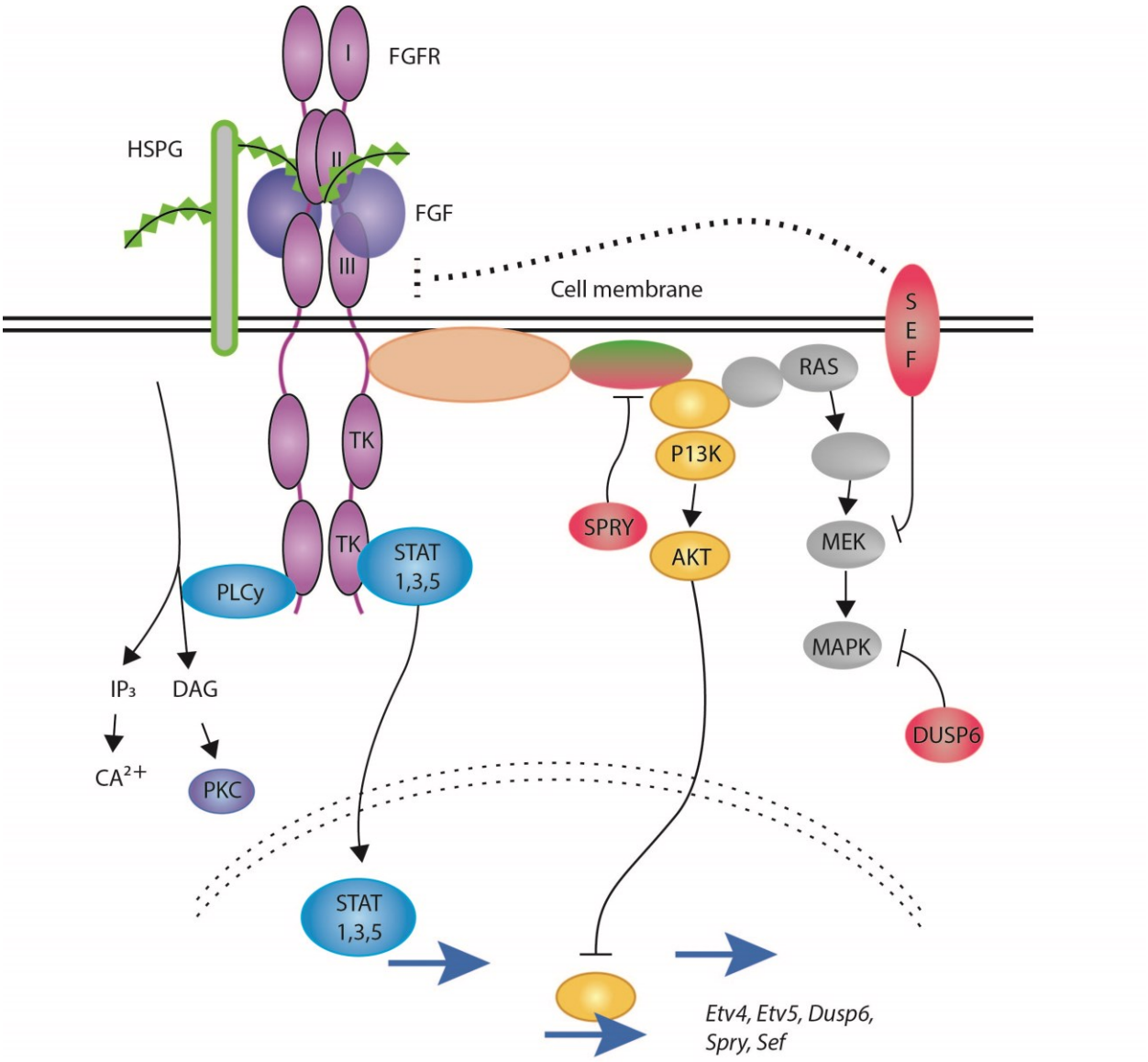
I
FGFR
HSPG
II
FGF
III
Cell membrane
S
E
F
RAS
TK
P13K
SPRY
TK
STAT
1,3,5
AKT
MEK
PLCy
MAPK
IP3
DAG
DUSP6
CA2+
PKC
STAT
1,3,5
Etv4, Etv5, Dusp6,
Spry, Sef

Figure 1.5

1.3.4. Fibroblast growth factor (FGF) Signalling

The FGF pathway is a major developmental pathway that is required for early embryogenesis and organ development. It also regulates angiogenesis and the wound healing response (Beer et al. 2005). Activation of the FGF pathway increases proliferation, differentiation, and anti-apoptotic signalling cascades (Katoh 2006). Even though it generally activates pro-survival signaling, its effects are determined by cellular context and in special circumstances, can result in cell cycle arrest (Krejci et al. 2008). Given its role in cell proliferation, malfunction of the FGF pathway is associated with developmental defects and several kinds of cancer (Ornitz and Itoh 2015, Brady et al. 2013).

The two main constituents of the FGF pathway, include FGF ligands and FGF receptors (FGFRs). FGF ligands are small, glycosylated proteins that are secreted to signal adjacent or distant cells. FGFRs are transmembrane tyrosine kinases. In humans, there are 18 genes that code for FGF ligands and five that code for FGFRs (Beenken and Mohammadi 2009). The FGF pathway output can be affected by the different affinities between FGF ligands and FGFRs. In mammals, different cells express a range of FGFR levels allowing differential stimulation by the same ligands (Hughes 1997).

FGFRs are members of the immunoglobulin superfamily. They are transmembrane tyrosine kinases anchored in the plasma membrane by a single hydrophobic domain (Ornitz and Itoh 2015). The intracellular region contains the catalytic kinase domain, while the extracellular region has the FGF ligand-binding domain. Of the five members of the human FGFR family, four have tyrosine kinase activity. FGFR5 can bind FGF but is

catalytically inactive and acts as a negative regulator of the pathway by decreasing ligand pools available to kinase-active FGFRs (Steinberg et al. 2010).

Stimulation of FGFRs targets mainly four downstream pathways (Figure 1.4). To limit FGFR signaling, there are a number of inhibitory mechanisms, and depends on the specific FGF-FGFR complex that is activated. The inhibitory mechanisms include internalization of activated FGFRs and transcriptional upregulation of inhibitors. Internalization of FGF-FGFR complexes is a fast response, where complexes are targeted for degradation or recycling in a process partly controlled by ubiquitination (Reilly, Mizukoshi and Maher 2004, Haugsten et al. 2008). Sustained FGFR signaling promotes the transcriptional upregulation of phosphatase genes and other specific FGFR inhibitors. Two main inhibitors of this pathway have been described; Sprouty (SPRY) and Similar Expression to FGF (SEF) proteins. SPRY proteins inhibit the RAS-MAPK and PI3K-AKT pathways whereas SEF inhibits FGFR kinase activity by interacting with its extracellular domain (Cabrita and Christofori 2008, Hanafusa et al. 2002, Kovalenko et al. 2003). Lastly, upregulation of phosphatases that de-phosphorylate and thus inactivate downstream kinases in the FGFR pathway is employed to limit FGF signalling. An example is Dusp6 phosphatase, which specifically targets kinases of the MAPK pathway (Zhang et al. 2010).

1.4. Phosphatases

1.4.1 Overview

Protein phosphatases are perhaps not as well studied as kinases, but they play critical roles in every aspect of cellular function. The balance between the actions of kinases and phosphatases is what makes phosphorylation one of the most versatile post-transcriptional modifications. By counteracting the effects of kinases, phosphatases help regulate many diverse processes such as cell cycle, signalling cascades, motility and apoptosis (Olsen et al. 2006). Surprisingly, the human genome encodes only ~140 phosphatases, compared to over 500 kinases (Lander et al. 2001, Manning et al. 2002). Whereas tyrosine phosphatases and tyrosine kinases are similarly abundant (107 vs 90 respectively), there are >13-fold more serine/threonine kinases than serine/threonine phosphatases. In order to maintain the balance of regulation, the substrate range of many serine/threonine phosphatases is relatively high (Ceulemans and Bollen 2004, Cohen 2002, Lu and Wang 2008). This is accomplished by the use of multiple regulatory subunits that greatly increase the number of targets that can be acted on by phosphatases (Ceulemans and Bollen 2004).

Protein phosphatases catalyze the removal of a phosphate group from an amino acid residue, producing inorganic phosphate while restoring the hydroxyl group on the aminoacid side chain (Figure 1.3). Although they all catalyze the same reaction, phosphatases are known to use at least four different mechanisms, each of which can be traced back to a different ancestor (Shi 2009). Phosphatases that use the same mechanism also share sequence similarity. Based on this sequence similarity, phosphatases are subdivided into four groups: 1) Cysteine-dependant phosphatases; 2)

Phosphoprotein phosphatases; 3) Metal dependant phosphatases and; 4) Aspartate-dependant phosphatases.

Cysteine-dependant phosphatases. Members of this group share the conserved motif CxxxxxR, in which an active cysteine catalyzes phosphate removal (Alonso et al. 2004). It is the largest and most diverse phosphatase group. In addition to their catalytic domains, they share other characteristics, including: i) Functioning as monomers (Schaapveld, Wieringa and Hendriks 1997); ii) Regulatory domains that provide specificity without the need for regulatory subunits (Gandhi et al. 2005); and iii) A regulatory cysteine residue at the core of the catalytic domain that can be controlled by reversible oxidation (van Montfort et al. 2003). All tyrosine phosphatases, including receptor, non-receptor, and dual-specificity phosphatases, belong to this group (Alonso et al. 2004).

Phosphoprotein Phosphatases. Members of this group share the protein phosphatase 2A (PP2A) catalytic domain, an approximately 280 amino acid residue domain that is highly conserved among eukaryotes (Cohen 2002, Ceulemans and Bollen 2004). Phosphoprotein phosphatases act exclusively on serine/threonine residues and, although there are only nine members of this family, they are involved in virtually every aspect of cell function as each member of this group can dephosphorylate hundreds of different targets.

The members of this family are PP1, PP2A, PP2B, PP4, PP5, PP6 and PP7. Except for PP2B (also known as calcineurin) they do not contain regulatory domains. To form a fully active holoenzyme, members of this family must interact with one or more regulatory subunits. To date, more than 200 regulatory subunits of phosphoprotein phosphatases have been identified (Bollen et al. 2010, Cohen 2002, Shi 2009). These,

include activators, inhibitors and scaffold subunits. The large number of different complexes that can be formed by interactions of phosphatases with various combinations of the regulatory subunits allows for a wide range of substrates and regulatory mechanisms (Moorhead, Trinkle-Mulcahy and Ulke-Lemée 2007).

Metal-dependant phosphatases. With 16 members, this is the largest group of serine/threonine phosphatases. Their catalytic domains require coordination of Mn^{2+} / Mg^{2+} for enzymatic activity (Das et al. 1996). Although they are involved in many diverse activities, including differentiation, meiosis, and apoptosis, their activities appear to be largely involved in response to stress (Lu and Wang 2008). Their functions are not well characterized, but evidence suggests that unlike phosphoprotein phosphatases they are not be controlled by regulatory subunits. Rather, there are large number of isoforms encoded by splice variants, each with different subcellular localizations and activities (Brognard et al. 2007).

Aspartate-dependant phosphatases. This group of serine/threonine phosphatases is the smallest and least studied group (Shi 2009). Their catalytic subunit relies on a aspartate residues in their cores. The main target of this group is RNA polymerase II, and therefore, their actions influence transcriptional activity (Ghosh, Shuman and Lima 2008).

1.5. Objectives

Since its discovery 19 years ago, RNAi has emerged as an invaluable tool for the study of gene and protein function. RNAi is also a major posttranscriptional regulatory pathway that controls the expression of most protein-encoding genes. While much is known about RNAi mechanisms that control expression of mRNAs, relatively little is known about the regulation of RNAi itself. At the outset of this study, evidence was beginning to emerge that RNAi activity is modulated by post-translational modifications on Ago proteins. Ago proteins are phosphorylated on multiple sites yet very little was known about the this modification affected Ago function. The goal of my thesis research was to characterize the effects of Ago protein phosphorylation in RNAi function. I hypothesized that Ago2 phosphorylation modulates RNAi activity by influencing their spatial localization and/or function. Accordingly, mutations that blocked or mimicked Ago2 phosphorylation would affect its activity and/or subcellular localization. My findings suggest that specific phosphorylation events on Ago2 can dramatically affect its subcellular localization while having minimal effects on its function. I also performed a genome-wide screen to identify the kinases and phosphatases that regulate Ago2 and characterized several receptor tyrosine kinases that inhibit RNAi. Further analyses revealed that other cell surface receptors negatively regulate RNAi silencing. The results described in this thesis advance our understanding of Ago2 control by phosphorylation.

Chapter 2

Materials & Methods

2.1 Materials

All commercial materials, chemicals and reagents were used according to manufacturers recommendations unless otherwise stated.

2.1.1 Reagents

Table 2.1 – Commercial sources of materials, chemicals and reagents

Reagent	Source
0.25% Trypsin-EDTA	Thermo Fisher Scientific
1-bromo 3-chloropropane	Sigma-Aldrich
1mm and 2 mM Electroporation Cuvettes	Bio-Rad
2-Mercaptoethanol	Thermo Fisher Scientific
4-(2-hydroxyethyl)-1piperazineethanesulfonic acid (HEPES)	Thermo Fisher Scientific
4-(2-hydroxyethyl)-1-piperazineethanesulphonic acid (HEPES)	Thermo Fisher Scientific
40% acrylamide /bis-acrylamide solution (29:1)	Bio-Rad
Accutase® Cell Detachment Solution	Thermo Fisher Scientific
Adenosine triphosphate (ATP)	Sigma-Aldrich
Agar	Sigma-Aldrich
Agarose, ultrapure, electrophoresis grade	Thermo Fisher Scientific
Ammonium acetate	Thermo Fisher Scientific
Ammonium persulphate	Sigma-Aldrich
Ampicillin	Sigma-Aldrich
Adenosine Triphosphate (ATP) αP^{32}	PerkinElmer
Bacto-tryptone	Becton, Dickinson & Company
Bacto-yeast extract	Becton, Dickinson & Company
BGJ398 (Fibroblast growth factor receptor inhibitor)	Adooq
Blasticidin	Thermo Fisher Scientific
Bovine serum albumin (BSA)	Sigma-Aldrich
Bromophenol blue	Sigma-Aldrich
Casein, enzymatic hydrolysate	Sigma-Aldrich
Chloroform	Thermo Fisher Scientific
Cycloheximide	Sigma-Aldrich
CO_2-independent cell culture medium	Thermo Fisher Scientific
Complete™ EDTA-free protease inhibitor	Roche
DAPI (4',6-diamidino-2-phenylindole)	Thermo Fisher Scientific
Dharmafect 1 Transfection reagent	GE Healthcare
Dimethyl sulphoxide (DMSO)	Sigma-Aldrich
Dimethylpimelimidate (DMP)	Thermo Fisher Scientific
Disodium hydrogen orthophosphate	Becton, Dickinson & Company

Table 2.1 – Continued

Reagent	Source
Dithiothreitol (DTT)	Sigma-Aldrich
Dulbecco's modified Eagle's medium (DMEM) High Glucose	Thermo Fisher Scientific
Ethanolamine	Thermo Fisher Scientific
Ethidium bromide solution	Sigma-Aldrich
Ethylene glycol tetraacetic acid (EGTA)	Sigma-Aldrich
Ethylenediaminetetraacetic acid (EDTA)	EMD Chemicals
Fetal bovine serum (FBS)	Thermo Fisher Scientific
Fibroblast growth factor 1 (FGF1)	AbCam
Glycerol	Thermo Fisher Scientific
Glycine	Calbiochem
Guanidine HCl	Thermo Fisher Scientific
HALT (Phosphatase Inhibitor)	Thermo Fisher Scientific
Hydrochloric Acid	Thermo Fisher Scientific
Isopropanol	Commercial Alcohols
Isopropanol (molecular biology grade)	Sigma-Aldrich
Kanamycin	Sigma-Aldrich
L-glutamine	Sigma-Aldrich
Lipofectamine 2000	Thermo Fisher Scientific
Lipofectamine RNAiMax	Thermo Fisher Scientific
Magnesium chloride hexahydrate	EMD Chemicals
Methanol	Thermo Fisher Scientific
N,N,N',N'-tetramethylenediamine (TEMED)	Sigma-Aldrich
Nonidet P-40 (NP-40) / Igepal CA-630	Sigma-Aldrich
OptiMEM	Thermo Fisher Scientific
Paraformaldehyde	Thermo Fisher Scientific
Penicillin-streptomycin solution (100x)	Thermo Fisher Scientific
Phenol, buffer-saturated	Sigma-Aldrich
Phenol: Chloroform: Isoamyl Alcohol	Sigma-Aldrich
Plasmocin	InvivoGen
Potassium acetate	Anachemia
Potassium chloride	Becton, Dickinson & Company
Potassium hydroxide	Becton, Dickinson & Company
ProLong Gold anti-fade mounting medium	Thermo Fisher Scientific
Protein G - sepharose Fast Flow	General Electric Healthcare
Puromycin	Sigma-Aldrich
Resazurin sodium salt	Sigma-Aldrich
Skim milk powder	Carnation
Sodium arsenite	Sigma-Aldrich
Sodium Borate	Sigma-Aldrich
Sodium chloride	Thermo Fisher Scientific
Sodium Deoxycolate	
Sodium dodecyl sulphate (SDS)	Bio-Rad
Sodium hydroxide	Becton, Dickinson & Company

Table 2.1 – Continued…

Reagent	**Source**
Sodium molybdate	Acros Organics
Sodium salicylate	EM Science
Sucrose	EMD Chemicals
Tumor necrosis factor (TNFα)	Roche
TRI Reagent / TRIZol	Thermo Fisher Scientific
Tris base	EMD Chemicals
UltraHyb Oligo buffer	Thermo Fisher Scientific
UltraPure distilled water	Thermo Fisher Scientific
Urea	Sigma-Aldrich
Xylene cyanol FF	Sigma-Aldrich

Table 2.2 – Molecular size standards

Standard	**Source**
GeneRuler 1 kb DNA Ladder Plus (SM1333)	Thermo Fisher Scientific
PageRuler™ Pre-stained Protein Ladder (SM0671)	Thermo Fisher Scientific
PageRuler™ Plus Prestained Protein Ladder, 10 to 250 kDa (SM26619)	Thermo Fisher Scientific

Table 2.3 – DNA / RNA modifying enzymes

Enzyme	***Source***
Calf intestinal alkaline phosphatase	Thermo Fisher Scientific
Antartic Phosphatase	Thermo Fisher Scientific
DNase I, amplification grade	Thermo Fisher Scientific
Restriction endonucleases	Thermo Fisher Scientific and New England Biolabs
RNase A	Thermo Fisher Scientific
T4 DNA ligase	Thermo Fisher Scientific
T4 Kinase	Thermo Fisher Scientific

Table 2.4 – Detection systems, analytical instruments and software

System	***Source***
BD LSRFortessa	BD Biosystems
FACSDiva Software	BD Biosystems
FluorChem Q	Cell BioSciences
ChemiDoc™ MP System	BioRad
GeneScreen Plus membrane	PerkinElmer
Hamamatsu EMCCD (C9100-13) digital camera.	Hamamatsu Photonics
iBrowser analysis software	Thorlabs Inc
iCys software	Thorlabs Inc
ImageQuant Software	GE Health Sciences
MX3005P	Stratagene
Nitrocellulose membrane, Trans-Blot Transfer Medium (0.45 µM)	Bio-Rad
Odyssey Infrared Imaging System	LiCor
Olympus IX-81 motorized microscope	Olympus
Precisely Wallac envision 2104	PerkinElmer
Spinning disk confocal unit CSU X1	Yokogawa Electric Corporation
Ultraviolet gel transilluminator	Thermo Fisher Scientific
Image Studio Lite Ver 5.0	LiCor
Wallac Envision manager software	PerkinElmer
Volocity software	PerkinElmer

Table 2.5 – Multi-component systems

System	***Source***
Expand Long Template PCR System	Roche
Platinum Taq PCR System	Thermo Fisher Scientific
QIAEX II gel extraction kit	QIAGEN
QIAGEN plasmid maxi kit	QIAGEN
QIAprep spin miniprep kit	QIAGEN
QIAquick Gel Extraction Kit	QIAGEN
QIAquick PCR purification kit	QIAGEN
QuickChange II mutagenesis kit	Agilent

2.1.2. Commonly used buffers

Table 2.6 – Buffers and solutions

Name	***Composition***
2X Urea Mix	8 M urea, 25 mM EDTA, 0.025% xylene cyanol (XC), 0.025% bromophenol blue
5x Protein sample buffer	62.5 mM Tris-HCl (pH 6.8), 25% (v/v) glycerol, 2% (w/v) SDS, 0.01% (w/v) bromophenol blue, 5% (v/v) β-mercaptoethanol
6x DNA gel loading buffer	40% (w/v) sucrose, 0.25% (w/v) bromophenol blue, 0.25% (w/v) xylene cyanol FF
Ago2 IP buffer	50 mM Tris-HCl (pH 7.4), 100 mM NaCl, 1 mM MgOAc, 1%, TritonX-100, 20 mM sodium molybdate
Bacteria resuspension buffer	50 mM Tris-HCl (pH 8.0), 10 mM EDTA, 100 µg/mL RNaseA
Cytomix	25 mM HEPES (pH 7.6), 10 mM KH2PO4, 120 mM KCl, 0.15 mM CaCl2, 2 mM ethylene glycol tetraacetic acid (EGTA), 5 mM MgCl2, 5 mM adenosine triphosphate (ATP), and 2 mM L-glutamine
Elution Buffer (EB)	10 mM Tris-Cl, pH 8.5
LB media	1% (w/v) Bacto-tryptone, 0.5% (w/v) Bacto-yeast extract, 0.5% (w/v) NaCl, 0.1% (v/v) 1 M NaOH
Neutralization buffer	3.0 M Potassium acetate (pH 5.5)
Oligo binding buffer	25 mM HEPES-KOH (pH 7.4), 50 mM KCl, 75 mM KOAc, 2 mM MgCl2, 1 mM DTT
PBS-T	137 mM NaCl, 2.7 mM KCl, 8 mM Na2HPO4 (pH 7.4), 0.05% (v/v) Tween-20
Phosphate-buffered saline (PBS)	137 mM NaCl, 2.7 mM KCl, 8 mM Na2HPO4 (pH 7.4)
RIPA	50 mM Tris-HCl (pH 7.4), 150mM NaCl, 1% TritonX-100, 0.5% Na Deoxycolate, 0.1% SDS, 1X CPI (Protease Inhibitor), 1X HALT (Phosphatase inhibitor)
SDS-PAGE running buffer	250 mM glycine, 0.1% (w/v) SDS, 100 mM Tris base (pH 8.3)
TAE	40 mM Tris-Acetate, 1 mM EDTA (pH 8.0)
TBS-T	137 mM NaCl, 2.7 mM KCl, 24 mM Tris-HCl (pH 7.4), 0.05% (v/v) Tween-20
Tris-buffered saline (TBS)	137 mM NaCl, 2.7 mM KCl, 24 mM Tris-HCl (pH 7.4)
Western blot transfer buffer	200 mM glycine, 25 mM Tris base (pH 8.3), 20% (v/v) methanol, 0.1% (w/v) SDS

2.1.3. Oligonucleotides

Table 2.7 – Oligonucleotides

Name	***Engineered site***	***Sequence***	***Usage (Section)***
miR21-Cassette	*EcoR1*	*5'- AAT TCT CAA CAT CAG TCT GAT AAG CTA GA; 5' AAT TCT AGC TTA TCA GAC TGA TGT TGA G*	*2.2.2.2.1*
Slicer-Cassette	*EcoR1*	*5'- AAT TCG TCG TTA ATC GCG TAT AAT ACA GAT CTG; 5'-AAT TCA GAT CTG TAT TAT ACG CGA TTA ACG ACG*	*2.2.2.2.2*
NonSlicer-Cassette	*EcoR1*	*5'- AAT TCC GTA TTA TAT TGA TTA ACG AAA CGG GAC GGC GCA CGC GCG TAT TAT ATT GAT TAA CGA AAC GGG ACG GCG CAC GCG CGT ATT ATA TTG ATT AAC GGG GCC AGA TCT G; 5'-AAT TCA GAT CTG GCC CCG TTA ATC AAT ATA ATA CGC GCG TGC GCC GTC CCG TTT CGT TAA TCA ATA TAA TAC GCG CGT GCG CCG TCC CGT TTC GTT AAT CAA TAT AAT ACG G*	*2.2.2.2.3*
BFP2-Nhe1-F	*Nhe1*	*5'-TAT AGC TAG CGC TAC CGG ACT CAG ATC CAT CGC CAC CAT GGT GTC TAA GGG CGA AGA GCT G*	*2.2.2.3*
BFP2-Not1-R	*Not1*	*5'-TAT AGC GGC CGC ATT AAT TAA GCT TGT GCC CCA GTT TG*	*2.2.2.3*
Bp-FGFR2b-Not1-F	*Not1*	*5'-GAG CGG CCG CAT GGG ATT AAC GTC CAC ATG G*	*2.2.2.4*
Bp-FGFR2b-Xba1-R	*Xba1*	*5'-GGC ACG CAG TCT AGA TGT TTT AAC ACT GCC GTT TAT GTG*	*2.2.2.4*
Bp-FGFR3c-BamH1-F	*BamH1*	*5'-GAC GGA TCC ATG GGC GCC CCT G*	*2.2.2.5*
Bp-FGFR3c-Not1-R	*Not1*	*5'-AGC GGC CGC TCA CGT CCG CGA G*	*2.2.2.5*

2.1.4. Mutagenesis Primers

Table 2.8 – Mutagenesis Primers

Mutant	***Forward primer***	***Reverse primer***
pcDNA4/TO/myc-Ago2 S253A	*5' CAA AAA CCT CTG ACA GAT GCC CAA CGC GTA AAG TTT ACC AAA GAA 3'*	*5' TTC TTT GGT AAA CTT TAC GCG TTG GGC ATC TGT CAG AGG TTT TTG 3'*
pcDNA4/TO/myc-Ago2 S253D	*5' CAA AAA CCT CTG ACA GAT GAC CAA CGC GTA AAG TTT ACC AAA GAA 3'*	*5' TTC TTT GGT AAA CTT TAC GCG TTG GTC ATC TGT CAG AGG TTT TTG3'*
pcDNA4/TO/myc-Ago2 T303A	*5' C CCG CTG CAG CAG GAG AGT GGC CAG GCG GTG GAG TGC GCG GTG GCC CAG TAT TTC AAG 3'*	*5' CTT GAA ATA CTG GGC CAC CGC GCA CTC CAC CGC CTG GCC ACT CTC CTG CTG CAG CGG G 3'*
pcDNA4/TO/myc-Ago2 T303D	*5' C CCG CTG CAG CAG GAG AGT GGC CAG GAT GTG GAG TGC GCG GTG GCC CAG TAT TTC AAG 3'*	*5' CTT GAA ATA CTG GGC CAC CGC GCA CTC CAC ATC CTG GCC ACT CTC CTG CTG CAG CGG G 3'*
pcDNA4/TO/myc-Ago2 T307A	*5' C CCG CTG CAG CAG GAG AGT GGC CAG ACG GTG GAG TGC GCG GTG GCC CAG TAT TTC AAG 3'*	*5' CTT GAA ATA CTG GGC CAC CGC GCA CTC CAC CGT CTG GCC ACT CTC CTG CTG CAG CGG G 3'*
pcDNA4/TO/myc-Ago2 T307D	*5' C CCG CTG CAG CAG GAG AGT GGC CAG ACG GTG GAG TGC GAT GTG GCC CAG TAT TTC AAG 3'*	*5' CTT GAA ATA CTG GGC CAC ATC GCA CTC CAC CGT CTG GCC ACT CTC CTG CTG CAG CGG G 3'*
pcDNA4/TO/myc-Ago2 S387A	*5' ATT AGC AAA TTG ATG CGA TCG GCC GCT TTC AAC ACA GAT CCA TAC 3'*	*5' GTA TGG ATC TGT GTT GAA AGC GGC CGA TCG CAT CAA TTT GCT AAT 3'*
pcDNA4/TO/myc-Ago2 S387D	*5' ATT AGC AAA TTG ATG CGA TCG GCC GAT TTC AAC ACA GAT CCA TAC 3'*	*5' GTA TGG ATC TGT GTT GAA ATC GGC CGA TCG CAT CAA TTT GCT AAT 3'*
pcDNA4/TO/myc-Ago2 Y393F	*5' CGA AGT GCA AGT TTC AAC ACG GAT CCA TTC GTC CGT GAA TTT GGA ATC 3'*	*5' GAT TCC AAA TTC ACG GAC GAA TGG ATC CGT GTT GAA ACT TGC ACT TCG 3'*
pcDNA4/TO/myc-Ago2 Y393E	*5' CGA AGT GCA AGT TTC AAC ACG GAT CCA GAG GTC CGT GAA TTT GGA ATC 3'*	*5' GAT TCC AAA TTC ACG GAC CTC TGG ATC CGT GTT GAA ACT TGC ACT TCG 3'*
pcDNA4/TO/myc-Ago2 Y529F	*5' ATC CTG CCC GGC AAG ACG CCC GTG TTC GCC GAG GTC AAA CGC GTG GGA GAC ACG GTG CTG GGG 3'*	*5' CCC CAG CAC CGT GTC TCC CAC GCG TTT GAC CTC GGC GAA CAC GGG CGT CTT GCC GGG CAG GAT 3'*
pcDNA4/TO/myc-Ago2 Y529E	*5' ATC CTG CCC GGC AAG ACG CCC GTG GAA GCC GAG GTC AAA CGC GTG GGA GAC ACG GTG CTG GGG 3'*	*5' CCC CAG CAC CGT GTC TCC CAC GCG TTT GAC CTC GGC TTC CAC GGG CGT CTT GCC GGG CAG GAT 3'*
pcDNA4/TO/myc-Ago2 S798A	*5' CGC TGC ACA CGC TCC GTG GCC ATC CCG GCG CCA GCA TAC TAC GCT C 3'*	*5' G AGC GTA GTA TGC TGG CGC CGG GAT GGC CAC GGA GCG TGT GCA GCG 3'*

Table 2.8 – *Continued…*

Mutant	***Forward primer***	***Reverse primer***

pcDNA4/TO/myc-Ago2 S798D	*5' CGC TGC ACA CGC TCC GTG GAC ATC CCG GCG CCA GCA TAC TAC GCT C 3'*	*5' G AGC GTA GTA TGC TGG CGC CGG GAT GTC CAC GGA GCG TGT GCA GCG 3'*
pcDNA4/TO/myc-Ago2 RARA	*5' CTG ACA GAT TCC CAA AGG GCC CGG GCT ACC AAA GAA ATT AAA GGT C 3'*	*5' GAC CTT TAA TTT CTT TGG TAG CCC GGG CCC TTT GGG AAT CTG TCA G 3'*

2.1.5. siRNAs

Table 2.9 – siRNAs

siRNA	***Source***
Casp8 siRNA	Thermo Fisher Scientific
Ago2 siRNA	Thermo Fisher Scientific
Silencer® Select Negative Control No. 1 siRNA	Thermo Fisher Scientific
FGFR3 siRNA	Thermo Fisher Scientific
Ambion Silencer Human Kinase siRNA Library	Thermo Fisher Scientific
Ambion Silencer Human Phosphatase siRNA Library	Thermo Fisher Scientific
Dicer Substrate NC-1	IDT DNA

2.1.6 Plasmid vectors

Table 2.10 – Plasmid vectors

Plasmid	***Source***
pcDNA 3.1/ pD2eGFP	C.S Sullivan (University of Texas)
pcDNA 3.1/ pD2eGFP-mir21	Constructed in this study
pcDNA 3.1/ pD2eGFP-NonSlicer	Constructed in this study
pcDNA 3.1/ pD2eGFP-Slicer	Constructed in this study
pcDNA 3/ myc-Ago2-H634P	Greg Hannon (Cold Spring Harbor)
pcDNA 4/TO/ Myc-Ago2 S253A	Constructed in this study
pcDNA 4/TO/ Myc-Ago2 S253D	Constructed in this study
pcDNA 4/TO/ Myc-Ago2 S387A	Constructed in this study
pcDNA 4/TO/ Myc-Ago2 S387D	Constructed in this study
pcDNA 4/TO/ Myc-Ago2 S798A	Constructed in this study

Table 2.10 – Continued…

Plasmid	***Source***
pcDNA 4/TO/ Myc-Ago2 S798D	Constructed in this study

pcDNA 4/TO/ Myc-Ago2 T303A	Constructed in this study
pcDNA 4/TO/ Myc-Ago2 T303D	Constructed in this study
pcDNA 4/TO/ Myc-Ago2 T303D	Constructed in this study
pcDNA 4/TO/ Myc-Ago2 T307A	Constructed in this study
pcDNA 4/TO/ Myc-Ago2 T307D	Constructed in this study
pcDNA 4/TO/ Myc-Ago2 WT	J. M Pare (University of Alberta)
pcDNA 4/TO/ Myc-Ago2 Y393E	Constructed in this study
pcDNA 4/TO/ Myc-Ago2 Y393F	Constructed in this study
pcDNA 4/TO/ Myc-Ago2 Y529E	Constructed in this study
pcDNA 4/TO/ Myc-Ago2 Y529F	Constructed in this study
pcDNA3/ myc-Ago2-PAZ9	Greg Hannon (Cold Spring Harbor)
pBFP2	Constructed in this study
pBFP2-ACTA	Dr Paul Melançon (University of Alberta)
pBFP2-PP1CA	Constructed in this study
pBp-FGFR2b-WT	Addgene plasmid#45698
pBp-FGFR3c-WT	Addgene plasmid#45711
pcDNA 5/TO	Thermo Fisher Scientific
pcDNA 5/TO/ FGFR2	Constructed in this study
pcDNA 5/TO/ FGFR3	Constructed in this study
pDsRed / TIA-1	J. M Pare (University of Alberta)
pDsRed-C1-Monomer	Clontech
pEYFP(C1)-PP1CA	Addgene plasmid#44231

2.1.7 Antibodies

Table 2.11 – Primary antibodies

Antibody	***Dilution***	***Application****	***Source***
Rabbit anti-Ago2 (2D4, PAZ)	1:1,000	WB	Hobman lab
Goat anti-hp90 (sc-1055)	1:1,000	WB	Santa Cruz Biotechnology
Human anti-GW182	1:1,000	WB	Dr. M.J. Fritzler, University of Calgary
Mouse anti-Actin (ab8227)	1:1,000	WB	Abcam
Mouse anti-Dicer (ab14601)	1:1,000	WB	Abcam
Mouse anti-FGFR2 (ab58201)	1:1,000	WB	Abcam
Rabbit anti-FGFR3 (ab137084)	1:1,000	WB	Abcam

Table 2.11 – Continued…

Antibody	***Dilution***	***Application****	***Source***

Rabbit anti-GFP	1:20,000 / 1:1,000	WB / IP	Dr. L.G. Berthiaume, University of Alberta
Rat anti-Ago2	1:100	WB	Dr. G.Meister, Max Planck Institute of Biochemistry
Human anti-GW182	1:1,000	IIF	Dr. M.J. Fritzler, University of Calgary
Rabbit anti-Dcp1 (ab47811)	1:500	IIF	Abcam
Goat anti-TIA (sc-1751)	1:200	IIF	Santa Cruz Biotechnology
Mouse anti-myc (9E10)	1:1,000	IP	Hobman lab

*-WB:western blot; IIF:indirect immunofluorescence; IP:immunoprecipitation

Table 2.12 – Secondary antibodies

Antibody::Conjugate	***Dilution***	***Application****	***Source (product ID)***
Goat anti-rabbit IgG::Alexa750	1:10,000	WB	Thermo Fisher Scientific (A21039)
Donkey anti-mouse IgG::Alexa680	1:10,000	WB	Thermo Fisher Scientific (A10038)
Donkey anti-goat IgG::Alexa680	1:10,000	WB	Thermo Fisher Scientific (A21084)
Donkey anti-rabbit IgG::IR-Dye 800	1:10,000	WB	Li-Cor Biosciences (P/N 925-32213)
Donkey anti-rabbit IgG::Alexa647	1:1,000	IIF	Thermo Fisher Scientific (A31573)
Goat anti-rabbit IgG::Alexa594	1:1,000	IIF	Thermo Fisher Scientific (A11037)
Donkey anti-mouse IgG::Alexa488	1:1,000	IIF	Thermo Fisher Scientific (A21202)
Donkey anti-rabbit IgG::Alexa488	1:1,000	IIF	Thermo Fisher Scientific (A21206)
Donkey anti-human IgG::TexasRed	1:1,000	IIF	Jackson ImmunoResearch Laboratories
Chicken anti-goat IgG::Alexa647	1:1,000	IIF	Thermo Fisher Scientific (A21469)
Chicken anti-goat IgG::Alexa594	1:1,000	IIF	Thermo Fisher Scientific (A21468)
Donkey anti-mouse IgG::Alexa 647	1:1,000	IIF	Thermo Fisher Scientific (A31571)
Chicken anti-mouse IgG::Alexa594	1:1,000	IIF	Thermo Fisher Scientific (A21201)

Table 2.12 – Continued…

Antibody	***Dilution***	***Application****	***Source***

Donkey anti-goat IgG::Alexa 647	1:1,000	IIF	Thermo Fisher Scientific (A21469)
Goat anti-human IgG::Alexa647	1:1,000	IIF	Thermo Fisher Scientific (A21445)

*-WB:western blot; IIF:indirect immunofluorescence; IP:immunoprecipitation

2.1.8. Cell lines

Table 2.13 – Mammalian cell culture lines

Cell line	***Source***
HeLa	ATCC
HeLa TNF sensitive	Dr. Edan Foley, University of Alberta
MEF Ago2 -/-	Dr. Greg Hannon, Cold Spring harbor
HEK293T	ATCC
SKBR3	Dr. Ing Swie Goping, University of Alberta

2.2 Methods

2.2.1 Molecular Biology

2.2.1.1 Isolation of plasmid DNA from Escherichia coli

Small scale plasmid DNA extractions were carried out using QIAprep spin miniprep kit (Table 2.5) following manufacturer's recommendations. Preparation procedures were performed on plasmid-transformed DH5α *E. coli (Genotype: F^- Φ80lacZΔM15 Δ(lacZYA-argF) U169 recA1 endA1 hsdR17(r_k^-, m_k^+) phoA supE44 thi-1 gyrA96 relA1 λ^-)*, grown overnight in 3-5 mL cultures of LB (Table 2.6).

Plasmids used to transfect mammalian cell lines were extracted from 200 – 300 mL overnight cultures using QIAGEN plasmid Maxi kits (Table 2.5) following manufacturer's recommendations.

2.2.1.2 Restriction endonuclease digestion

Reactions were typically performed in a volume of 10 - 20 µL containing 0.5 - 5 µg of plasmid DNA and 1 - 10 U of restriction endonuclease and appropriate reaction buffer (Table 2.3).

2.2.1.3 Dephosphorylation of linearized vectors

To reduce occurrences of self-ligation following restriction digest, vector DNA was dephosphorylated using calf intestinal alkaline phosphatase or Antarctic Phosphatase (Table 2.3) per manufacturer's recommendations.

2.2.1.4 Polymerase chain reaction

DNA was amplified using the Expand Long Template PCR system (Table 2.5) or Platinum *Taq* (Table 2.5). A typically reaction contained 10 – 50 ng of plasmid DNA (linearized by restriction endonuclease digestion), 500 nM dNTPs, 10 µM of each primer and 1 – 5 U of the polymerase. Reactions were performed using a TC-312 thermocycler (Techne).

2.2.1.5 Agarose gel electrophoresis

Ultrapure agarose (Table 2.1) was dissolved in TAE via heating (Table 2.6). Before pouring the gel [1% - 2% (w/v)] into the casting tray, ethidium bromide (Table 2.1) was added to a final concentration of 0.5 µg/mL. The gel was submerged in TAE and the DNA samples were combined with 6x DNA gel loading buffer (Table 2.6) and applied to the gel. Gels were electrophoretically resolved typically using 100 -150 V. Bands of DNA were visualized using an Ultraviolet transilluminator (Table 2.4) or images were captured using a ChemiDoc™ MP System (Table 2.4).

2.2.1.6 Purification of DNA fragments

To purify DNA products following completion of polymerase chain reaction or restriction digest, a QIAquick PCR purification kit (Table 2.5) was used to remove proteins and salts, and small (<100nt) cleavage products that were to be excluded from subsequent ligations. For purification of DNA fragments larger than 100nt, which were not compatible for exclusion by the above kit, agarose gel electrophoresis was performed. Followed by the excision of the bands of interest with a clean razor blade, and extraction

of the fragment DNA from the gel using the QIAquick Gel Extraction Kit or QIAEX II gel extraction kit (Table 2.5).

2.2.1.7 Ligation of DNA

Restriction digested DNA fragments and vectors were mixed in molar ratios ranging from 2:1 – 6:1, typically using a mass of 25 - 50 ng of vector DNA, 1nM of rATP and 2 – 5 U of T4 DNA ligase (Table 2.3). Reactions were carried out in 15 - 20 uL volume and ligations were performed for at least one hour at room temperature (for cohesive end ligations) or overnight at 16 ^{o}C (for blunt-end ligations).

2.2.1.8 Site-directed mutagenesis

To perform single or multiple nucleotide mutations, the QuickChange™ site-directed mutagenesis kit (Table 2.5) was used according to manufacturer's recommendations. Mutagenic primers (Table 2.8) were purchased from Integrated DNA Technologies (IDT). Mutations in the cDNAs were confirmed by Sanger sequencing using The Applied Genomics Core (TAGC) at the Department of Medical Genetics, University of Alberta.

2.2.1.9 Chemical transformation of Escherichia coli

Chemically competent OneShot ChemicalCompetent (Thermo Scientific), XL10Gold Ultracompetent cells (Genotype: TetrΔ (*mcrA*)*183* Δ(*mcrCB-hsdSMR-mrr*)*173 endA1 supE44 thi-1 recA1 gyrA96 relA1* lac Hte. [*F' proAB* lacIqZΔM15 Tn10 (*Tetr*) *Amy* Camr]) (Agilent) and SubCloning Efficiency DH5α *(Genotype: F^{-} Φ80lacZΔM15 Δ(lacZYA-argF) U169 recA1 endA1 hsdR17(r_k^{-}, m_k^{+}) phoA supE44 thi-1 gyrA96 relA1 λ^{-})*

competent (Thermo Scientific) strains were used during the course of this work. In all cases, cells were transformed and subsequently cultured following the manufacturer's recommendations.

2.2.1.10 Electro transformation of Escherichia coli

E. coli electro-competent cells ElectroMAX™ DH10B™ (Genotype: F$^-$*mcr*A Δ(*mrr-hsd*RMS-*mcr*BC) Φ80*lac*ZΔM15 Δ*lac*X74 *rec*A1 *end*A1 *ara*D139Δ(*ara*, *leu*)7697 *gal*U *gal*K λ$^-$*rps*L *nup*G) were electroporated using 1 mm electroporation cuvettes (Table 2.1) according manufacturer's instructions.

2.2.2 Construction of recombinant plasmids

Information regarding primers and DNA duplexes used for the construction of the plasmids described below can be found in Table 2.7. All plasmids and their sources are listed in Table 2.10. The sequence of each plasmid that was constructed using PCR was verified by DNA sequencing at The Applied Genomics Core (TAGC) at the Department of Medical Genetics, University of Alberta.

2.2.2.1 pcDNA4/TO / myc-hAgo2 Phospho-mutants

A total of 14 Ago2 phospho-mutants were created from the myc-tagged Ago2 WT plasmid (pcDNA 4/TO/ Myc-Ago2 WT) using the QuickChange™ site-directed mutagenesis kit (Table 2.5) using primers described in Table 2.8.

Table 2.14 Ago2 phosphomutants

Phospho-Residue	Non-phosphorylatable substitution	Phospho-mimetic Substitution
Ago2-S253	Ago2-S253**A**	Ago2-S253**D**
Ago2-T303	Ago2-T303**A**	Ago2-T303**D**
Ago2-T307	Ago2-T307**A**	Ago2-T307**D**
Ago2-S387	Ago2-S387**A**	Ago2-S387**D**
Ago2-Y393	Ago2-Y393**F**	Ago2-Y393**E**
Ago2-Y529	Ago2-Y529**F**	Ago2-Y529**E**
Ago2-S798	Ago2-S798**A**	Ago2-S798**D**

2.2.2.2 pcDNA 3.1/ pD2eGFP RNAi reporters

All the dsGFP RNAi reporters used in this study were constructed from a plasmid encoding the enhanced Green Fluorescent Protein (eGFP) destabilized with the mouse ornithine decarboxylase proline-glutamate-serine-threonine (PEST) signal (pcDNA 3.1/ pD2eGFP) (*Sullivan and Ganem, 2005)*.

2.2.2.2.1 pcDNA 3.1/ pD2eGFP-miR21

pcDNA 3.1/ pD2eGFP-mir21 was constructed by ligating the miR21-Cassette cDNA (Table 2.7) into the EcoR1 site of pcDNA3.1-pD2eGFP.

2.2.2.2.2 pcDNA 3.1/ pD2eGFP-Slicer

pcDNA 3.1/ pD2eGFP-Slicer was constructed by ligating the Slicer-Cassette cDNA (Table 2.7) into the EcoR1 site of pcDNA3.1-pD2eGFP.

2.2.2.2.3 pcDNA 3.1/ pD2eGFP-NonSlicer

pcDNA 3.1/ pD2eGFP-NonSlicer was constructed by ligating the NonSlicer-Cassette cDNA (Table 2.7) into the EcoR1 site of pcDNA3.1-pD2eGFP.

2.2.2.3 pEBFP-N1

The BFP2 cDNA which encodes the Blue Fluorescent Protein (BFP), was amplified by PCR from using pBFP2-ACTA as the template together with the primers BFP2-Nhe1-F and BFP2-Not1-R. The resulting product (764 base pairs) was digested with Nhe1 and Not1 and then ligaged into the plasmid pEGP-N1, which had been digested with Nhe1 and Not1 to release the eGFP cassette.

2.2.2.4 pcDNA 5/TO/ FGFR2

The FGFR2 cDNA was amplified by PCR using the plasmid template pBp-FGFR2b-WT (Table 2.10) with the forward primer Bp-FGFR2b-Not1-F and the reverse primer Bp-FGFR2b-Xba1-R (Table 2.7). The resulting PCR fragment (2473 base pairs) was digested with Not1 and Xba1 before ligation into the corresponding sites in pcDNA 5TO.

2.2.2.5 pcDNA 5/TO/ FGFR3

The FGFR3 cDNA was amplified by PCR using the plasmid template pBp-FGFR3c-WT with the forward primer Bp-FGFR3c-BamH1-F and the reverse primer Bp-FGFR3c-Not1-R. The resulting PCR fragment (2418 base pairs) FGFR3 was digested with Not1 and BamHI before ligation into the corresponding sites in pcDNA 5TO.

2.2.2.5 pBFP/ PP1CA

The PP1CA cDNA was released from pEYFP(C1)-PP1alpha (Table 2.10) by digestion with EcoR1 and Sal2 and then ligated into the corresponding sites in pEBFP-N1 (Table 2.10).

2.2.3 Culture and transfection of mammalian cell lines

2.2.3.1 Cell line maintenance

HeLa, HEK293T, SKBR3 and MEF Ago2 -/- cells were cultured in Dulbecco's Modified Eagle Medium (DMEM) containing 10% heat-inactivated fetal bovine serum (FBS), 10 mM 4-(2-hydroxyethyl)-1-piperazineethanesulfonic acid (HEPES), and 2.5 µg/mL Plasmocin (Table 2.1) at 37°C in a humidified atmosphere 5% CO_2 atmosphere.

2.2.3.2 Transient transfection of cell lines

HeLa, HEK293T and SKBR3 cells were transiently transfected with plasmid DNA using Lipofectamine 2000 (Table 2.1). Cells were seeded 24 hours before transfection. HeLa cells were seeded in six wells plates at a density of $2x10^5$ cells/well. HEK293T and SKBR3 cells were seeded in 24 wells plates at a density of $2.5x10^5$ cells/well. HeLa cells were transfected with 1 µg of plasmid DNA and 2.5 µL of Lipofectamine 2000 in 1 mL of OptiMEM per six well plate well. HEK293T and SKBR3 cells were transfected with 0.5 µg of plasmid DNA and 1.25 µL of Lipofectamine 2000 in 0.5 mL of OptiMEM per 24 well plate well, respectively. Cells were incubated with the DNA-lipocomplexes for 16 hours.

The supernatants were then removed and the cells were rinsed with PBS before addition of complete culture media to the wells. To achieve a high degree of double transfection in the cells, plasmids were transfected in a 1:2 molar ratio of BFP and GFP respectively. Using this ratio more than 99% of the cells that were BFP-positive were also dsGFP-positive (data not shown).

2.2.3.3 Transient electroporation of cell lines

Electroporation was used to introduce plasmid DNA into Ago2-/- MEF cells. MEFs ($1x10^6$ cells) were resuspended in 100 µL of Cytomix (Table 2.6) and added to 2 mm cuvettes (Table 2.1) containing 2µg of DNA. Electroporation setting was 260 volts and 500 micro-Faradays. After electroporation, the cells were recovered from the cuvettes using 2 mL of complete culture media and seeded in 35 mm plates. In these experiments, delivery of BFP:dsGFP:Ago2 plasmids was achieved by electroporating those plasmids in a molar ratio of 1:4:16 respectively. Using this molar ratio, more than 99% of the BFP-positive cells also contained plasmids encoding dsGFP and Ago2 (data not shown).

2.2.4 Microscopy

2.2.4.1 Indirect Immunofluorescence

HeLa cells were cultured on glass coverslips and processed for indirect immunofluorescence microscopy post-transfection at times indicated. Where indicated, stress granules were induced by treating the cells with sodium arsenite at a final concentration of 500 µM in the culture media for 45 minutes before fixation. Cells on coverslips were first washed with PBS and then fixed with 2% (w/v) paraformaldehyde for

10 minutes. Fixed cells were rinsed with PBS two more times prior to permeabilization with PBS containing 0.2% (v/v) TritonX-100 for 3 minutes. Following permeabilization, coverslips were again rinsed two times with PBS and then blocked for 30 min in PBS containing 5% skim milk powder (Table 2.6). Primary antibody (diluted as indicated in Table 2.11) incubations were performed in PBS containing 5% skim milk powder for at least 2 hours at room temperature or overnight at 4^{o}C. Following primary antibody incubation, coverslips were washed three times for 10 minutes in PBS while rocking. Secondary antibody (Table 2.12) incubations were performed in PBS for 1 hour at room temperature followed by three additional PBS washes for a total of 30 min, while rocking. Coverslips were then incubated for 10 minutes in PBS containing 4′,6-diamidino-2-phenylindole (DAPI) (Table 2.1) at 1 µg/mL followed by mounting with ProLong Gold (Table 2.1). Samples were examined at the Faculty of Medicine & Dentistry Cell Imaging Centre (http://microscopy.med.ualberta.ca) using an Olympus IX-81 motorized microscope equipped with a spinning disk confocal unit CSU X1. Images were acquired with a Hamamatsu EMCCD (C9100-13) digital camera and analyzed using Volocity software (Table 2.4).

2.2.5 Laser scanning cytometry

2.2.5.1 iBrowser high content imaging analysis

High-content quantitative imaging of Ago2 mutants expressed in HeLa cells was performed using a laser scanning cytometer system equipped with 405, 488, 561 and 640 nm lasers, iBrowser analysis software (Table 2.4) and a 40x objective (0.45 N.A.). A step

size of 0.25 μm was used to capture a composite image formed of 81 or 100 images per sample (rectangles of 9x9 or 10x10 images). Voltages were set allowing for a background pixel intensity of between 200 and 500 (arbitrary units) to limit saturation of the images. The cells were identified using the nuclear stain DAPI (Table 2.1) and the localization of myc-tagged Ago2 relative to P-bodies and stress granules was determined using object-based segmentation using iCys software (Table 2.4). Data was represented by plotting the integrated signals of myc-Ago2 integral versus that of P-bodies or stress granules. Background fluorescence levels were set by measuring the signal from cells transfected with the empty vector pcDNA-5/TO (Table 2.10). At least 500 transfected cells were analysed for each mutant or control. Paired sample t-test was used to determine the statistical significance of differences. “Statistics run” data was exported to a Microsoft Excel file format and analysed.

2.2.5.1 iBrowser segmentation

iBrowser analysis software was configured to detect cell-associated objects outside of cell nuclei (defined by DAPI staining). P-bodies were defined as objects between 0.1μM^2 and 2 μM^2, with a minimum of 2,500 arbitrary units of pixel intensity in the dcp1a channel. Stress granules were defined as objects between 5μM^2 and 20 μM^2, with a minimum of 1,500 arbitrary units of pixel intensity in the TIA channel. For each object detected (either a P-body or a stress granule) the pixel intensity of either dcp1a or TIA and Ago2 channels were recorded.

Data analyses were performed by plotting pixel intensities of either TIA or dcp1a channels against the Ago2 channel. Ago2 WT plots were used as baseline colocalization, and all Ago2 mutants were compared against Ago2 WT baseline.

2.2.6 Flow cytometry

2.2.6.1 Cell harvesting and preparation for flow cytometry

Cells were rinsed with PBS prior addition of 200 µL of 0.25% Trypsin-EDTA or Accutase (Table 2.1) for detach them from dishes. Once detached, 500 µL of PBS 5% FBS was added to the cells which were recovered by centrifugation at 1,000 x g for 3 minutes. The supernatant was discarded and the cells were resuspended in PBS containing with 1% BSA and 5 mM EDTA before analysis on a BD LSRFortessa cell analyzer equipped with FACSDiva Software (Table 2.4).

2.2.6.2 Hierarchy organization and analysis

Cells transfected with a plasmid not encoding a fluorescence protein were used to determine background fluorescence. 10,000 cells in which either BFP or DsRed fluorescence was higher than the background threshold were gated, the means for BFP and GFP as well as DsRed and GFP were recorded (No GFP threshold was used). Cell doublets were excluded from these analyses by using a forward-scatter-width-discrimination. The real GFP levels of the samples were determined by normalizing the GFP fluorescence to the BFP or DsRed fluorescence. The normalizations were calculated by dividing the mean GFP fluorescence value over the mean BFP or DsRed fluorescence values of the same sample.

2.2.7 Protein gel electrophoresis and immunoblotting

2.2.7.1 Sodium dodecyl-sulphate polyacrylamide gel electrophoresis (SDS-PAGE)

Proteins in samples were separated by gel electrophoresis, using a 5% stacking gel paired with 8% or 10% resolving gel. Stacking gels were prepared adding pre-prepared acrylamide/bis-acrylamide (29:1) to final concentration of 5% to 125 mM TrisHCl (pH 6.0) containing 0.1% ammonium persulphate and 0.1% TEMED. Resolving gels were prepared by combining pre-prepared acrylamide/bis-acrylamide (29:1) to 8% or 10% final concentration in 375 mM Tris-HCl (pH 8.8), 0.1% ammonium persulphate and 0.1% TEMED. Prior electrophoresis, protein samples were mixed with 5x protein sample buffer (Table 2.6) and then denatured at 95^{o}C for 5 minutes. Electrophoresis was performed using the Bio-Rad mini-protean III system with SDS-PAGE running buffer (Table 2.6) at 150 – 200 Volts. Following electrophoresis, the gels were prepared for immunoblot analysis as described in section 2.2.7.2.

2.2.7.2 Immunoblot analysis

After SDS-PAGE had been completed, proteins in the gels were transferred to nitrocellulose membranes (Table 2.4). Then, membranes were equilibrated in western blot transfer buffer (Table 2.6) for 5 -10 minutes at room temperature. The Mini Trans-Blot Electrophoresis transfer cell apparatus (Bio-Rad) was used for the immunoblot procedures. Protein transfer was carried out using western blot transfer buffer, pre-chilled to 4^{o}C at 140 V or 320 mA for 1 hour. After the transfer had completed, the membranes

were air-dried and then blocked in PBS (Table 2.6) containing 5% (w/v) skim milk powder for at least 20 min. The nitrocellulose membranes were incubated with primary antibodies diluted, as described in Table 2.11, in PBS containing 5% (w/v) bovine serum albumin for 1 hour at room temperature or overnight at 4^{o}C. Following incubation with primary antibodies, membranes were washed three times with PBS-T at room temperature for a total of 1 hour. Secondary antibody incubations were performed using antibodies, diluted as indicated in Table 2.12, in PBS containing 1% (w/v) skim milk powder for 30 minutes at room temperature. Finally, membranes were washed three times with PBS for a total of 30 minutes before detection as described in Section 2.2.7.3.

2.2.7.3 Detection of fluorophore-conjugated secondary antibodies and analysis

Membranes were placed face-down on the scanner bed of an Odyssey Infrared Imaging system (Table 2.4) and then scanned at 84 µm resolution on a quality setting of “High”. Image annotations and analysis were done using the Image Studio Lite Software (Table 2.4).

2.2.8 Biochemical analysis of protein-protein interactions

2.2.8.1 Crosslinking myc antibody to sepharose beads

Protein G-Sepharose 4 fast flow beads were washed twice with PBS, then incubated at room temperature for an hour with 9E10 anti-myc antibody (5mg/ml of beads), followed by washing once with ten volumes of 100 mM sodium borate (Table 2.1).

The crosslinking reagent dimethylpimelimidate (20 mM) was added to the beads for 30 minutes at room temperature, followed by two washes with ten volumes of 200 mM ethanolamine (Table 2.1). Beads were then incubated at room temperature with 200 mM ethanolamine (Table 2.1) for 2 hours before washing three times with ten volumes of PBS. Finally, beads were stored as a 50% slurry in PBS at 4°C until use in immunoprecipitation experiments.

2.2.8.2 Co-Immunoprecipitation of Ago2 interacting proteins

Dishes (100 mm) of HeLa cells transiently expressing myc-Ago2 were lysed in Ago2 IP buffer (Table 2.6) supplemented with Complete™ Protease Inhibitor (Roche) (Table 2.1) after which lysates were cleared via centrifugation at 14,000 x *g* for 10 minutes at 4°C. Immunoprecipitation of clarified lysates was performed with 15-20 µL of protein G-sepharose beads crosslinked to anti-myc antibody (Section 2.2.8.1). Immunoprecipitations were performed for 1 hour at 4°C with rotation after which the beads were washed one time with Ago2 IP buffer before boiling in Protein sample buffer and subjected to SDS-PAGE and immunoblot analysis (Section 2.2.7.1 and 2.2.7.2).

2.2.9 Biochemical analysis of protein-RNA interactions

2.2.9.1 Immunoprecipitation of myc-Ago2 and detection of associated miRNAs

Dishes (100 mm) of HeLa cells transiently transfected for 24 hours with plasmids encoding myc-Ago2 proteins were lysed using RIPA buffer (Table 2.6) or Ago2 IP buffer supplemented with Complete™ Protease Inhibitors. Lysates were clarified via

centrifugation at 15,000 x *g* for 10 minutes at 4°C. Immunoprecipitation of clarified lysates was performed with 15-20 µL of protein G-sepharose beads crosslinked to anti-myc antibody (Section 2.2.8.1) for 1 hour at 4°C with rotation. Beads were collected via centrifugation at 500 x *g* for 3 minutes at 4°C and washed once in RIPA buffer. Samples then were harvested in 500 µL of TRI Reagent for RNA extraction (Section 2.2.10.1).

2.2.10 RNA techniques

2.2.10.1 RNA isolation

Total RNA, including small RNA species such as miRNAs, was isolated from samples using TRI Reagent (Thermo Fisher Scientific) (Table 2.1) according to the manufaturer's recommendations.

2.2.10.2 Northern blot detection of miRNAs

Total RNA was resolved on 15% acrylamide gels (19:1 acrylamide/bisacrylamide) containing 8M Urea before transfer to GeneScreen Plus membranes (PerkinElmer). The membranes were probed in UltraHyb Oligo buffer at 42°C containing 5'-[^{32}P]-end-labeled DNA oligonucleotides with exact complementarity to the mature miRNA sequences. U6 RNA was detected with a radioactive probe as a loading control. The levels of miRNAs were quantified using ImageQuant software (Table 2.4).

2.2.10.2.1 DNA oligonucleotides 5'-[^{32}P]-end-labeled labeling

DNA oligonucleotides perfectly complementary to mature miRNAs were 5' end labeled using γ-^{32}P ATP as a substrate with T4 kinase (Thermo Fisher Scientific) following manufacturer recommendations.

2.2.10.3 Analysis of RNA integrity

The total RNA samples prepared as in section 2.2.10.1 were analyzed using a NanoDrop 2000c spectrophotometer (Thermo Fisher Scientific). Samples with A260/A280 and A260/A230 ratios greater than 1.8 were resolved by 15% acrylamide gels (19:1 acrylamide/bisacrylamide) containing 8M Urea. The gel was subsequently stained using ethidium bromide in PBS to a final concentration of 5 µg/mL for at least 10 minutes at room temperature with rocking. After staining the gel was imaged using a ChemiDoc™ MP System (Table 2.4) imaging system. The presence of discrete ribosomal RNA bands indicated RNA of high quality.

2.2.11 siRNA knockdown genome-wide screens

2.2.11.1 siRNA libraries

siRNA libraries (Table 2.9) for all known human kinase and phosphatase genes were acquired. These libraries contained a pool of five siRNAs targeting each known kinase or phosphatase in the human genome.

2.2.11.2 Genome wide screen of kinases and phosphatases involved in RNAi.

siRNA libraries and siRNAs used for the RNAi screens and validation respectively are listed in Table 2.9. Cell seeding, transfection and treatment was performed using the Perkin Elmer JANUS^{TM}, Automated liquid handling system. HeLa cells, sensitive to Tumor Necrosis Factor (TNF) and cycloheximide (CHX) (Table 2.1) treatment, were seeded at $1x10^4$ per well in 96 wells plates Greiner (Cell star, Cat # 655180). Cells were reverse-transfected in quadruplicate using Dharmafect1 (Table 2.1) transfection reagent with the siRNA kinase library "Ambion Silencer Human Kinase siRNA Library" or the siRNA phosphatase library "Ambion Silencer Human Phosphatase siRNA Library" and Caspase 8 siRNAs. Caspase 8 siRNAs were cotransfected with *Silencer*® Select Negative Control No. 1 siRNA or Argonaute2 siRNA as negative or positive control respectively. After 72 h, two of the quadruplicates were treated with fresh culture media or media containing 10 ng/mL TNF and 5 µg/mL *CHX* (Table 2.1). Thirteen and one half hours later, Resazurin sodium salt (Sigma-Aldrich) (Table 2.1) was added to a final concentration of 44 µM. Cell viability was assessed using a photometer plate reader (Perkin Elmer Precisely Wallac envision 2104 multilabel reader) (Table 2.4) at 544 nM excitation and 590 nM Emission. The data were acquired using the software Wallac Envision manager (Table 2.4). Death indexes (DI) were calculated as the signal ratio of cells not treated with TNF/CHX divided by cells treated with TNF/CHX.

To calculate the variability of the DI results, it was assumed that the variability between repeats follows a normal distribution. Therefore, to determine a 95% confidence interval of the screen duplicate, the upper and lower limits of the DI confidence interval were calculated using the formula $L= \overline{x} \pm 1.96*(SE)$: where L is the limit, $\overline{x}$ is the mean of

the DI and SE is the standard error of the mean. If the total span of the DI confidence interval of a sample did not include 1 (which is the value of the control sample) the sample was recorded as statistically different from the control. Conversely, if the DI confidence interval of a sample included 1, then the sample was considered as not having a statistically significant effect.

Chapter 3

Phosphorylation of Ago2 at Serine-798 alters its spatial localization but has minimal effect on RNAi

A version of this chapter was previously published in:

"LOPEZ-OROZCO J., PARE J.M., HOLME A.L., CHAULK S.G., FAHLMAN R.P., and HOBMAN T.C. (2015) Functional analyses of phosphorylation events in human Argonaute 2. *RNA* **21**:1–9"

3.1 Rationale

RNAi is a conserved mechanism for regulation of gene expression that controls >50% of all mammalian genes (Friedman et al. 2009). Therefore, RNAi components must be highly regulated. At the core of the RNAi machinery are Ago proteins. One effective mechanism for regulating RNAi activity is through post-translational modification of Ago proteins. In humans, the Ago protein subfamily consists of four members, of which hAgo2 is the only member than can cleave targeted mRNAs (Liu et al. 2004b). Ago2 is also the most widely expressed and predominant Ago isoform in somatic cells (Liu et al. 2004a). Mounting evidence indicates that the activity of Ago2 is indeed extensively regulated through several post-translational modifications, including phosphorylation on several sites (Rudel et al. 2011, Horman et al. 2013, Shen et al. 2013, Zeng et al. 2008). Mass spectrometry analyses indicate that Ago2 is phosphorylated on at least seven amino acid residues (Rudel et al. 2011). Most of these phospho-residues are located within important domains of Ago proteins (Figure 3.1). Moreover, these amino acids are positionally conserved across Agos in many different organisms, particularly in mammals (Rudel et al. 2011). This strongly suggests that they play important roles in Ago protein functions.

To date, seven phosphorylation sites have been reported on human Ago2, but the functional consequences of only three of these events have been studied in any significant detail. Specifically, evidence indicates that phosphorylation of serine-387 and tyrosines-393 and -529 regulate hAgo2 activity by three different mechanisms. Phosphorylation at S-387 was reported to decrease endonucleolytic activity and increase P-Body localization. While tyrosine-393 phosphorylation partially inhibits interaction of Ago2 to Dicer and certain types of miRNAs, phosphorylation of Ago2 at tyrosine-529

blocks interaction with small RNAs (Zeng et al. 2008, Horman et al. 2013, Shen et al. 2013, Rudel et al. 2011, Mazumder et al. 2013). However, the role of phosphorylation at other sites in Ago2 has not been reported. Here, I used site-directed mutagenesis to create a panel of 14 mutants in which each known phosphoamino acid residue was converted to either a non-phosphorylatable amino acid residue or a mimic of a constitutively phosphorylated amino acid residue. Serines and threonines were substituted with alanines (non-phosphorylatable) or aspartic acid (phospho-mimetic), whereas tyrosine residues were changed to either phenylalanine (non-phosphorylatable) or glutamic acid (phospho-mimetic). I analyzed the subcellular localizations as well as endonuclease-dependent and –independent gene-silencing activities of these mutants to wild type (WT) Ago2.

Figure 3.1. Schematic representation of Ago2 domains and known phosphoamino acid residues. Ago proteins have three conserved domains. PAZ domain which binds dsRNA 2 nt overhangs characteristic of miRNAs. The MID domain anchors the 5’ end of miRNAs, and the PIWI domain gives Ago2 the RNAse H activity to cleave mRNAs with extensive base pairing to miRNAs.

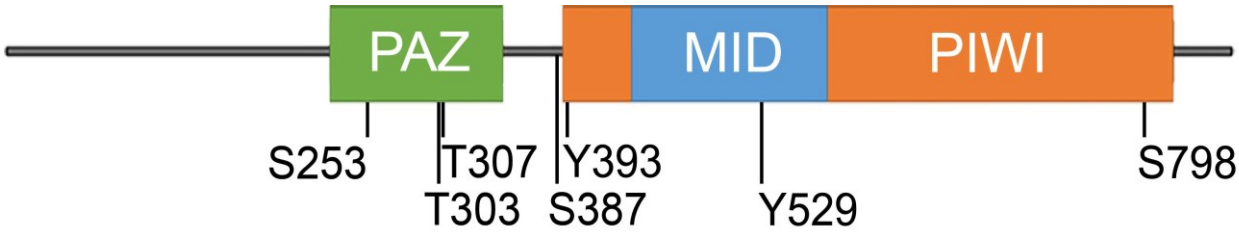

Figure 3.1

3.2 Results

3.2.1 Analysis of Ago2 phosphomutants subcellular localization

3.2.1.1 Phospho-mimetic mutation of Ago2 at Serine-798 does not co-localize to P-bodies.

Earlier reports have drawn a correlation between Ago2 activity and its interaction with cytoplasmic ribonucleoprotein granules such as P-bodies and stress granules (Eulalio et al. 2007b, Chu and Rana 2006, Eulalio et al. 2007a, Franks and Lykke-Andersen 2008). The relationship between RNAi-mediated silencing activity and localization to P-bodies is not fully understood, but targeting of Ago2 to these granules is dependent on small RNA binding (Pare, Lopez-Orozco and Hobman 2011a). This observation was consistent with the idea that Ago2 localizes to RNA granules as a consequence of its mRNA silencing activity, as opposed to a previous theory, which espoused that RNAi activity was confined to these structures. To determine whether changes in phosphorylation altered Ago2 localization, I performed a high content, unbiased, automated image analysis of the 14 phosphomutants (Table 2.14) using laser-scanning cytometry.

HeLa cells were transfected with plasmids encoding myc-tagged versions of each of the 14 phospho-mutants, WT, as well as Ago2-PAZ9 and Ago2-H634P, which served as controls. The Ago2-PAZ9 mutant has been characterized previously (Liu et al. 2005b). Because of multiple site-directed mutations the PAZ domain, cannot bind to small RNAs, and is therefore inactive in both slicer-mediated and slicer-independent silencing. Conversely, the Ago2-H634P mutant retains its small-RNA-binding and slicer-

independent silencing activities, but is catalytically inactive due to a mutation in the endonuclease domain active site (Liu et al. 2004a). As such, it is unable to cleave targeted mRNAs. At 24 hours post-transfection, cells were processed for indirect immunofluorescence microscopy using antibodies to myc and Dcp1a, a well-characterized P-body component (van Dijk et al. 2002a). At least 500 cells were analyzed for each sample (n=3) after which the mean co-localizations between Ago2 mutants and Dcp1a were plotted relative to that observed for wild type (myc-Ago2-WT, Figure 3.2A). As expected, Ago2-PAZ9 and Ago2-Y529E, two mutants that cannot bind miRNAs, did not co-localize with P-bodies. Decreased co-localization was also observed for Ago2-Y529F, an observation that is consistent with a previous report from this laboratory (Pare et al. 2011b). Interestingly, very little of the Ago2-S798D mutant was found to associate with P-bodies, whereas the Ago2 T303D mutant showed a small, yet significant, increase in co-localization with P-bodies compared to Ago2-WT (Figure 3.2A). In contrast to a previous report (Zeng et al. 2008), we found that changing serine 387 to alanine (Ago2-S387A) had no effect on localization of the Ago2 to P-bodies. This may be due to the fact that different methodologies were used to determine the extent of co-localization to P-bodies. Zeng et al. used the H1299 cell line and manually counted “FLAG-Ago2-stained” P-bodies in 40 cells. In contrast, we used HeLa cells, and relied on automated analysis software to count the number of myc-Ago2-positive P-bodies (as indicated by co-localization with co-stained Dcp1a) in a minimum of 500 cells.

The aberrant localization of Ago2-S798D (Figure 3.2B) was confirmed using confocal microscopy. HeLa cells were transfected with plasmids expressing myc-Ago2-WT, 3xmyc-Ago2-PAZ9 or myc-Ago2-S798D, endogenous Dcp1a was used as a marker

for P-bodies. Ago2-PAZ9 and Ago2-S798D were distributed diffusely throughout the cytoplasm, and did not overlap with Dcp1a-positive P-bodies (Figure 3.2B).

Figure 3.2. Localization of Ago2 phosphorylation mutants relative to P-bodies. A) HeLa cells transiently transfected with plasmids expressing WT or mutant Ago2 were processed for indirect immunofluorescence (IIF) microscopy. Dcp1a-positive P-bodies were analyzed for Ago2 signal using quantitative laser scanning cytometry. The co-localization between Ago2 and Dcp1a for all mutants is relative to WT, which was set to 1.0. Paired student's two-tailed t-test were used to compare relative co-localization of mutant Ago2 and RNA granule to that of Ago2-WT, (*) $p < 0.05$; (**) $p < 0.01$. Error bars indicate SE. **B)** HeLa cells transiently transfected with plasmids expressing myc-tagged Ago2 (WT, PAZ9, or S798D) were processed for IIF microscopy. Exogenously expressed Ago2 was detected using an anti-myc antibody. Dcp1a-positive P-bodies are denoted by arrows.

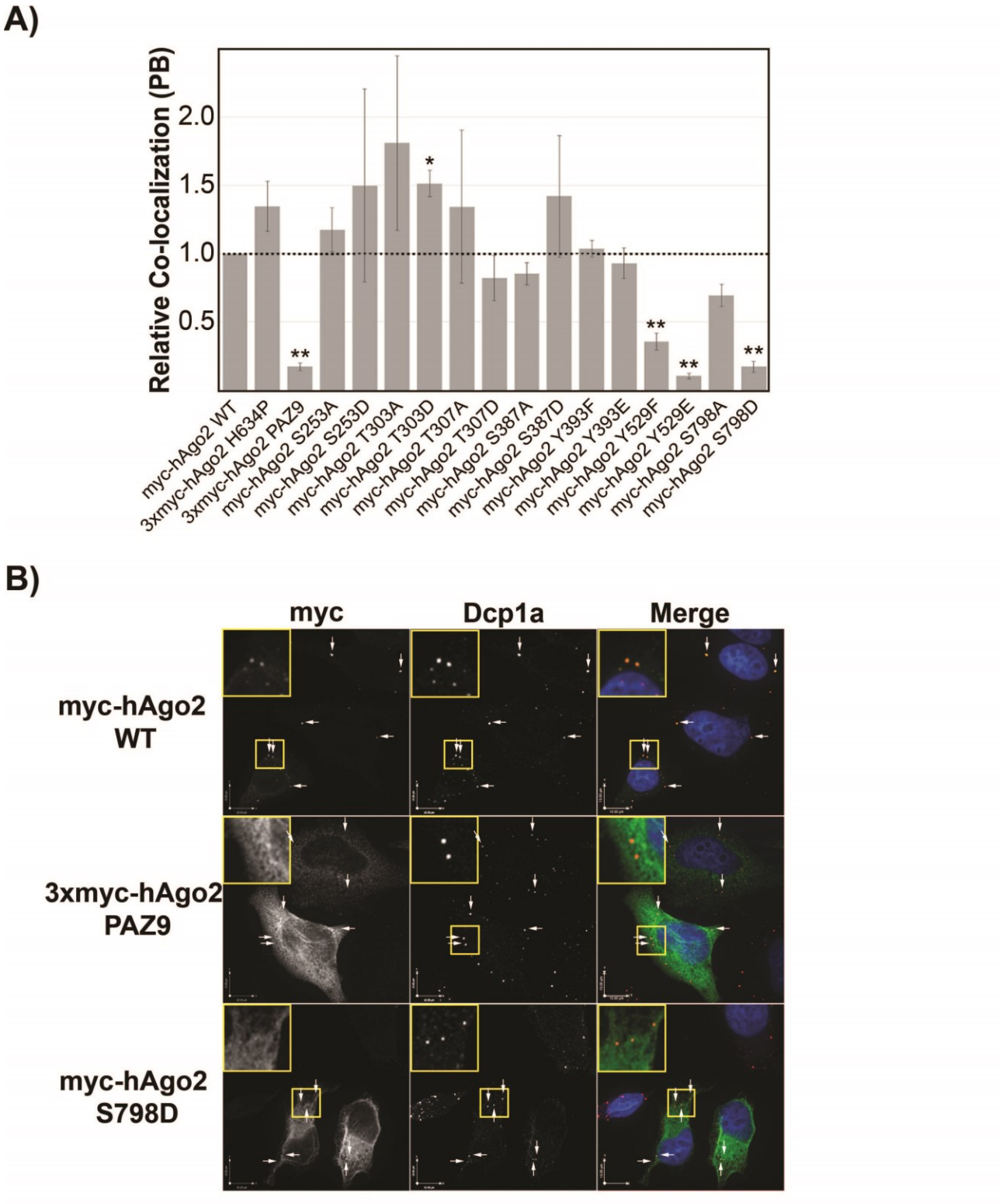
A)
Relative Co-localization (PB)
2.0
1.5
1.0
0.5
*
**
**
**
**
myc-hAgo2 WT
3xmyc-hAgo2 H634P
3xmyc-hAgo2 PAZ9
myc-hAgo2 S253A
myc-hAgo2 S253D
myc-hAgo2 T303A
myc-hAgo2 T303D
myc-hAgo2 T307A
myc-hAgo2 T307D
myc-hAgo2 S387A
myc-hAgo2 S387D
myc-hAgo2 Y393F
myc-hAgo2 Y393E
myc-hAgo2 Y529F
myc-hAgo2 Y529E
myc-hAgo2 S798A
myc-hAgo2 S798D
B)
myc
Dcp1a
Merge
myc-hAgo2 WT
3xmyc-hAgo2 PAZ9
myc-hAgo2 S798D

Figure 3.2

3.2.1.2 Phospho-mimetic mutation at Serine-798 blocks association of Ago2 with stress granules.

Similar to P-bodies, localization of Ago2 to stress granules requires small RNA binding (Pare et al. 2011a). It is therefore assumed that targeting of Ago2 to these structures was a consequence of its role in RNAi and is mediated by its interaction with targeted mRNAs. I next sought to determine whether recruitment of Ago2 to stress granules was affected by changes in Ago2 phosphorylation. Transfected HeLa cells expressing myc-tagged Ago2 mutants were employed in a similar approach as above except, 45 minutes prior to fixation, media containing the oxidative stressor sodium arsenite (500 μM) was added to cells, to induce the formation of stress granules. Cells were then processed for indirect fluorescence with antibodies to myc and TIA-1, a stress granule resident protein (Kedersha et al. 1999). Computational analysis of the data showed that, as with targeting to P-bodies, recruitment of Ago2-PAZ9, Ago2-Y529E, Ago2-Y529F, and the Ago2-S798D mutants to stress granules was significantly impaired (Figure 3.3A). Similar to what was observed for Ago2 T303D and P-bodies, targeting of Ago2-S387D to TIA-1 positive stress granules was slightly, but significantly, increased compared to Ago2-WT.

The aberrant localization of Ago2-S798D to stress granules (Figure 3.3A) was then confirmed using confocal microscopy. HeLa cells were transfected with plasmids expressing myc-Ago2-WT, 3xmyc-Ago2-PAZ9 or myc-Ago2-S798D. A plasmid expressing DsRed-tagged TIA-1 was co-transfected into cells treated with arsenite for 45 minutes prior to fixation. Ago2-PAZ9 and Ago2-S798D were distributed diffusely

throughout the cytoplasm, and did not overlap with TIA-1-positive stress granules (Figure 3.3B).

Figure 3.3 Localization of Ago2 phosphorylation mutants relative to stress granules. A) HeLa cells were transiently co-transfected with plasmids expressing WT or mutant Ago2. Prior to processing for IIF microscopy, cells were treated with 500 μM sodium arsenite for 1 hour. Stress granules positive for endogenous TIA-1 were assessed for Ago2 signal using quantitative laser scanning cytometry. The co-localization between Ago2 and TIA-1 for all mutants is relative to WT, which was set to 1.0. Paired student's two-tailed t-test were used to compare relative co-localization of mutant Ago2 and RNA granule to that of wildtype Ago2, (*) $p < 0.05$; (**) $p < 0.01$; (***) $p < 0.001$; (****) $p < 0.0001$. Error bars indicate SE. **B)** HeLa cells were transiently co-transfected with plasmids expressing myc-tagged Ago2 (WT, PAZ9, or S798D) and DsRed-tagged TIA-1. Following treatment with 500 μM sodium arsenite for 1 hour cells were processed for IIF microscopy. Exogenously expressed Ago2 was detected using an anti-myc antibody. TIA-1-positive stress granules are marked by arrowheads. Outlined regions are expanded in inset. Axis lines at the bottom left corner represent 10 μm.

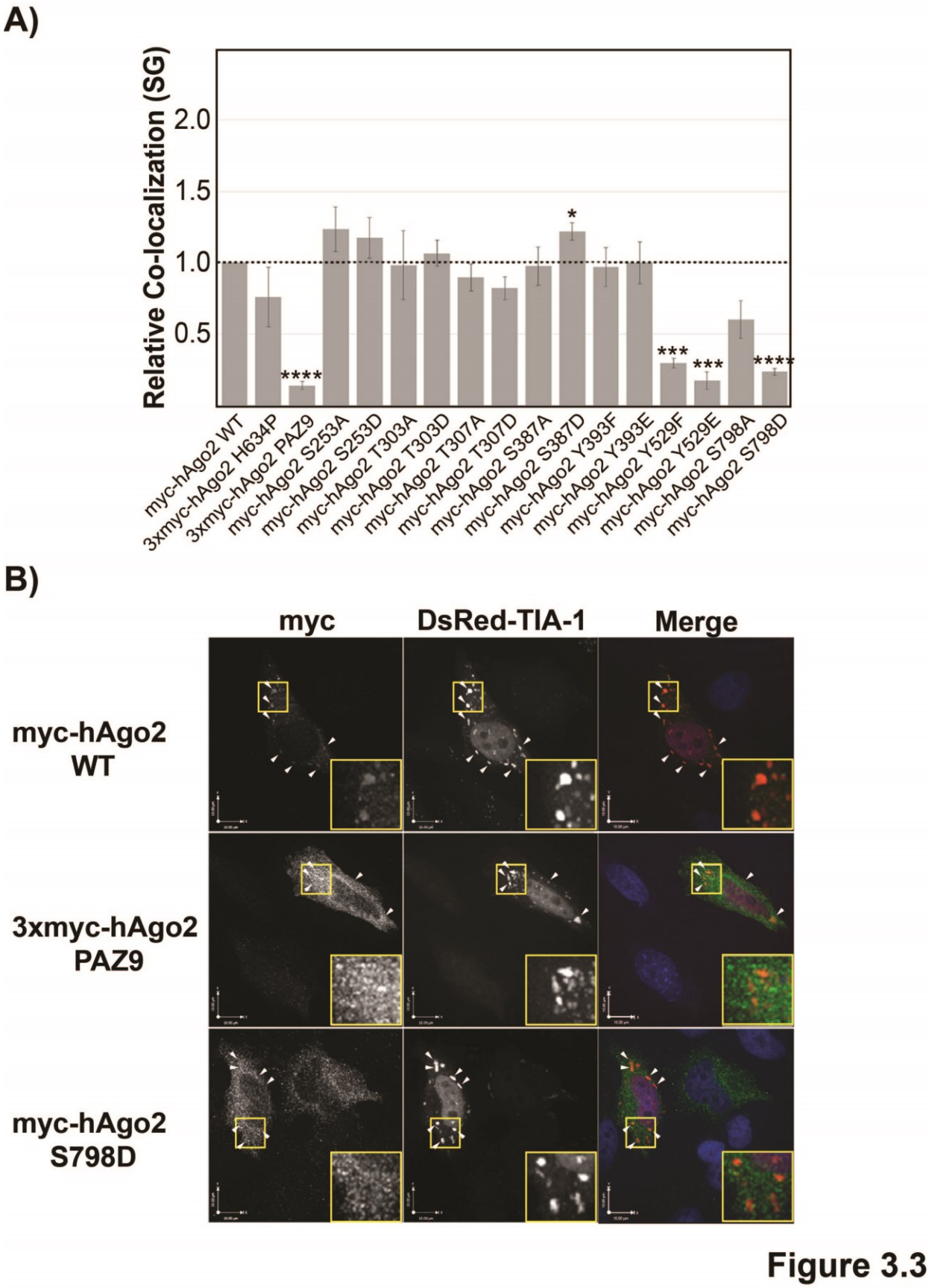
A)
Relative Co-localization (SG)
2.0
1.5
1.0
0.5
*
****
***
***
****
myc-hAgo2 WT
3xmyc-hAgo2 H634P
3xmyc-hAgo2 PAZ9
myc-hAgo2 S253A
myc-hAgo2 S253D
myc-hAgo2 T303A
myc-hAgo2 T303D
myc-hAgo2 T307A
myc-hAgo2 T307D
myc-hAgo2 S387A
myc-hAgo2 S387D
myc-hAgo2 Y393F
myc-hAgo2 Y393E
myc-hAgo2 Y529F
myc-hAgo2 Y529E
myc-hAgo2 S798A
myc-hAgo2 S798D
B)
myc
DsRed-TIA-1
Merge
myc-hAgo2 WT
3xmyc-hAgo2 PAZ9
myc-hAgo2 S798D

Figure 3.3

Using confocal microscopy, I also validated the localization data of the remaining mutants by transfecting plasmids expressing all 14 myc-tagged Ago2 mutants into HeLa cells that were subsequently treated with or without arsenite prior to fixation. Endogenous Dcp1a was used as a marker for P-bodies, while endogenous TIA-1 was used to detect stress granules. Together, results from these experiments confirmed that Y529F, Y529E and S798D are the only phospho-mutants of Ago2 with marked localization defects (Figure 3.4 A & B).

Figure 3.4 Subcellular localization of Ago2 phospho-mutants. A) HeLa cells were transiently transfected with plasmids encoding myc-tagged Ago2 individually mutated at each known phospho-site to prevent phosphorylation. Following treatment with 500 μM arsenite for 45 min, cells were processed for indirect immunofluorescence microscopy. **B)** HeLa cells were transiently transfected with plasmids expressing myc-tagged Ago2 individually mutated at each known phospho-site to mimic phosphorylation. Following treatment with 500 μM arsenite for 45 min, cells were processed for indirect immunofluorescence microscopy. Dcp1a-positive P-bodies are marked with arrows; TIA-1-positive stress granules are marked with arrowheads. Axis lines at the bottom left corner represent 15 μm.

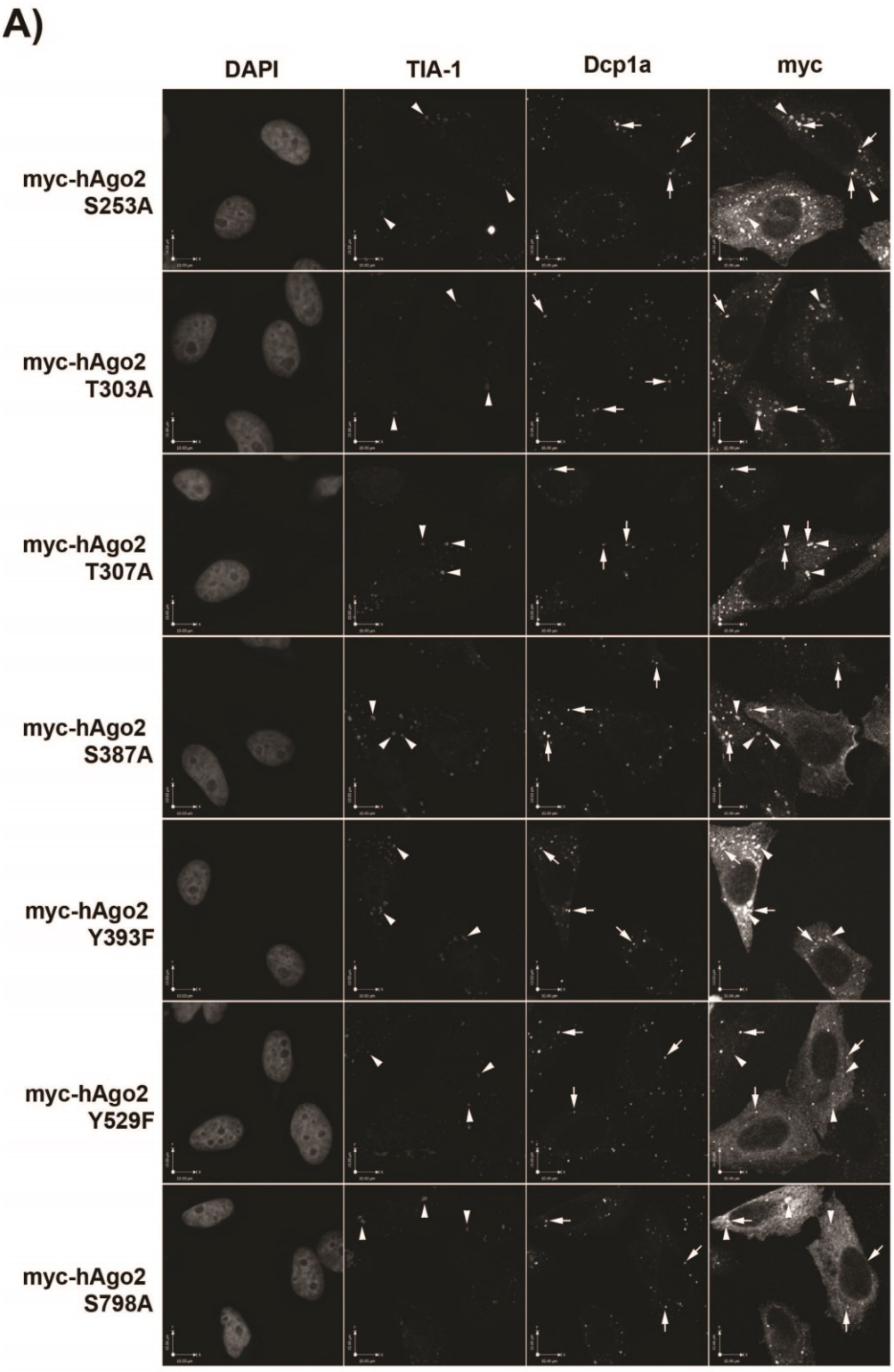
A)
DAPI
TIA-1
Dcp1a
myc
myc-hAgo2 S253A
myc-hAgo2 T303A
myc-hAgo2 T307A
myc-hAgo2 S387A
myc-hAgo2 Y393F
myc-hAgo2 Y529F
myc-hAgo2 S798A

Figure 3.4

Figure 3.4 Continued

B)

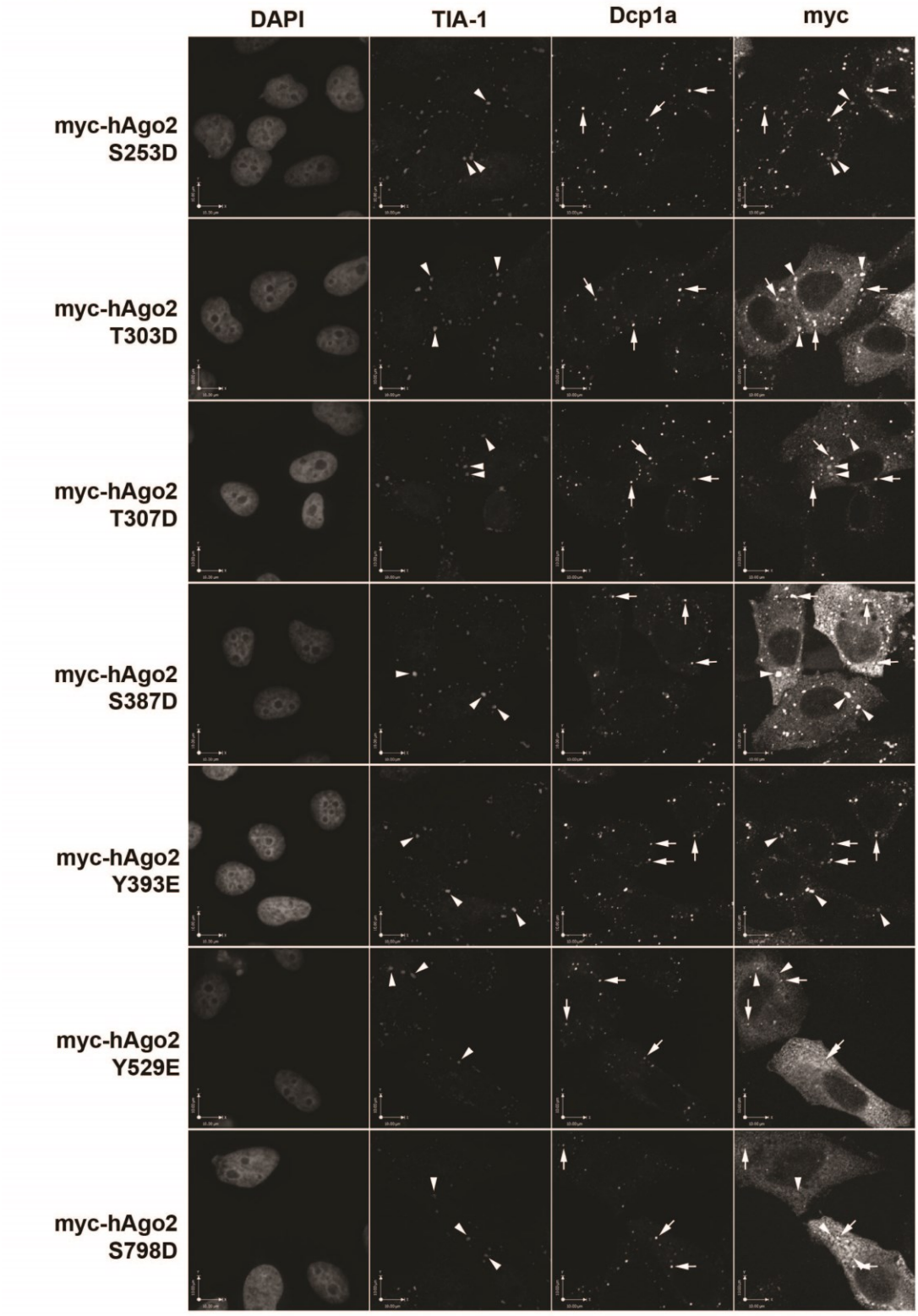

3.2.2 myc-Ago2-WT and myc-Ago2 mutants are expressed at comparable levels and their expression does not disrupt RNA granule formation.

Comparing exogenously expressed proteins can be complicated as multiple variables are often at play. One potential variable is differing expression levels of the different Ago2 mutants. For example, it is possible that the mutants Ago2-S798D or Ago2-Y529F are expressed below detectable levels. To address this possibility, the expression levels of the Ago constructs were measured by immunoblot analyses. For the most part, expression of each of the 14 phospho-mutants was comparable to that of exogenously expressed myc-Ago2-WT and, in all cases, higher than endogenous Ago2 (Figure 3.5). As such, the observed decreased localization of Ago2-S798D to P-bodies or stress granules was not due to lower expression. Moreover, expression levels of two other myc-tagged mutants (Ago2-S798A and Ago2 Y393E) were routinely lower than Ago2-S798D, however no appreciable decrease in granule localization was observed in these cases.

I considered that expression of some Ago2 mutants may disrupt the formation of P-bodies and/or stress granules in cells, however this was not the case. Data from laser scanning cytometry high content analysis shows that the total number of granules was unchanged in cells expressing WT or mutant Ago2 proteins (Figure 3.6).

Figure 3.5 Ago2 mutants are expressed at comparable levels in transfected HeLa cells. Cells were transiently transfected with plasmids encoding WT or phospho-mutant Ago2 proteins, and dsGFP as a control. Cells were harvested 24 hours post-transfection and the lysates were subjected to SDS-PAGE and immunoblotting for Ago, actin, and GFP. Signal intensities for Ago were normalized against the levels of actin. The numbers below the blot indicate expression of each Ago2 phospho-mutant relative to Ago2-WT. Endogenous Agos are indicated by an arrowhead. n=1.

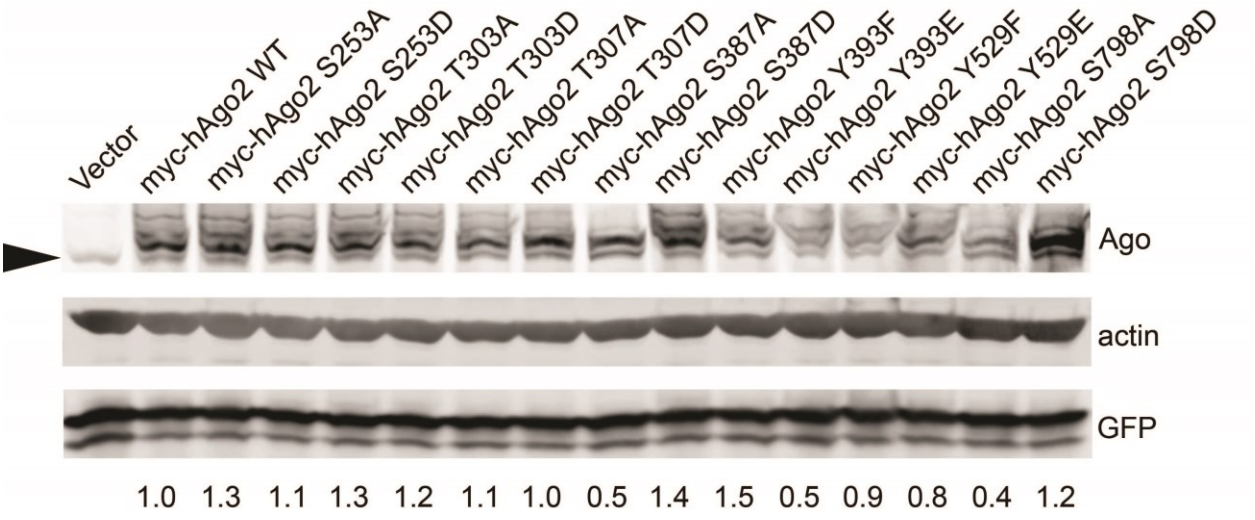
Vector
myc-hAgo2 WT
myc-hAgo2 S253A
myc-hAgo2 S253D
myc-hAgo2 T303A
myc-hAgo2 T303D
myc-hAgo2 T307A
myc-hAgo2 T307D
myc-hAgo2 S387A
myc-hAgo2 S387D
myc-hAgo2 Y393F
myc-hAgo2 Y393E
myc-hAgo2 Y529F
myc-hAgo2 Y529E
myc-hAgo2 S798A
myc-hAgo2 S798D
Ago
actin
GFP
1.0 1.3 1.1 1.3 1.2 1.1 1.0 0.5 1.4 1.5 0.5 0.9 0.8 0.4 1.2

Figure 3.5

Figure 3.6 Quantitation of P-bodies and stress granules in cells expressing WT and mutant Ago2 proteins. HeLa cells transiently transfected with plasmids expressing WT or mutant Ago2 were processed for indirect immunofluorescence (IIF) microscopy. The numbers of P-bodies and stress granules were determined by quantitative laser scanning cytometry**. A)** Numbers of Dcp1a-positive P-bodies in vector or myc-Ago2 transfected cells are shown. **B)** Numbers of TIA1-positive stress granules in vector and myc-Ago2 transfected cells are shown. Note- prior to processing for IIF microscopy, cells were treated with 500 μM sodium arsenite for 1 hour to induce stress granules. Paired student's two-tailed t-test was used to compare relative co-localization of mutant Ago2 and RNA granules to that of Ago2-WT. Error bars indicate SE.

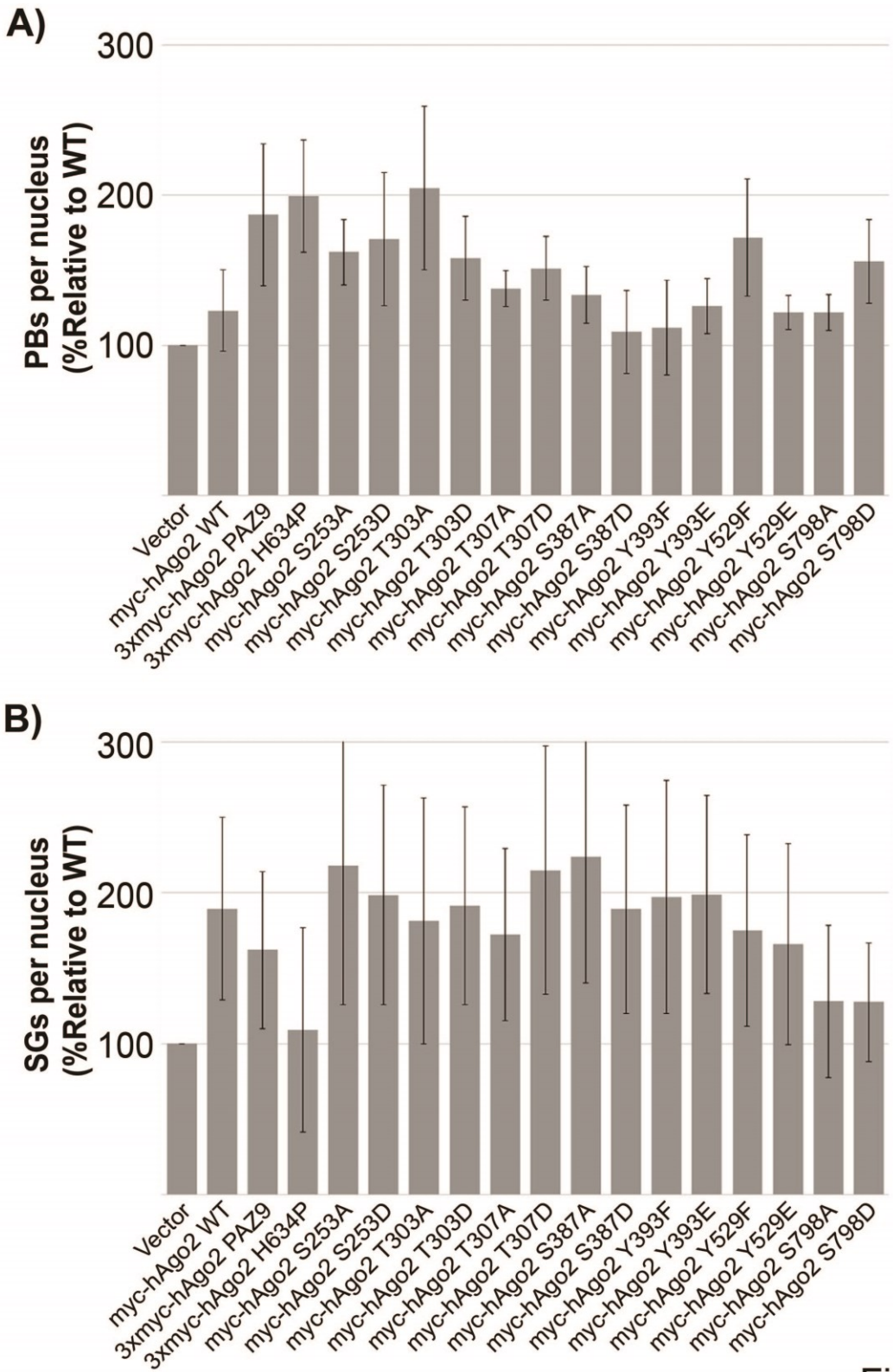
A)
PBs per nucleus (%Relative to WT)
300
200
100
Vector
myc-hAgo2 WT
3xmyc-hAgo2 PAZ9
3xmyc-hAgo2 H634P
myc-hAgo2 S253A
myc-hAgo2 S253D
myc-hAgo2 T303A
myc-hAgo2 T303D
myc-hAgo2 T307A
myc-hAgo2 T307D
myc-hAgo2 S387A
myc-hAgo2 S387D
myc-hAgo2 Y393F
myc-hAgo2 Y393E
myc-hAgo2 Y529F
myc-hAgo2 Y529E
myc-hAgo2 S798A
myc-hAgo2 S798D
B)
SGs per nucleus (%Relative to WT)
300
200
100
Vector
myc-hAgo2 WT
3xmyc-hAgo2 PAZ9
3xmyc-hAgo2 H634P
myc-hAgo2 S253A
myc-hAgo2 S253D
myc-hAgo2 T303A
myc-hAgo2 T303D
myc-hAgo2 T307A
myc-hAgo2 T307D
myc-hAgo2 S387A
myc-hAgo2 S387D
myc-hAgo2 Y393F
myc-hAgo2 Y393E
myc-hAgo2 Y529F
myc-hAgo2 Y529E
myc-hAgo2 S798A
myc-hAgo2 S798D

Figure 3.6

3.2.3 Phospho-mimetic substitution at position 798 does not affect interaction of Ago2 with mature miRNAs or RISC-loading complex components Dicer and Hsp90

In some cases, point mutations can have profound effects on the folding of proteins, resulting in altered three-dimensional structures. To address the possibility that loss of RNA granule targeting was due to Ago2-S798D being misfolded, we assessed its ability to interact with the well-characterized RISC-loading proteins (Hsp90 and Dicer) and nucleic acid (miRNAs) binding partners (Pare et al. 2009, Pare, LaPointe and Hobman 2013, Tahbaz et al. 2004, Wang et al. 2013). HeLa cells were transfected with plasmids encoding myc-tagged Ago2 (WT, PAZ9, S798A or S798D) and then processed for co-immunoprecipitation and immunoblotting. Data in Figure 3.7A show that both Hsp90 and Dicer co-immunoprecipitated with the Ago2-S798D mutant. Levels of co-immunoprecipitated Hsp90 and Dicer were normalized to the amount of Ago2 bound by the anti-myc beads. The relative amounts of Hsp90 and Dicer detected in the co-immunoprecipitates are shown in figure 3.7B. Similar to Ago2-PAZ9, significantly more Hsp90 and Dicer were bound to Ago2-S798D than to Ago2-WT. One interpretation of these results is that the transfer of the miRNA from Dicer to Ago triggers the dissolution of the RISC loading complex; therefore, Ago2 mutants that cannot be efficiently loaded with miRNA, dwell in complex with Dicer and the loading machinery. In contrast to Ago2-S798D, the amount of Dicer and Hsp90 associated with Ago2-S798A was not significantly different from Ago2-WT.

The localization defect associated with Ago2-S798D (Figure 3.2) closely resembles that of two other Ago2 mutants (Ago2-PAZ9 and Ago2-Y529E), which are unable to bind to small RNAs. Moreover, both S798D and PAZ9 Ago2 mutants bind

significantly more Hsp90 and Dicer than Ago2-WT (Figure 3.7B). Analysis of the crystal structure of Ago2 in complex with a miRNA suggests that serine-798 interacts with the phosphate backbone at position five of the miRNA (Schirle and MacRae 2012). According to this structure, serine-798 is predicted to have limited surface availability; which would restrict access by protein kinases. However, tyrosine-529 has similar predicted surface availability and increasing evidence indicates that it is phosphorylated *in vivo* (Mazumder et al. 2013, Rudel et al. 2011). This may indicate that Ago2 adopts a conformation where one or both of these amino acid residues are accessible to kinases. Based on these data, I predicted that Ago2-S798D would not bind small RNAs due to electrostatic repulsion. To test this, the relative levels of two endogenous miRNAs (hsa-let-7b and hsa-miR-21) bound to myc-tagged WT and mutant Ago2 proteins were determined by co-immunoprecipitation and Northern blotting. Data in Figure 3.7C revealed, unexpectedly, that Ago2-S798D behaves similarly to Ago2-WT in binding endogenous mature miRNAs. These observations appear to rule out the possibility that at position 798 (unlike at position 529) the presence of a large, negative charge serves to prevent binding of the small RNA.

Although it seems unlikely, we cannot rule out the possibility that the substituted aspartic acid at position 798 is differentially aligned within the structure of Ago2 than a phosphoserine at this position; thereby allowing for the interaction with the negatively charged phosphate backbone of the small RNA, whereas phosphorylation of the native serine residue may have more significant effects on small RNA binding. Irrespective of the mechanism, to my knowledge, this is the first mutation of Ago2 that uncouples miRNA binding from targeting to cytoplasmic RNA granules.

Figure 3.7 Interaction of myc-hAgo2-S798D with components of the RISC-loading complex and small RNAs. A) HeLa cells transiently transfected with plasmids encoding WT or mutant Ago2 were lysed 16 h post-transfection and subjected to co-immunoprecipitation with anti-myc antibodies. Total cell lysates (Input) and bound fractions were subjected to SDS-PAGE and immunoblotted for Ago2, Hsp90, and Dicer as indicated. **B)** Signal intensities for Hsp90 and Dicer were quantitated and normalized to levels of immunoprecipitated Ago2. The bar graph indicates the fold change in the amount of each co-immunoprecipitated Ago2-binding partner relative to the amount associated with Ago2-WT. Paired student's two-tailed t-test was used to compare amounts of co-immunoprecipitated Hsp90 and Dicer to amounts bound to Ago2-WT, * $p < 0.05$; ** $p < 0.01$. Error bars indicate SE. **C)** HeLa cells transiently transfected with plasmids encoding WT or mutant Ago2 were lysed 16 h post-transfection and subjected to immunoprecipitation using sepharose beads coated with anti-myc antibodies. RNA was extracted from the bound fractions (IP α-myc) and subjected to UREA-PAGE. Cells transfected with empty vector were used as the negative control for immunoprecipitation (labeled "Vector"). Loading of RNA was normalized to level of bound Ago2 (immunoblot of 3% of immunoprecipitated protein shown below). MiRNAs detected by Northern blotting using ^{32}P-labeled oligonucleotide probes. Total RNA isolated from cell lysate included as a control (Input RNA).

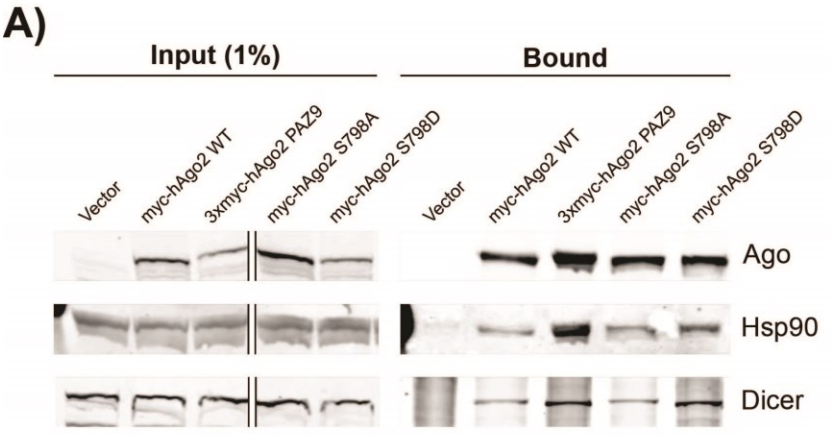
A)
Input (1%)
Bound
Vector
myc-hAgo2 WT
3xmyc-hAgo2 PAZ9
myc-hAgo2 S798A
myc-hAgo2 S798D
Ago
Hsp90
Dicer

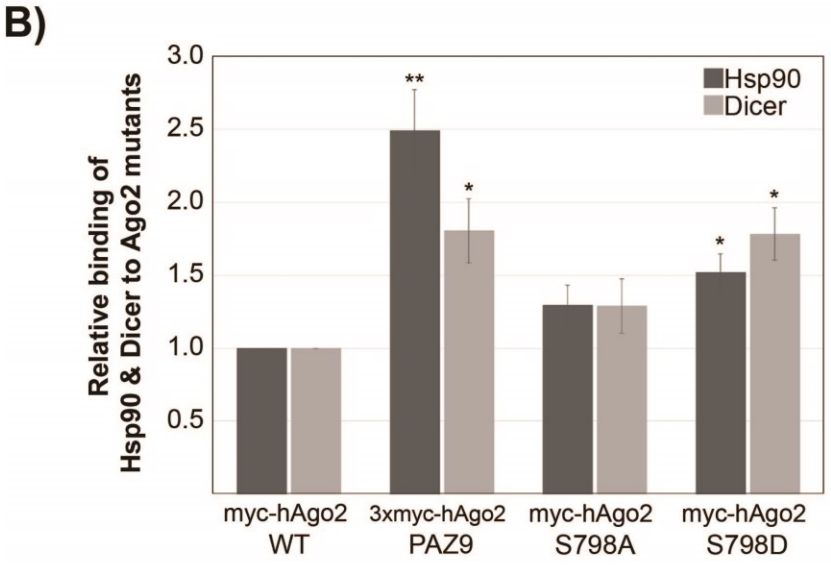
B)
Relative binding of Hsp90 & Dicer to Ago2 mutants
3.0
2.5
2.0
1.5
1.0
0.5
Hsp90
Dicer
**
*
*
*
myc-hAgo2 WT
3xmyc-hAgo2 PAZ9
myc-hAgo2 S798A
myc-hAgo2 S798D

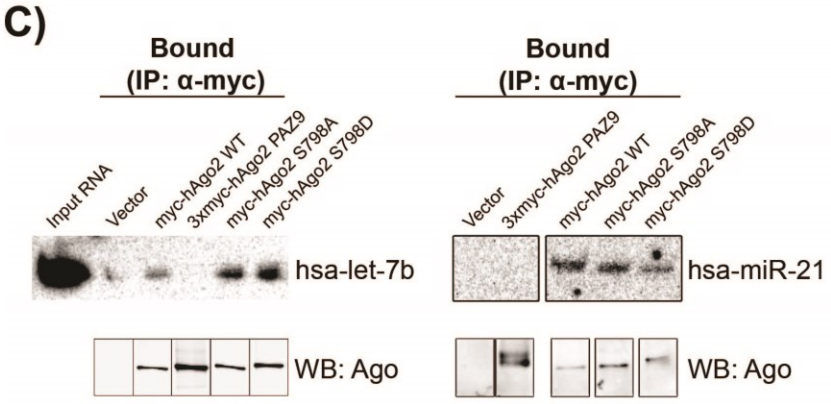
C)
Bound (IP: α-myc)
Bound (IP: α-myc)
Input RNA
Vector
myc-hAgo2 WT
3xmyc-hAgo2 PAZ9
myc-hAgo2 S798A
myc-hAgo2 S798D
hsa-let-7b
hsa-miR-21
WB: Ago
WB: Ago

Figure 3.7

To further demonstrate that mutations at S798 do not cause misfolding of Ago2, I assessed whether Ago2-S798A and S798D were able to interact with proteins of the RISC complex. Data in Figure 3.8 demonstrates that Ago2-WT, Ago2-S798A, and Ago2-S798D all formed stable complexes with Dcp1a. However, the significance of this interaction remains unclear as Ago2-PAZ9, which does not associate with P-bodies, also binds Dcp1a (Figure 3.8 and (Liu et al. 2005b)). Furthermore, it has been shown that Ago2-Y529E, despite being functionally inactive and not localized to RNA granules, interacts with GW182, a P-body resident protein and critical component to the RNAi-mediated silencing pathway (Rudel et al. 2011). Given that Ago2-S798D interacts with two critical proteins involved in RISC-loading (Dicer and Hsp90), as well as miRNAs and Dcp1a, I conclude that point mutations at position 798 do not result in misfolding of Ago2.

Figure 3.8 Interaction of WT and Ago2 phospho-mutants with the P-body resident protein Dcp1a. HeLa cells transiently transfected with plasmids encoding WT or mutant Ago2 were lysed 16 h post-transfection and subjected to co-immunoprecipitation with anti-myc antibodies. Total cell lysates (Input) and bound fractions were subjected to SDS-PAGE and immunoblotted for Ago2 and Dcp1a as indicated. Enhanced contrast image of co-immunoprecipitated Dcp1a is shown. n=1.

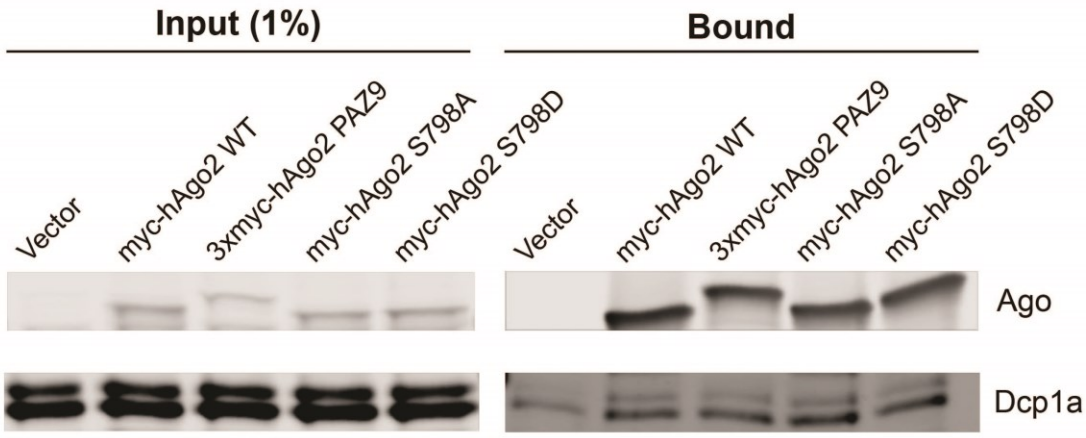
Input (1%)
Bound
Vector
myc-hAgo2 WT
3xmyc-hAgo2 PAZ9
myc-hAgo2 S798A
myc-hAgo2 S798D
Vector
myc-hAgo2 WT
3xmyc-hAgo2 PAZ9
myc-hAgo2 S798A
myc-hAgo2 S798D
Ago
Dcp1a

Figure 3.8

3.2.4 The silencing activity of Ago2 is mildly affected by phospho-mimetic mutation of Serine-798

Given the evidence linking Ago2 localization to cytoplasmic RNA granules and gene-silencing function, we next explored the consequence of mutating phosphoamino acid residues on the gene-silencing activity of Ago2. To measure endonuclease-dependent silencing activity, we constructed a reporter (pdsGFP-miR21) encoding destabilized GFP (dsGFP) and a single perfectly complementary binding site to mouse miR-21 (Figure 3.9A), a miRNA that is highly expressed in MEFs. A plasmid encoding dsGFP and an untargeted 3' UTR site (pdsGFP-nsc), was used as a negative control. MEF cells lacking the gene encoding Ago2 (Liu et al. 2004a) were electroporated with plasmids encoding either Ago2-WT or the phospho-mutants; pDsRed-C1-Monomer; and pdsGFP-miR21 reporter (or pdsGFP-nsc control). The molar ratios of plasmids in the electroporation ensured that all DsRed-expressing cells were co-transfected with Ago2 and the dsGFP-encoding reporters. Expression of dsGFP and DsRed was determined by flow cytometry 24 hours after electroporation, followed by normalization of dsGFP against DsRed. GFP expression is represented as a percent of the total expression of the pdsGFP-nsc control. As expected, co-expression of Ago2-WT caused a 91% reduction in the fluorescence of cells transfected with pdsGFP-miR21 cells co-transfected with plasmids Ago2-WT and dsGFP with an untargeted 3' UTR site (pdsGFP-nsc) (Figure 3.9B). Levels of dsGFP expression in cells transfected with plasmids encoding the slicer-dead (Ago2-H634P) or small RNA-binding mutants (Ago2-PAZ9 and Ago2-Y529E) of Ago2 were not significantly different from those expressing vector alone. Paired sample t-tests were performed to confirm that the differences in GFP expression, relative to Ago2-

WT, were significant for Ago2-H634P, Ago2-PAZ9, Ago2-Y529E and Ago2-S798D. However, while the slicer-dependent silencing activity of Ago2-S798D was significantly lower than Ago2-WT, it was not as impaired as the Ago2-H634P, Ago2-PAZ9, or Ago2-Y529E mutants (Figure 3.9B).

Figure 3.9 Slicer-dependent activities of Ago2 phospho-mutants. A) Schematic representation of expression cassette in the pdsGFP-miR21 reporter used to assay slicer-dependent silencing activity. TGA is the stop codon. A(n) represents the mRNA poly(A) tail. The straight line between the stop codon and the poly(A) tail represents the perfectly complementary miR21 site. **B)** Ago2 -/- mouse embryonic fibroblast cells were electroporated with plasmids encoding WT or mutant Ago2 proteins together pdsGFP-miR21 or pdsGFP-nsc (negative control), and pDsRed-C1-monomer. GFP expression was determined by flow cytometry and normalized against DsRed expression. The bar graph represents the GFP expression from pdsGFP-miR21 relative to pdsGFP-nsc for each Ago2 construct.

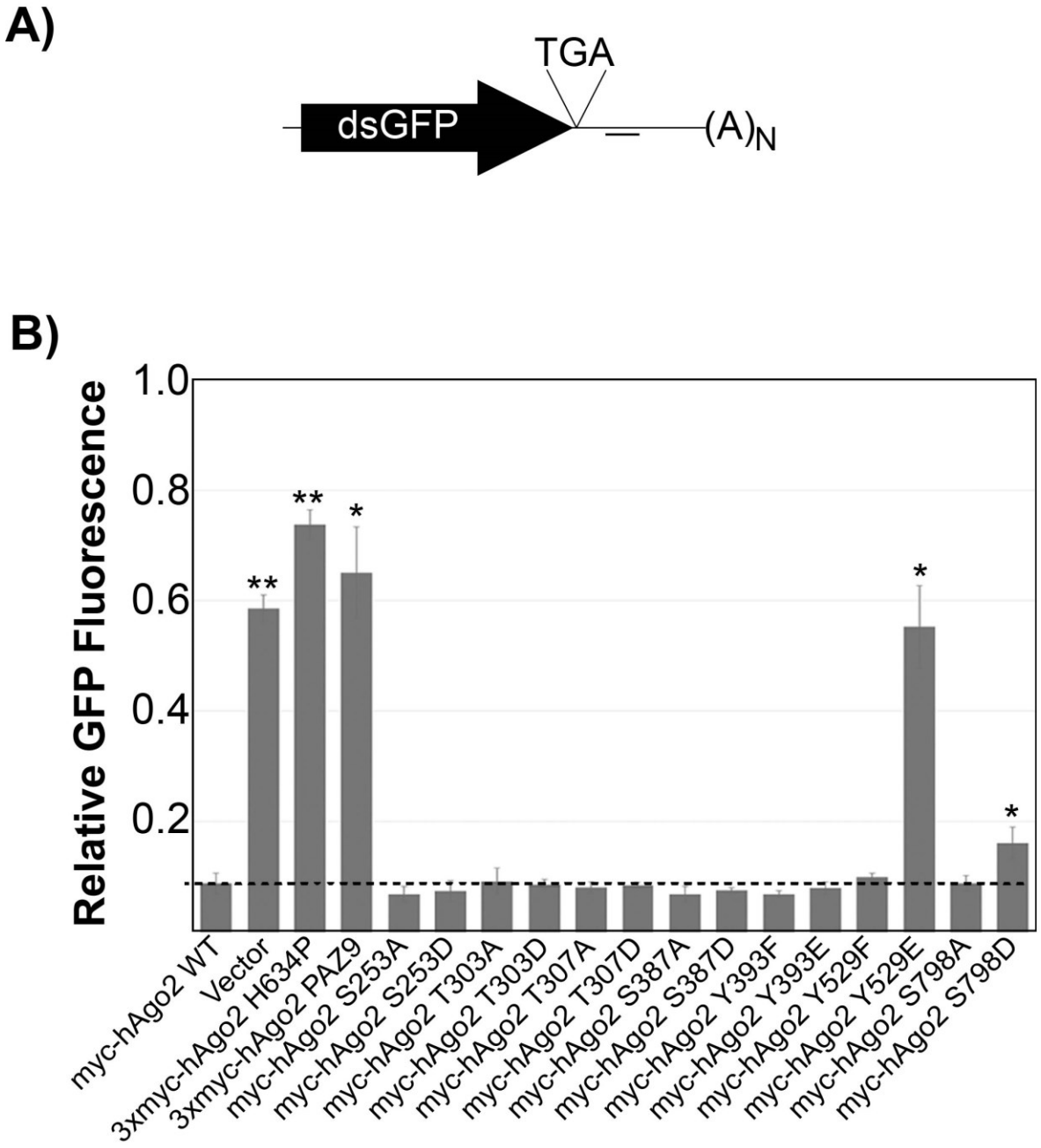
A)
TGA
dsGFP
(A)N
B)
Relative GFP Fluorescence
1.0
0.8
0.6
0.4
0.2
**
**
*
*
*
myc-hAgo2 WT
Vector
3xmyc-hAgo2 H634P
3xmyc-hAgo2 PAZ9
myc-hAgo2 S253A
myc-hAgo2 S253D
myc-hAgo2 T303A
myc-hAgo2 T303D
myc-hAgo2 T307A
myc-hAgo2 T307D
myc-hAgo2 S387A
myc-hAgo2 S387D
myc-hAgo2 Y393F
myc-hAgo2 Y393E
myc-hAgo2 Y529F
myc-hAgo2 Y529E
myc-hAgo2 S798A
myc-hAgo2 S798D

Figure 3.9

To measure endonuclease-independent silencing activity of Ago2 mutants, I constructed the reporter plasmid pdsGFP-Nonslicer (Figure 3.10A). This plasmid includes a synthetic 107 bp 3' UTR containing three binding sites for a Dicer-substrate siRNA that does not target any mammalian (including murine) genomic sequences. To prevent Ago2-mediated cleavage of the mRNA target, the binding sites within the synthetic 3' UTR were mismatched at positions nine and ten (Bartel 2004). Finally, the binding sites within the 3' UTR were spaced in a manner to bias non-slicer dependent silencing by Ago2 (Broderick et al. 2011).

Using the same experimental conditions described above, followed by transfection of the Dicer-substrate siRNA, I assessed the ability of the Ago2 phospho-mutants to repress translation of the targeted mRNAs. Following normalization to DsRed expression, expression of dsGFP from the pdsGFP-Nonslicer plasmid was determined relative to expression from the non-silenced control plasmid (Figure 3.10B). Consistent with my expectations, co-expression of Ago2-PAZ9 or Ago2-Y529E did not cause an appreciable decrease in fluorescence compared to vector alone. That is, Ago2-PAZ9 and Ago2-Y529E were relatively ineffective (compared to Ago2-WT) in suppressing expression of the pdsGFP-Nonslicer reporter. The mean GFP fluorescence in cells expressing the Ago2 phospho-mutants was somewhat variable, likely due to silencing functions of the three remaining endogenous Ago proteins 1, 3, and 4. Despite this background silencing activity, Ago2-S798D was the only other mutant whose silencing activity was statistically different from Ago2-WT. However, in contrast to what we observed in the slicer-dependent silencing assay, the activity of Ago2-S798D in the slicer-independent silencing assay was slightly increased relative to Ago2-WT (Figure 3.10B).

A recent study showed that phosphorylation at tyrosine-393 impairs maturation of long-loop miRNAs (Shen et al. 2013). Therefore, the phosphomimetic mutant Ago2-Y393E should have reduced activity compared to Ago2-WT when long-loop miRNAs are involved but data in Figures 3.9 and 3.10 show no significant differences between them. However, because neither miR-21 nor the Dicer-substrate siRNA are of this type, it was not unexpected that Ago2-Y393E exhibited normal silencing activity in these assays.

Figure 3.10 Endonuclease-independent silencing activities of Ago2 phospho-mutants. A) Schematic representation of expression cassette in the pdsGFP-Nonslicer reporter used to assay slicer-independent silencing activity. TGA is the stop codon. A(n) represents the mRNA poly(A) tail. The three lines between the stop codon and the poly(A) tail represent the imperfect complementary sites to the synthetic Dicer-substrate siRNA. **B)** Ago2 -/- mouse embryonic fibroblast cells were transiently electroporated with plasmids encoding WT or mutant Ago2 proteins together with pdsGFP-NonSlicer or pdsGFP-nsc (negative control), and pDsRed-C1-monomer. Cells were then transfected with Dicer substrate siRNA. GFP expression was determined by flow cytometry and normalized against DsRed expression. The bar graph represents the expression GFP from pdsGFP-NonSlicer relative to pdsGFP-nsc for each Ago2 construct. Paired student's two-tailed t-test was used to compare amounts of dsGFP expression in cells co-transfected with mutant Ago2 constructs to those co-transfected with Ago2-WT, * $p < 0.05$; ** $p < 0.01$. Error bars indicate SE.

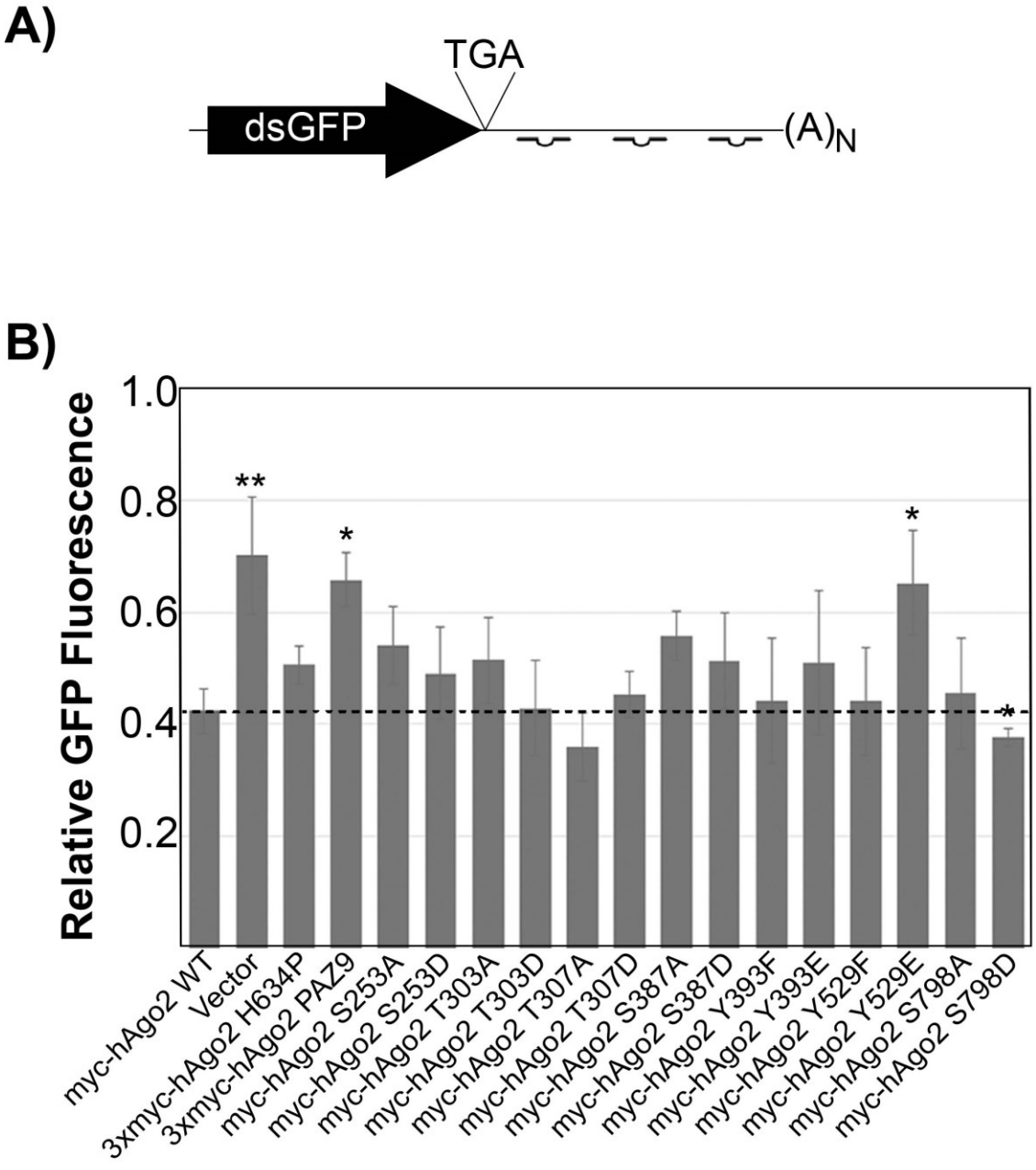
A)
TGA
dsGFP
(A)N
B)
Relative GFP Fluorescence
1.0
0.8
0.6
0.4
0.2
**
*
*
*
myc-hAgo2 WT
Vector
3xmyc-hAgo2 H634P
3xmyc-hAgo2 PAZ9
myc-hAgo2 S253A
myc-hAgo2 S253D
myc-hAgo2 T303A
myc-hAgo2 T303D
myc-hAgo2 T307A
myc-hAgo2 T307D
myc-hAgo2 S387A
myc-hAgo2 S387D
myc-hAgo2 Y393F
myc-hAgo2 Y393E
myc-hAgo2 Y529F
myc-hAgo2 Y529E
myc-hAgo2 S798A
myc-hAgo2 S798D

Figure 3.10

3.2.5 Phospho-mimetic mutation of Ago2 at Serine-798 alters Ago2 interaction with pre-miRNAs

It is well established that Ago proteins stably interact with mature miRNAs. (Liu et al. 2004; Rudel et al. 2011). However, very little information regarding the interaction of Ago proteins with pre-miRNAs is available. Since Ago2 is necessary for the processing of Dicer-independent miRNAs, *i.e.* miR-45, it could be inferred that Ago2 can interact to some pre-miRNAs independently of Dicer (Cheloufi et al. 2010). Nevertheless, there is no direct evidence of the interaction of Ago proteins with pre-miRNAs.

When performing the co-immunoprecipitation analysis described in figure 3.7. It was unexpected to observe that Ago2-WT co-immunoprecipitated with mature miRNAs as well as pre-miRNAs. Therefore, I next sought to investigate the interaction of pre-miRNA with Ago2 mutants. Using the same experimental conditions described in figure 3.7C, Ago2-WT, Ago2-PAZ9, Ago2-S798A and Ago2-S798D were analyzed for interaction with pre-miRNAs. Consistent with data in figure 3.7C, only Ago2-PAZ9 does not bind mature miRNAs while Ago2-WT, Ago2-S798A, and Ago2-S798D do bind mature miRNAs. However, only Ago2-WT and Ago2-S798A co-immunoprecipitated with pre-miRNAs. Neither Ago2-PAZ9 nor Ago2-S798D co-immunoprecipitated with detectable amounts of pre-miRNAs. Moreover, the co-immunoprecipitation of Ago2 to pre-miRNAs cannot be explained by the interaction to Dicer since Ago2-PAZ9 and Ago2-S798D pulled down more Dicer than Ago2-WT or Ago2-S798A.

Figure 3.11 The Ago-S798D mutant forms stable complexes with mature miRNAs but not with pre-miRNAs. HeLa cells transiently transfected with plasmids encoding WT or mutant Ago2 were lysed 16 h post-transfection and then subjected to immunoprecipitation with sepharose beads coated with anti-myc antibodies. RNA was extracted from the bound fractions (IP α-myc) and subjected to UREA-PAGE. Cells transfected with empty vector were used as the negative control for immunoprecipitation (labeled “Vector”). Loading of RNA was normalized to the level of bound Ago2 in each sample (immunoblot of 3% of immunoprecipitated protein shown below). MiRNAs were detected by Northern blotting using ^{32}P-labeled oligonucleotide probes. Total RNA isolated from cell lysates was included as a control (Input RNA). n=2.

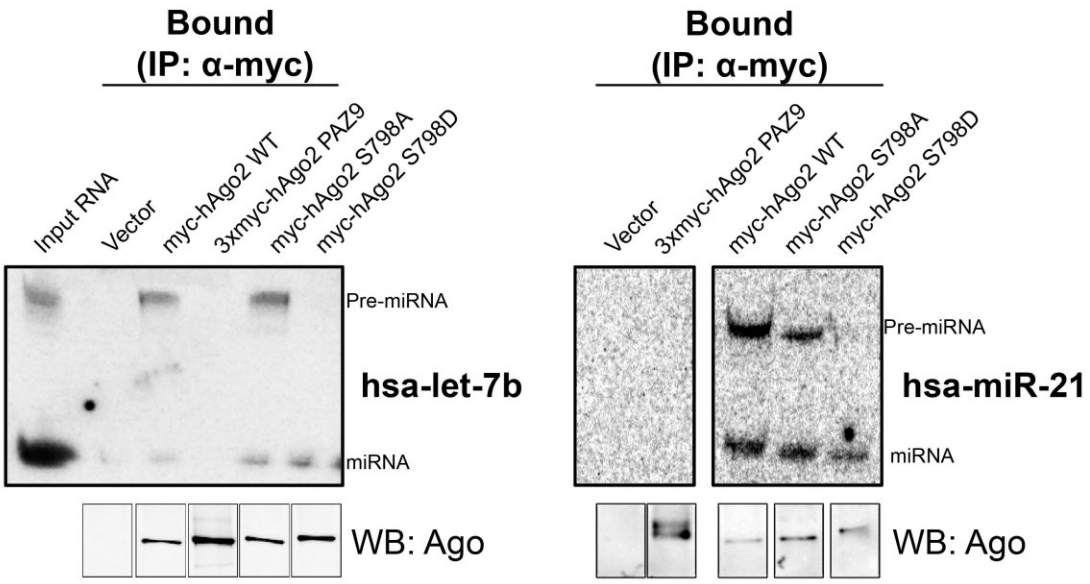
Bound
(IP: α-myc)
Input RNA
Vector
myc-hAgo2 WT
3xmyc-hAgo2 PAZ9
myc-hAgo2 S798A
myc-hAgo2 S798D
Pre-miRNA
hsa-let-7b
miRNA
WB: Ago
Bound
(IP: α-myc)
Vector
3xmyc-hAgo2 PAZ9
myc-hAgo2 WT
myc-hAgo2 S798A
myc-hAgo2 S798D
Pre-miRNA
hsa-miR-21
miRNA
WB: Ago

Figure 3.11

3.3. Summary

In this section, I analyzed the phenotypes of mutations that mimic the non-phosphorylated state and mutations that partially mimic constitutive phosphorylation at every known phospho-amino acid residue in hAgo2. During the course of my research a number of related studies (Rudel et al. 2011, Horman et al. 2013, Shen et al. 2013) were published that described how phosphorylation of S387, Y393 and Y529 affect Ago2 function. Unique to my studies is finding that phospho-mimetic substitution of aspartate for serine at position 798, dramatically alters the subcellular localization of Ago2. The data suggest that phosphorylation of S798 prevents Ago2 from associating with P-bodies and stress granules, but does not affect the formation of these RNA granules *per se*. Conversely, association of the Ago2-T303D mutant with RNA granules was increased compared to Ago2-WT. While a phospho-mimetic mutation at S798 completely changes Ago2 subcellular localization, the effect on the RNAi activity of Ago2 was less pronounced. Whereas other studies have shown that microscopic P-bodies are not required for RNAi (Eulalio et al. 2007b, Behm-Ansmant et al. 2006, Chu and Rana 2006), this is the first evidence indicating that the association of Ago2 with cytoplasmic RNA granules can be uncoupled from its role in gene-silencing. My data also suggest that the phosphomimic mutant Ago2-S798D increases the rate of miRNA maturation.

Chapter 4

Kinases modulate RNAi activity

(Unpublished data)

4.1. Rationale

A substantial amount of evidence suggests that phosphorylation plays a major role in controlling RNAi (Lopez-Orozco et al. 2015, Rüdel et al. 2011, Paroo et al. 2009, Shen et al. 2013, Horman et al. 2013, Zeng et al. 2008). Mass spectrometry analyses have revealed that some of the key components of the RNAi machinery are phosphorylated *in vivo* (Rüdel et al. 2011, Drake et al. 2014). However, we know comparatively little about how phosphorylation affects their functions and which kinases and phosphatases are involved. Identifying the kinases and phosphatases involved in the modification of RNAi pathway proteins is essential for understanding how RNAi is coordinated with other cellular functions.

RNAi is a ubiquitous process that relies on a group of sequentially acting proteins and RNAs that are located in different subcellular compartments (see Figure 1.1). Key components of this pathway are likely to be phosphorylated at every step. My work as described in Chapter 3 together with other studies, strongly suggests that RNAi can be modulated at late stages through the phosphorylation of Ago proteins (Horman et al. 2013, Shen et al. 2013). The objective in this chapter was to identify kinases and phosphatases whose functions affect RNAi in late stages, rather than during miRNA biogenesis or during nucleus-to-cytoplasm transfer (See Figure 1.1 and Figure 4.1A). Candidate kinases were further examined to confirm their effects in RNAi regulation and the mechanisms involved.

4.2. Results

4.2.1. Human genome-wide screen identified important kinases that function as regulators of siRNA-mediated gene silencing.

My first objective was to identify the kinases involved in the regulation of the late stages of the RNAi pathway. By adapting a screening methodology developed in the Foley laboratory (Schindler and Foley 2010), I was able to rapidly and robustly screen for human kinases involved in RNAi. The screen involves inducing apoptosis in siRNA-transfected HeLa cells with a combination of Tumor Necrosis Factor (TNF) and cycloheximide (TNF/CHX). The readout of the screen is cell survival, which was measured using the Resazurin salt assay. Cells treated with TNF/CHX undergo apoptosis via the death receptor pathway that requires caspase 8. TNF binds and activates death receptors on the cell membrane that in turn activate caspase 8 in the cell. Once activated, caspase 8 induces an apoptotic cascade. The screen exploits the need for adequate levels of caspase8 to trigger cell death. If the RNAi pathway is functional, then providing cells with caspase8-specific siRNAs will result in low caspase8 protein levels, and therefore, TNF/CHX will be less effective in triggering cell death. Prior to TNF/CHX treatment, the cells were transfected with a combination of siRNAs against caspase8 and all known human kinase genes. Cells that are transfected with siRNAs against a kinase that is important or required for RNAi function, then efficient downregulation of caspase8 protein does not occur and the level of cell death is high. Conversely, if the siRNA targets a kinase that is not important for RNAi, then caspase8 protein levels will be low and the level of induced cell death will be low. For example, in cells transfected with siRNAs against caspase8 and a non-silencing siRNA (that does not have a target in the human

genome) resulted in a low rate of cell death after treatment with TNF/CHX. In contrast, a combination of siRNAs against caspase8 and Ago2 resulted in high cell death because the latter is essential for RNAi. The screen methodology is described in section 2.2.11.2 and a schematic is shown in Figure 4.1A.

While it is quite likely that the RNAi pathway is regulated at most if not all stages, my screen was designed to identify kinases that are required for the endonuclease-dependent gene-silencing activity of Ago2, the last step in the canonical RNAi pathway. By employing 22 nt siRNAs that resemble Dicer cleavage products, kinases that regulate upstream steps in RNAi pathways including miRNA transcription, nuclear processing, transport of small RNAs from the nucleus to the cytoplasm, and cytoplasmic processing may not be identified here. Moreover, kinases that modulate RNAi factors that function by suppressing translation and/or directly degrading of mRNAs such as GW182, Dcp1a, and XRN1 may be missed in my screen (see section 1.1.2.4). Based on these criteria, the screen is designed to maximize the chances of detecting kinases involved in phosphorylation of Ago2.

Statistical analysis of the two repeats of the screen revealed with a 95% degree of confidence, many kinases that either reduced or increased RNAi activity (Figure 4.1B). As expected, most kinases (79%) did not have a statistically significant effect on RNAi. Out of the 150 kinases that had an effect on Ago2 function, 142 (~95%) increased RNAi, while eight (~5%) had an inhibitory effect. Conspicuously, of the eight kinases detected as inhibitory of RNAi, six are tyrosine kinases. This is consistent with reports that phosphorylation of two tyrosines in Ago proteins have inhibitory effects (Rüdel et al. 2011, Shen et al. 2013). One of the strongest effects on RNAi detected was the knockdown of

fibroblast growth factor receptor 3 (FGFR3). FGFR2 had a similar effect as FGFR3 but was not initially noticed in my screen because it did not fall within the 95% confidence interval. Nevertheless, I decided to further investigate the potential role the FGFR family members on RNAi.

Large-scale screens like the one described above have limitations and it is important to keep these caveats in mind. For example, although most of the siRNAs employed in my screen were validated by the supplier, some were not. As such, it is not known how efficiently or accurately they downregulate their targets and it would be cost-prohibitive and impractical to validate each target knockdown using immunoblotting or flow cytometry. Another caveat is that the cell line (HeLa) used in my screen does not express every kinase that was targeted by siRNAs. Accordingly, a kinase that does in fact regulate Ago2 function (positively or negatively), but it is not expressed in the cell line, would not be picked up in the screen. Finally, given the possibility of off-target effects of some siRNAs, it was critical to validate all “hits” using independent assays.

Figure 4.1 A genome-wide screen identified human kinases whose expression affects Ago2-mediated gene-silencing. A) Schematic of the assay used to identify kinases regulators of RNAi. **B)** Kinase screen results. List of the kinases identified, in red are kinases that decreased and in green are kinases that increased Ago2 activity. The reference bar at the bottom shows the range from the lowest to highest death index obtained in the screen.

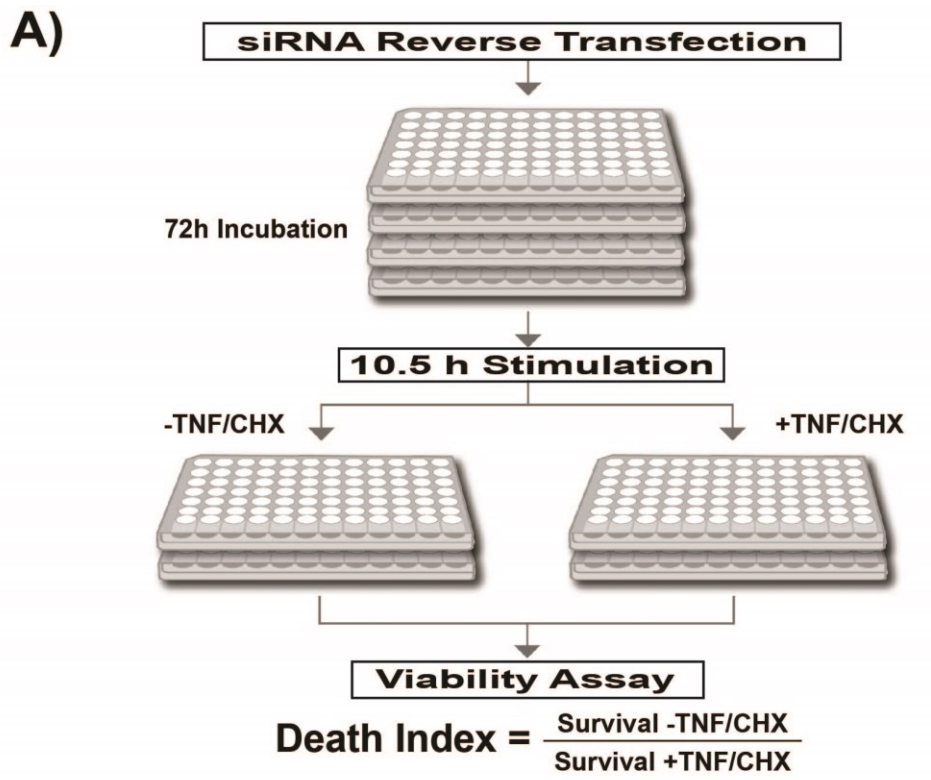

B)

BMX	FLJ13052	PLK4	MGC42105	CHEK1
FGFR3	SKP2	PRPSAP2	CSNK1A1	LOC442075
PXK	MAP2K2	LOC441047	CSNK1A1L	LRRK2
TEK	ITPKA	CAMK2G	PLXNB3	LOC441787
EPHB1	PKN1	RAF1	MAPKAPK2	FN3K
MPP1	LOC340371	PAPSS2	MARK1	FLJ25006
EPHA1	ATR	HIPK3	DYRK3	LAK
LOC441708	MPP6	CDKL1	MAPK11	C9orf96
RIPK3	ROR1	LOC440345	SIK2	SBK1
GLYCTK	STK32C	SRPK2	SPHK1	PNCK
MARK4	AK3	ADCK5	PKLR	LOC400301
BMPR1B	LOC389599	PRKG1	CALM3	LOC392347
PCTK1	FGFR4	STK32A	TYK2	GUK1
ERBB4	PTK2	FLJ37794	GK	XM_290793
PRKG2	AKAP2	TPK1	MAPKAPK5	MAP3K1
SYK	STK4	RYK	IHPK3	C19orf35
SRPK1	PIK3C3	NME7	STK24	GALK2
RPS6KA2	PLK2	ERK8	FLJ32685	MAP2K5
MAP4K2	EPHA7	CDC2L2	ACVR1C	XYLB
CDK8	MFHAS1	PRKCH	PRKCG	GSK3A
ADRBK1	ASB10	CDK10	MELK	EIF2AK3
TAF1L	AURKC	RP26	FLJ16518	AURKB
LOC283846	MAP2K7	AKT3	ADK	MAP2K1
GALK1	CNKSR1	PLXNA2	PRKCZ	PIK3AP1
COL4A3BP	IKBKG	LOC375328	FLJ34389	TESK1
ALS2CR2	FGFR1	LOC391295	DGKI	LOC390877
PIK3R4	MAPK7	NEK5	FRK	IRAK2
ROR2	TLK2	STK6	PIM3	NRK
RPS6KA1	ERBB2	NEK6	PIP5KL1	MAPK9
TOPK	AKAP28	PRKDC	RPS6KB1	MAP3K7IP2

Figure 4.1

4.2.2. Validation of FGFR3 kinase in the regulation of silencing activity

To validate the effect of FGFR2 and FGFR3 depletion on Ago2 function, I obtained new and certified siRNAs from another commercial source. Moreover, instead of using HeLa cells (which were used for the initial screen), I used HEK293T cells for the validation assay. Finally, instead of measuring cell survival as the output for Ago2 activity, a GFP-based assay was employed. Changing these parameters minimized the chances of a false positive result in the validation assay.

The validation assay involved measuring the expression of a destabilized form of GFP (dsGFP) during various treatments (siRNA transfection or kinase gene over-expression). To be able to evaluate both types of silencing, two dsGFP reporters were created for the assays; one for endonuclease-dependent and one for endonuclease-independent silencing activity. The dsGFP reporter for endonuclease-independent RNAi activity was previously described in section 3.2.4; hereafter this reporter will be referred to as dsGFP-NonSlicer. The dsGFP plasmid designed to measure endonuclease-dependent RNAi activity has a single site that is perfectly complementary with a Dicer-substrate siRNA that was engineered not to target any mammalian (including human) genomic sequences; hereafter this reporter will be referred to as dsGFP-Slicer. GFP expression from dsGFP-Slicer and dsGFP-NonSlicer are only silenced when a specific siRNA is co-transfected with the reporter plasmids. GFP expression in transfected cells was measured using flow cytometry.

HEK293T cells were co-transfected with the plasmids pBFP-N1, dsGFP-Slicer or dsGFP-NonSlicer and various amounts of the siRNA that targets the dsGFP reporters. Cells were transfected using molar ratios of plasmids that ensured that cells expressing

BFP were also co-transfected with the dsGFP reporters and siRNA. Twenty-four hours post-transfection, dsGFP and BFP expression were determined by flow cytometry after which the level of GFP expression was normalized against BFP. The benchmark used for maximum GFP expression was cells transfected with reporter plasmids but no siRNA. Data in figure 4.2A shows that both dsGFP reporters are silenced proportionately to the amount of siRNA added. As expected, dsGFP-Slicer was more strongly silenced than dsGFP-NonSlicer, needing approximately ten-fold less siRNA to silence the reporter to ~50% of expression. This is because Ago2-mediated cleavage of mRNA targets is more efficient that translational repression (Broderick et al. 2011). Moreover, by controlling the siRNA that targets the reporter, I could use any cell line that is readily transfected. Furthermore, controlling the siRNA allowed me to control the level of silencing observed, since both RNAi reporter plasmids are repressed in an siRNA dose-dependent manner (Figure 4.2 A).

To further investigate the effect of FGFR3 on Ago2 activity, levels of FGFR3 were reduced by siRNA transfection and RNAi activity was measured as described above. Briefly, HEK293T cells were reverse-transfected with an siRNA against FGFR3 or a non-targeting siRNA (negative control). Twenty-four hours post-seeding, the cells were co-transfected with pBFP-N1, dsGFP-Slicer or dsGFP-NonSlicer, and siRNAs against the silencing construct. The reporter-specific siRNA was used at a concentration previously determined to silence the reporter approximately 50% compared to the negative siRNA control. The molar ratios of plasmids in the transfection ensured that all BFP-expressing cells were co-transfected with the dsGFP-based reporters and siRNA. Expression of dsGFP and BFP were determined by flow cytometry 24 hours after transfection, followed

by normalization of GFP against BFP. In cells with normal levels of FGFR3, GFP-silencing was calculated by dividing the normalized GFP signal from cells transfected with siRNA against normalized GFP signal from cells without siRNA. Silencing in cells with normal levels of FGFR3 was used as control, therefore it was set as 100% relative silencing. The same procedure was used to determine reporter silencing in cells with reduced levels of FGFR3, and the relative silencing activity was expressed compared to the cells with normal levels of FGFR3.

Using this assay, I was able to validate that FGFR3 acts as an inhibitor of endonuclease-dependent Ago2 activity (Figure 4.2 B). Cells with reduced levels of FGFR3 protein had higher silencing activity than cells with normal levels of FGFR3. Interestingly, endonuclease-independent silencing was not significantly affected by decreasing levels of FGFR3. These results suggest that the effect of FGFR3 may be restricted to Ago2.

Since all FGFRs activate the same downstream pathways (Figure 1.5), it is likely that if one of the FGFRs inhibits RNAi activity, the other receptors will inhibit RNAi as well. As mentioned above, in the kinase screen, FGFR2 had a similar effect on RNAi as FGFR3. Unfortunately, in HEK293T cells, the level of FGFR2 was too low to produce any effect on RNAi by further knocking down FGFR2 levels using siRNAs. Therefore, to further validate the effect of FGFRs on silencing, I measured silencing activity in cells overexpressing FGFRs.

Figure 4.2 Validating FGFR3 as a regulator of RNAi using dsGFP-based reporters. **A)** The endonuclease-dependent and endonuclease-independent dsGFP reporters (dsGFP-Slicer and dsGFP-NonSlicer respectively) are silenced proportionately to the amount of siRNA transfected (n=1). **B)** Using dsGFP-Slicer and dsGFP-NonSlicer reporters, endonuclease-dependent and -independent silencing, was measured in HEK293T cells with normal or reduced levels of FGFR3. The bar graph represents the silencing of dsGFP-Slicer or dsGFP-NonSlicer in cells with FGFR3 knockdown relative to dsGFP-Slicer or dsGFP-NonSlicer in cells with normal levels of FGFR. Paired student's two-tailed t-test was used to compare the relative silencing, * $p < 0.05$. Error bars indicate SE.

A)

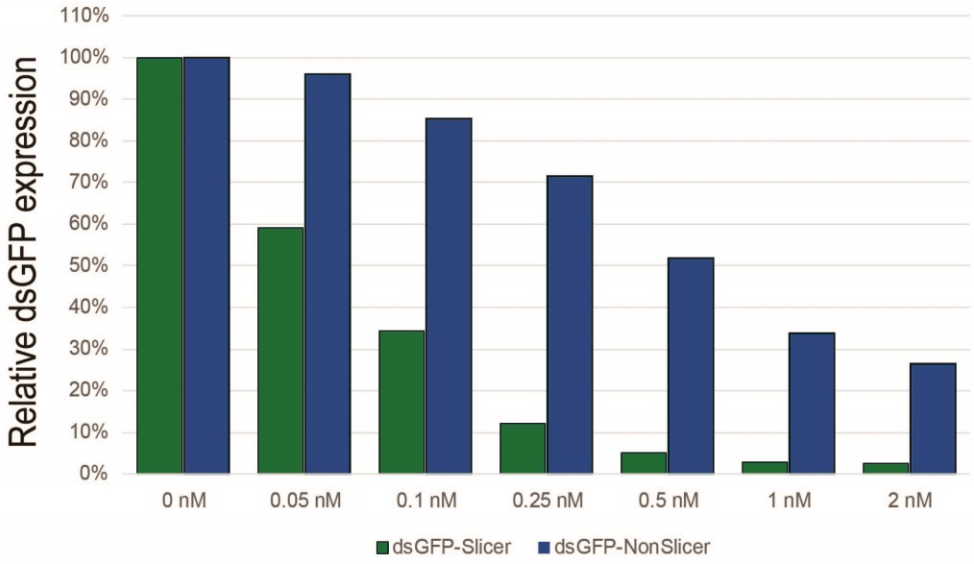
110%
100%
90%
80%
70%
60%
50%
40%
30%
20%
10%
0%
Relative dsGFP expression
0 nM
0.05 nM
0.1 nM
0.25 nM
0.5 nM
1 nM
2 nM
dsGFP-Slicer
dsGFP-NonSlicer

B)

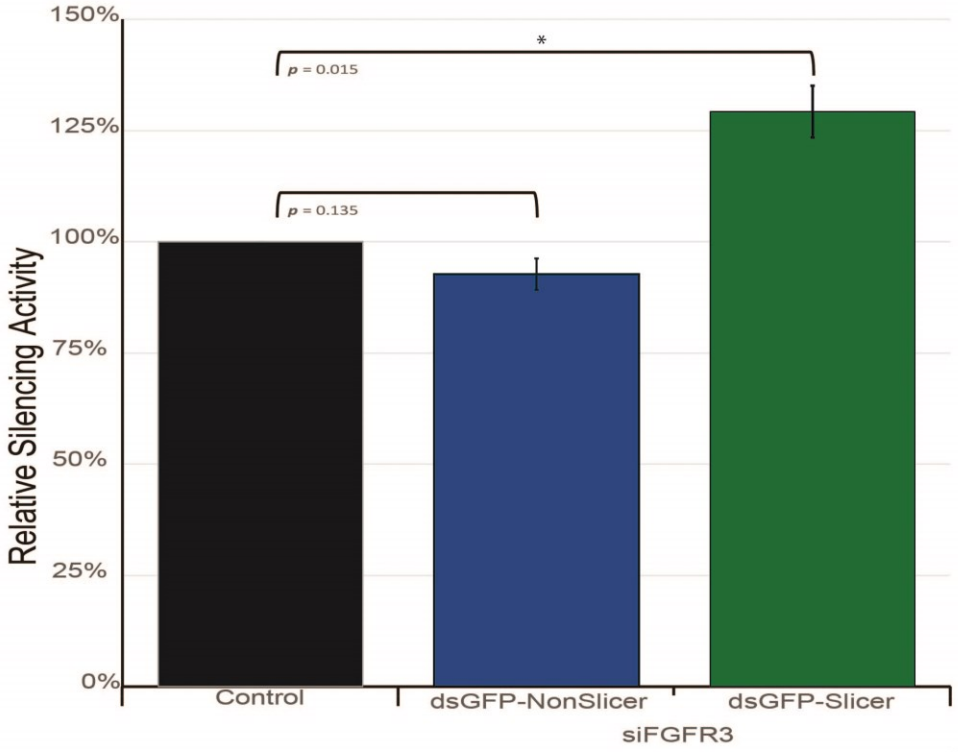
150%
125%
100%
75%
50%
25%
0%
Relative Silencing Activity
*
p = 0.015
p = 0.135
Control
dsGFP-NonSlicer
dsGFP-Slicer
siFGFR3

Figure 4.2

4.2.3. Ectopic expression of FGFR2 and FGFR3 impair endonuclease-dependent and endonuclease-independent silencing activity

If reducing expression of FGFRs increases RNAi activity, then overexpressing FGFRs should decrease RNAi activity. FGFRs become activated after dimerization and high concentrations of FGFRs increase the chances of their dimerization and activation. I used the dsGFP-based assay to evaluate the effect of transient overexpression of FGFRs on silencing activity. As a control, cells were also transfected with a plasmid that encodes DsRed, a non-toxic protein that should not affect RNAi. Also, introducing the DsRed plasmid was necessary to control for promoter competition from the FGFRs plasmids, because all plasmids in this assay (including the reporter plasmids) contain the same CMV promoter.

HEK293T cells were co-transfected with the pBFP-N1, pcDNA 5/TO/ FGFR2 or pcDNA 5/TO/ FGFR3 (or pDsRed-C1-Monomer as control), pdsGFP-Slicer or pdsGFP-NonSlicer, and ± siRNA. The siRNA was used at a predetermined amount sufficient to achieve approximately 50% silencing of the reporter. Again, the molar ratios of plasmids in the transfection ensured that all BFP-expressing cells were co-transfected with the FGF receptor, dsGFP-based reporters and siRNA. Expression of dsGFP and BFP was determined using flow cytometry 24 hours after transfection, followed by the normalization of dsGFP against BFP. In the cells expressing DsRed, silencing activity was calculated by dividing the normalized dsGFP from cells transfected with siRNA against normalized dsGFP from cells without siRNA. Silencing activity in cells expressing DsRed was used as the reference point and was set as 100% relative silencing activity. The same

procedure was used to calculate silencing in cells expressing FGFR2 or FGFR3, and their relative silencing activities were expressed compared to the cells expressing DsRed.

As expected, overexpression of FGFR2 and FGFR3 inhibited RNAi silencing. Moreover, this was the first time that I observed inhibition in both endonuclease-dependent and endonuclease-independent silencing (Figure 4.3). The effect of FGFR2 on silencing was stronger than that of FGFR3, reducing both types of silencing by approximately 40% compared to a 25% reduction by FGFR3. Overall, these data further demonstrate that FGFRs regulate activity of RNAi. The next step was to measure silencing after activation of FGFRs by FGF ligand.

Figure 4.3 Ectopic overexpression of FGFR2 and FGFR3 inhibit RNAi silencing activity. HEK293T cells were transiently transfected with plasmids encoding FGFR2, FGFR3 or DsRed together with dsGFP-Slicer or dsGFP-NonSlicer with or without siRNA. Relative endonuclease-dependent (**A**) and -independent silencing (**B**) was measured in cells ectopically overexpressing FGFR2 or FGFR3 compared to cells overexpressing DsRed. Paired student's two-tailed t-test was used to compare the relative silencing, * $p < 0.05$; ** $p < 0.01$. Error bars indicate SE.

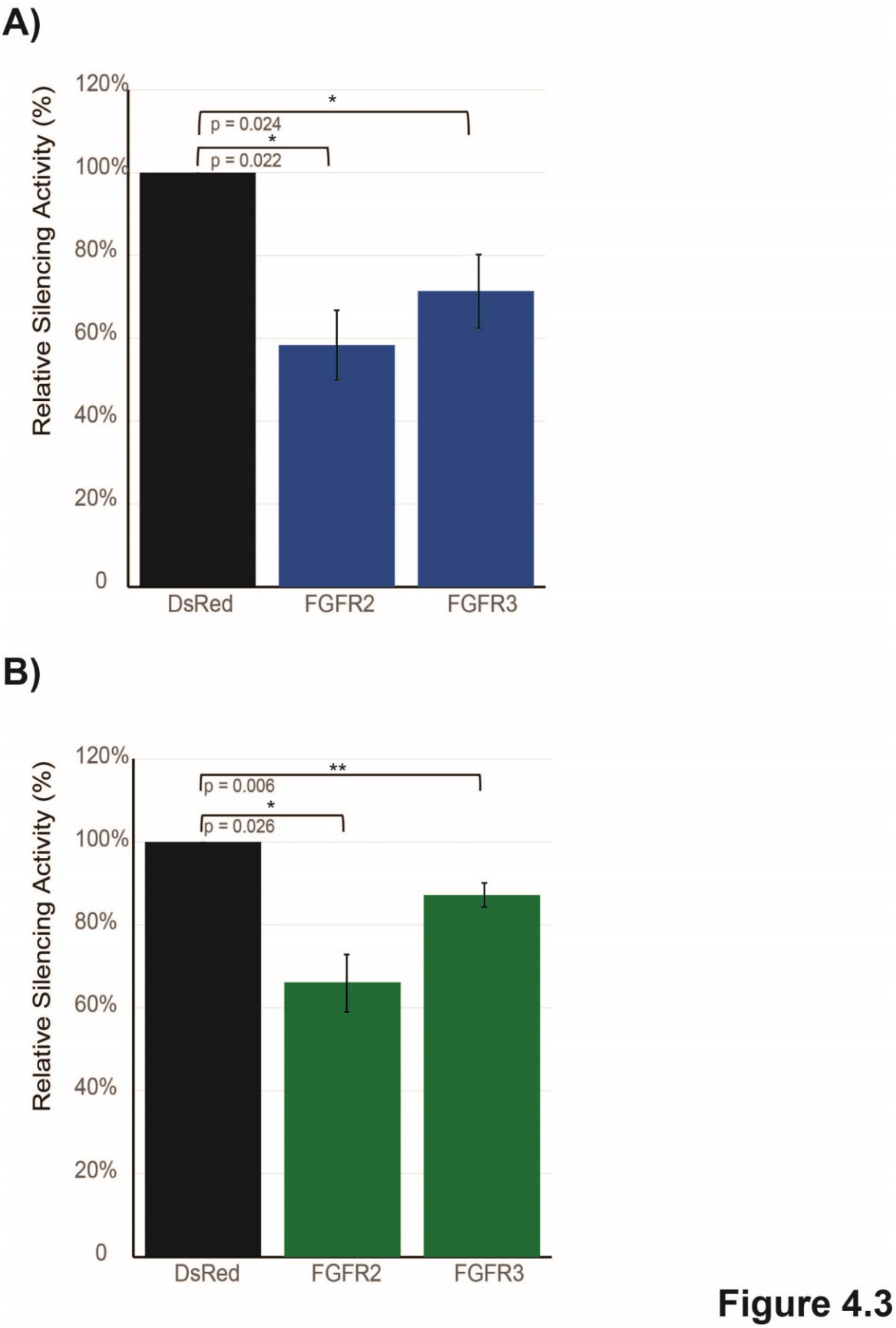
A)
Relative Silencing Activity (%)
120%
100%
80%
60%
40%
20%
0
*
p = 0.024
*
p = 0.022
DsRed
FGFR2
FGFR3
B)
Relative Silencing Activity (%)
120%
100%
80%
60%
40%
20%
0
**
p = 0.006
*
p = 0.026
DsRed
FGFR2
FGFR3

Figure 4.3

4.2.4. FGF1 ligand-dependent signaling inhibits RNAi

In vivo, cells communicate via chemical signals, some of which are growth factors; small secreted polypeptides that bind to the extracellular domains of membrane receptors to activate intracellular pathways. Members of the FGF ligand family bind to and activate FGFRs (Goetz et al. 2009). Receptor activation stimulates downstream pathways that primarily induces cell proliferation and survival (Borello et al. 2008, Feng et al. 2013, Feng et al. 2015, Nagamatsu et al. 2015). In an effort to mimic *in vivo* FGFR activation, FGF1 ligand was added to the media of cultured cells and relative silencing activity was determined using the dsGFP reporter system described above.

FGF1 was used for these experiments because it is the only known FGF ligand that activates all FGFRs (Ornitz and Itoh 2015). Accordingly, its effect should be the result of simultaneous activation of all FGFRs in the cells. HEK293T cells were co-transfected with the plasmids pBFP-N1, dsGFP-Slicer or dsGFP-NonSlicer, and siRNA (or not) to silence the reporter to approximately 50% expression. As before, the molar ratios of plasmids in the transfection ensured that all BFP-expressing cells were co-transfected with the dsGFP-based reporters and siRNA. Twenty-four hours post-transfection, cells were supplemented with fresh media ±125ng/mL FGF1 ligand. Expression of dsGFP and BFP was determined by flow cytometry 24 hours after FGF1 treatment, followed by normalization of dsGFP against BFP. Silencing activity was calculated by dividing the normalized dsGFP from cells transfected with siRNA against normalized dsGFP from cells without siRNA. Silencing in cells not treated with FGF1 was used as control and was set to 100% relative silencing. The same procedure was used to calculate silencing in cells supplemented with FGF1 ligand. The silencing activity after FGF1 treatment was

expressed relative to the control cells. To further validate the inhibitory effect of FGF1 on RNAi, I employed an FGFR inhibitor in the silencing assays. Here, silencing was measured in HEK293 cells following the same procedure described above for figure 4.4A. As indicated, cells were treated with or without the pan-FGFR inhibitor BGJ-398. The results show that the negative effect of FGF1 on RNAi is completely blocked by the pan-FGFR inhibitor (Figure 4.4C).

The data in figure 4.4 show that the activation of endogenous FGFRs inhibits endonuclease-dependent and -independent silencing. Addition of FGF1 reduced endonuclease-dependent silencing by ~26% and endonuclease-independent silencing by ~30%. Although FGF1-dependent inhibition of endonuclease-independent silencing appeared to be slightly stronger than inhibition of endonuclease-dependent silencing, the difference was not statistically significant. These data indicate that Ago2 activity can be inhibited by physiological activation of FGFRs.

A recent study reported that the EGFR inhibits RNAi activity in a manner that is associated with poor prognosis of breast cancer patients (Adams, Claffey and White 2009). FGF and EGF receptors share multiple similarities. Both are membrane-anchored tyrosine kinases that are activated by extracellular ligands. Moreover, they share multiple downstream pathways (Carraway and Cantley 1994, Chen et al. 1987, Dudka, Sweet and Heath 2010). Although it would be tempting to speculate that FGFRs act the same manner as EGFR, this is unlikely because EGFR is proposed to inhibit RNAi by blocking loading of “long loop” miRNAs onto Ago proteins. However, the assay used here to measure silencing activity relies on Dicer substrate siRNAs, which are non-loop-pre-miRNA

synthetic mimics. Based on what we know from (Shen et al. 2013), EGFR-dependent inhibition of Ago2 would not be observed when using Dicer substrate siRNAs.

Figure 4.4 FGF1 ligand inhibits RNAi even though Ago protein levels increase. A) HEK293T cells were transiently transfected with the plasmids pBFP-N1; dsGFP-Slicer or dsGFP-NonSlicer; ±siRNA. Twenty-four hours post-transfection the cells were treated with or without FGF1 ligand. Endonuclease-dependent and -independent silencing was measured 24h after FGF1 treatment by assaying GFP expression from dsGFP-Slicer and dsGFP-NonSlicer plasmids. The bar graphs represent the relative silencing of dsGFP-Slicer or dsGFP-NonSlicer in FGF1- or mock-treated cells. Paired student's two-tailed t-test was used to compare the relative silencing, *** $p < 0.001$; **** $p < 0.0001$. Error bars indicate SE. **B)** HEK293T cells treated with or without FGF1 for 24h were lysed and subjected to SDS-PAGE and immunoblotting for Agos and actin proteins. Signal intensities for Ago were normalized against the level of actin. The numbers below the blot indicate the expression of normalized Agos relative to the -FGF control. n=2. **A)** Following the same approach as in Figure 4.4A, silencing activity was assayed in HEK293T cells. At 24 hours post-transfection, cells were treated with or without FGF1 ligand and/or the Pan-FGFR inhibitor BGJ-398 as indicated. The bar graphs represent the relative silencing of dsGFP-Slicer or dsGFP-NonSlicer in FGF1- or mock-treated cells. Paired student's two-tailed t-test was used to compare the relative silencing, *** $p < 0.001$; **** $p < 0.0001$. Error bars indicate SE. n=3.

A)

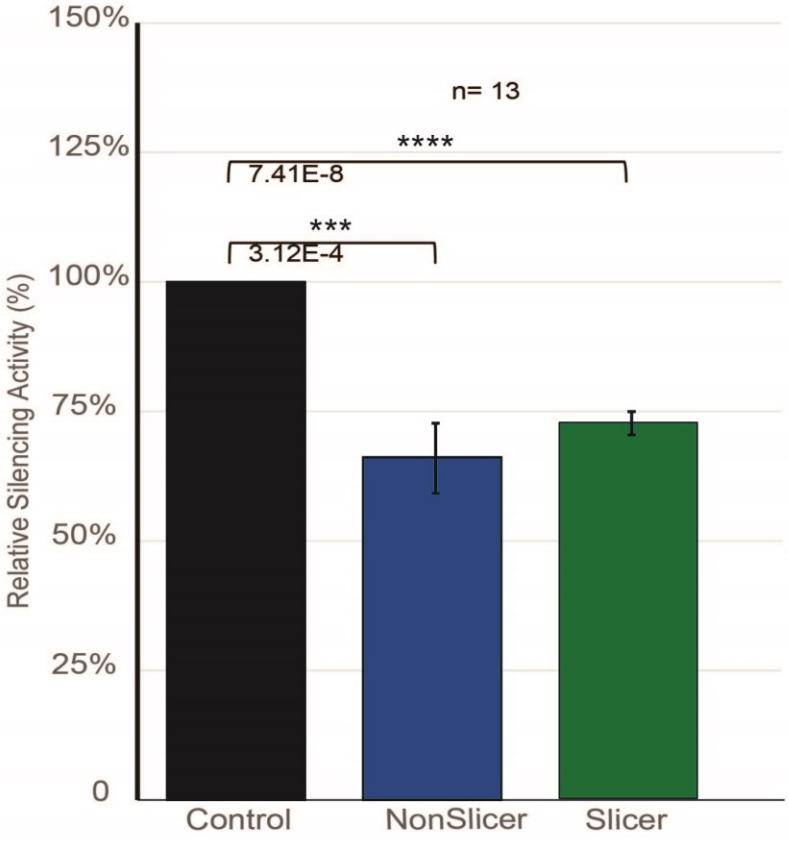
150%
125%
100%
75%
50%
25%
0
Relative Silencing Activity (%)
n= 13
****
7.41E-8
***
3.12E-4
Control
NonSlicer
Slicer

B)

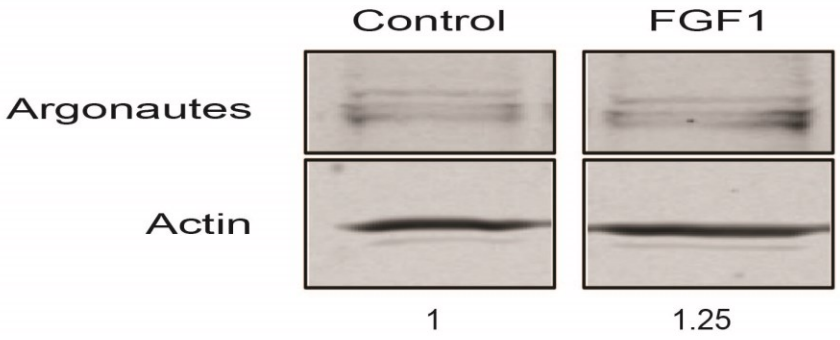
Control
FGF1
Argonautes
Actin
1
1.25

Figure 4.4

Figure 4.4 continued

C)

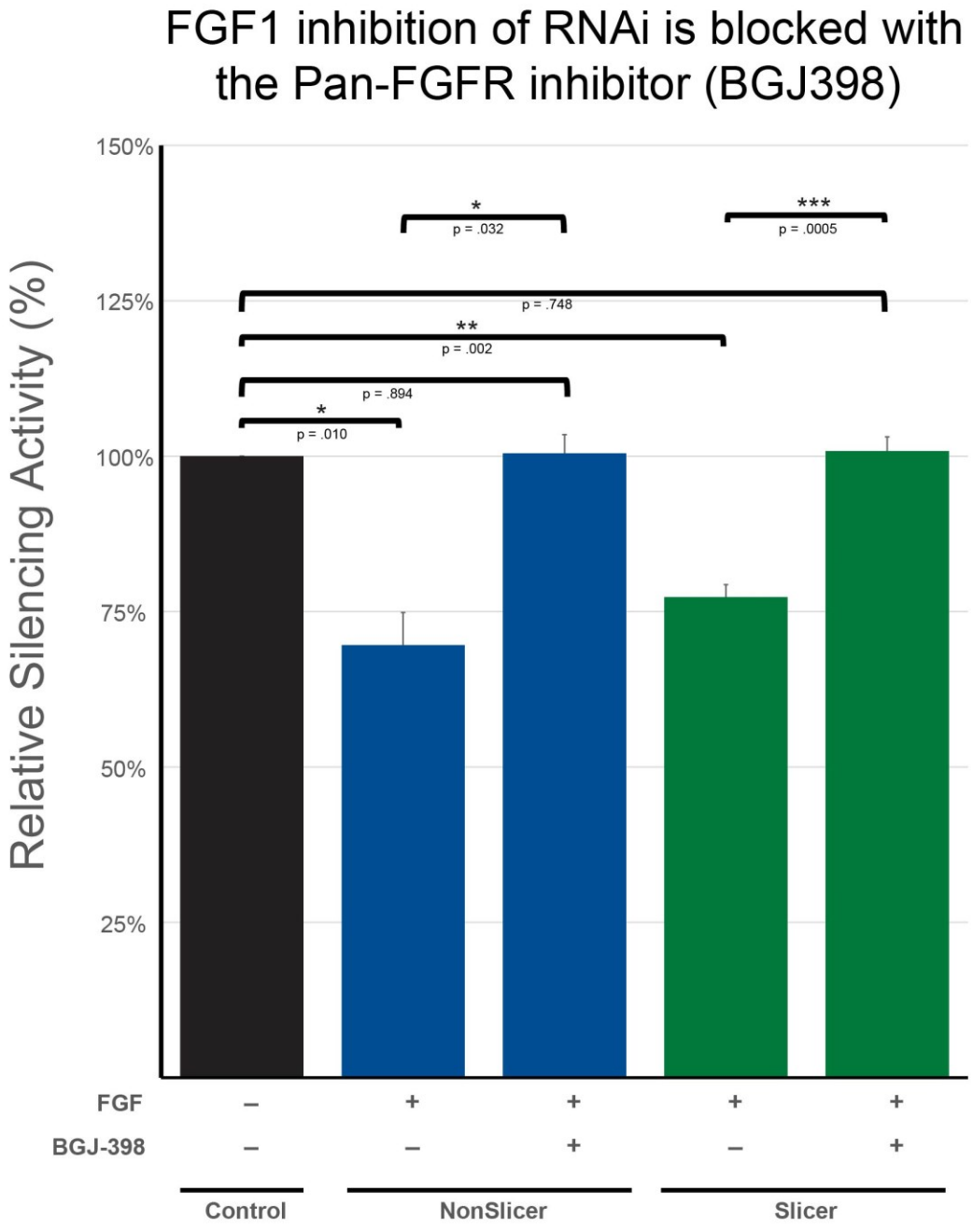

Figure 4.4

4.2.5. FGFR2 and FGFR3 interact with myc-hAgo2

The canonical RNAi silencing mechanism involves endonuclease-dependent cleavage of targeted mRNAs, a process that is performed only by an Ago2 molecule loaded with a small RNA with perfect complementarity to the mRNA. It does not require other cofactors such as GW182 that are involved in endonuclease-independent translational repression of mRNAs (see section 1.1.2.4). Given that FGF receptor activity inhibits endonuclease-dependent and -independent silencing to the same extent, I hypothesized that the effect of FGFR activation is exerted directly on Ago proteins.

Activation of FGFRs can positively or negatively affect different transcription factors, which in turn can alter protein expression. It was possible that the FGF1-dependent inhibition of RNAi was caused by a reduction in the expression levels of Ago proteins. To determine if FGF1 treatment affected Ago protein levels, lysates from HEK293T cells treated for 24h with or without FGF1 were resolved by SDS-PAGE and then subjected to immunoblotting with a pan-Ago antibody. These experiments showed that cells treated with FGF1 actually had higher (25% more) levels of Ago proteins, but 30% less silencing activity. Based on these results, it is possible that FGFRs directly phosphorylate Ago proteins in a manner that inhibits their silencing activities.

If FGFRs phosphorylate Ago proteins, they must physically interact at least briefly. To test whether FGFRs and Ago proteins form stable complexes, I performed co-immunoprecipitation assays. To maximize the changes of detecting interaction, I ectopically expressed Ago2 and FGFR2 or FGFR3 using plasmids. HEK293T cells were transfected with plasmids encoding myc-tagged Ago2 together with FGFR2 or FGFR3.

Twenty-four hours post transfection, the cells were processed for co-immunoprecipitation using beads conjugated to a myc-antibody, followed by immunoblotting. To control for non-specific binding of FGFR2 or FGFR3 to the beads, I used lysates from cells transfected with plasmids encoding only FGFR2 or FGFR3. Ago2 was selected for the co-immunoprecipitation analysis over the other isoforms of Ago because activated FGFRs inhibit endonuclease-dependent silencing. If this inhibition is accomplished through the phosphorylation of Ago proteins, then Ago2 must be the target as it is the only Ago that has endonuclease activity. Data in Figure 4.5A show that both FGFR2 and FGFR3 co-immunoprecipitated with the Ago2.

To further corroborate the interaction between FGFRs and Ago proteins, I performed reciprocal co-immunoprecipitations -- that is, I used beads crosslinked to FGFR antibodies to immunoprecipitate FGFRs and probe for Ago2 co-immunoprecipitation. Interestingly, under the conditions used for the immunoprecipitations, Ago2 only co-immunoprecipitated with FGFR2 but not FGFR3. This correlates well with the functional analysis shown in figure 4.3, which revealed that ectopically expressed FGFR2 had a stronger inhibitory effect on silencing than FGFR3. However, the lack of co-immunoprecipitation between Ago2 and FGFR3 could be explained by the FGFR3 antibody binding to a region important for the FGFR3-Ago2 interaction. It remains to be determined whether the Ago2-FGFR interaction is direct or additional proteins are involved.

Figure 4.5 Interaction of myc-hAgo2 with FGFR2 and FGFR3. HEK293T cells were transiently transfected with plasmids encoding myc-hAgo2 and FGFR2 or FGFR3. Twenty-four hours later, cell lysates were subjected to co-immunoprecipitation with **(A)** anti-myc antibodies or **(B)** anti-FGFR2 or -FGFR3 antibodies. Bound fractions were subjected to SDS-PAGE and immunoblotting for Ago2, FGFR2 or FGFR3 as indicated. n=2.

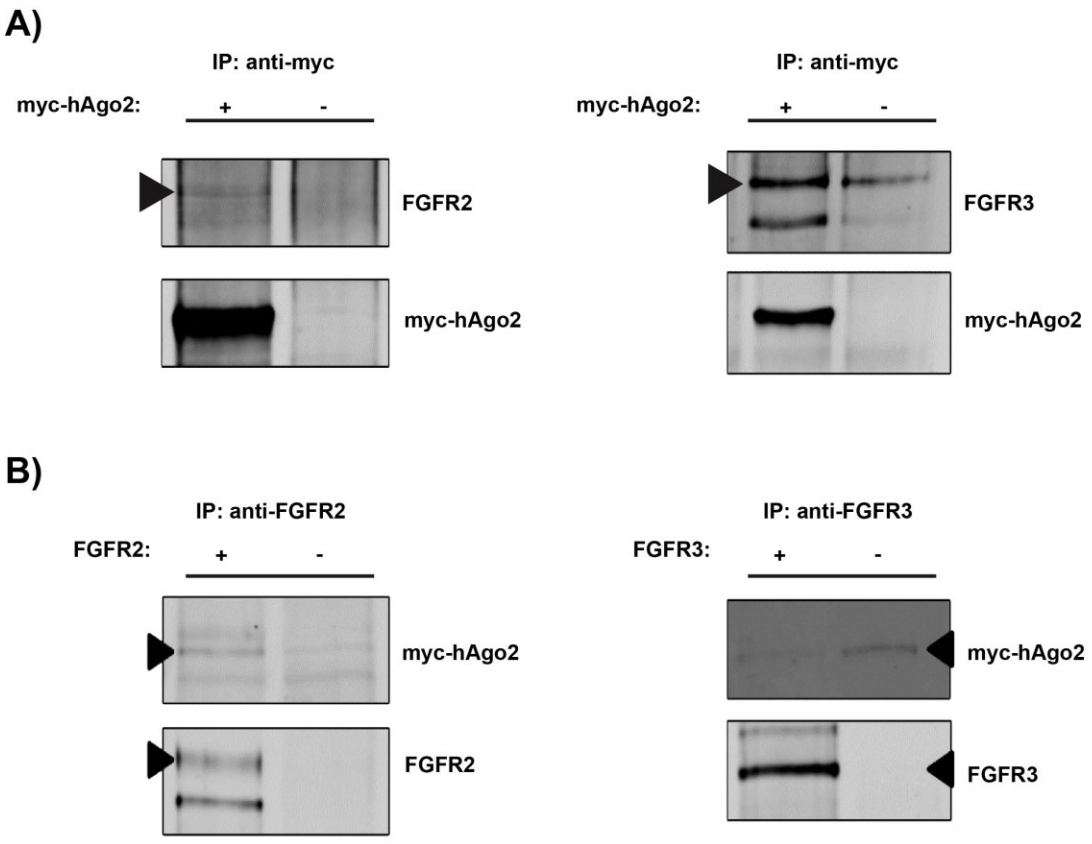
A)
IP: anti-myc
myc-hAgo2:
+
-
FGFR2
myc-hAgo2
IP: anti-myc
myc-hAgo2:
+
-
FGFR3
myc-hAgo2
B)
IP: anti-FGFR2
FGFR2:
+
-
myc-hAgo2
FGFR2
IP: anti-FGFR3
FGFR3:
+
-
myc-hAgo2
FGFR3

Figure 4.5

4.3 Summary

Through a genome-wide screen, I was able to identify several human kinases that affect Ago2 function. A disproportionate number of the inhibitory kinases were tyrosine kinases; an observation that is even more intriguing given that tyrosine kinases make up but a small fraction of the total kinome. Two members of FGFR family that had among the strongest inhibitory effects on Ago2 activity were further investigated. Using different silencing assays, I confirmed that FGFR2 and FGFR3 inhibit Ago2 activity and thus validated the results obtained from the initial kinase screen. Ligand (FGF1)-induced activation of FGFRs inhibited endonuclease-dependent and endonuclease-independent reporter gene silencing to the same extent, suggesting that the mechanism involves a component(s) shared in both pathways. This is likely to be Ago proteins. Consistent with this theory, I showed that Ago2 forms a complex with FGFR2.

Presently, it is unknown which amino acid residue(s) are modified on Ago proteins by FGFRs. Since FGFRs inhibit endonuclease-dependent and -independent silencing, it can be assumed that this mechanism does not involve blocking endonuclease activity or promoting one form of silencing over the other as has been suggested for phosphorylation of Serine 387.

Chapter 5

PP1 inhibits RNAi activity
(Unpublished data)

5.1 Rationale

Evidence from our lab and others shows that phosphorylation is a major regulator of RNAi (Lopez-Orozco et al. 2015, Rüdel et al. 2011, Paroo et al. 2009). However, most of the research has been focused on the identification of kinases. The reversible nature of phosphorylation makes it a dynamic post-translational modification, and dephosphorylation reactions catalyzed by phosphatases, are an integral part of the phosphorylation process (see Chapter 1, Figure 1.4). As with kinase-mediated phosphorylation, protein phosphatases can also have significant consequences for protein activity. Therefore, I investigated the potential roles of phosphatases in RNAi.

Examination of the sequences of human Ago proteins revealed a putative protein phosphatase 1 (PP1)-binding motif. PP1 is one of the most important phosphatases as it has thousands of substrates that are involved in virtually every cellular process (Cohen 2002, Ceulemans and Bollen 2004). The objective of this chapter was to examine the potential roles of PP1 and other phosphatases in Ago2 function.

5.2 Results

5.2.1 PP1 interacts with Ago2

Mammalian Ago proteins contain a putative RVxF PP1 binding motif in their PAZ domains (Figure 5.1A). The crystal structure of Ago2 shows that this motif is accessible on the surface of the protein, which is necessary for interaction with the phosphatase. PP1 binds substrates via the RVxF motif through a binding groove on the opposite side of the catalytic region. If the RVxF motif does in fact mediate binding of PP1, the target

for the phosphatase could be Ago2 or another protein that is in close proximity (Egloff et al. 1997). Regardless of whether Ago2 was a direct target of PP1 or not, it was important to determine whether a PP1-Ago2 interaction could be detected before considering a potential role for this phosphatase in regulation of RNAi.

To test whether Ago2 and PP1 form a complex, I performed co-immunoprecipitations using lysates from HEK293T cells transfected with plasmids encoding myc-Ago2 and GFP-PP1. Following the protocol described in section 4.2.5, I was able to show that PP1α co-immunoprecipitated with Ago2 (Figure 5.1 B). Moreover, the interaction between Ago2 and PP1 does not involve miRNAs because the Ago2 mutant PAZ9, which does not bind small RNAs, also interacted with PP1. Surprisingly, mutating the canonical PP1-binding motif encoded in Ago2 did not block interaction between Ago2-PP1 (Figure 5.1 B).

Figure 5.1 Interaction of myc-hAgo2 with PP1α. A) RVxF motif is conserved among human Ago isoforms. RVXF motifs are highlighted in red letters. **B)** HEK293T cells were transiently transfected with plasmids encoding myc-Ago2 WT, myc-Ago2 PAZ9, myc-Ago2 RARA, GFP-N1, GFP-PP1α or vector alone as indicated on the top of the blots. Twenty-four hours post-transfection, cell lysates were subjected to co-immunoprecipitation with anti-myc antibodies. Bound fractions were subjected to SDS-PAGE and immunoblotting for myc or GFP as indicated.

A)

hs Ago1 241... IDEQPKPLTD SQRVRFTKEI KGLKVEVTHC ... 270
hs Ago2 241... KSIEEQQKPL TDSQRVKFTK EIKGLKVEIT ... 270
hs Ago3 241... IHNIDEQPRP LTDSHRVKFT KEIKGLKVEV... 270
hs Ago4 241... TDSQRVKFTK EIRGLKVEVT HCGQMKRKYR ... 270

B)

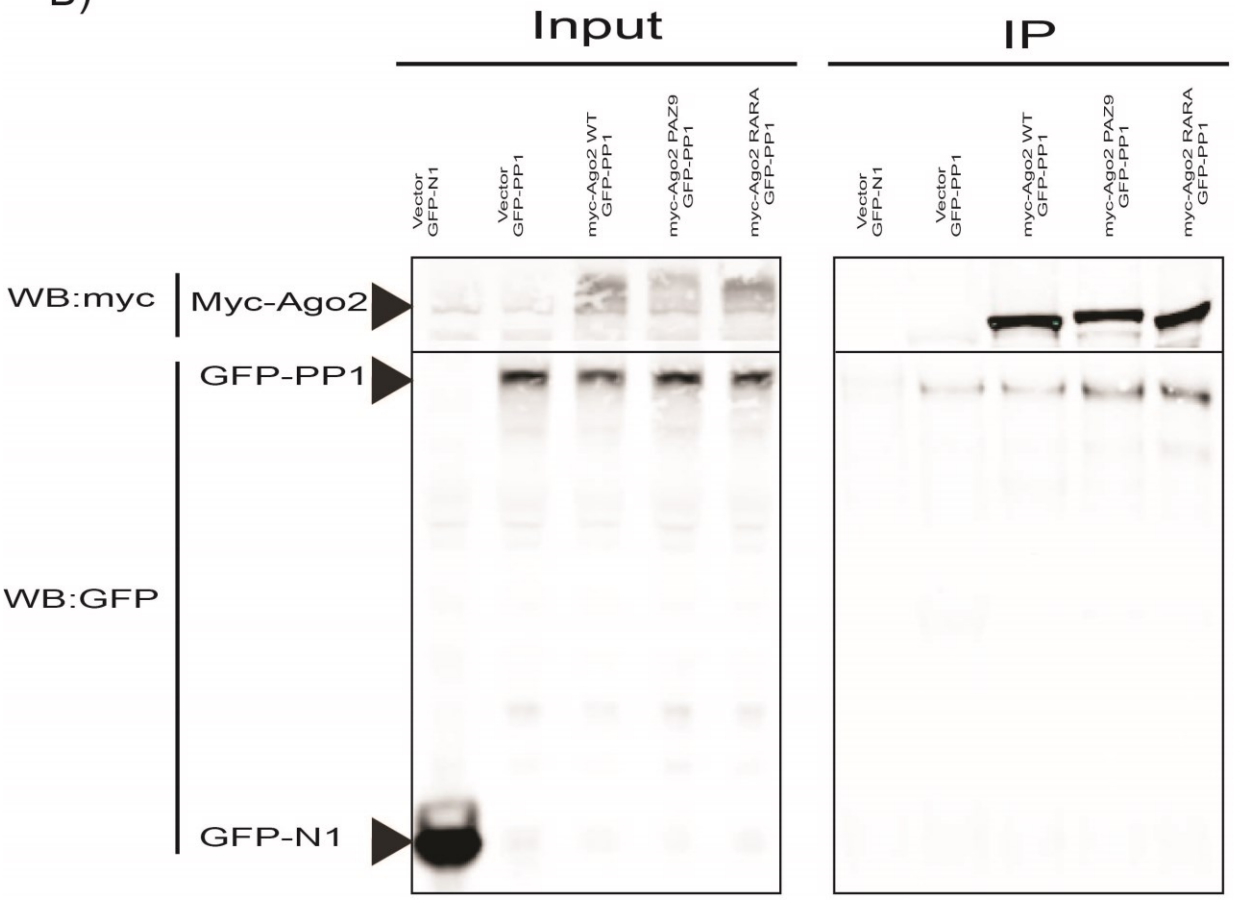

Figure 5.1

5.2.2 PP1α is not recruited to P-bodies.

Agos are known to form stable complexes with proteins that are not present in P-bodies (*i.e.* Dicer, Hsp90) (Pare et al. 2009). Because PP1α can interact with the PAZ9 Ago2 mutant, which is not targeted to P-bodies because it cannot be loaded with small RNAs, it can be concluded that the Ago2-PP1 interaction does not require association with P-bodies. Nevertheless, investigating whether PP1α co-localizes with P-bodies can identify a spatial location where the phosphatase could dephosphorylate and regulate important components of the RNAi machinery. To address this issue, I examined the subcellular localizations of PP1α and Ago2 using confocal microscopy. HeLa cells expressing GFP-PP1α and myc-Ago2 were processed for indirect immunofluorescence 24 hours post-transfection. As shown in figure 5.2, PP1α localized mainly to the cytoplasm in non-membranous foci but was also detected in the nucleus. The PP1α-positive foci did not co-localize with Ago2-positive P-bodies; however, many of the PP1α foci were adjacent to and partially overlapping with P-bodies. The presence of the overlapping regions between P-bodies and PP1α foci is certainly consistent with a scenario by which this enzymes regulates proteins in the RNAi pathway.

Figure 5.2 PP1α is not recruited to P-bodies. HeLa cells transiently transfected with plasmids encoding myc-Ago2 WT and GFP-PP1α or myc-Ago2 WT and GFP-N1 were processed for indirect immunofluorescence microscopy. Panels show localization of myc-Ago2 WT, GFP-PP1α or GFP-N1 as indicated. Axis lines at the bottom left corner represent 10 μm.

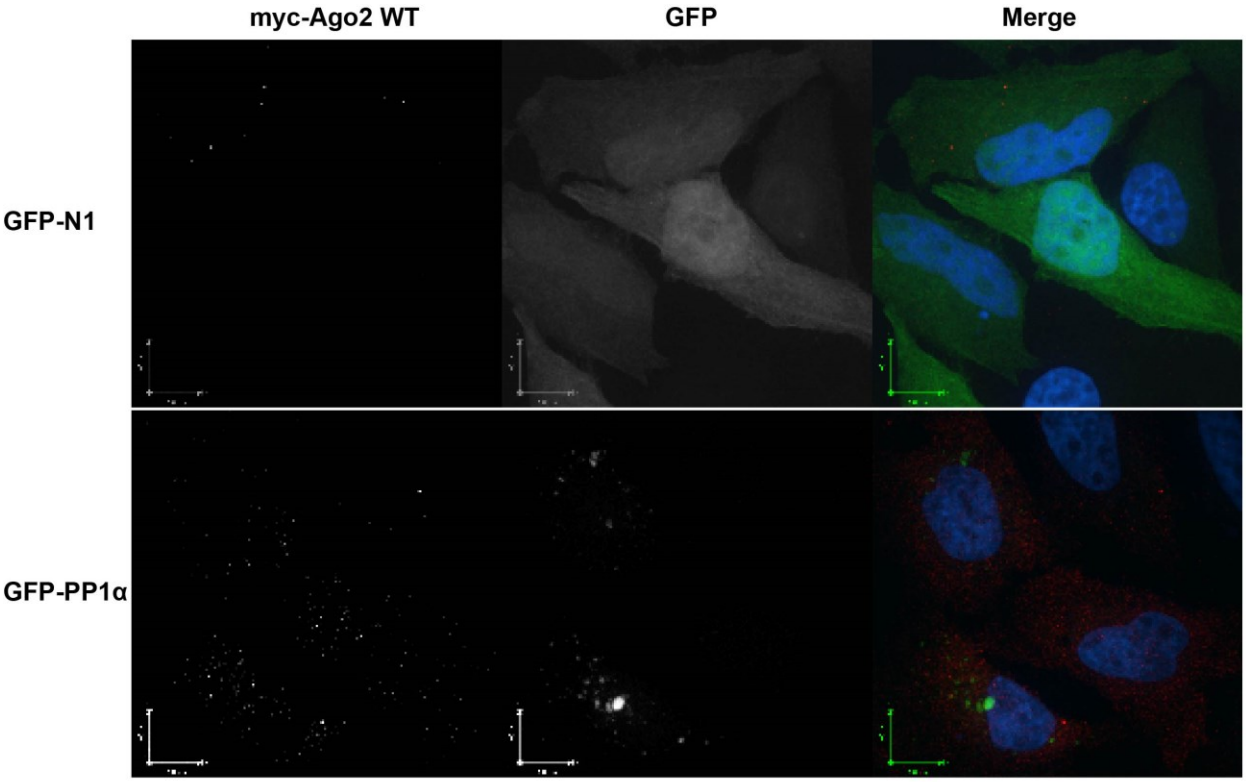

Figure 5.2

5.2.3 Human genome-wide screen identified key phosphatases involved in regulating siRNA-mediated gene silencing

The kinase screen described in Chapter 4 revealed that many kinases affect RNAi activity, mostly in a positive manner. Accordingly, I hypothesized that multiple phosphatases are required to activate and in some cases, inhibit RNAi. Certainly, the data in figures 5.1 and 5.2 showing that PP1 interacts with Ago2 and localizes close to P-bodies is consistent with my hypothesis. In addition to PP1, it is possibly and quite likely that many other phosphatases affect RNAi by acting on Ago2 or other components of the RNAi pathway. Therefore, I employed a screen to determine how expression of all known human phosphatases and their regulatory subunits affect Ago2 activity.

Data in figure 5.3 show the results of the phosphatase screen that used the same output assay as described for the kinase screen described in section 4.2.1. As expected, most phosphatases (~79%) did not have a statistically significant effect on RNAi. Of the 53 phosphatases found to affect Ago2 function, 14 increased RNAi activity and 39 reduced RNAi activity. Consistent with the results of the kinase screen, most of the phosphatases had an inhibitory effect on RNAi, whereas most kinases increased RNAi activity.

The phosphatase siRNA library used in this screen contained siRNAs targeting all known phosphatases: tyrosine phosphatases, serine/threonine catalytic and some regulatory subunits (see section 2.2.11.1). Most of the phosphatases that influenced RNAi are phosphatases of the cysteine-dependent family which comprises the tyrosine and dual function phosphatases (target tyrosine and serine/threonine residues). Moreover, the phosphatases of the cysteine-based family were largely identified as having the most

robust effect, in both increasing and decreasing RNAi activity. Few serine/threonine catalytic or regulatory subunits were identified in the screen and of the subunit hits that were identified, none had a robust effect on RNAi. The bias of these results toward tyrosine phosphatases may be a consequence of the inherent differences between the two types of phosphatases. Whereas cysteine-dependent phosphatases function as monomers with a relatively well defined set of targets, the serine/threonine phosphatases typically function as heterodimers, usually requiring one catalytic subunit and a regulatory subunit. They target a wide variety of substrates depending on the composition of the heterodimer (see section 1.4.1). During the screening process, siRNAs targeted only one protein at the time. This would effectively reduce the activity of a protein that functions as a monomer (i.e tyrosine phosphatases or kinases), but may not be effective for targeting multicomponent holoenzymes such as the serine/threonine phosphatases. The situation may be further compounded by the fact that the regulatory subunits of this family have overlapping functions. Ultimately, due to the nature of the phosphoprotein phosphatase family, this screen may not be well suited for determining their potential activies in RNAi.

Unexpectedly, knockdown of the three PP1 isoforms did not have a statistically significant effect on RNAi function (Figure 5.3 B). On top of the methodological limitations discussed above, the three PP1 isoforms share more than 90% identity at the amino acid residue level (Peti, Nairn and Page 2013). As such, it is possible that PP1 isoforms functionally compensate for each other in the RNAi pathway. Data in figure 5.3 B shows the effect on RNAi after knockdown of PP1 or the other phosphoprotein catalytic subunits. Knockdown of Ago2 is also shown as a positive control. Although RNAi was not significantly affected in this particular assay by knockdown of any of the PP1 isoforms,

reducing PP1α expression had the biggest effect. Therefore, I further investigated the potential role of PP1α on RNAi using over-expression approaches and addition siRNA knockdown experiments.

Figure 5.3 A genome-wide screen identified human phosphatases whose expression affects Ago2-mediated gene-silencing. A) Heat map list with the phosphatases identified in the screen. Phosphatases whose knockdown decreased or increased Ago2 activity are identified in red and green, respectively. **B)** Catalytic subunits of serine/threonine phosphatases values selected from screen data. Ago2 knockdown is shown as a positive control. Error bars represent 95% confidence intervals. The reference bar at the bottom shows the range from the lowest to highest death index obtained in the screen.

A)

PPA2	PPP3CA	PHACTR4
PTEN	NUDT3	ACP6
SKIP	INPP1	PIP3AP
PPP3CC	PPEF2	PPP1R16A
NUDT5	SBF1	DUSP13
IMPA2	ANP32E	PPP3R2
SYNJ1	INPP5A	PFKFB1
PPM2C	ANP32C	PHACTR1
TENS1	PPAP2A	FLJ40125
PDXP	ACP2	PFKFB3
DUSP12	PPP3CB	PPM1F
INPP5B	ALPI	PTPN18
INPPL1	NAP1L5	PTPN6
MTMR9	SYNJ2	G6PC2
OCRL	PPP1R12C	PFKFB4
MTMR8	PHACTR3	ANP32D
TPTE2	TNS	LOC390760
PTPN9	ANP32F	

B)

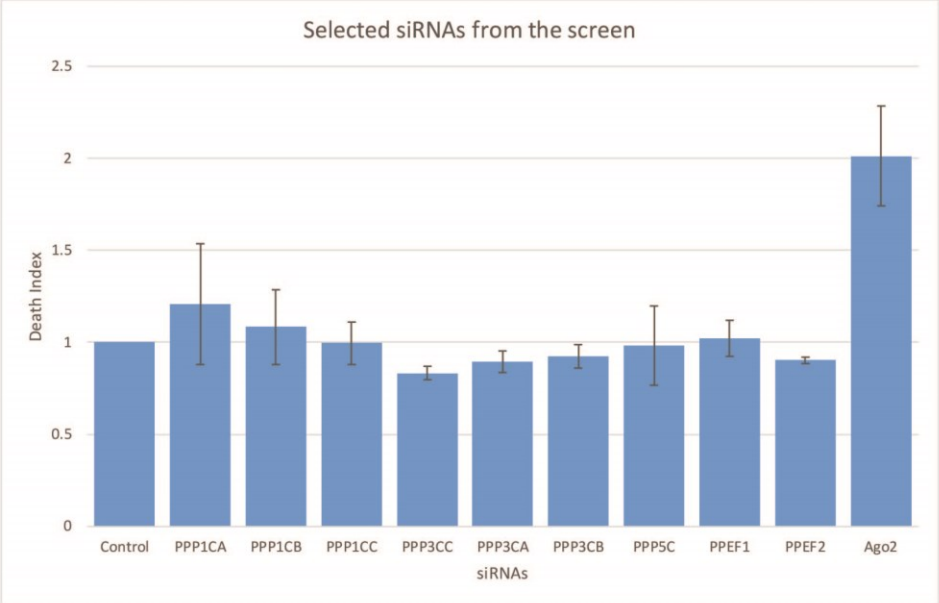

Figure 5.3

5.2.4 Knockdown of PP1α does not affect RNAi activity

Using a new and validated siRNA (different from those used in the screen) against PP1α, I measured endonuclease-dependent activity of Ago2 in HEK293T cells with reduced levels of PP1α. Data in figure 5.4A show that the PP1α-specific siRNA reduced levels of the phosphatase by more than 95%. However, Ago2-dependent endonuclease activity was not significantly affected by knockdown of PP1α (Figure 5.4B). As mentioned earlier, it is possible that the other PP1 isoforms (PP1β and PP1γ) compensate for the reduced levels of PP1α. Therefore, I tested whether ectopic overexpression of PP1α affected RNAi.

Figure 5.4 Reducing PP1α expression does not affect Ago2-dependent gene-silencing activity. A) HEK293T cells were transfected with a PP1α-specific siRNA or a non-targeting control siRNA for 24h after which cells were lysed and subjected to SDS-PAGE and immunoblotting for PP1α and actin. **B)** Using the dsGFP-Slicer and dsGFP-NonSlicer reporter plasmids, the relative endonuclease-dependent activities of Ago2 were assessed in HEK293T cells with normal or reduced levels of PP1α.

A)

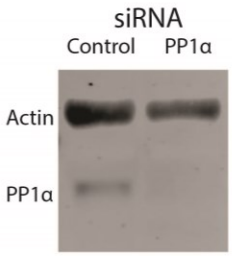
siRNA
Control
PP1α
Actin
PP1α

B)

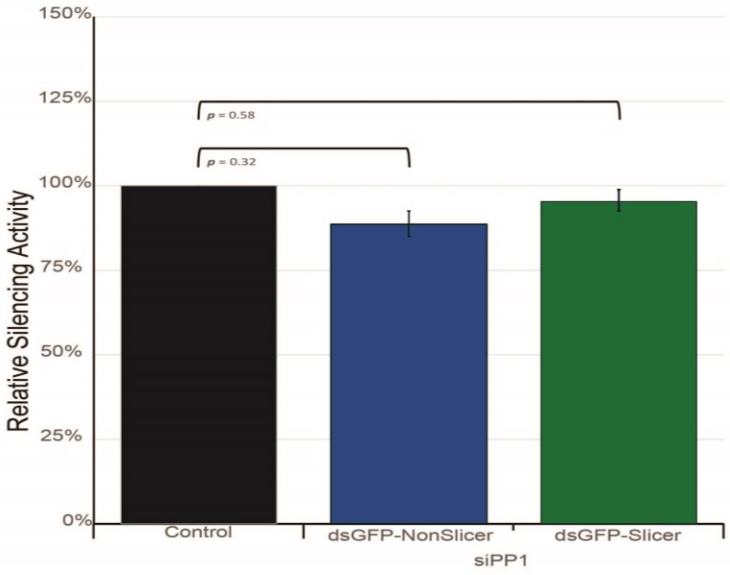
150%
125%
100%
75%
50%
25%
0%
Relative Silencing Activity
p = 0.58
p = 0.32
Control
dsGFP-NonSlicer
dsGFP-Slicer
siPP1

Figure 5.4

5.2.5 Ectopic overexpression of PP1α inhibits RNAi activity.

To further test if PP1 influenced RNAi activity, I resorted to measure RNAi activity on cells overexpressing PP1α. HEK293T cells were transiently transfected with a plasmid encoding PP1α or vector alone (or DsRed) and after 24 hours, RNAi activity was measured using the procedure described in section 4.2.3. Cells over-expressing PP1α exhibited reduced silencing activity (see Figure 5.5B), displaying ~30% less silencing activity in both, endonuclease-dependent and -independent silencing, than control cells. These data suggest the PP1α inhibits the RNAi pathway but it is not clear whether it does so by acting on Ago2 or another component.

Figure 5.5 Ectopic overexpression of PP1α inhibits RNAi activity. HEK293T cells were transiently transfected with plasmids encoding PP1α or DsRed together with dsGFP-Slicer or dsGFP-NonSlicer with or without siRNA against the reporter vectors. Relative endonuclease-dependent and -independent silencing was measured in cells ectopically overexpressing PP1α and compared to cells overexpressing DsRed. Paired student's two-tailed t-test was used to compare the relative silencing, * $p < 0.05$; ** $p < 0.01$. Error bars indicate standard error of the mean.

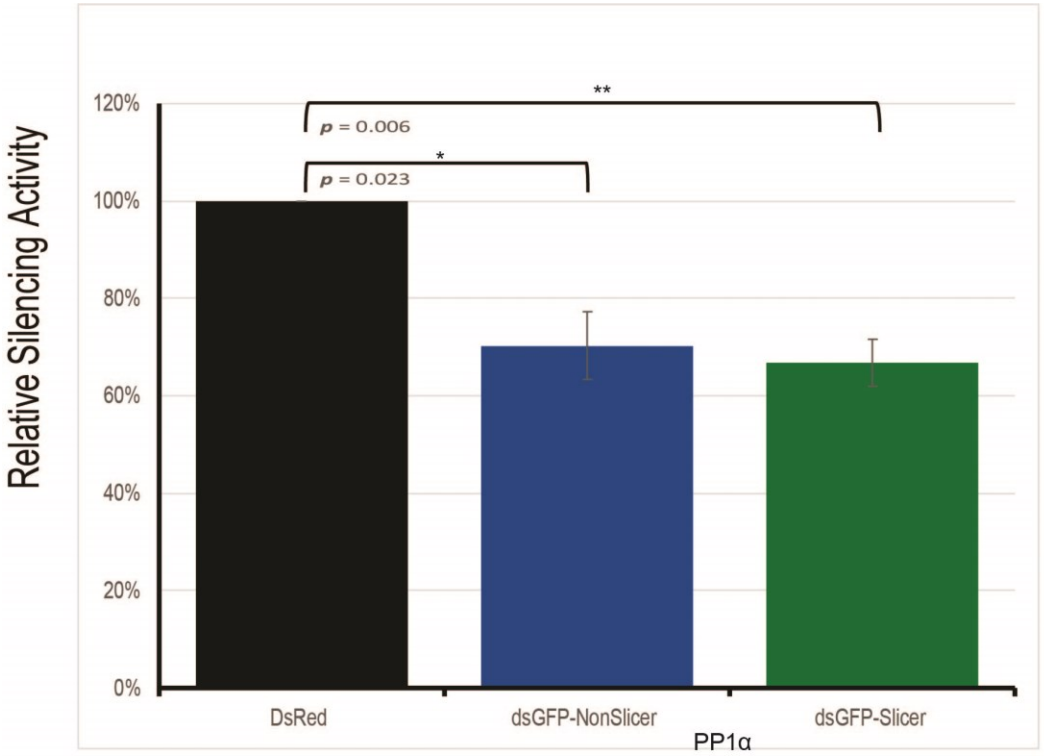
Relative Silencing Activity
120%
100%
80%
60%
40%
20%
0%
**
p = 0.006
*
p = 0.023
DsRed
dsGFP-NonSlicer
dsGFP-Slicer
PP1α

Figure 5.5

5.3 Summary

Mammalian Ago proteins contain a canonical RVxF PP1 binding motif that based on the crystal structure of Ago2 is on the surface of the proteins thereby making it available for PP1 interaction. Using co-immunoprecipitation, I showed that Ago2 interaction with PP1α is not dependent on miRNAs. Unexpectedly, mutating the canonical PP1-binding motif in Ago2 did not affect Ago2-PP1 interaction. While PP1α does not appear to be a component of P-bodies, PP1α–positive foci were observed in close proximity to P-bodies.

To gain a broader view of the regulation of RNAi by phosphorylation, and to complement the kinase data described in Chapter 4, I performed a screen to identify phosphatases involved in RNAi regulation. The results of this screen showed that, of those that had an effect, most phosphatases decreased RNAi activity. Predictably, this is the opposite of what was observed from the kinase screen. The screen overwhelmingly detected proteins of the tyrosine phosphatase family as affecting RNAi; however, it remains unclear whether members of the phosphoprotein phosphatase family were not detected due to their lack of involvement with RNAi or because inherent shortcomings of the screen design. Nevertheless, PTPN6 and PTPN18 tyrosine phosphatases are interesting candidates for future investigation because of the inhibitor effects of receptor tyrosine kinases on RNAi (Monast, Furcht and Lazzara 2012, Luo et al. 2009).

None of the PP1 isoforms were detected as regulators of RNAi in the phosphatase screen. It is possible that this is a false negative because of the nature of the PP1 holoenzyme, or because the three PP1 isoforms have overlapping functions. Using over-expression, I demonstrated that PP1α inhibits RNAi in cultured cell lines. Because PP1

has hundreds if not thousands of substrates that function in all major cellular pathways, it would therefore not unexpected that PP1 also regulates RNAi (Bollen et al. 2010, Ceulemans and Bollen 2004, Cohen 2002, Hendrickx et al. 2009, Küntziger et al. 2006, Peti et al. 2013, Rojas, Vasconcelos and Dever 2015, Tabba et al. 2010, Terrak et al. 2004). Further investigation is needed to determine whether the PP1-Ago2 interaction contributes to the regulation of RNAi or whether other RNAi pathway components are substrates for PP1. Moreover, if Ago2 is the main substrate of PP1 during RNAi regulation, the mechanism by which dephosphorylation of Ago2 inhibits silencing activity is an important mechanism to unravel.

Chapter 6

Discussion

6.1 Overview

The objective of this thesis was to investigate the regulation of small RNA-mediated silencing through phosphorylation of Ago proteins. Agos are highly conserved proteins that form the cores of the RNAi machinery. Using small RNAs to provide specificity, Ago proteins regulate more than half of all human genes at the post-transcriptional level (Friedman et al. 2009). Accordingly, regulation of Ago activity can affect gene expression on a large, potentially global scale. The main hypothesis of my PhD research is that phosphorylation of Ago proteins affects their activities through multiple mechanisms. Consistent with this prediction, several reports that emerged during the course of my research showed that post-transcriptional modifications of Ago proteins affect RNAi (Horman et al. 2013, Rüdel et al. 2011, Zeng et al. 2008, Shen et al. 2013, Qi et al. 2008, Leung et al. 2011, Sahin et al. 2014). Moreover, it has been reported that there are at least seven phosphorylation sites on human Ago2 (Rüdel et al. 2011), many of which are conserved among other Ago proteins in other eukaryotes. One of the unexpected findings from my thesis research is that certain phosphorylation events can dramatically affect the localization of Ago2 while having only a modest effect on RNAi activity. I also discovered a family of receptor tyrosine kinases whose activity significantly inhibits Ago2 function. Specifically, stimulation of FGF receptors decreased the endonuclease-dependent as well as translational repressing activities of Ago2. Finally, the Ago2 binding-protein phosphatase 1 (PP1) was observed to inhibit RNAi activity when over-expressed. However, much still remains to be discovered regarding regulation of Ago proteins by kinases and phosphatases.

6.2 Ago proteins association to RNA granules

RNA granules are non-membranous organelles formed by the accumulation of RNA and RNA binding proteins. There are several types of RNA granules, and their function, as well as composition, is diverse (Section 1.2). For example, while P-bodies and stress granules are present in most cell types, neuronal granules and germinal granules are cell type-specific (Schisa, Pitt and Priess 2001, Navarro and Blackwell 2005). P-bodies are centers for mRNA degradation and are enriched in proteins involved in mRNA decay (Bashkirov et al. 1997, Eystathioy et al. 2002, Ingelfinger et al. 2002, van Dijk et al. 2002b). Stress granules are only formed after exposure to stress and these structures are thought to allow cells to conserve energy by storing and repressing translation of mRNAs that encode non-essential proteins (Kedersha et al. 1999, Nover et al. 1989, Kedersha et al. 2002). Although neuronal granules contain many of the same components as stress granules, they are omnipresent in certain cell types as opposed to being formed after cellular stress (Krichevsky and Kosik 2001). Their function is to shuttle mRNAs away from the nucleus after which they are translated in specific regions of the cytoplasm. However, is important to recognize that all these functions, mRNA degradation, sequestering from translating and shuttling can be performed in the absence of RNA granules. Notably, despite their distinct functions and composition, all RNA granules contain Ago proteins (Liu et al. 2005a, Savas et al. 2010, Leung et al. 2006).

Because the association of Ago proteins with RNA granules was linked to their activity in gene-silencing (Leung et al. 2006, Liu et al. 2005a, Pare et al. 2011b), it was assumed that their association with P-bodies and stress granules is a consequence of RNAi activity. The function of Ago-miRNA complexes is to sequester mRNAs from

translating and/or target them for degradation, processes that occur in stress granules and P-bodies (Eulalio et al. 2007b). However, the Ago-miRNA complexes can perform these functions outside stress granules and P-bodies (Eulalio et al. 2007a, Eulalio et al. 2007b, Kedersha and Anderson 2002, Mollet et al. 2008). The data presented here are the first to show that Ago proteins that do not associate with RNA granules can still efficiently function in RNAi.

By demonstrating that the ability to carry out RNAi is not sufficient to target Ago2 to RNA granules, I predict that an additional signal is needed to drive association of Ago with P-bodies and stress granules and it is likely that this mechanism is controlled by phosphorylation. In support of this theory, it has been suggested that post-transcriptional modifications on Ago proteins regulate their association to RNA granules. For instance, ribosylation of Ago proteins reportedly regulates their association with stress granules (Leung et al. 2011) and phosphorylation of Ago2 at S387 increases its association with P-bodies (Zeng et al. 2008). However, while phosphorylation at S387 increases targeting to P-bodies, blocking phosphorylation at this site does not affect association of Ago2 with P-bodies (Zeng et al. 2008, Lopez-Orozco et al. 2015). Together, these data are consistent with a model in which Ago localization is not strictly dictated by its gene-silencing activity but rather, other factors are involved in their targeting to these structures. This is potentially an important mechanism as it would result in separate pools of active and inactive Ago proteins to specific regions of the cell.

6.3 New RISC loading model

The major steps of RISC loading are relatively well understood. After pre-miRNAs are exported from the nucleus to the cytoplasm they are processed to mature miRNAs by Dicer in complex with TRBP and/or PACT (Parker, Maity and Bass 2008, Wang et al. 2009, Wilson et al. 2015, Macrae et al. 2006b). MiRNAs duplexes are loaded on Ago proteins, aided by Hsp90 chaperone and its co-chaperones after which the passenger strand is removed (Pare et al. 2009, Pare et al. 2013, Iwasaki et al. 2010, Miyoshi et al. 2010). While we know the sequence of steps in miRNA loading onto Ago complexes, the regulation of this process is less understood. My analyses indicate that interaction of Ago2 with Dicer and Hsp90 can occur in the absence of small RNA loading. Specifically, immunoprecipitation of Ago2-Y529E and PAZ9 mutants (which do not bind small RNAs) also pulled down Dicer and Hsp90. My data also show that while Ago2-WT and the mutant Ago2-S798A co-immunoprecipitated with pre-miRNAs and mature miRNAs, the phospho-mimetic mutant Ago2-S798D co-immunoprecipitated only with mature miRNAs.

A model that accommodates the observations described above is that the Ago-Dicer-Hsp90 complex is assembled prior to interaction with pre-miRNA, which is then delivered to the Ago complex by TRBP and/or PACT (Parker et al. 2008, Yamashita et al. 2011). The rate of pre-miRNA processing into mature miRNA is dependent upon combined signaling through Ago and Dicer proteins (Figure 3.11) (Wostenberg et al. 2012). One of the triggers that may initiate the processing of pre-miRNAs into miRNAs is phosphorylation of Ago2 at S798. If so, this could explain why only mature miRNAs but not pre-miRNAs co-purified with the Ago2-S798D mutant (Figure 3.11). If phosphorylation of S798 indeed triggers rapid processing of pre-miRNAs to miRNAs, then only miRNAs

would be expected to associate with the phosphomimetics mutant Ago2-S798D. However, because the non-phosphorylatable mutant Ago2-S798A, which displays similar RNAi activity to wild type Ago, it is likely that phosphorylation of S798 is not the only signal that induces processing of pre-miRNA by Dicer.

Ago-Dicer-pre-miRNA dwell in a complex, effectively sequestering all of these components from functioning and therefore, it is possible that during this stage, pre-miRNA binds only transiently to the Ago-Dicer complex, and can still exchange with the free pre-miRNA pool until a signal to process the pre-miRNA to miRNA is detected by the complex. The fact that the Ago-Dicer-pre-miRNA complex is stable and can be co-immunoprecipitated together (Figure 3.7 and 3.11), is consistent with a scenario in which a signal is required to trigger Dicer-dependent processing of pre-miRNAs.

Loading of small RNAs onto Ago2 is also regulated by phosphorylation at Y529 (Lopez-Orozco et al. 2015, Rüdel et al. 2011). Together with my own data, which suggests that phosphorylation at S798 affects processing of pre-miRNAs into miRNAs, the data of Rüdel et al strongly support a role for phosphorylation in regulating the loading of Agos. This is a key checkpoint in RISC maturation and as such, the panel of Ago2 phosphomutants created in this PhD research project, promises to be an important tool for further analysis of RISC loading and the regulation of this process.

Figure 6.1 Revised model for loading of small RNAs onto Ago complexes. Prior to interaction with pre-miRNAs, Ago proteins form complexes with Hsp90 and Dicer. Subsequently, pre-miRNAs are delivered to this complex by the Dicer-binding proteins TRBP and/or PACT. After processing of pre-miRNA into mature miRNAs, the Ago-Dicer complex dissociates during or after which loading of Ago with a miRNA duplex occurs. Removal of the passenger strand of the miRNA is the last step in activation of the Ago protein. Kinases play a role in loading small RNAs in part through phosphorylation of Y529 and S798 in Ago.

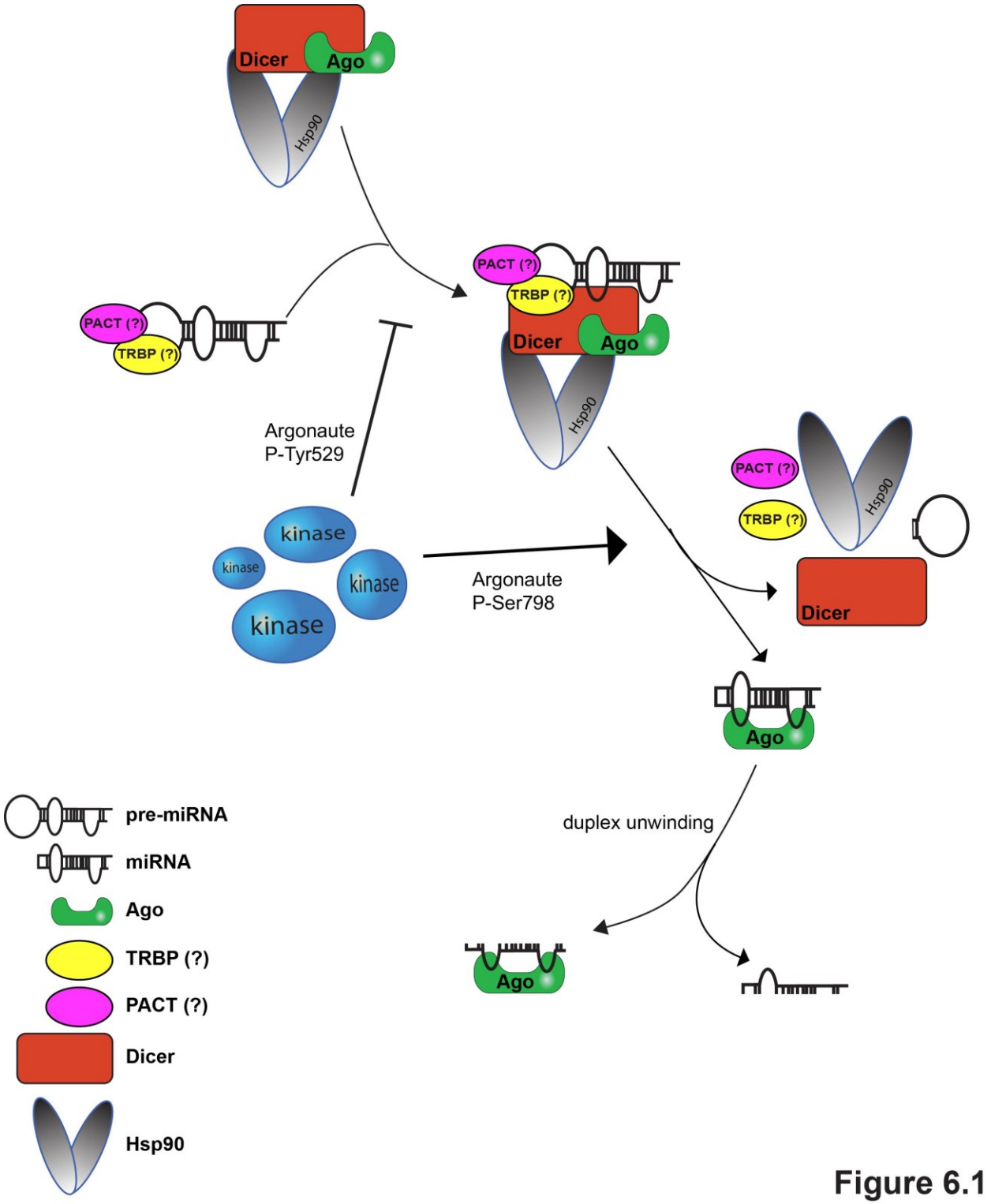
Dicer
Ago
Hsp90
PACT (?)
TRBP (?)
Argonaute
P-Tyr529
kinase
Argonaute
P-Ser798
duplex unwinding
pre-miRNA
miRNA
Ago
TRBP (?)
PACT (?)
Dicer
Hsp90

Figure 6.1

6.4 Reprogramming of Ago proteins in response to extracellular stimuli

In response to external stimuli, cells often transduce signals through intracellular kinase cascades. The organization of these pathways is hierarchical in manner where an upstream kinase activates downstream kinases, which in turn, activate several other downstream kinases and so on until effector proteins are activated. The outcome after activation of a given upstream pathway depends on multiple factors including cell type and the duration of the stimulus. There is now evidence that RNAi pathways are influenced by external stimuli that activate downstream signalling pathways. For example, during cell stress, the P38/Akt pathway regulates RNAi through phosphorylation of Agos and Drosha as well as promoting cell survival (Zeng et al. 2008, Horman et al. 2013, Yang et al. 2015). It is quite likely that other downstream pathways also modulate RNAi.

Several lines of evidence have shown that RNAi can be inhibited by multiple stimuli, including oxidative stress, EGF, or lipopolysaccharide (LPS) treatment (Leung et al. 2011, Shen et al. 2013, Mazumder et al. 2013). My recent data indicate that stimulation of FGF receptors also impairs RNAi activity. While all these stimuli have been proposed to reduce RNAi activity by promoting post-translational modification of Ago proteins, they appear to employ different mechanisms. For example, oxidative stress induces ADP-ribosylation of Ago proteins leading to their sequestration in stress granules (Leung et al. 2011). Conversely, EGF treatment during hypoxia induces phosphorylation of Ago2 at Y393, resulting in reduced maturation and inability to load long-loop miRNAs (Shen et al. 2013). LPS treatment transiently inactivates RISC through phosphorylation of Ago proteins (Mazumder et al. 2013). Significantly FGF, EGF, oxidative stress, and LPS all activate signaling pathways that lead to changes in the transcriptional profiles of cells.

Moreover, EGF and FGF stimulation are known to affect expression of miRNAs (Yin et al. 2008, Bobbs et al. 2012, Nazarov et al. 2013). As such, it is tempting to speculate that in order to efficiently regulate a new cohort of mRNAs, changes to miRNA expression is also required. The kinase screen I conducted led to identification of several receptor tyrosine kinases as well as non-receptor tyrosine kinases that inhibit RNAi activity. Of note, activation of most if not all receptor tyrosine kinases result in changes to the cellular transcriptome (Segatto, Anastasi and Alemà 2011, Yang, Sharrocks and Whitmarsh 2013, Avraham and Yarden 2011, Kholodenko 2009).

Based on the data described above, I propose a model in which FGF, and other stimuli, inhibit RNA-mediated silencing by de-stabilizing Ago-miRNA interactions. In doing so, Agos could be loaded with different miRNAs rather than being inactivated and/or degraded (Figure 6.2). This model proposes a mechanism to recycle Agos by displacing old miRNAs with new miRNAs that are expressed in response to the stimulus. Since activation of receptor tyrosine kinases leads to changes in the transcriptome, one of the predictions of this model is that these kinases should also inhibit RNA-mediated silencing in a way that allows loading of the newly transcribed miRNAs. My preliminary data (Appendix Figure 1) showing that EGF and insulin treatment inhibit RNAi is consistent with this prediction. EGF, insulin, and FGF are ligands that stimulate receptor tyrosine kinases classes I, II and IV, respectively (Robinson, Wu and Lin 2000, Wagner et al. 2013). While it was previously reported that EGF inhibits RNAi activity by phosphorylating Ago2 at Y393, this was found to occur only during hypoxia and only long loop miRNAs were affected (Shen et al. 2013). In contrast, my experiments were conducted using cells treated with EGF under normal oxygen levels and the RNAi assays employed synthetic

miRNAs lacking long loop structures. That fact that EGF also did inhibited RNAi under these conditions may indicate that EGF inhibits RNAi through different mechanisms depending upon oxygen levels. In addition to growth factors, other extracellular stimuli such as cytokines may inhibit RNA-mediated silencing, as they activate some of the same downstream pathways as EGF, insulin, and FGF. Indeed, my preliminary data (Appendix Figure 1) demonstrate that tumor necrosis factor (TNF) inhibits RNA-mediated silencing further supporting my proposed model.

A number of issues regarding the mechanism(s) that promote Ago unloading and RISC reprogramming remain unanswered. For example, do cells use a similar mechanism to reprogram Agos in the absence of receptor activation by external stimuli? Also, the consequences for short-term and long-term cell viability when this process is deregulated remain to be determined. Given that Ago proteins are quite stable (half-lives > five days (Olejniczak et al. 2013)), it is possible that they are recycled and reprogrammed continuously for days. I expect that this process is more important when cells undergo substantial changes to their transcriptome, as opposed to transient upregulation of a few genes. For example, transitioning from one miRNA profile is important for cell differentiation and during development. Given the central role of RNAi-mediated silencing pathways in modulating gene expression on a global scale, a more detailed knowledge of their regulation is warranted.

My studies on growth factors and cytokines and regulation of RNAi have potential relevance to human diseases, in particular cancer. Because of their roles in promoting cell survival, proliferation and apoptotic pathways, unregulated and/or aberrant signalling within growth factor and cytokine pathways are consistently associated with development

and progression of various cancers. As such, pharmaceutical targeting of these pathways, particularly those activated by EGF and FGF, has resulted in substantial benefits to cancer patients (Vermorken et al. 2007, Cunningham et al. 2004, Brady et al. 2013). I predict that further understanding of their roles in RNAi may lead to yet more efficacious therapies and better outcomes for patients.

Figure 6.2 miRNA reprogramming of Agos induced by cell surface receptor activation. Extracellular stimuli trigger membrane receptor activity which in turn, activates multiple downstream kinase signaling pathways. Some of these kinases activate transcription factors, leading to significant changes in expression of mRNAs and miRNAs. Concurrently, other kinase(s) phosphorylate Ago proteins resulting in weakened association with miRNAs. This allows reloading of Agos with new miRNAs. After or during reloading, I predict that Ago proteins are dephosphorylated to allow them to stably bind new miRNAs. Ultimately, the re-loading of Ago coordinates the transition to use the new miRNA cohort to regulate the new mRNA population.

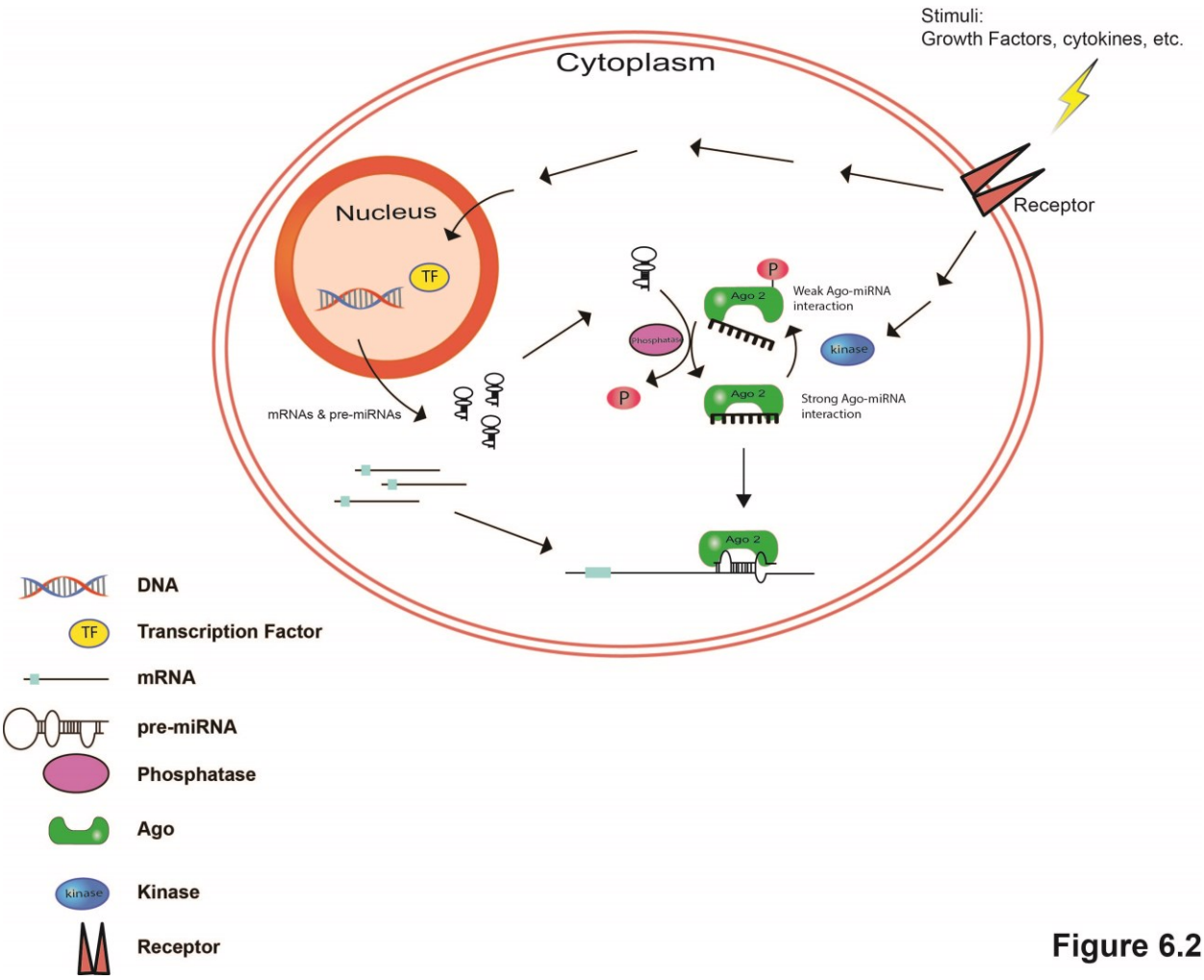
Stimuli:
Growth Factors, cytokines, etc.
Cytoplasm
Receptor
Nucleus
TF
mRNAs & pre-miRNAs
P
Ago 2
Weak Ago-miRNA interaction
Phosphatase
kinase
P
Ago 2
Strong Ago-miRNA interaction
Ago 2
DNA
TF
Transcription Factor
mRNA
pre-miRNA
Phosphatase
Ago
kinase
Kinase
Receptor

Figure 6.2

6.5 Protein phosphatase 1 and Ago2 activity

Protein phosphatase 1 (PP1) catalytic subunit is an indiscriminate serine/threonine phosphatase that is expressed in virtually all mammalian cell types (Cohen 2002, Ceulemans and Bollen 2004). It is one of the most highly expressed proteins in mammalian cells and accounts for a large part of the serine/threonine phosphatase activity (Peti et al. 2013). It is estimated that more than 70% of all cellular proteins are phosphorylated on serine/threonine residues, and therefore, is not surprising that PP1 regulates such a large number of cellular processes including but not limited to: cell cycle, differentiation, transcription, and apoptosis (Sharma et al. 2014). To gain specificity, PP1 forms dimeric and trimeric holoenzymes by binding regulatory subunits (Bollen et al. 2010, Peti et al. 2013). There are more than 200 regulatory subunits and three distinct PP1 isoforms, and together, the different combinations of these proteins allow for a remarkable degree of substrate specificity and control over PP1 activity. A detailed examination of the PP1 biology is not warranted here, however, the potential role in the regulation of RNA-mediated silencing merits discussion.

In light of what was discussed above, it is perhaps not unexpected that PP1 may be involved in the regulation of RNAi, however, this is just starting to be explored. Many of the proteins involved in the RNAi pathway are phosphorylated (Drake et al. 2014, Rüdel et al. 2011, Yang et al. 2015, Herbert et al. 2013, Paroo et al. 2009), although the consequences of such modification are largely unknown. Nevertheless, given that the majority of the phosphatase activity in mammalian cells is provided by PP1 or Protein Phosphatase 2A (PP2A), the involvement of PP1 in dephosphorylating proteins of the RNAi pathway seems highly likely. Data presented in Chapter 5 of this thesis suggest that

PP1 inhibits RNAi activity through an as yet unidentified mechanism. PP1 may affect RNAi activity by modulating AKT and MAPK kinases, both of which are known to phosphorylate Ago proteins (Horman et al. 2013, Zeng et al. 2008). My data also show that Ago2-PP1 interact in an miRNA independent manner. Although Ago2 has a conserved PP1-binding motif (RVxF), the mutation of this site to “RARA”, which was expected to disrupt PP1 binding, did not in fact affect Ago2-PP1 interaction. There are several possible explanations for this result. First, binding of PP1 to Ago2 could be mediated by another site. The PIWI domain of Ago2 contains the tetrapeptide RIIF which is slightly different from RVxF. However, valine and isoleucine have similar structures and it would be of interest to determine if RIIF is required for Ago2-PP1 interaction. Alternatively, the interaction of Ago2 with PP1 could be mediated by PP1 regulatory subunits (Wakula et al. 2003, Rojas et al. 2015). In this case, the regulatory subunits would be expected to bind to Ago2 in a manner that does not involved RVxF motifs (Rojas et al. 2015).

The RVxF motif in the PAZ domain of Ago proteins is located one amino acid residue downstream from a phosphoserine residue (S253). While S253 is too close to the RVxF motif to be acted upon by PP1 (if it bound to this motif), it is tempting to speculate that phosphorylation at S253 controls PP1 binding. In this scenario, PP1 could dephosphorylate proteins that come into proximity to Ago proteins. Previous evidence exists where phosphorylation of the flanking residues of the RVxF motif has been shown to block PP1 interaction (Beullens et al. 1999, Küntziger et al. 2006). Similarly, phosphorylation of Ago next to the RVxF motif, at S253, could impair PP1 binding. The data presented in this thesis suggest a potentially important role for PP1 in the regulation

of the RNAi pathway but we are just beginning to understand this process and further investigation is clearly warranted.

6.6 Future directions and perspective

A great deal of information is to be gained by studying the activity of my panel of Ago2 mutants in knockout cell lines. For example, it should be possible to identify phosphoamino acid residues that play a role in FGF- or other stimuli (EGF, TNF, etc.) mediated inhibition of RNAi. The same approach, but using other Ago mutants, could be used to identify mutants that are refractory to inhibition when overexpressing PP1 or one of its many regulatory partners.

The identification of other phosphorylation sites in Ago2 that regulate miRNA reloading should also be a priority. It is possible for example, that none of the seven known phosphorylation sites in Ago2 are directly or indirectly affected by FGF or the other stimuli described in this thesis. Although not published yet, we have been informed that Ago2 is phosphorylated on additional sites (Dr. Gunter Meister, Universität Regensburg, personal communication). The mass spectrometry analyses of Ago2 that detected the seven known phosphoresidues was performed using extracts from cells grown under “normal” culture conditions (Rüdel et al. 2011). As such, it possible and quite likely that other phosphorylation events in Ago2 would only be detected after cells have been treated with various stimuli (e.g., growth factors, stress). This highlights the importance of studying RNAi in the context of different physiological conditions.

The central hypothesis of my model is that extracellular stimuli triggers reprogramming of Agos with small RNAs. This could be achieved by phosphorylation

and/or other post-translational modifications on Ago proteins. It is conceivable that kinase pathways promote other post-translational modifications on Ago proteins. To account for this scenario, further investigation could employ mass spectrometry analysis to identify posttranslational modifications on Ago proteins when treated with FGF ligand or other stimuli that have been shown to inhibit RNAi. Identification of factors that guide the reprogramming of Ago proteins with new miRNAs is critical for understanding how the RNAi pathway responds to various stimuli and pathological conditions.

Based on the reprograming model, I predict that the pool of Ago in stimuli-treated cells will be loaded with new miRNAs faster than Ago from untreated cells. To test this prediction, northern blots or quantitative PCR can be used to measure the time it requires for newly introduced siRNAs/miRNAs to be loaded onto Ago proteins. Alternatively, reporters encoding proteins with extremely short half-lives could be used to measure silencing soon after new siRNAs/miRNAs are introduced. An example of such a reporter is GFP tagged with a combination of the mouse ornithine decarboxylase PEST signal and the cyclin B destruction box which can reduce eGFP half-life to 1-2 hours (Kitsera, Khobta and Epe 2007). If the model I propose is correct, silencing in stimulated cells should be detected faster than in non-stimulated cells.

Given that most of the stimuli tested here inhibit RNAi to similar levels, it is tempting to speculate that common downstream components are activated by the upstream signaling. Using inhibitors of key downstream kinases, future experiment could identify the pathway(s) used to modify RISC directly. It is possible that several pathways work together, or in a redundant fashion to modify RISC components. Redundancy among pathways would undoubtedly complicate identification of key components, but it is still

worth pursuing. The identification of those pathways will be essential for understanding how the RNAi machinery and global gene-expression are regulated by a combination of extracellular and intracellular cues.

The research in this thesis points to a mechanism that may integrate the RNAi machinery into cellular signaling networks that control transcription in response to environmental stimuli. Moreover, it presents many testable hypotheses regarding the role of Ago phosphorylation as a central point of control for the RNAi pathway. It should be noted that the validation of this working model still requires a great deal of work, however, the more knowledge we gain about RNAi-based gene silencing, the more we will improve our ability to manipulate it and apply this knowledge to unlock its therapeutic potential.

Lastly, it is worth discussing the GFP-based RNAi measuring assay described in Chapter 4 of this thesis. Several assays to measure RNAi-mediated silencing are available, however, to the best of my knowledge, the GFP-based described here is the first system where the level of silencing can be easily and accurately titrated. Moreover, this assay can be used to separate the endonuclease-dependant and -independent silencing activities of Ago2 in virtually any mammalian cell line. Finally, by comparing normal and transformed cell lines, we can further elucidate the role that RNAi plays in cancer progression.

References

Adams, B. D., K. P. Claffey & B. A. White (2009) Argonaute-2 expression is regulated by epidermal growth factor receptor and mitogen-activated protein kinase signaling and correlates with a transformed phenotype in breast cancer cells. *Endocrinology,* 150**,** 14-23.

Adams, J. A. (2001) Kinetic and catalytic mechanisms of protein kinases. *Chem Rev,* 101**,** 2271-90.

Aizer, A., Y. Brody, L. W. Ler, N. Sonenberg, R. H. Singer & Y. Shav-Tal (2008) The dynamics of mammalian P body transport, assembly, and disassembly in vivo. *Mol Biol Cell,* 19**,** 4154-66.

Alonso, A., J. Sasin, N. Bottini, I. Friedberg, A. Osterman, A. Godzik, T. Hunter, J. Dixon & T. Mustelin (2004) Protein tyrosine phosphatases in the human genome. *Cell,* 117**,** 699-711.

Ameres, S. L. & P. D. Zamore (2013) Diversifying microRNA sequence and function. *Nat Rev Mol Cell Biol,* 14**,** 475-88.

Anderson, P., N. Kedersha & P. Ivanov (2015) Stress granules, P-bodies and cancer. *Biochim Biophys Acta,* 1849**,** 861-70.

Andrei, M. A., D. Ingelfinger, R. Heintzmann, T. Achsel, R. Rivera-Pomar & R. Lührmann (2005) A role for eIF4E and eIF4E-transporter in targeting mRNPs to mammalian processing bodies. *RNA,* 11**,** 717-27.

Aravin, A., D. Gaidatzis, S. Pfeffer, M. Lagos-Quintana, P. Landgraf, N. Iovino, P. Morris, M. J. Brownstein, S. Kuramochi-Miyagawa, T. Nakano, M. Chien, J. J. Russo, J. Ju, R. Sheridan, C. Sander, M. Zavolan & T. Tuschl (2006) A novel class of small RNAs bind to MILI protein in mouse testes. *Nature,* 442**,** 203-7.

Ashe, A., A. Sapetschnig, E. M. Weick, J. Mitchell, M. P. Bagijn, A. C. Cording, A. L. Doebley, L. D. Goldstein, N. J. Lehrbach, J. Le Pen, G. Pintacuda, A. Sakaguchi, P. Sarkies, S. Ahmed & E. A. Miska (2012) piRNAs can trigger a multigenerational epigenetic memory in the germline of C. elegans. *Cell,* 150**,** 88-99.

Aukerman, M. J. & H. Sakai (2003) Regulation of flowering time and floral organ identity by a MicroRNA and its APETALA2-like target genes. *Plant Cell,* 15**,** 2730-41.

Avraham, R. & Y. Yarden (2011) Feedback regulation of EGFR signalling: decision making by early and delayed loops. *Nat Rev Mol Cell Biol,* 12**,** 104-17.

Baillat, D. & R. Shiekhattar (2009) Functional dissection of the human TNRC6 (GW182-related) family of proteins. *Mol Cell Biol,* 29**,** 4144-55.

Barber, G. N. (2005) The dsRNA-dependent protein kinase, PKR and cell death. *Cell Death Differ,* 12**,** 563-70.

Bartel, D. P. (2004) MicroRNAs: genomics, biogenesis, mechanism, and function. *Cell,* 116**,** 281-97.

Bashkirov, V. I., H. Scherthan, J. A. Solinger, J. M. Buerstedde & W. D. Heyer (1997) A mouse cytoplasmic exoribonuclease (mXRN1p) with preference for G4 tetraplex substrates. *J Cell Biol,* 136**,** 761-73.

Beenken, A. & M. Mohammadi (2009) The FGF family: biology, pathophysiology and therapy. *Nat Rev Drug Discov,* 8**,** 235-53.

Beer, H. D., M. Bittner, G. Niklaus, C. Munding, N. Max, A. Goppelt & S. Werner (2005) The fibroblast growth factor binding protein is a novel interaction partner of FGF-7, FGF-10 and FGF-22 and regulates FGF activity: implications for epithelial repair. *Oncogene,* 24**,** 5269-77.

Behm-Ansmant, I., J. Rehwinkel, T. Doerks, A. Stark, P. Bork & E. Izaurralde (2006) mRNA degradation by miRNAs and GW182 requires both CCR4:NOT deadenylase and DCP1:DCP2 decapping complexes. *Genes Dev,* 20**,** 1885-98.

Berezikov, E., W. J. Chung, J. Willis, E. Cuppen & E. C. Lai (2007) Mammalian mirtron genes. *Mol Cell,* 28**,** 328-36.

Bernstein, E., A. A. Caudy, S. M. Hammond & G. J. Hannon (2001) Role for a bidentate ribonuclease in the initiation step of RNA interference. *Nature,* 409**,** 363-6.

Beullens, M., A. Van Eynde, V. Vulsteke, J. Connor, S. Shenolikar, W. Stalmans & M. Bollen (1999) Molecular determinants of nuclear protein phosphatase-1 regulation by NIPP-1. *J Biol Chem,* 274**,** 14053-61.

Bobbs, A. S., A. V. Saarela, T. A. Yatskievych & P. B. Antin (2012) Fibroblast growth factor (FGF) signaling during gastrulation negatively modulates the abundance of microRNAs that regulate proteins required for cell migration and embryo patterning. *J Biol Chem,* 287**,** 38505-14.

Bohmert, K., I. Camus, C. Bellini, D. Bouchez, M. Caboche & C. Benning (1998) AGO1 defines a novel locus of Arabidopsis controlling leaf development. *EMBO J,* 17**,** 170-80.

Boland, A., F. Tritschler, S. Heimstädt, E. Izaurralde & O. Weichenrieder (2010) Crystal structure and ligand binding of the MID domain of a eukaryotic Argonaute protein. *EMBO Rep,* 11**,** 522-7.

Bollen, M., W. Peti, M. J. Ragusa & M. Beullens (2010) The extended PP1 toolkit: designed to create specificity. *Trends Biochem Sci,* 35**,** 450-8.

Borello, U., I. Cobos, J. E. Long, J. R. McWhirter, C. Murre & J. L. Rubenstein (2008) FGF15 promotes neurogenesis and opposes FGF8 function during neocortical development. *Neural Dev,* 3**,** 17.

Boswell, R. E. & A. P. Mahowald (1985) tudor, a gene required for assembly of the germ plasm in Drosophila melanogaster. *Cell,* 43**,** 97-104.

Brady, N., P. Chuntova, L. K. Bade & K. L. Schwertfeger (2013) The FGF/FGFR axis as a therapeutic target in breast cancer. *Expert Rev Endocrinol Metab,* 8**,** 391-402.

Brennecke, J., A. A. Aravin, A. Stark, M. Dus, M. Kellis, R. Sachidanandam & G. J. Hannon (2007) Discrete small RNA-generating loci as master regulators of transposon activity in Drosophila. *Cell,* 128**,** 1089-103.

Brennecke, J., D. R. Hipfner, A. Stark, R. B. Russell & S. M. Cohen (2003) bantam encodes a developmentally regulated microRNA that controls cell proliferation and regulates the proapoptotic gene hid in Drosophila. *Cell,* 113**,** 25-36.

Brennecke, J., A. Stark, R. B. Russell & S. M. Cohen (2005) Principles of microRNA-target recognition. *PLoS Biol,* 3**,** e85.

Broderick, J. A., W. E. Salomon, S. P. Ryder, N. Aronin & P. D. Zamore (2011) Argonaute protein identity and pairing geometry determine cooperativity in mammalian RNA silencing. *RNA,* 17**,** 1858-69.

Brognard, J., E. Sierecki, T. Gao & A. C. Newton (2007) PHLPP and a second isoform, PHLPP2, differentially attenuate the amplitude of Akt signaling by regulating distinct Akt isoforms. *Mol Cell,* 25**,** 917-31.

Burger, K. & M. Gullerova (2015) Swiss army knives: non-canonical functions of nuclear Drosha and Dicer. *Nat Rev Mol Cell Biol,* 16**,** 417-30.

Cabrita, M. A. & G. Christofori (2008) Sprouty proteins, masterminds of receptor tyrosine kinase signaling. *Angiogenesis,* 11**,** 53-62.

Carmell, M. A., A. Girard, H. J. van de Kant, D. Bourc'his, T. H. Bestor, D. G. de Rooij & G. J. Hannon (2007) MIWI2 is essential for spermatogenesis and repression of transposons in the mouse male germline. *Dev Cell,* 12**,** 503-14.

Carmichael, J. B., C. Stoica, H. Parker, J. M. McCaffery, A. J. Simmonds & T. C. Hobman (2006) RNA interference effector proteins localize to mobile cytoplasmic puncta in Schizosaccharomyces pombe. *Traffic,* 7**,** 1032-44.

Carraway, K. L. & L. C. Cantley (1994) A neu acquaintance for erbB3 and erbB4: a role for receptor heterodimerization in growth signaling. *Cell,* 78**,** 5-8.

Cerutti, L., N. Mian & A. Bateman (2000) Domains in gene silencing and cell differentiation proteins: the novel PAZ domain and redefinition of the Piwi domain. *Trends Biochem Sci,* 25**,** 481-2.

Ceulemans, H. & M. Bollen (2004) Functional diversity of protein phosphatase-1, a cellular economizer and reset button. *Physiol Rev,* 84**,** 1-39.

Chapman, E. J. & J. C. Carrington (2007) Specialization and evolution of endogenous small RNA pathways. *Nat Rev Genet,* 8**,** 884-96.

Cheloufi, S., C. O. Dos Santos, M. M. Chong & G. J. Hannon (2010) A dicer-independent miRNA biogenesis pathway that requires Ago catalysis. *Nature,* 465**,** 584-9.

Chen, C., J. Jin, D. A. James, M. A. Adams-Cioaba, J. G. Park, Y. Guo, E. Tenaglia, C. Xu, G. Gish, J. Min & T. Pawson (2009a) Mouse Piwi interactome identifies binding mechanism of Tdrkh Tudor domain to arginine methylated Miwi. *Proc Natl Acad Sci U S A,* 106**,** 20336-41.

Chen, C. Y. & A. B. Shyu (2011) Mechanisms of deadenylation-dependent decay. *Wiley Interdiscip Rev RNA,* 2**,** 167-83.

Chen, C. Y., D. Zheng, Z. Xia & A. B. Shyu (2009b) Ago-TNRC6 triggers microRNA-mediated decay by promoting two deadenylation steps. *Nat Struct Mol Biol,* 16**,** 1160-6.

Chen, C. Z., L. Li, H. F. Lodish & D. P. Bartel (2004) MicroRNAs modulate hematopoietic lineage differentiation. *Science,* 303**,** 83-6.

Chen, W. S., C. S. Lazar, M. Poenie, R. Y. Tsien, G. N. Gill & M. G. Rosenfeld (1987) Requirement for intrinsic protein tyrosine kinase in the immediate and late actions of the EGF receptor. *Nature,* 328**,** 820-3.

Chen, X. (2004) A microRNA as a translational repressor of APETALA2 in Arabidopsis flower development. *Science,* 303**,** 2022-5.

Chendrimada, T. P., R. I. Gregory, E. Kumaraswamy, J. Norman, N. Cooch, K. Nishikura & R. Shiekhattar (2005) TRBP recruits the Dicer complex to Ago2 for microRNA processing and gene silencing. *Nature,* 436**,** 740-4.

Chu, C. Y. & T. M. Rana (2006) Translation repression in human cells by microRNA-induced gene silencing requires RCK/p54. *PLoS Biol,* 4**,** e210.

Clancy, J. L., G. H. Wei, N. Echner, D. T. Humphreys, T. H. Beilharz & T. Preiss (2011) mRNA isoform diversity can obscure detection of miRNA-mediated control of translation. *RNA,* 17**,** 1025-31.

Cohen, P. T. (2002) Protein phosphatase 1--targeted in many directions. *J Cell Sci,* 115**,** 241-56.

Cougot, N., A. Cavalier, D. Thomas & R. Gillet (2012) The dual organization of P-bodies revealed by immunoelectron microscopy and electron tomography. *J Mol Biol,* 420**,** 17-28.

Cox, D. N., A. Chao, J. Baker, L. Chang, D. Qiao & H. Lin (1998) A novel class of evolutionarily conserved genes defined by piwi are essential for stem cell self-renewal. *Genes Dev,* 12**,** 3715-27.

Cunningham, D., Y. Humblet, S. Siena, D. Khayat, H. Bleiberg, A. Santoro, D. Bets, M. Mueser, A. Harstrick, C. Verslype, I. Chau & E. Van Cutsem (2004) Cetuximab monotherapy and cetuximab plus irinotecan in irinotecan-refractory metastatic colorectal cancer. *N Engl J Med,* 351**,** 337-45.

Czech, B., C. D. Malone, R. Zhou, A. Stark, C. Schlingeheyde, M. Dus, N. Perrimon, M. Kellis, J. A. Wohlschlegel, R. Sachidanandam, G. J. Hannon & J. Brennecke (2008) An endogenous small interfering RNA pathway in Drosophila. *Nature,* 453**,** 798-802.

Daniels, S. M., C. E. Melendez-Peña, R. J. Scarborough, A. Daher, H. S. Christensen, M. El Far, D. F. Purcell, S. Lainé & A. Gatignol (2009) Characterization of the TRBP domain required for dicer interaction and function in RNA interference. *BMC Mol Biol,* 10**,** 38.

Das, A. K., N. R. Helps, P. T. Cohen & D. Barford (1996) Crystal structure of the protein serine/threonine phosphatase 2C at 2.0 A resolution. *EMBO J,* 15**,** 6798-809.

Decker, C. J. & R. Parker (2012) P-bodies and stress granules: possible roles in the control of translation and mRNA degradation. *Cold Spring Harb Perspect Biol,* 4**,** a012286.

Decker, C. J., D. Teixeira & R. Parker (2007) Edc3p and a glutamine/asparagine-rich domain of Lsm4p function in processing body assembly in Saccharomyces cerevisiae. *J Cell Biol,* 179**,** 437-49.

Denli, A. M., B. B. Tops, R. H. Plasterk, R. F. Ketting & G. J. Hannon (2004) Processing of primary microRNAs by the Microprocessor complex. *Nature,* 432**,** 231-5.

Dever, T. E. (2002) Gene-specific regulation by general translation factors. *Cell,* 108**,** 545-56.

Domenicali Pfister, D., G. Burkard, S. Morand, C. K. Renggli, I. Roditi & E. Vassella (2006) A Mitogen-activated protein kinase controls differentiation of bloodstream forms of Trypanosoma brucei. *Eukaryot Cell,* 5**,** 1126-35.

Drake, M., T. Furuta, K. M. Suen, G. Gonzalez, B. Liu, A. Kalia, J. E. Ladbury, A. Z. Fire, J. B. Skeath & S. Arur (2014) A requirement for ERK-dependent Dicer phosphorylation in coordinating oocyte-to-embryo transition in C. elegans. *Dev Cell,* 31**,** 614-28.

Drinnenberg, I. A., D. E. Weinberg, K. T. Xie, J. P. Mower, K. H. Wolfe, G. R. Fink & D. P. Bartel (2009) RNAi in budding yeast. *Science,* 326**,** 544-50.

Dudka, A. A., S. M. Sweet & J. K. Heath (2010) Signal transducers and activators of transcription-3 binding to the fibroblast growth factor receptor is activated by receptor amplification. *Cancer Res,* 70**,** 3391-401.

Egloff, M. P., D. F. Johnson, G. Moorhead, P. T. Cohen, P. Cohen & D. Barford (1997) Structural basis for the recognition of regulatory subunits by the catalytic subunit of protein phosphatase 1. *EMBO J,* 16**,** 1876-87.

Eichhorn, S. W., H. Guo, S. E. McGeary, R. A. Rodriguez-Mias, C. Shin, D. Baek, S. H. Hsu, K. Ghoshal, J. Villén & D. P. Bartel (2014) mRNA destabilization is the dominant effect of mammalian microRNAs by the time substantial repression ensues. *Mol Cell,* 56**,** 104-15.

El-Shami, M., D. Pontier, S. Lahmy, L. Braun, C. Picart, D. Vega, M. A. Hakimi, S. E. Jacobsen, R. Cooke & T. Lagrange (2007) Reiterated WG/GW motifs form functionally and evolutionarily conserved ARGONAUTE-binding platforms in RNAi-related components. *Genes Dev,* 21**,** 2539-44.

Elbashir, S. M., W. Lendeckel & T. Tuschl (2001a) RNA interference is mediated by 21- and 22-nucleotide RNAs. *Genes Dev,* 15**,** 188-200.

Elbashir, S. M., J. Martinez, A. Patkaniowska, W. Lendeckel & T. Tuschl (2001b) Functional anatomy of siRNAs for mediating efficient RNAi in Drosophila melanogaster embryo lysate. *EMBO J,* 20**,** 6877-88.

Elkayam, E., C. D. Kuhn, A. Tocilj, A. D. Haase, E. M. Greene, G. J. Hannon & L. Joshua-Tor (2012) The structure of human argonaute-2 in complex with miR-20a. *Cell,* 150**,** 100-10.

Emery, J. F., S. K. Floyd, J. Alvarez, Y. Eshed, N. P. Hawker, A. Izhaki, S. F. Baum & J. L. Bowman (2003) Radial patterning of Arabidopsis shoots by class III HD-ZIP and KANADI genes. *Curr Biol,* 13**,** 1768-74.

Ender, C. & G. Meister (2010) Argonaute proteins at a glance. *J Cell Sci,* 123**,** 1819-23.

Eulalio, A., I. Behm-Ansmant & E. Izaurralde (2007a) P bodies: at the crossroads of post-transcriptional pathways. *Nat Rev Mol Cell Biol,* 8**,** 9-22.

Eulalio, A., I. Behm-Ansmant, D. Schweizer & E. Izaurralde (2007b) P-body formation is a consequence, not the cause, of RNA-mediated gene silencing. *Mol Cell Biol,* 27**,** 3970-81.

Eulalio, A., S. Helms, C. Fritzsch, M. Fauser & E. Izaurralde (2009a) A C-terminal silencing domain in GW182 is essential for miRNA function. *RNA,* 15**,** 1067-77.

Eulalio, A., J. Rehwinkel, M. Stricker, E. Huntzinger, S. F. Yang, T. Doerks, S. Dorner, P. Bork, M. Boutros & E. Izaurralde (2007c) Target-specific requirements for enhancers of decapping in miRNA-mediated gene silencing. *Genes Dev,* 21**,** 2558-70.

Eulalio, A., F. Tritschler & E. Izaurralde (2009b) The GW182 protein family in animal cells: new insights into domains required for miRNA-mediated gene silencing. *RNA,* 15**,** 1433-42.

Eystathioy, T., E. K. Chan, S. A. Tenenbaum, J. D. Keene, K. Griffith & M. J. Fritzler (2002) A phosphorylated cytoplasmic autoantigen, GW182, associates with a unique population of human mRNAs within novel cytoplasmic speckles. *Mol Biol Cell,* 13**,** 1338-51.

Faehnle, C. R., E. Elkayam, A. D. Haase, G. J. Hannon & L. Joshua-Tor (2013) The making of a slicer: activation of human Argonaute-1. *Cell Rep,* 3**,** 1901-9.

Fasken, M. B. & A. H. Corbett (2005) Process or perish: quality control in mRNA biogenesis. *Nat Struct Mol Biol,* 12**,** 482-8.

Feng, S., O. Dakhova, C. J. Creighton & M. Ittmann (2013) Endocrine fibroblast growth factor FGF19 promotes prostate cancer progression. *Cancer Res,* 73**,** 2551-62.

Feng, S., J. Wang, Y. Zhang, C. J. Creighton & M. Ittmann (2015) FGF23 promotes prostate cancer progression. *Oncotarget,* 6**,** 17291-301.

Filippov, V., V. Solovyev, M. Filippova & S. S. Gill (2000) A novel type of RNase III family proteins in eukaryotes. *Gene,* 245**,** 213-21.

Fire, A., S. Xu, M. K. Montgomery, S. A. Kostas, S. E. Driver & C. C. Mello (1998) Potent and specific genetic interference by double-stranded RNA in Caenorhabditis elegans. *Nature,* 391**,** 806-11.

Fortin, K. R., R. H. Nicholson & A. W. Nicholson (2002) Mouse ribonuclease III. cDNA structure, expression analysis, and chromosomal location. *BMC Genomics,* 3**,** 26.

Franks, T. M. & J. Lykke-Andersen (2008) The control of mRNA decapping and P-body formation. *Mol Cell,* 32**,** 605-15.

Friedman, R. C., K. K. Farh, C. B. Burge & D. P. Bartel (2009) Most mammalian mRNAs are conserved targets of microRNAs. *Genome Res,* 19**,** 92-105.

Fujimura, K., J. Katahira, F. Kano, Y. Yoneda & M. Murata (2009) Microscopic dissection of the process of stress granule assembly. *Biochim Biophys Acta,* 1793**,** 1728-37.

Förstemann, K., Y. Tomari, T. Du, V. V. Vagin, A. M. Denli, D. P. Bratu, C. Klattenhoff, W. E. Theurkauf & P. D. Zamore (2005) Normal microRNA maturation and germ-line stem cell maintenance requires Loquacious, a double-stranded RNA-binding domain protein. *PLoS Biol,* 3**,** e236.

Gandhi, T. K., S. Chandran, S. Peri, R. Saravana, R. Amanchy, T. S. Prasad & A. Pandey (2005) A bioinformatics analysis of protein tyrosine phosphatases in humans. *DNA Res,* 12**,** 79-89.

Gebauer, F., T. Preiss & M. W. Hentze (2012) From cis-regulatory elements to complex RNPs and back. *Cold Spring Harb Perspect Biol,* 4**,** a012245.

Ghildiyal, M., H. Seitz, M. D. Horwich, C. Li, T. Du, S. Lee, J. Xu, E. L. Kittler, M. L. Zapp, Z. Weng & P. D. Zamore (2008) Endogenous siRNAs derived from transposons and mRNAs in Drosophila somatic cells. *Science,* 320**,** 1077-81.

Ghosh, A., S. Shuman & C. D. Lima (2008) The structure of Fcp1, an essential RNA polymerase II CTD phosphatase. *Mol Cell,* 32**,** 478-90.

Gilks, N., N. Kedersha, M. Ayodele, L. Shen, G. Stoecklin, L. M. Dember & P. Anderson (2004) Stress granule assembly is mediated by prion-like aggregation of TIA-1. *Mol Biol Cell,* 15**,** 5383-98.

Girard, A., R. Sachidanandam, G. J. Hannon & M. A. Carmell (2006) A germline-specific class of small RNAs binds mammalian Piwi proteins. *Nature,* 442**,** 199-202.

Goetz, R., K. Dover, F. Laezza, N. Shtraizent, X. Huang, D. Tchetchik, A. V. Eliseenkova, C. F. Xu, T. A. Neubert, D. M. Ornitz, M. Goldfarb & M. Mohammadi (2009) Crystal structure of a fibroblast growth factor homologous factor (FHF) defines a conserved surface on FHFs for binding and modulation of voltage-gated sodium channels. *J Biol Chem,* 284**,** 17883-96.

Good, M., G. Tang, J. Singleton, A. Reményi & W. A. Lim (2009) The Ste5 scaffold directs mating signaling by catalytically unlocking the Fus3 MAP kinase for activation. *Cell,* 136**,** 1085-97.

Grentzinger, T., C. Armenise, C. Brun, B. Mugat, V. Serrano, A. Pelisson & S. Chambeyron (2012) piRNA-mediated transgenerational inheritance of an acquired trait. *Genome Res,* 22**,** 1877-88.

Grivna, S. T., E. Beyret, Z. Wang & H. Lin (2006) A novel class of small RNAs in mouse spermatogenic cells. *Genes Dev,* 20**,** 1709-14.

Gunawardane, L. S., K. Saito, K. M. Nishida, K. Miyoshi, Y. Kawamura, T. Nagami, H. Siomi & M. C. Siomi (2007) A slicer-mediated mechanism for repeat-associated siRNA 5' end formation in Drosophila. *Science,* 315**,** 1587-90.

Guo, H., N. T. Ingolia, J. S. Weissman & D. P. Bartel (2010) Mammalian microRNAs predominantly act to decrease target mRNA levels. *Nature,* 466**,** 835-40.

Haase, A. D., L. Jaskiewicz, H. Zhang, S. Lainé, R. Sack, A. Gatignol & W. Filipowicz (2005) TRBP, a regulator of cellular PKR and HIV-1 virus expression, interacts with Dicer and functions in RNA silencing. *EMBO Rep,* 6**,** 961-7.

Han, J., Y. Lee, K. H. Yeom, J. W. Nam, I. Heo, J. K. Rhee, S. Y. Sohn, Y. Cho, B. T. Zhang & V. N. Kim (2006) Molecular basis for the recognition of primary microRNAs by the Drosha-DGCR8 complex. *Cell,* 125**,** 887-901.

Hanafusa, H., S. Torii, T. Yasunaga & E. Nishida (2002) Sprouty1 and Sprouty2 provide a control mechanism for the Ras/MAPK signalling pathway. *Nat Cell Biol,* 4**,** 850-8.

Harashima, H., N. Dissmeyer, P. Hammann, Y. Nomura, K. Kramer, H. Nakagami & A. Schnittger (2016) Modulation of plant growth in vivo and identification of kinase substrates using an analog-sensitive variant of CYCLIN-DEPENDENT KINASE A;1. *BMC Plant Biol,* 16**,** 209.

Hari, S. B., E. A. Merritt & D. J. Maly (2013) Sequence determinants of a specific inactive protein kinase conformation. *Chem Biol,* 20**,** 806-15.

Haugsten, E. M., J. Malecki, S. M. Bjørklund, S. Olsnes & J. Wesche (2008) Ubiquitination of fibroblast growth factor receptor 1 is required for its intracellular sorting but not for its endocytosis. *Mol Biol Cell,* 19**,** 3390-403.

Hendrickson, D. G., D. J. Hogan, H. L. McCullough, J. W. Myers, D. Herschlag, J. E. Ferrell & P. O. Brown (2009) Concordant regulation of translation and mRNA abundance for hundreds of targets of a human microRNA. *PLoS Biol,* 7**,** e1000238.

Hendrickx, A., M. Beullens, H. Ceulemans, T. Den Abt, A. Van Eynde, E. Nicolaescu, B. Lesage & M. Bollen (2009) Docking motif-guided mapping of the interactome of protein phosphatase-1. *Chem Biol,* 16**,** 365-71.

Herbert, K. M., G. Pimienta, S. J. DeGregorio, A. Alexandrov & J. A. Steitz (2013) Phosphorylation of DGCR8 increases its intracellular stability and induces a progrowth miRNA profile. *Cell Rep,* 5**,** 1070-81.

Heyam, A., D. Lagos & M. Plevin (2015) Dissecting the roles of TRBP and PACT in double-stranded RNA recognition and processing of noncoding RNAs. *Wiley Interdiscip Rev RNA,* 6**,** 271-89.

Horman, S. R., M. M. Janas, C. Litterst, B. Wang, I. J. MacRae, M. J. Sever, D. V. Morrissey, P. Graves, B. Luo, S. Umesalma, H. H. Qi, L. J. Miraglia, C. D. Novina & A. P. Orth (2013) Akt-mediated phosphorylation of argonaute 2 downregulates cleavage and upregulates translational repression of MicroRNA targets. *Mol Cell,* 50**,** 356-67.

Houwing, S., E. Berezikov & R. F. Ketting (2008) Zili is required for germ cell differentiation and meiosis in zebrafish. *EMBO J,* 27**,** 2702-11.

Houwing, S., L. M. Kamminga, E. Berezikov, D. Cronembold, A. Girard, H. van den Elst, D. V. Filippov, H. Blaser, E. Raz, C. B. Moens, R. H. Plasterk, G. J. Hannon, B. W. Draper & R. F. Ketting (2007) A role for Piwi and piRNAs in germ cell maintenance and transposon silencing in Zebrafish. *Cell,* 129**,** 69-82.

Huang, H., Q. Gao, X. Peng, S. Y. Choi, K. Sarma, H. Ren, A. J. Morris & M. A. Frohman (2011) piRNA-associated germline nuage formation and spermatogenesis require MitoPLD profusogenic mitochondrial-surface lipid signaling. *Dev Cell,* 20**,** 376-87.

Hughes, S. E. (1997) Differential expression of the fibroblast growth factor receptor (FGFR) multigene family in normal human adult tissues. *J Histochem Cytochem,* 45**,** 1005-19.

Hunter, T. (2000) Signaling--2000 and beyond. *Cell,* 100**,** 113-27.

Huntzinger, E. & E. Izaurralde (2011) Gene silencing by microRNAs: contributions of translational repression and mRNA decay. *Nat Rev Genet,* 12**,** 99-110.

Ingelfinger, D., D. J. Arndt-Jovin, R. Lührmann & T. Achsel (2002) The human LSm1-7 proteins colocalize with the mRNA-degrading enzymes Dcp1/2 and Xrnl in distinct cytoplasmic foci. *RNA,* 8**,** 1489-501.

Iwasaki, S., M. Kobayashi, M. Yoda, Y. Sakaguchi, S. Katsuma, T. Suzuki & Y. Tomari (2010) Hsc70/Hsp90 chaperone machinery mediates ATP-dependent RISC loading of small RNA duplexes. *Mol Cell,* 39**,** 292-9.

Jakymiw, A., S. Lian, T. Eystathioy, S. Li, M. Satoh, J. C. Hamel, M. J. Fritzler & E. K. Chan (2005) Disruption of GW bodies impairs mammalian RNA interference. *Nat Cell Biol,* 7**,** 1267-74.

Jaskiewicz, L. & W. Filipowicz (2008) Role of Dicer in posttranscriptional RNA silencing. *Curr Top Microbiol Immunol,* 320**,** 77-97.

Johnston, R. J. & O. Hobert (2003) A microRNA controlling left/right neuronal asymmetry in Caenorhabditis elegans. *Nature,* 426**,** 845-9.

Katoh, M. (2006) FGF signaling network in the gastrointestinal tract (review). *Int J Oncol,* 29**,** 163-8.

Kaufman, R. J. (2004) Regulation of mRNA translation by protein folding in the endoplasmic reticulum. *Trends Biochem Sci,* 29**,** 152-8.

Kawamata, T. & Y. Tomari (2010) Making RISC. *Trends Biochem Sci,* 35**,** 368-76.

Kawamura, Y., K. Saito, T. Kin, Y. Ono, K. Asai, T. Sunohara, T. N. Okada, M. C. Siomi & H. Siomi (2008) Drosophila endogenous small RNAs bind to Argonaute 2 in somatic cells. *Nature,* 453**,** 793-7.

Kedersha, N. & P. Anderson (2002) Stress granules: sites of mRNA triage that regulate mRNA stability and translatability. *Biochem Soc Trans,* 30**,** 963-9.

Kedersha, N., S. Chen, N. Gilks, W. Li, I. J. Miller, J. Stahl & P. Anderson (2002) Evidence that ternary complex (eIF2-GTP-tRNA(i)(Met))-deficient preinitiation complexes are core constituents of mammalian stress granules. *Mol Biol Cell,* 13**,** 195-210.

Kedersha, N., G. Stoecklin, M. Ayodele, P. Yacono, J. Lykke-Andersen, M. J. Fritzler, D. Scheuner, R. J. Kaufman, D. E. Golan & P. Anderson (2005) Stress granules and processing bodies are dynamically linked sites of mRNP remodeling. *J Cell Biol,* 169**,** 871-84.

Kedersha, N. L., M. Gupta, W. Li, I. Miller & P. Anderson (1999) RNA-binding proteins TIA-1 and TIAR link the phosphorylation of eIF-2 alpha to the assembly of mammalian stress granules. *J Cell Biol,* 147**,** 1431-42.

Kemp, C. & J. L. Imler (2009) Antiviral immunity in drosophila. *Curr Opin Immunol,* 21**,** 3-9.

Kemp, C., S. Mueller, A. Goto, V. Barbier, S. Paro, F. Bonnay, C. Dostert, L. Troxler, C. Hetru, C. Meignin, S. Pfeffer, J. A. Hoffmann & J. L. Imler (2013) Broad RNA interference-mediated antiviral immunity and virus-specific inducible responses in Drosophila. *J Immunol,* 190**,** 650-8.

Kholodenko, B. N. (2009) Spatially distributed cell signalling. *FEBS Lett,* 583**,** 4006-12.

Kim, V. N. (2005) MicroRNA biogenesis: coordinated cropping and dicing. *Nat Rev Mol Cell Biol,* 6**,** 376-85.

Kimball, S. R. (2001) Regulation of translation initiation by amino acids in eukaryotic cells. *Prog Mol Subcell Biol,* 26**,** 155-84.

Kirino, Y., N. Kim, M. de Planell-Saguer, E. Khandros, S. Chiorean, P. S. Klein, I. Rigoutsos, T. A. Jongens & Z. Mourelatos (2009) Arginine methylation of Piwi proteins catalysed by dPRMT5 is required for Ago3 and Aub stability. *Nat Cell Biol,* 11**,** 652-8.

Kirino, Y. & Z. Mourelatos (2007a) 2'-O-methyl modification in mouse piRNAs and its methylase. *Nucleic Acids Symp Ser (Oxf)***,** 417-8.

--- (2007b) Mouse Piwi-interacting RNAs are 2'-O-methylated at their 3' termini. *Nat Struct Mol Biol,* 14**,** 347-8.

--- (2007c) The mouse homolog of HEN1 is a potential methylase for Piwi-interacting RNAs. *RNA,* 13**,** 1397-401.

Kitsera, N., A. Khobta & B. Epe (2007) Destabilized green fluorescent protein detects rapid removal of transcription blocks after genotoxic exposure. *Biotechniques,* 43**,** 222-7.

Klattenhoff, C., D. P. Bratu, N. McGinnis-Schultz, B. S. Koppetsch, H. A. Cook & W. E. Theurkauf (2007) Drosophila rasiRNA pathway mutations disrupt embryonic axis specification through activation of an ATR/Chk2 DNA damage response. *Dev Cell,* 12**,** 45-55.

Knighton, D. R., J. H. Zheng, L. F. Ten Eyck, N. H. Xuong, S. S. Taylor & J. M. Sowadski (1991) Structure of a peptide inhibitor bound to the catalytic subunit of cyclic adenosine monophosphate-dependent protein kinase. *Science,* 253**,** 414-20.

Knowles, J. R. (1980) Enzyme-catalyzed phosphoryl transfer reactions. *Annu Rev Biochem,* 49**,** 877-919.

Knowles, R. B., J. H. Sabry, M. E. Martone, T. J. Deerinck, M. H. Ellisman, G. J. Bassell & K. S. Kosik (1996) Translocation of RNA granules in living neurons. *J Neurosci,* 16**,** 7812-20.

Kok, K. H., M. H. Ng, Y. P. Ching & D. Y. Jin (2007) Human TRBP and PACT directly interact with each other and associate with dicer to facilitate the production of small interfering RNA. *J Biol Chem,* 282**,** 17649-57.

Kolobova, E., A. Efimov, I. Kaverina, A. K. Rishi, J. W. Schrader, A. J. Ham, M. C. Larocca & J. R. Goldenring (2009) Microtubule-dependent association of AKAP350A and CCAR1 with RNA stress granules. *Exp Cell Res,* 315**,** 542-55.

Kovalenko, D., X. Yang, R. J. Nadeau, L. K. Harkins & R. Friesel (2003) Sef inhibits fibroblast growth factor signaling by inhibiting FGFR1 tyrosine phosphorylation and subsequent ERK activation. *J Biol Chem,* 278**,** 14087-91.

Krejci, P., L. Salazar, H. S. Goodridge, T. A. Kashiwada, M. J. Schibler, P. Jelinkova, L. M. Thompson & W. R. Wilcox (2008) STAT1 and STAT3 do not participate in FGF-mediated growth arrest in chondrocytes. *J Cell Sci,* 121**,** 272-81.

Krichevsky, A. M. & K. S. Kosik (2001) Neuronal RNA granules: a link between RNA localization and stimulation-dependent translation. *Neuron,* 32**,** 683-96.

Krishnamoorthy, T., G. D. Pavitt, F. Zhang, T. E. Dever & A. G. Hinnebusch (2001) Tight binding of the phosphorylated alpha subunit of initiation factor 2 (eIF2alpha) to the regulatory subunits of guanine nucleotide exchange factor eIF2B is required for inhibition of translation initiation. *Mol Cell Biol,* 21**,** 5018-30.

Kunii, K., L. Davis, J. Gorenstein, H. Hatch, M. Yashiro, A. Di Bacco, C. Elbi & B. Lutterbach (2008) FGFR2-amplified gastric cancer cell lines require FGFR2 and Erbb3 signaling for growth and survival. *Cancer Res,* 68**,** 2340-8.

Kuzuoğlu-Öztürk, D., D. Bhandari, E. Huntzinger, M. Fauser, S. Helms & E. Izaurralde (2016) miRISC and the CCR4-NOT complex silence mRNA targets independently of 43S ribosomal scanning. *EMBO J,* 35**,** 1186-203.

Kwon, S. C., T. A. Nguyen, Y. G. Choi, M. H. Jo, S. Hohng, V. N. Kim & J. S. Woo (2016) Structure of Human DROSHA. *Cell,* 164**,** 81-90.

Küntziger, T., M. Rogne, R. L. Folstad & P. Collas (2006) Association of PP1 with its regulatory subunit AKAP149 is regulated by serine phosphorylation flanking the RVXF motif of AKAP149. *Biochemistry,* 45**,** 5868-77.

Lander, E. S., L. M. Linton, B. Birren, C. Nusbaum, M. C. Zody, J. Baldwin, K. Devon, K. Dewar, M. Doyle, W. FitzHugh, R. Funke, D. Gage, K. Harris, A. Heaford, J. Howland, L. Kann, J. Lehoczky, R. LeVine, P. McEwan, K. McKernan, J. Meldrim, J. P. Mesirov, C. Miranda, W. Morris, J. Naylor, C. Raymond, M. Rosetti, R. Santos, A. Sheridan, C. Sougnez, Y. Stange-Thomann, N. Stojanovic, A. Subramanian, D. Wyman, J. Rogers, J. Sulston, R. Ainscough, S. Beck, D. Bentley, J. Burton, C. Clee, N. Carter, A. Coulson, R. Deadman, P. Deloukas, A. Dunham, I. Dunham, R. Durbin, L. French, D. Grafham, S. Gregory, T. Hubbard, S. Humphray, A. Hunt, M. Jones, C. Lloyd, A. McMurray, L. Matthews, S. Mercer, S. Milne, J. C. Mullikin, A. Mungall, R. Plumb, M. Ross, R. Shownkeen, S. Sims, R. H. Waterston, R. K. Wilson, L. W. Hillier, J. D. McPherson, M. A. Marra, E. R. Mardis, L. A. Fulton, A. T. Chinwalla, K. H. Pepin, W. R. Gish, S. L. Chissoe, M. C. Wendl, K. D. Delehaunty, T. L. Miner, A. Delehaunty, J. B. Kramer, L. L. Cook, R. S. Fulton, D. L. Johnson, P. J. Minx, S. W. Clifton, T. Hawkins, E. Branscomb, P. Predki, P. Richardson, S. Wenning, T. Slezak, N. Doggett, J. F. Cheng, A. Olsen, S. Lucas, C. Elkin, E. Uberbacher, M. Frazier, et al. (2001) Initial sequencing and analysis of the human genome. *Nature,* 409**,** 860-921.

Lazzaretti, D., I. Tournier & E. Izaurralde (2009) The C-terminal domains of human TNRC6A, TNRC6B, and TNRC6C silence bound transcripts independently of Argonaute proteins. *RNA,* 15**,** 1059-66.

Lee, E. J., S. Banerjee, H. Zhou, A. Jammalamadaka, M. Arcila, B. S. Manjunath & K. S. Kosik (2011) Identification of piRNAs in the central nervous system. *RNA,* 17**,** 1090-9.

Lee, H. Y., K. Zhou, A. M. Smith, C. L. Noland & J. A. Doudna (2013) Differential roles of human Dicer-binding proteins TRBP and PACT in small RNA processing. *Nucleic Acids Res,* 41**,** 6568-76.

Lee, R. C., R. L. Feinbaum & V. Ambros (1993) The C. elegans heterochronic gene lin-4 encodes small RNAs with antisense complementarity to lin-14. *Cell,* 75**,** 843-54.

Lee, Y., C. Ahn, J. Han, H. Choi, J. Kim, J. Yim, J. Lee, P. Provost, O. Rådmark, S. Kim & V. N. Kim (2003) The nuclear RNase III Drosha initiates microRNA processing. *Nature,* 425**,** 415-9.

Lemmon, M. A. & J. Schlessinger (2010) Cell signaling by receptor tyrosine kinases. *Cell,* 141**,** 1117-34.

Leung, A. K., J. M. Calabrese & P. A. Sharp (2006) Quantitative analysis of Argonaute protein reveals microRNA-dependent localization to stress granules. *Proc Natl Acad Sci U S A,* 103**,** 18125-30.

Leung, A. K. & P. A. Sharp (2013) Quantifying Argonaute proteins in and out of GW/P-bodies: implications in microRNA activities. *Adv Exp Med Biol,* 768**,** 165-82.

Leung, A. K., S. Vyas, J. E. Rood, A. Bhutkar, P. A. Sharp & P. Chang (2011) Poly(ADP-ribose) regulates stress responses and microRNA activity in the cytoplasm. *Mol Cell,* 42**,** 489-99.

Lewis, B. P., I. H. Shih, M. W. Jones-Rhoades, D. P. Bartel & C. B. Burge (2003) Prediction of mammalian microRNA targets. *Cell,* 115**,** 787-98.

Li, H. & S. J. Roux (1992) Purification and characterization of a casein kinase 2-type protein kinase from pea nuclei. *Plant Physiol,* 99**,** 686-92.

Li, S. & D. J. Patel (2016) Drosha and Dicer: Slicers cut from the same cloth. *Cell Res,* 26**,** 511-2.

Liu, J., M. A. Carmell, F. V. Rivas, C. G. Marsden, J. M. Thomson, J. J. Song, S. M. Hammond, L. Joshua-Tor & G. J. Hannon (2004a) Argonaute2 Is the Catalytic Engine of Mammalian RNAi. *Science*.

--- (2004b) Argonaute2 is the catalytic engine of mammalian RNAi. *Science,* 305**,** 1437-41.

Liu, J., M. A. Valencia-Sanchez, G. J. Hannon & R. Parker (2005a) MicroRNA-dependent localization of targeted mRNAs to mammalian P-bodies. *Nat Cell Biol,* 7**,** 719-23.

--- (2005b) MicroRNA-dependent localization of targeted mRNAs to mammalian P-bodies. *Nat Cell Biol,* 7**,** 719-23.

Liu, Y. P., M. Karg, A. Harwig, E. Herrera-Carrillo, A. Jongejan, A. van Kampen & B. Berkhout (2015) Mechanistic insights on the Dicer-independent AGO2-mediated processing of AgoshRNAs. *RNA Biol,* 12**,** 92-100.

Lopez-Orozco, J., J. M. Pare, A. L. Holme, S. G. Chaulk, R. P. Fahlman & T. C. Hobman (2015) Functional analyses of phosphorylation events in human Argonaute 2. *RNA,* 21**,** 2030-8.

Lu, G. & Y. Wang (2008) Functional diversity of mammalian type 2C protein phosphatase isoforms: new tales from an old family. *Clin Exp Pharmacol Physiol,* 35**,** 107-12.

Lund, E., S. Güttinger, A. Calado, J. E. Dahlberg & U. Kutay (2004) Nuclear export of microRNA precursors. *Science,* 303**,** 95-8.

Luo, Y., C. Yang, C. Jin, R. Xie, F. Wang & W. L. McKeehan (2009) Novel phosphotyrosine targets of FGFR2IIIb signaling. *Cell Signal,* 21**,** 1370-8.

Lytle, J. R., T. A. Yario & J. A. Steitz (2007) Target mRNAs are repressed as efficiently by microRNA-binding sites in the 5' UTR as in the 3' UTR. *Proc Natl Acad Sci U S A,* 104**,** 9667-72.

Ma, E., I. J. MacRae, J. F. Kirsch & J. A. Doudna (2008) Autoinhibition of human dicer by its internal helicase domain. *J Mol Biol,* 380**,** 237-43.

Macrae, I. J., F. Li, K. Zhou, W. Z. Cande & J. A. Doudna (2006a) Structure of Dicer and mechanistic implications for RNAi. *Cold Spring Harb Symp Quant Biol,* 71**,** 73-80.

Macrae, I. J., K. Zhou, F. Li, A. Repic, A. N. Brooks, W. Z. Cande, P. D. Adams & J. A. Doudna (2006b) Structural basis for double-stranded RNA processing by Dicer. *Science,* 311**,** 195-8.

Mallory, A. & H. Vaucheret (2010) Form, function, and regulation of ARGONAUTE proteins. *Plant Cell,* 22**,** 3879-89.

Malone, C. D., J. Brennecke, M. Dus, A. Stark, W. R. McCombie, R. Sachidanandam & G. J. Hannon (2009) Specialized piRNA pathways act in germline and somatic tissues of the Drosophila ovary. *Cell,* 137**,** 522-35.

Manning, G., D. B. Whyte, R. Martinez, T. Hunter & S. Sudarsanam (2002) The protein kinase complement of the human genome. *Science,* 298**,** 1912-34.

Mazumder, A., M. Bose, A. Chakraborty, S. Chakrabarti & S. N. Bhattacharyya (2013) A transient reversal of miRNA-mediated repression controls macrophage activation. *EMBO Rep,* 14**,** 1008-16.

Mazzoni, C., I. D'Addario & C. Falcone (2007) The C-terminus of the yeast Lsm4p is required for the association to P-bodies. *FEBS Lett,* 581**,** 4836-40.

Meister, G., C. Eggert, D. Bühler, H. Brahms, C. Kambach & U. Fischer (2001) Methylation of Sm proteins by a complex containing PRMT5 and the putative U snRNP assembly factor pICln. *Curr Biol,* 11**,** 1990-4.

Miyoshi, T., A. Takeuchi, H. Siomi & M. C. Siomi (2010) A direct role for Hsp90 in pre-RISC formation in Drosophila. *Nat Struct Mol Biol,* 17**,** 1024-6.

Mollet, S., N. Cougot, A. Wilczynska, F. Dautry, M. Kress, E. Bertrand & D. Weil (2008) Translationally repressed mRNA transiently cycles through stress granules during stress. *Mol Biol Cell,* 19**,** 4469-79.

Monast, C. S., C. M. Furcht & M. J. Lazzara (2012) Computational analysis of the regulation of EGFR by protein tyrosine phosphatases. *Biophys J,* 102**,** 2012-21.

Moorhead, G. B., L. Trinkle-Mulcahy & A. Ulke-Lemée (2007) Emerging roles of nuclear protein phosphatases. *Nat Rev Mol Cell Biol,* 8**,** 234-44.

Morita, S., T. Horii, M. Kimura, Y. Goto, T. Ochiya & I. Hatada (2007) One Argonaute family member, Eif2c2 (Ago2), is essential for development and appears not to be involved in DNA methylation. *Genomics,* 89**,** 687-96.

Moser, J. J., T. Eystathioy, E. K. Chan & M. J. Fritzler (2007) Markers of mRNA stabilization and degradation, and RNAi within astrocytoma GW bodies. *J Neurosci Res,* 85**,** 3619-31.

Muckenthaler, M., N. Gunkel, R. Stripecke & M. W. Hentze (1997) Regulated poly(A) tail shortening in somatic cells mediated by cap-proximal translational repressor proteins and ribosome association. *RNA,* 3**,** 983-95.

Muhlrad, D., C. J. Decker & R. Parker (1995) Turnover mechanisms of the stable yeast PGK1 mRNA. *Mol Cell Biol,* 15**,** 2145-56.

Nagamatsu, H., J. Teishima, K. Goto, H. Shikuma, H. Kitano, K. Shoji, S. Inoue & A. Matsubara (2015) FGF19 promotes progression of prostate cancer. *Prostate,* 75**,** 1092-101.

Navarro, R. E. & T. K. Blackwell (2005) Requirement for P granules and meiosis for accumulation of the germline RNA helicase CGH-1. *Genesis,* 42**,** 172-80.

Nazarov, P. V., S. E. Reinsbach, A. Muller, N. Nicot, D. Philippidou, L. Vallar & S. Kreis (2013) Interplay of microRNAs, transcription factors and target genes: linking dynamic expression changes to function. *Nucleic Acids Res,* 41**,** 2817-31.

Nishida, K. M., T. N. Okada, T. Kawamura, T. Mituyama, Y. Kawamura, S. Inagaki, H. Huang, D. Chen, T. Kodama, H. Siomi & M. C. Siomi (2009) Functional involvement of Tudor and dPRMT5 in the piRNA processing pathway in Drosophila germlines. *EMBO J,* 28**,** 3820-31.

Nover, L., K. D. Scharf & D. Neumann (1989) Cytoplasmic heat shock granules are formed from precursor particles and are associated with a specific set of mRNAs. *Mol Cell Biol,* 9**,** 1298-308.

Nowotny, M., S. A. Gaidamakov, R. J. Crouch & W. Yang (2005) Crystal structures of RNase H bound to an RNA/DNA hybrid: substrate specificity and metal-dependent catalysis. *Cell,* 121**,** 1005-16.

Ohn, T., N. Kedersha, T. Hickman, S. Tisdale & P. Anderson (2008) A functional RNAi screen links O-GlcNAc modification of ribosomal proteins to stress granule and processing body assembly. *Nat Cell Biol,* 10**,** 1224-31.

Okamura, K., J. W. Hagen, H. Duan, D. M. Tyler & E. C. Lai (2007) The mirtron pathway generates microRNA-class regulatory RNAs in Drosophila. *Cell,* 130**,** 89-100.

Okamura, K. & E. C. Lai (2008) Endogenous small interfering RNAs in animals. *Nat Rev Mol Cell Biol,* 9**,** 673-8.

Olejniczak, S. H., G. La Rocca, J. J. Gruber & C. B. Thompson (2013) Long-lived microRNA-Argonaute complexes in quiescent cells can be activated to regulate mitogenic responses. *Proc Natl Acad Sci U S A,* 110**,** 157-62.

Olsen, J. V., B. Blagoev, F. Gnad, B. Macek, C. Kumar, P. Mortensen & M. Mann (2006) Global, in vivo, and site-specific phosphorylation dynamics in signaling networks. *Cell,* 127**,** 635-48.

Olsen, P. H. & V. Ambros (1999) The lin-4 regulatory RNA controls developmental timing in Caenorhabditis elegans by blocking LIN-14 protein synthesis after the initiation of translation. *Dev Biol,* 216**,** 671-80.

Ornitz, D. M. & N. Itoh (2015) The Fibroblast Growth Factor signaling pathway. *Wiley Interdiscip Rev Dev Biol,* 4**,** 215-66.

Palatnik, J. F., E. Allen, X. Wu, C. Schommer, R. Schwab, J. C. Carrington & D. Weigel (2003) Control of leaf morphogenesis by microRNAs. *Nature,* 425**,** 257-63.

Pane, A., K. Wehr & T. Schüpbach (2007) zucchini and squash encode two putative nucleases required for rasiRNA production in the Drosophila germline. *Dev Cell,* 12**,** 851-62.

Parang, K., J. H. Till, A. J. Ablooglu, R. A. Kohanski, S. R. Hubbard & P. A. Cole (2001) Mechanism-based design of a protein kinase inhibitor. *Nat Struct Biol,* 8**,** 37-41.

Pare, J. M., P. LaPointe & T. C. Hobman (2013) Hsp90 cochaperones p23 and FKBP4 physically interact with hAgo2 and activate RNA interference-mediated silencing in mammalian cells. *Mol Biol Cell,* 24**,** 2303-10.

Pare, J. M., J. Lopez-Orozco & T. C. Hobman (2011a) MicroRNA-binding is required for recruitment of human Argonaute 2 to stress granules and P-bodies. *Biochem Biophys Res Commun,* 414**,** 259-64.

Pare, J. M., J. López-Orozco & T. C. Hobman (2011b) MicroRNA-binding is required for recruitment of human Argonaute 2 to stress granules and P-bodies. *Biochem Biophys Res Commun,* 414**,** 259-64.

Pare, J. M., N. Tahbaz, J. López-Orozco, P. LaPointe, P. Lasko & T. C. Hobman (2009) Hsp90 regulates the function of argonaute 2 and its recruitment to stress granules and P-bodies. *Mol Biol Cell,* 20**,** 3273-84.

Parker, G. S., T. S. Maity & B. L. Bass (2008) dsRNA binding properties of RDE-4 and TRBP reflect their distinct roles in RNAi. *J Mol Biol,* 384**,** 967-79.

Paroo, Z., X. Ye, S. Chen & Q. Liu (2009) Phosphorylation of the human microRNA-generating complex mediates MAPK/Erk signaling. *Cell,* 139**,** 112-22.

Perkel, J. M. (2013) Visiting "noncodarnia". *Biotechniques,* 54**,** 301, 303-4.

Peti, W., A. C. Nairn & R. Page (2013) Structural basis for protein phosphatase 1 regulation and specificity. *FEBS J,* 280**,** 596-611.

Piatek, M. J. & A. Werner (2014) Endogenous siRNAs: regulators of internal affairs. *Biochem Soc Trans,* 42**,** 1174-9.

Pillai, R. S., S. N. Bhattacharyya, C. G. Artus, T. Zoller, N. Cougot, E. Basyuk, E. Bertrand & W. Filipowicz (2005) Inhibition of translational initiation by Let-7 MicroRNA in human cells. *Science,* 309**,** 1573-6.

Provost, P., D. Dishart, J. Doucet, D. Frendewey, B. Samuelsson & O. Rådmark (2002) Ribonuclease activity and RNA binding of recombinant human Dicer. *EMBO J,* 21**,** 5864-74.

Qi, H. H., P. P. Ongusaha, J. Myllyharju, D. Cheng, O. Pakkanen, Y. Shi, S. W. Lee & J. Peng (2008) Prolyl 4-hydroxylation regulates Argonaute 2 stability. *Nature,* 455**,** 421-4.

Rehwinkel, J., I. Behm-Ansmant, D. Gatfield & E. Izaurralde (2005) A crucial role for GW182 and the DCP1:DCP2 decapping complex in miRNA-mediated gene silencing. *RNA,* 11**,** 1640-7.

Reijns, M. A., R. D. Alexander, M. P. Spiller & J. D. Beggs (2008) A role for Q/N-rich aggregation-prone regions in P-body localization. *J Cell Sci,* 121**,** 2463-72.

Reilly, J. F., E. Mizukoshi & P. A. Maher (2004) Ligand dependent and independent internalization and nuclear translocation of fibroblast growth factor (FGF) receptor 1. *DNA Cell Biol,* 23**,** 538-48.

Reinhart, B. J., F. J. Slack, M. Basson, A. E. Pasquinelli, J. C. Bettinger, A. E. Rougvie, H. R. Horvitz & G. Ruvkun (2000) The 21-nucleotide let-7 RNA regulates developmental timing in Caenorhabditis elegans. *Nature,* 403**,** 901-6.

Robinson, D. R., Y. M. Wu & S. F. Lin (2000) The protein tyrosine kinase family of the human genome. *Oncogene,* 19**,** 5548-57.

Rojas, M., G. Vasconcelos & T. E. Dever (2015) An eIF2α-binding motif in protein phosphatase 1 subunit GADD34 and its viral orthologs is required to promote dephosphorylation of eIF2α. *Proc Natl Acad Sci U S A,* 112**,** E3466-75.

Rudel, S., Y. Wang, R. Lenobel, R. Korner, H. H. Hsiao, H. Urlaub, D. Patel & G. Meister (2011) Phosphorylation of human Argonaute proteins affects small RNA binding. *Nucleic Acids Res,* 39**,** 2330-43.

Ruhe, J. E., S. Streit, S. Hart & A. Ullrich (2006) EGFR signaling leads to downregulation of PTP-LAR via TACE-mediated proteolytic processing. *Cell Signal,* 18**,** 1515-27.

Rüdel, S., Y. Wang, R. Lenobel, R. Körner, H. H. Hsiao, H. Urlaub, D. Patel & G. Meister (2011) Phosphorylation of human Argonaute proteins affects small RNA binding. *Nucleic Acids Res,* 39**,** 2330-43.

Sacks, D. B. (2006) The role of scaffold proteins in MEK/ERK signalling. *Biochem Soc Trans,* 34**,** 833-6.

Sahin, U., P. Lapaquette, A. Andrieux, G. Faure & A. Dejean (2014) Sumoylation of human argonaute 2 at lysine-402 regulates its stability. *PLoS One,* 9**,** e102957.

Saito, K., H. Ishizu, M. Komai, H. Kotani, Y. Kawamura, K. M. Nishida, H. Siomi & M. C. Siomi (2010) Roles for the Yb body components Armitage and Yb in primary piRNA biogenesis in Drosophila. *Genes Dev,* 24**,** 2493-8.

Saito, K., K. M. Nishida, T. Mori, Y. Kawamura, K. Miyoshi, T. Nagami, H. Siomi & M. C. Siomi (2006) Specific association of Piwi with rasiRNAs derived from retrotransposon and heterochromatic regions in the Drosophila genome. *Genes Dev,* 20**,** 2214-22.

Savas, J. N., B. Ma, K. Deinhardt, B. P. Culver, S. Restituito, L. Wu, J. G. Belasco, M. V. Chao & N. Tanese (2010) A role for huntington disease protein in dendritic RNA granules. *J Biol Chem,* 285**,** 13142-53.

Schaapveld, R., B. Wieringa & W. Hendriks (1997) Receptor-like protein tyrosine phosphatases: alike and yet so different. *Mol Biol Rep,* 24**,** 247-62.

Schindler, A. & E. Foley (2010) A functional RNAi screen identifies hexokinase 1 as a modifier of type II apoptosis. *Cell Signal,* 22**,** 1330-40.

Schirle, N. T. & I. J. MacRae (2012) The crystal structure of human Argonaute2. *Science,* 336**,** 1037-40.

Schisa, J. A., J. N. Pitt & J. R. Priess (2001) Analysis of RNA associated with P granules in germ cells of C. elegans adults. *Development,* 128**,** 1287-98.

Schwartz, D. C. & R. Parker (1999) Mutations in translation initiation factors lead to increased rates of deadenylation and decapping of mRNAs in Saccharomyces cerevisiae. *Mol Cell Biol,* 19**,** 5247-56.

Segatto, O., S. Anastasi & S. Alemà (2011) Regulation of epidermal growth factor receptor signalling by inducible feedback inhibitors. *J Cell Sci,* 124**,** 1785-93.

Sharma, K., R. C. D'Souza, S. Tyanova, C. Schaab, J. R. Wiśniewski, J. Cox & M. Mann (2014) Ultradeep human phosphoproteome reveals a distinct regulatory nature of Tyr and Ser/Thr-based signaling. *Cell Rep,* 8**,** 1583-94.

Shen, J., W. Xia, Y. B. Khotskaya, L. Huo, K. Nakanishi, S. O. Lim, Y. Du, Y. Wang, W. C. Chang, C. H. Chen, J. L. Hsu, Y. Wu, Y. C. Lam, B. P. James, X. Liu, C. G. Liu, D. J. Patel & M. C. Hung (2013) EGFR modulates microRNA maturation in response to hypoxia through phosphorylation of AGO2. *Nature,* 497**,** 383-7.

Shi, Y. (2009) Serine/threonine phosphatases: mechanism through structure. *Cell,* 139**,** 468-84.

Shirayama, M., M. Seth, H. C. Lee, W. Gu, T. Ishidate, D. Conte & C. C. Mello (2012) piRNAs initiate an epigenetic memory of nonself RNA in the C. elegans germline. *Cell,* 150**,** 65-77.

Song, J. J., J. Liu, N. H. Tolia, J. Schneiderman, S. K. Smith, R. A. Martienssen, G. J. Hannon & L. Joshua-Tor (2003) The crystal structure of the Argonaute2 PAZ domain reveals an RNA binding motif in RNAi effector complexes. *Nat Struct Biol,* 10**,** 1026-32.

Song, J. J., S. K. Smith, G. J. Hannon & L. Joshua-Tor (2004) Crystal structure of Argonaute and its implications for RISC slicer activity. *Science,* 305**,** 1434-7.

Steinberg, F., L. Zhuang, M. Beyeler, R. E. Kälin, P. E. Mullis, A. W. Brändli & B. Trueb (2010) The FGFRL1 receptor is shed from cell membranes, binds fibroblast growth factors (FGFs), and antagonizes FGF signaling in Xenopus embryos. *J Biol Chem,* 285**,** 2193-202.

Stoecklin, G. & N. Kedersha (2013) Relationship of GW/P-bodies with stress granules. *Adv Exp Med Biol,* 768**,** 197-211.

Stöhr, N., M. Lederer, C. Reinke, S. Meyer, M. Hatzfeld, R. H. Singer & S. Hüttelmaier (2006) ZBP1 regulates mRNA stability during cellular stress. *J Cell Biol,* 175**,** 527-34.

Sun, G., Y. Wang, L. Sun, H. Luo, N. Liu, Z. Fu & Y. You (2011) Clinical significance of Hiwi gene expression in gliomas. *Brain Res,* 1373**,** 183-8.

Swarts, D. C., K. Makarova, Y. Wang, K. Nakanishi, R. F. Ketting, E. V. Koonin, D. J. Patel & J. van der Oost (2014) The evolutionary journey of Argonaute proteins. *Nat Struct Mol Biol,* 21**,** 743-53.

Tabba, S., S. Mangat, R. McCartney & M. C. Schmidt (2010) PP1 phosphatase-binding motif in Reg1 protein of Saccharomyces cerevisiae is required for interaction with both the PP1 phosphatase Glc7 and the Snf1 protein kinase. *Cell Signal,* 22**,** 1013-21.

Tahbaz, N., F. A. Kolb, H. Zhang, K. Jaronczyk, W. Filipowicz & T. C. Hobman (2004) Characterization of the interactions between mammalian PAZ PIWI domain proteins and Dicer. *EMBO Rep,* 5**,** 189-94.

Takimoto, K., M. Wakiyama & S. Yokoyama (2009) Mammalian GW182 contains multiple Argonaute-binding sites and functions in microRNA-mediated translational repression. *RNA,* 15**,** 1078-89.

Terrak, M., F. Kerff, K. Langsetmo, T. Tao & R. Dominguez (2004) Structural basis of protein phosphatase 1 regulation. *Nature,* 429**,** 780-4.

Thomson, T. & H. Lin (2009) The biogenesis and function of PIWI proteins and piRNAs: progress and prospect. *Annu Rev Cell Dev Biol,* 25**,** 355-76.

Till, S., E. Lejeune, R. Thermann, M. Bortfeld, M. Hothorn, D. Enderle, C. Heinrich, M. W. Hentze & A. G. Ladurner (2007) A conserved motif in Argonaute-interacting proteins mediates functional interactions through the Argonaute PIWI domain. *Nat Struct Mol Biol,* 14**,** 897-903.

Tourrière, H., K. Chebli, L. Zekri, B. Courselaud, J. M. Blanchard, E. Bertrand & J. Tazi (2003) The RasGAP-associated endoribonuclease G3BP assembles stress granules. *J Cell Biol,* 160**,** 823-31.

Tucker, M., R. R. Staples, M. A. Valencia-Sanchez, D. Muhlrad & R. Parker (2002) Ccr4p is the catalytic subunit of a Ccr4p/Pop2p/Notp mRNA deadenylase complex in Saccharomyces cerevisiae. *EMBO J,* 21**,** 1427-36.

Tudzarova, S., P. Mulholland, A. Dey, K. Stoeber, A. L. Okorokov & G. H. Williams (2016) p53 controls CDC7 levels to reinforce G1 cell cycle arrest upon genotoxic stress. *Cell Cycle,* 15**,** 2958-2972.

Ubersax, J. A. & J. E. Ferrell (2007) Mechanisms of specificity in protein phosphorylation. *Nat Rev Mol Cell Biol,* 8**,** 530-41.

Vagin, V. V., A. Sigova, C. Li, H. Seitz, V. Gvozdev & P. D. Zamore (2006) A distinct small RNA pathway silences selfish genetic elements in the germline. *Science,* 313**,** 320-4.

van Dijk, E., N. Cougot, S. Meyer, S. Babajko, E. Wahle & B. Seraphin (2002a) Human Dcp2: a catalytically active mRNA decapping enzyme located in specific cytoplasmic structures. *EMBO J,* 21**,** 6915-24.

van Dijk, E., N. Cougot, S. Meyer, S. Babajko, E. Wahle & B. Séraphin (2002b) Human Dcp2: a catalytically active mRNA decapping enzyme located in specific cytoplasmic structures. *EMBO J,* 21**,** 6915-24.

van Montfort, R. L., M. Congreve, D. Tisi, R. Carr & H. Jhoti (2003) Oxidation state of the active-site cysteine in protein tyrosine phosphatase 1B. *Nature,* 423**,** 773-7.

van Wolfswinkel, J. C. (2014) Piwi and potency: PIWI proteins in animal stem cells and regeneration. *Integr Comp Biol,* 54**,** 700-13.

Vermorken, J. B., J. Trigo, R. Hitt, P. Koralewski, E. Diaz-Rubio, F. Rolland, R. Knecht, N. Amellal, A. Schueler & J. Baselga (2007) Open-label, uncontrolled, multicenter

phase II study to evaluate the efficacy and toxicity of cetuximab as a single agent in patients with recurrent and/or metastatic squamous cell carcinoma of the head and neck who failed to respond to platinum-based therapy. *J Clin Oncol,* 25**,** 2171-7.

Wagner, J. P., A. Wolf-Yadlin, M. Sevecka, J. K. Grenier, D. E. Root, D. A. Lauffenburger & G. MacBeath (2013) Receptor tyrosine kinases fall into distinct classes based on their inferred signaling networks. *Sci Signal,* 6**,** ra58.

Wakula, P., M. Beullens, H. Ceulemans, W. Stalmans & M. Bollen (2003) Degeneracy and function of the ubiquitous RVXF motif that mediates binding to protein phosphatase-1. *J Biol Chem,* 278**,** 18817-23.

Wang, G. & V. Reinke (2008) A C. elegans Piwi, PRG-1, regulates 21U-RNAs during spermatogenesis. *Curr Biol,* 18**,** 861-7.

Wang, H. W., C. Noland, B. Siridechadilok, D. W. Taylor, E. Ma, K. Felderer, J. A. Doudna & E. Nogales (2009) Structural insights into RNA processing by the human RISC-loading complex. *Nat Struct Mol Biol,* 16**,** 1148-53.

Wang, X. H., R. Aliyari, W. X. Li, H. W. Li, K. Kim, R. Carthew, P. Atkinson & S. W. Ding (2006) RNA interference directs innate immunity against viruses in adult Drosophila. *Science,* 312**,** 452-4.

Wang, Y., R. Mercier, T. C. Hobman & P. LaPointe (2013) Regulation of RNA interference by Hsp90 is an evolutionarily conserved process. *Biochim Biophys Acta,* 1833**,** 2673-81.

Wang, Z. & P. A. Cole (2014) Catalytic mechanisms and regulation of protein kinases. *Methods Enzymol,* 548**,** 1-21.

Wee, L. M., C. F. Flores-Jasso, W. E. Salomon & P. D. Zamore (2012) Argonaute divides its RNA guide into domains with distinct functions and RNA-binding properties. *Cell,* 151**,** 1055-67.

Wek, R. C., H. Y. Jiang & T. G. Anthony (2006) Coping with stress: eIF2 kinases and translational control. *Biochem Soc Trans,* 34**,** 7-11.

Wightman, B., I. Ha & G. Ruvkun (1993) Posttranscriptional regulation of the heterochronic gene lin-14 by lin-4 mediates temporal pattern formation in C. elegans. *Cell,* 75**,** 855-62.

Wilczynska, A., C. Aigueperse, M. Kress, F. Dautry & D. Weil (2005) The translational regulator CPEB1 provides a link between dcp1 bodies and stress granules. *J Cell Sci,* 118**,** 981-92.

Wilson, R. C., A. Tambe, M. A. Kidwell, C. L. Noland, C. P. Schneider & J. A. Doudna (2015) Dicer-TRBP complex formation ensures accurate mammalian microRNA biogenesis. *Mol Cell,* 57**,** 397-407.

Wostenberg, C., J. W. Lary, D. Sahu, R. Acevedo, K. A. Quarles, J. L. Cole & S. A. Showalter (2012) The role of human Dicer-dsRBD in processing small regulatory RNAs. *PLoS One,* 7**,** e51829.

Wu, H., H. Xu, L. J. Miraglia & S. T. Crooke (2000) Human RNase III is a 160-kDa protein involved in preribosomal RNA processing. *J Biol Chem,* 275**,** 36957-65.

Wu, Y., Z. Chen & A. Ullrich (2003) EGFR and FGFR signaling through FRS2 is subject to negative feedback control by ERK1/2. *Biol Chem,* 384**,** 1215-26.

Xu, P., S. Y. Vernooy, M. Guo & B. A. Hay (2003) The Drosophila microRNA Mir-14 suppresses cell death and is required for normal fat metabolism. *Curr Biol,* 13**,** 790-5.

Yamashita, A., T. C. Chang, Y. Yamashita, W. Zhu, Z. Zhong, C. Y. Chen & A. B. Shyu (2005) Concerted action of poly(A) nucleases and decapping enzyme in mammalian mRNA turnover. *Nat Struct Mol Biol,* 12**,** 1054-63.

Yamashita, S., T. Nagata, M. Kawazoe, C. Takemoto, T. Kigawa, P. Güntert, N. Kobayashi, T. Terada, M. Shirouzu, M. Wakiyama, Y. Muto & S. Yokoyama (2011) Structures of the first and second double-stranded RNA-binding domains of human TAR RNA-binding protein. *Protein Sci,* 20**,** 118-30.

Yang, Q., W. Li, H. She, J. Dou, D. M. Duong, Y. Du, S. H. Yang, N. T. Seyfried, H. Fu, G. Gao & Z. Mao (2015) Stress induces p38 MAPK-mediated phosphorylation and inhibition of Drosha-dependent cell survival. *Mol Cell,* 57**,** 721-34.

Yang, S. H., A. D. Sharrocks & A. J. Whitmarsh (2013) MAP kinase signalling cascades and transcriptional regulation. *Gene,* 513**,** 1-13.

Yang, Z., A. Jakymiw, M. R. Wood, T. Eystathioy, R. L. Rubin, M. J. Fritzler & E. K. Chan (2004) GW182 is critical for the stability of GW bodies expressed during the cell cycle and cell proliferation. *J Cell Sci,* 117**,** 5567-78.

Yigit, E., P. J. Batista, Y. Bei, K. M. Pang, C. C. Chen, N. H. Tolia, L. Joshua-Tor, S. Mitani, M. J. Simard & C. C. Mello (2006) Analysis of the C. elegans Argonaute family reveals that distinct Argonautes act sequentially during RNAi. *Cell,* 127**,** 747-57.

Yin, V. P., J. M. Thomson, R. Thummel, D. R. Hyde, S. M. Hammond & K. D. Poss (2008) Fgf-dependent depletion of microRNA-133 promotes appendage regeneration in zebrafish. *Genes Dev,* 22**,** 728-33.

Zeng, Y., H. Sankala, X. Zhang & P. R. Graves (2008) Phosphorylation of Argonaute 2 at serine-387 facilitates its localization to processing bodies. *Biochem J,* 413**,** 429-36.

Zhang, H., F. A. Kolb, V. Brondani, E. Billy & W. Filipowicz (2002) Human Dicer preferentially cleaves dsRNAs at their termini without a requirement for ATP. *EMBO J,* 21**,** 5875-85.

Zhang, Z., S. Kobayashi, A. C. Borczuk, R. S. Leidner, T. Laframboise, A. D. Levine & B. Halmos (2010) Dual specificity phosphatase 6 (DUSP6) is an ETS-regulated negative feedback mediator of oncogenic ERK signaling in lung cancer cells. *Carcinogenesis,* 31**,** 577-86.

Zheng, Y., C. Zhang, D. R. Croucher, M. A. Soliman, N. St-Denis, A. Pasculescu, L. Taylor, S. A. Tate, W. R. Hardy, K. Colwill, A. Y. Dai, R. Bagshaw, J. W. Dennis, A. C. Gingras, R. J. Daly & T. Pawson (2013) Temporal regulation of EGF signalling networks by the scaffold protein Shc1. *Nature,* 499**,** 166-71.

Zipprich, J. T., S. Bhattacharyya, H. Mathys & W. Filipowicz (2009) Importance of the C-terminal domain of the human GW182 protein TNRC6C for translational repression. *RNA,* 15**,** 781-93.

Appendix

Appendix Table 1. Full results of the kinase screen presented in Figure 4.1. Death Index, upper and lower limits of the 95% confidence interval and statistical significance calculations are described in detail in section 2.2.10.3. Kinases with dead indexes < 1 reduce RNAi activity and are presented in red. Kinases with death indexes > 1 increase RNAi activity and are presented in green.

Appendix Table 1

Death Index	Symbol	Upper limit 95% CI UL	Lower limit 95% CI LL	Statistical significance
0.74073583	BMX	0.96355012	0.517921532	Positive
0.77756551	FGFR3	0.915937828	0.639193201	Positive
0.82177867	MAP3K5	1.080605642	0.562951698	-
0.84786688	FGFR2	1.085588322	0.610145445	-
0.84880581	PXK	0.990355647	0.707255981	Positive
0.85032068	FGR	1.079213882	0.621427481	-
0.85033811	TEK	0.995346238	0.705329981	Positive
0.85351419	PACSIN3	1.198094135	0.508934242	-
0.86156898	PRKCD	1.190283146	0.532854823	-
0.87384995	FLJ22955	1.183598294	0.564101597	-
0.87411016	STYK1	1.111540282	0.636680037	-
0.87480974	BLK	1.212122456	0.53749702	-
0.87636993	GSK3B	1.320510775	0.432229089	-
0.87766679	EPHB1	0.988233515	0.767100072	Positive
0.87844326	FLT3	1.182133487	0.574753036	-
0.87885197	TGFBR1	1.221322943	0.536380993	-
0.87966765	EPHA2	1.346436224	0.412899073	-
0.88321937	MAP3K9	1.339458293	0.426980447	-
0.88416214	VRK3	1.183089089	0.5852352	-
0.88460015	FRAP1	1.238024219	0.531176074	-
0.88629568	PLK3	1.109552017	0.663039338	-
0.88803656	MAPK6	1.572985979	0.203087138	-
0.88897494	PCTK3	1.166233044	0.611716843	-
0.89071599	PRKCDBP	1.288716922	0.492715062	-
0.89272896	PAK3	1.126676995	0.65878092	-
0.89334084	PDGFRL	1.206088541	0.580593141	-
0.89376236	EPHB6	1.259031711	0.528493016	-
0.8984273	PRPS1	1.370595158	0.426259438	-
0.89951084	ITK	1.234247858	0.564773816	-
0.90084909	MPP1	0.956267787	0.845430383	Positive
0.90303013	STK39	1.080224054	0.725836199	-
0.90416235	DTYMK	1.090982581	0.717342119	-
0.90855627	MAP3K11	1.318751392	0.498361143	-
0.90870804	FLT1	1.214471936	0.602944136	-
0.90874404	PIP5K2C	1.442258624	0.375229449	-
0.91151643	C9orf95	1.193115898	0.629916954	-
0.91281968	MUSK	1.23981014	0.585829215	-
0.91338155	EPHA1	0.966151488	0.860611603	Positive
0.91468848	PDGFRA	1.176803387	0.652573579	-
0.91469414	CAMK2A	1.100377259	0.729011025	-
0.91545551	CDC42BPA	1.001762266	0.829148764	-
0.91795271	ERBB3	1.274858676	0.561046743	-
0.91887733	CAMK1D	1.216812657	0.620942003	-
0.92033765	LOC441708	0.999098367	0.84157694	Positive
0.92205825	MAP3K4	1.156902529	0.687213972	-

0.9226488	EPHA4	1.043111297	0.802186305	-
0.92310229	AK1	1.057227747	0.788976831	-
0.9236884	EPHB3	1.462378131	0.38499866	-
0.92536868	LTK	1.266708176	0.584029179	-
0.9254605	PGK2	1.217721726	0.633199277	-
0.9263269	ATM	1.13756556	0.715088234	-
0.92643539	NTRK3	1.159161478	0.693709301	-
0.92992542	NRGN	1.329879574	0.529971272	-
0.93134335	GCKR	1.184169011	0.678517685	-
0.93292796	BRAF	1.326567477	0.539288446	-
0.93337277	PAK2	1.346458007	0.520287528	-
0.93383228	NTRK1	1.268769671	0.598894893	-
0.93529423	GRK5	1.395178975	0.475409487	-
0.93726048	ADCK4	1.43840733	0.436113622	-
0.93938785	DGKG	1.387194358	0.491581339	-
0.93972741	SCGB2A1	1.438891843	0.440562972	-
0.94041788	MATK	1.287069788	0.593765981	-
0.94232136	DYRK1A	1.235997352	0.648645364	-
0.94305529	CSNK1D	1.369607316	0.516503259	-
0.94452656	KDR	1.392856221	0.496196901	-
0.94662624	JAK3	1.104529002	0.788723474	-
0.94795054	LY6G5B	1.377937976	0.517963114	-
0.94900378	FLT4	1.349590798	0.548416767	-
0.94972612	AKT2	1.314154681	0.58529755	-
0.94973263	IKBKB	1.267486715	0.631978537	-
0.95040417	PRKCABP	1.591570994	0.309237345	-
0.95289817	EPHA8	1.412522883	0.493273456	-
0.95510907	BTK	1.210447069	0.699771066	-
0.95882378	CD2	1.164494071	0.75315348	-
0.95935374	MOS	1.413962086	0.504745389	-
0.96032292	AXL	1.213886922	0.706758909	-
0.96076002	FLJ23074	1.287189517	0.634330527	-
0.96079404	PDGFRB	1.245344066	0.676244011	-
0.96497925	PRKAA1	1.126963319	0.802995181	-
0.96501461	MKNK2	1.356835235	0.573193988	-
0.96541031	DMPK	1.242391116	0.688429497	-
0.96992744	NME3	1.329112728	0.610742159	-
0.97015214	FES	1.448712188	0.491592084	-
0.97058747	CHUK	1.442759839	0.498415098	-
0.97059411	DGKQ	1.126218848	0.814969373	-
0.97107794	FER	1.093666233	0.848489655	-
0.97323396	KIAA2002	1.349507064	0.596960864	-
0.9759954	ITPK1	1.829480771	0.122510023	-
0.97720797	RPS6KL1	1.530725585	0.423690349	-
0.97805911	GCK	1.311059735	0.645058489	-
0.97921022	GK2	1.500399387	0.458021062	-
0.98201505	DDR1	1.263062684	0.700967413	-
0.98328075	CLK1	1.388531574	0.578029917	-
0.98603413	HK3	1.250691419	0.721376849	-

0.98805555	NYD-SP25	1.334720784	0.641390315	-
0.98877697	FLJ33655	1.138355147	0.839198795	-
0.98930319	CDK3	1.458062443	0.520543944	-
0.98935012	CSF1R	1.437047303	0.541652945	-
0.99047077	PAK6	1.674138343	0.306803194	-
0.99299217	MKNK1	1.228604419	0.75737992	-
0.99300642	AMHR2	1.373509299	0.612503547	-
0.99376411	PANK3	1.457758097	0.529770113	-
0.99442951	BUB1	1.147702663	0.841156356	-
0.99778411	NTRK2	1.375420025	0.620148188	-
0.99801766	KHK	1.374181424	0.621853897	-
0.99915803	PRKCSH	1.505191708	0.493124342	-
1.00289315	MAP2K6	1.253055624	0.75273068	-
1.00317465	ACVR2	1.436138548	0.570210754	-
1.00476718	BMP2K	1.414416112	0.595118255	-
1.00480723	ACVR2B	1.423203256	0.586411209	-
1.00579668	DGKB	1.334310653	0.677282702	-
1.00588234	ADRBK2	1.431262699	0.58050199	-
1.00896594	NME1	1.37062511	0.647306768	-
1.00912053	CSNK1G2	1.472230322	0.54601074	-
1.01080853	LOC388221	1.044372253	0.977244808	-
1.01156998	CLK2	1.299705377	0.723434586	-
1.01243673	STK22C	1.525379223	0.499494241	-
1.01295667	MAPK10	1.238006712	0.787906623	-
1.01619137	C9orf12	1.30660846	0.725774272	-
1.01632345	MPP3	1.260158085	0.772488808	-
1.01741449	DGKA	1.440837995	0.593990985	-
1.01809257	MAST4	1.314327145	0.721857999	-
1.01989632	PIK3CA	1.607435565	0.432357081	-
1.02158463	CIT	1.209494262	0.83367499	-
1.0221464	MPP2	1.517151076	0.527141715	-
1.02350632	PRPF4B	1.255512046	0.791500589	-
1.02413698	HGS	1.363648449	0.684625511	-
1.02419084	STK11IP	1.588479715	0.459901972	-
1.02467528	HCK	1.539685577	0.509664991	-
1.02560203	FUK	1.136636262	0.914567788	-
1.02596633	CAMKK1	1.467457993	0.584474662	-
1.02609342	PRKCI	1.435240317	0.616946516	-
1.02710796	RIPK4	1.567916387	0.486299525	-
1.02879741	NAGK	1.300449855	0.757144968	-
1.02906115	KIAA1361	1.452104259	0.606018041	-
1.02936838	PIP5K2A	1.104667969	0.954068787	-
1.03083478	CKMT2	1.537323791	0.524345773	-
1.03125851	MET	1.449588	0.612929011	-
1.03189134	PMVK	1.178991553	0.884791125	-
1.03235061	TRIB3	2.085984682	-0.021283456	-
1.03343133	CAMK1	1.18155914	0.885303518	-
1.03417173	LYK5	1.378613583	0.689729877	-
1.0348338	ROCK1	1.478586403	0.591081194	-

1.03609122	DGKH	1.448689423	0.623493017	-
1.03697798	HK2	2.060168192	0.01378776	-
1.03741779	EEF2K	1.285778403	0.78905718	-
1.03793017	PRKWNK3	1.518248009	0.557612327	-
1.03819945	INSRR	1.57338559	0.503013301	-
1.03906723	NEK1	1.511999711	0.566134743	-
1.04112398	RIPK3	1.081317662	1.000930304	Positive
1.04168815	RNASEL	1.414647919	0.668728376	-
1.04191885	HAK	1.496772115	0.587065583	-
1.0420175	TRIB1	1.413753491	0.6702815	-
1.04213421	C21orf7	1.602476893	0.481791535	-
1.04267792	KIAA1804	1.312052261	0.773303571	-
1.0430749	MAK	1.479033714	0.607116083	-
1.04359505	SCYL1	1.404782393	0.682407712	-
1.043998	CAMK4	1.753108524	0.334887482	-
1.04429446	PRKACA	1.819545531	0.269043394	-
1.04653792	CASK	1.335177844	0.757898003	-
1.04682419	YES1	1.443760589	0.649887791	-
1.04746878	GRIP2	1.450800205	0.644137362	-
1.047649	BMPR1A	1.340231034	0.755066975	-
1.04802195	TRRAP	1.459786102	0.636257801	-
1.04951988	PRKACG	1.450739913	0.648299847	-
1.04989247	SRC	1.30908184	0.7907031	-
1.05003347	SLK	1.4058626	0.694204338	-
1.05085101	GLYCTK	1.08417424	1.01752778	Positive
1.0508716	CALM2	1.153711039	0.948032169	-
1.05129945	ALK	1.436378178	0.666220731	-
1.05148023	MAP3K7	1.248335363	0.854625091	-
1.05170205	MAP2K4	1.809524338	0.293879764	-
1.05193615	CKMT1	1.464910502	0.638961802	-
1.05326608	MAPK14	1.341344656	0.765187508	-
1.05646633	STK22D	1.352850691	0.760081971	-
1.05740863	CSNK1E	1.554110537	0.560706719	-
1.0575756	MAP4K3	1.276914477	0.838236724	-
1.05865351	HK1	1.372721587	0.744585428	-
1.05876909	FGFRL1	1.479651061	0.637887114	-
1.05996623	PIM1	1.167499253	0.952433214	-
1.06109166	MPP5	1.494298647	0.627884667	-
1.0620495	LIMK1	1.148552318	0.975546683	-
1.06262592	MAP4K1	1.323009752	0.802242093	-
1.06282551	CDK2	1.487638688	0.638012341	-
1.06393384	DKFZP434C131	1.445918243	0.681949443	-
1.06401589	STK16	1.53304425	0.59498753	-
1.06421676	MGC4796	1.369948721	0.75848479	-
1.06603876	ACVRL1	1.534974504	0.597103024	-
1.06616432	DGUOK	1.469830371	0.662498259	-
1.06646549	NEK9	1.283431218	0.849499766	-
1.06650308	UCK1	1.312640943	0.820365225	-
1.06776494	STK36	1.717844731	0.417685143	-

1.06878478	MIDORI	1.652008004	0.485561565	-
1.06934118	DYRK2	1.46552391	0.673158452	-
1.06992558	ILK	1.486637982	0.653213186	-
1.07049132	TAF1	1.315006729	0.825975911	-
1.07096194	PRPS2	1.313972435	0.827951454	-
1.07159193	PTK2B	1.522655429	0.620528433	-
1.07194622	RIPK5	1.421172402	0.722720043	-
1.07208621	BMP2KL	1.263904886	0.88026754	-
1.07299704	AKAP8L	1.578223019	0.567771053	-
1.07333239	INSR	1.394793496	0.751871289	-
1.07344784	MAP2K3	1.309533622	0.83736205	-
1.07392826	JAK2	1.203541157	0.944315354	-
1.07428503	FLJ10986	1.639597732	0.508972334	-
1.07435104	DAPK1	1.414451379	0.734250704	-
1.0761511	EGFR	1.434247324	0.71805488	-
1.07634276	MGC40579	1.219828835	0.932856692	-
1.0765814	RPS6KA6	1.471584978	0.681577823	-
1.07806991	CSNK1G1	1.215396748	0.94074308	-
1.07829944	CDKL5	1.279674796	0.876924078	-
1.07861253	ALDH18A1	1.669877357	0.487347694	-
1.0788718	PINK1	1.352795538	0.804948061	-
1.07942649	PHKG1	1.430181607	0.728671379	-
1.07959853	MAST3	1.353966316	0.805230754	-
1.08024163	GRK4	1.496574033	0.663909225	-
1.08228128	UCK2	1.702094786	0.462467777	-
1.08238976	CKM	1.248749219	0.916030307	-
1.08243001	PRKCB1	1.465577061	0.699282965	-
1.08280982	RIOK2	1.289069563	0.87655007	-
1.08281871	PI4K2B	1.302545098	0.863092316	-
1.08375314	PIK3C2A	1.253459477	0.914046798	-
1.084325	GAK	1.413217907	0.755432086	-
1.08514228	NEK11	1.40625704	0.764027525	-
1.08621021	CDK7	1.497675615	0.674744814	-
1.08706174	CaMKIINalpha	1.724696442	0.449427036	-
1.08719516	CSNK1G3	1.388837483	0.785552836	-
1.08734793	LCK	1.45284681	0.721849057	-
1.08764821	MADD	1.571433831	0.603862592	-
1.0877773	RIOK3	1.703530618	0.472023989	-
1.08816752	MAPK8	1.273825338	0.902509693	-
1.08822742	KIAA1639	1.600221586	0.57623326	-
1.08845678	OSR1	1.375571291	0.801342278	-
1.08856527	CRIM1	1.17950771	0.997622827	-
1.08944716	SSTK	1.466244379	0.712649939	-
1.09013755	PNKP	1.503865097	0.67641001	-
1.09014021	MARK4	1.165683658	1.014596769	Positive
1.09029753	EPHB2	1.191046948	0.989548103	-
1.09055121	TTBK1	1.519192642	0.661909781	-
1.09063303	CALM1	1.402078129	0.779187934	-
1.09158707	MPP4	1.600020295	0.583153844	-

1.09180251	DKFZp761P0423	1.253532256	0.930072772	-
1.09238789	LMTK3	1.556797453	0.627978327	-
1.09309423	BMPR1B	1.171102193	1.015086276	Positive
1.09341341	NEK7	1.434474024	0.752352786	-
1.09390746	TLK1	1.68141113	0.506403791	-
1.09522367	DKFZp434B1231	1.711226391	0.479220944	-
1.09552996	VRK2	1.443081703	0.747978221	-
1.09564104	PKN2	1.363472164	0.827809922	-
1.09746102	SGKL	1.41373718	0.781184858	-
1.09793735	EIF2AK4	1.713597345	0.482277361	-
1.09810332	PCTK1	1.180717256	1.015489388	Positive
1.09868751	FLJ12476	1.610479858	0.58689517	-
1.09874136	ERBB4	1.149072927	1.048409788	Positive
1.09876518	PTK9	1.537111616	0.660418741	-
1.09896049	ROS1	2.020941527	0.176979455	-
1.09911414	ADCK2	1.482861926	0.715366347	-
1.09920682	JIK	1.362798488	0.835615147	-
1.09935405	PLXNB1	1.513694994	0.685013115	-
1.10005505	SNX16	1.780992706	0.419117393	-
1.1021327	CRK7	1.59788649	0.606378917	-
1.103509	MAP3K13	1.47457567	0.732442337	-
1.10361074	PRKCM	1.596949819	0.610271669	-
1.10369545	KIS	1.809354925	0.398035966	-
1.10379184	C9orf98	1.609531767	0.598051915	-
1.10405327	TBK1	1.524847768	0.683258769	-
1.1040584	PRKG2	1.164998937	1.04311786	Positive
1.10427128	DCK	1.390344259	0.818198294	-
1.10480147	PHKG2	1.310910245	0.898692696	-
1.10552397	PTK7	1.496700833	0.714347105	-
1.10606596	ALS2CR7	1.704832447	0.507299471	-
1.10641047	ITPKC	1.388303516	0.824517424	-
1.10645951	SYK	1.166910552	1.04600846	Positive
1.10702463	DCAMKL1	1.218892196	0.995157073	-
1.10783414	CAMK2B	1.65102848	0.564639806	-
1.10828652	STK10	1.944795361	0.271777677	-
1.10987015	MGC8407	1.655533247	0.56420706	-
1.11110085	MAP4K5	1.34440256	0.877799135	-
1.11149918	MYLK2	1.427445863	0.795552493	-
1.11280089	CDK6	1.296807231	0.928794544	-
1.1147718	SRPK1	1.149450394	1.0800932	Positive
1.11572728	FLJ22761	1.394565404	0.836889153	-
1.11626586	STK33	1.533222235	0.699309484	-
1.11688221	ULK1	1.569277923	0.664486489	-
1.11721797	MAP3K14	1.611539754	0.622896176	-
1.11741507	EPHB4	1.747443588	0.487386553	-
1.11814807	EPHA3	1.517337623	0.718958509	-
1.11866606	CHEK2	1.545316023	0.692016096	-
1.11874577	KIAA1765	1.373594725	0.863896825	-
1.118879	LOC391533	1.614967373	0.622790631	-

1.1189403	MAP3K10	1.278794007	0.959086602	-
1.11951409	PSKH1	1.426649693	0.812378485	-
1.11965847	ABL2	1.286888475	0.952428458	-
1.11970395	LOC442141	1.562475014	0.676932879	-
1.11999243	RPS6KA4	1.993915594	0.246069262	-
1.12010185	TK2	1.515062816	0.725140885	-
1.12162754	LOC91807	1.611128618	0.632126453	-
1.12187003	RPS6KA2	1.168118097	1.075621967	Positive
1.12245142	FYN	1.693991952	0.550910898	-
1.12273445	CSNK2A2	1.261338848	0.984130051	-
1.12288629	PFKM	1.310230532	0.935542045	-
1.12388761	RFK	2.186191433	0.061583789	-
1.12400652	KIAA0999	1.368418782	0.879594261	-
1.12450464	MAP4K2	1.203442044	1.04556724	Positive
1.12473437	AKT1	1.329828872	0.919639871	-
1.12476735	TEX14	1.559953846	0.689580864	-
1.12482979	CDK8	1.210296564	1.039363026	Positive
1.12483193	NRBP	1.444879241	0.804784617	-
1.12499302	TSKS	1.641906984	0.608079065	-
1.12594056	GRK6	1.406780615	0.845100507	-
1.12655878	LMTK2	1.434526531	0.818591037	-
1.1272837	MINK	1.459550607	0.795016794	-
1.12739292	UCKL1	1.732491267	0.522294568	-
1.12749227	CDK11	1.438001404	0.816983139	-
1.12786487	ADRBK1	1.150844489	1.10488525	Positive
1.1279775	MGC45428	1.512315143	0.743639864	-
1.12844101	MASTL	1.428391106	0.828490912	-
1.12846123	DGKD	1.507676959	0.749245491	-
1.12983693	CDC42BPB	1.359695715	0.899978148	-
1.13141275	MAST2	1.490454742	0.77237075	-
1.13170025	IHPK2	1.339987243	0.923413257	-
1.13235159	ERN2	1.363315991	0.901387182	-
1.13279184	PRKXP1	1.354367757	0.911215925	-
1.13348069	TAF1L	1.262418013	1.004543357	Positive
1.13353768	RPS6KA3	1.375325513	0.891749856	-
1.13442165	GSG2	1.528323961	0.740519344	-
1.13496616	HRI	1.301081327	0.968850983	-
1.13592464	LYN	1.289002265	0.982847009	-
1.13603835	PIP5K1C	1.625334047	0.646742654	-
1.13618577	AIP1	1.807048722	0.465322826	-
1.13704957	CDK4	1.423827761	0.850271383	-
1.13807372	PAK1	2.056472634	0.219674797	-
1.13823501	PLXNA4A	1.533844751	0.742625267	-
1.1387985	TGFBR2	1.550290979	0.727306014	-
1.14041168	PIK4CA	1.392435949	0.888387401	-
1.14097605	NLK	1.388889989	0.893062109	-
1.14178187	STK25	1.469903055	0.81366069	-
1.14182385	LOC283846	1.219302606	1.06434509	Positive
1.14197029	PRKCN	1.51539034	0.768550242	-

1.14240347	IRAK3	1.394978347	0.889828595	-
1.14280908	AK5	1.507396274	0.778221882	-
1.14353628	RBKS	1.826745692	0.460326868	-
1.14410446	GALK1	1.286911205	1.001297708	Positive
1.14447632	PIP5K2B	1.54609494	0.7428577	-
1.14463058	TK1	1.298252967	0.991008194	-
1.14488611	FLJ10842	1.518296113	0.771476115	-
1.14489234	MAP2K1IP1	1.496229959	0.79355473	-
1.14518926	RPS6KB2	2.156349614	0.13402891	-
1.14528926	SRMS	1.508697382	0.781881129	-
1.14609146	KIAA1811	1.558643137	0.733539779	-
1.14779945	PAK7	1.66085716	0.63474174	-
1.14784313	BMPR2	1.728287836	0.567398432	-
1.14956525	CLK4	1.565203244	0.733927262	-
1.15043822	MARK2	1.336548861	0.964327573	-
1.15067332	NEK8	1.496097359	0.805249286	-
1.15122882	DYRK4	1.446160588	0.856297058	-
1.15127027	PIP5K1A	1.33371642	0.968824129	-
1.15167723	NEK4	1.55577338	0.74758109	-
1.15179722	PIK3R3	1.337837238	0.96575721	-
1.15221668	COL4A3BP	1.276061262	1.028372099	Positive
1.15242519	PRKACB	1.439180467	0.865669909	-
1.1527061	ARAF1	1.373082155	0.932330037	-
1.1528671	PACE-1	1.536506139	0.769228052	-
1.15319926	KIAA0551	1.445203624	0.861194905	-
1.15353271	PANK1	1.421566392	0.885499021	-
1.15383631	ETNK2	1.445172686	0.862499943	-
1.15389432	SGK2	1.342548477	0.965240163	-
1.15389562	CHKA	1.586075283	0.72171595	-
1.15439764	PRKX	1.593059111	0.715736174	-
1.15457498	GNE	1.468990394	0.840159571	-
1.15461469	ALS2CR2	1.23355263	1.075676753	Positive
1.1552275	ROCK2	1.459389073	0.851065925	-
1.15579337	UMP-CMPK	1.527755305	0.783831437	-
1.15598967	MST4	1.689320308	0.622659034	-
1.15681408	PKM2	1.649969439	0.663658713	-
1.1568314	MAPK13	1.456272519	0.857390272	-
1.15721595	CSK	1.382790691	0.931641204	-
1.15855989	MAGI-3	1.330534306	0.986585472	-
1.1589488	RIOK1	1.551567138	0.766330467	-
1.15908025	PIK3R4	1.203902779	1.11425772	Positive
1.15910437	SPHK2	1.597361894	0.720846843	-
1.16010674	DKFZP586B1621	1.335733237	0.984480245	-
1.16084589	ZAP70	1.603742322	0.717949462	-
1.16158106	PIK3C2B	1.384956948	0.938205174	-
1.16238609	PANK2	1.538807796	0.785964375	-
1.16264224	DGKK	1.380724273	0.944560211	-
1.16380679	MRC2	1.562172068	0.765441512	-
1.16389887	LIMK2	1.397954955	0.929842793	-

1.16457698	PDK3	1.336002817	0.99315115	-
1.16458011	PRPSAP1	1.482476291	0.846683923	-
1.16477763	STK22B	1.38834317	0.941212081	-
1.16487674	PFKL	1.520875532	0.808877952	-
1.16516317	MAP3K2	1.558009735	0.772316611	-
1.16547021	STK29	1.463033456	0.86790697	-
1.16557204	DNAJC6	1.491890695	0.839253386	-
1.16560039	LRRK1	1.651630567	0.679570213	-
1.16601594	LOC392226	1.348977805	0.983054067	-
1.16603463	MVK	1.673178267	0.658890987	-
1.16773995	PLXNC1	1.519615678	0.81586422	-
1.16777647	PTK9L	1.480792752	0.854760183	-
1.16982912	ICK	1.348111476	0.99154676	-
1.16983623	ROR2	1.306091299	1.033581161	Positive
1.17059947	PLXNA3	1.909332619	0.431866327	-
1.17078349	ERN1	1.476451368	0.86511561	-
1.17110922	ACVR1	1.39498943	0.947229002	-
1.17113414	FN3KRP	1.505537354	0.836730925	-
1.17212903	RPS6KA1	1.305637578	1.038620485	Positive
1.17227579	TTK	1.745282372	0.599269205	-
1.17258044	FLJ20574	2.595605089	-0.25044421	-
1.17396901	TOPK	1.339889173	1.008048856	Positive
1.17398828	CDKL4	1.438114504	0.90986206	-
1.17488294	KSR2	1.407987686	0.941778204	-
1.17488829	CSNK2A1	1.439975313	0.909801274	-
1.17518519	DDR2	1.399978879	0.95039151	-
1.17550986	DKFZp434G0625	1.643803392	0.707216334	-
1.17559208	PKN3	1.492521358	0.858662808	-
1.17576182	ARK5	1.382341262	0.96918237	-
1.17608794	PI4KII	1.583946438	0.768229439	-
1.17634815	FLJ13052	1.280443143	1.072253163	Positive
1.17753161	KIT	1.59425253	0.760810684	-
1.17794437	AK3L1	1.647921203	0.707967546	-
1.17865372	PLXNA1	1.40960792	0.947699514	-
1.17895744	CCRK	1.437210879	0.920704001	-
1.17896252	PASK	1.523668845	0.834256196	-
1.18160161	SKP2	1.216821094	1.146382124	Positive
1.18210653	MAP3K8	1.617227164	0.746985906	-
1.18212386	MAP2K2	1.263444394	1.100803319	Positive
1.18256072	ITPKA	1.329411968	1.03570948	Positive
1.1828011	RIPK2	1.870870632	0.494731574	-
1.18348636	PKN1	1.281841633	1.085131078	Positive
1.18366536	LOC440332	1.384972023	0.982358701	-
1.18401784	PRKWNK2	1.527660435	0.840375255	-
1.18429379	CDC2L5	2.169285024	0.199302553	-
1.18467554	LOC340371	1.323965183	1.045385894	Positive
1.18521531	STK3	1.579611782	0.790818842	-
1.18547406	PFTK1	1.457605174	0.913342938	-
1.18596505	ATR	1.225793508	1.146136601	Positive

1.18606599	VRK1	1.485211376	0.886920607	-
1.18621579	NEK3	1.464752104	0.907679468	-
1.18626001	PRKD2	1.472414237	0.900105791	-
1.18635526	ANKK1	1.704606049	0.668104473	-
1.18706912	NME4	2.225222302	0.14891593	-
1.18743264	STK35	1.440610362	0.934254925	-
1.18869791	PLXND1	1.425308619	0.952087205	-
1.19127419	PRKWNK4	1.633116855	0.749431533	-
1.19143453	PTK6	1.634206826	0.74866224	-
1.1915135	ETNK1	1.514744431	0.868282565	-
1.19275018	MPP6	1.295671689	1.089828675	Positive
1.19294781	SMG1	1.428199848	0.957695765	-
1.19409615	PSKH2	1.578596954	0.809595349	-
1.19415947	ROR1	1.315415021	1.072903927	Positive
1.19428821	STK32C	1.350239556	1.038336872	Positive
1.1950494	HUNK	1.559534854	0.830563945	-
1.19578044	PACSIN2	1.442842013	0.948718868	-
1.19579998	AK3	1.366690307	1.024909654	Positive
1.19611199	PRPS1L1	1.781383528	0.610840459	-
1.19614574	LOC389599	1.353076349	1.039215126	Positive
1.19642117	TEC	1.644064432	0.748777905	-
1.1967047	SNARK	1.623076396	0.770332995	-
1.19716369	FGFR4	1.364502158	1.029825224	Positive
1.19726408	PIK3CB	1.52114503	0.873383135	-
1.1978011	PTK2	1.32812154	1.06748066	Positive
1.19811505	PRKY	1.403111157	0.99311894	-
1.19864991	AKAP12	1.469481068	0.927818754	-
1.1989312	AKAP2	1.334434006	1.063428403	Positive
1.19903095	PIK3C2G	1.408062442	0.98999946	-
1.19904577	STK4	1.23630218	1.161789355	Positive
1.20029352	ULK2	1.684512353	0.716074678	-
1.20084237	PIK3C3	1.356237056	1.045447693	Positive
1.20249047	ACVR1B	1.585058189	0.81992275	-
1.20283686	STK38L	1.510746332	0.894927389	-
1.2030335	TXNDC6	1.426733062	0.979333933	-
1.20350174	AAK1	1.468295597	0.938707892	-
1.20363936	ABL1	1.442303387	0.964975335	-
1.2037792	CHKB	1.447089139	0.960469257	-
1.20403564	IHPK1	1.41010802	0.997963266	-
1.20437313	PLK2	1.320600248	1.088146021	Positive
1.20527823	EPHA7	1.255763134	1.154793325	Positive
1.20698591	DGKE	1.64776566	0.766206168	-
1.20717213	PIK3CG	1.441536218	0.972808049	-
1.20752335	MFHAS1	1.36014042	1.054906282	Positive
1.2076244	PIK4CB	1.451409566	0.96383923	-
1.20878529	MYLK	1.465250901	0.952319674	-
1.20919636	PIK3CD	1.441465005	0.976927722	-
1.20940837	LOC340156	1.711823529	0.706993206	-
1.20994289	ASB10	1.341952813	1.077932966	Positive

1.20999189	STK23	1.478202041	0.941781747	-
1.21111089	C14orf20	1.438978454	0.98324332	-
1.21127646	COASY	1.615369507	0.80718342	-
1.21135022	TAO1	1.596775185	0.825925251	-
1.21179328	AURKC	1.363591928	1.059994628	Positive
1.21193009	PDXK	2.520545754	-0.096685583	-
1.21208372	ACK1	1.516016473	0.908150971	-
1.21304822	IRAK4	1.44671274	0.979383698	-
1.21340921	MAP2K7	1.371953739	1.054864679	Positive
1.21385127	CNKSR1	1.416266469	1.011436079	Positive
1.21465132	CDC2	1.662589464	0.76671317	-
1.21498805	CDC42SE2	1.434071716	0.995904385	-
1.215167	TNK1	1.569969192	0.860364816	-
1.21564635	IKBKG	1.354366694	1.076925997	Positive
1.21579907	STK17B	1.588120143	0.843477997	-
1.21581895	MAST1	1.560127195	0.871510705	-
1.21603645	PAK4	1.654886789	0.777186111	-
1.21629646	WEE1	2.763227309	-0.330634394	-
1.21664849	FGFR1	1.399499421	1.03379756	Positive
1.21717726	MAPK7	1.358923835	1.07543068	Positive
1.2179641	SH3BP4	1.500637871	0.935290335	-
1.21853052	STK17A	1.455110881	0.981950153	-
1.21899274	IGF1R	1.858376721	0.579608763	-
1.21976961	TLK2	1.35100842	1.088530803	Positive
1.21990046	NIPA	1.715054298	0.724746624	-
1.21996787	BAIAP1	1.524254967	0.915680779	-
1.22017278	LOC392265	2.042210066	0.398135485	-
1.22205149	ERBB2	1.304099641	1.140003335	Positive
1.2233532	AKAP28	1.380447934	1.066258468	Positive
1.22459395	TXK	1.643223283	0.805964607	-
1.2249993	PLK4	1.331287551	1.118711056	Positive
1.22511838	LOC149420	1.497229906	0.953006849	-
1.22560175	PRPSAP2	1.296486909	1.154716598	Positive
1.22606089	LOC441047	1.409676809	1.042444974	Positive
1.22635999	CAMK2G	1.26892587	1.183794103	Positive
1.22646226	PACSIN1	1.453613568	0.999310944	-
1.22666861	RAF1	1.397450706	1.055886517	Positive
1.2267099	PAPSS2	1.451421614	1.001998191	Positive
1.22808315	GRK1	1.588599441	0.867566862	-
1.22868092	HIPK3	1.300240309	1.157121528	Positive
1.22871157	CDKL1	1.307457901	1.149965241	Positive
1.22871192	LOC440345	1.409431915	1.047991925	Positive
1.23008305	SRPK2	1.371169961	1.088996136	Positive
1.2305878	ADCK5	1.358269664	1.102905937	Positive
1.23114179	DYRK1B	1.698910315	0.763373275	-
1.23150669	RIPK1	1.573206493	0.889806896	-
1.23160398	PRKG1	1.439032274	1.024175686	Positive
1.23214825	STK32A	1.417651787	1.046644708	Positive
1.23385939	FLJ37794	1.30802698	1.159691793	Positive

1.23413794	TPK1	1.439854959	1.028420925	Positive
1.23537929	DAPK3	1.506632816	0.964125757	-
1.23635018	RYK	1.295261972	1.177438383	Positive
1.23708748	AKAP8	1.623036785	0.851138166	-
1.23714754	PRKCBP1	1.626983532	0.847311541	-
1.23736188	AKIP	1.729067143	0.745656613	-
1.23748408	TYRO3	1.859296737	0.615671417	-
1.23854757	TRIB2	1.597639321	0.879455827	-
1.23860837	NME7	1.313292144	1.163924602	Positive
1.2388611	DKFZp434C1418	1.771786349	0.705935844	-
1.23914881	ITGB1BP3	1.890563351	0.587734274	-
1.23936296	ERK8	1.321808434	1.156917494	Positive
1.24048099	SNRK	1.628039135	0.852922836	-
1.24077672	CDC2L2	1.403561522	1.077991918	Positive
1.24130557	PRKCH	1.404728456	1.07788268	Positive
1.2413741	CDK10	1.441028231	1.041719961	Positive
1.24137481	RP26	1.472100492	1.010649136	Positive
1.24147753	AKT3	1.389298396	1.093656667	Positive
1.2423871	AK2	1.675584	0.809190206	-
1.24242867	PLXNA2	1.466646559	1.018210789	Positive
1.24312847	PDPK1	1.486955438	0.999301498	-
1.24439836	PRKCE	1.677286204	0.811510517	-
1.24495975	PRKWNK1	2.236841368	0.253078126	-
1.24575391	LOC375328	1.394087871	1.097419943	Positive
1.2458963	CIB1	1.559358958	0.932433637	-
1.24680105	FASTK	1.549502212	0.944099884	-
1.24726191	LOC391295	1.417641087	1.076882728	Positive
1.24786532	NEK2	1.499308993	0.996421651	-
1.24933979	PANK4	1.868921747	0.629757828	-
1.24987432	NME6	1.976955739	0.522792908	-
1.25018462	NEK5	1.443162849	1.057206394	Positive
1.25053091	FLJ10074	1.89623037	0.604831451	-
1.25078175	STK6	1.416778913	1.084784584	Positive
1.25092746	NEK6	1.365817363	1.13603755	Positive
1.25472091	KIAA0431	1.744580505	0.764861307	-
1.25538605	MERTK	1.519818337	0.990953764	-
1.25652618	TXNDC3	1.781144598	0.731907764	-
1.25684022	PIP5K1B	1.903184539	0.610495897	-
1.25686127	T3JAM	1.606387195	0.907335346	-
1.25692879	IKBKE	1.58585539	0.928002191	-
1.25710759	HIPK4	1.607271236	0.90694394	-
1.25723782	AK7	1.516110005	0.998365625	-
1.25733581	PRKDC	1.406159855	1.108511774	Positive
1.25783934	BCKDK	2.145380591	0.370298079	-
1.25802153	PDK2	1.59016593	0.925877122	-
1.25851997	SCAP1	1.644011903	0.873028028	-
1.25857656	MAP3K6	2.023833413	0.493319706	-
1.25858914	MGC42105	1.499671186	1.017507098	Positive
1.25929147	IRAK1	1.790090501	0.728492445	-

1.26020849	PRKCQ	1.585163469	0.93525352	-
1.26034277	MAP3K3	1.798488767	0.722196771	-
1.26304743	DGKZ	1.979859302	0.546235568	-
1.26315646	SGK	1.843378353	0.682934562	-
1.26320223	GRK7	1.974210611	0.552193855	-
1.26488899	NME2	1.592724515	0.937053458	-
1.26511086	MAP4K4	1.571522315	0.958699403	-
1.26566776	CSNK1A1	1.415602301	1.115733212	Positive
1.26588843	CSNK1A1L	1.530040243	1.001736609	Positive
1.2661342	PLXNB3	1.327127327	1.205141081	Positive
1.26641805	MAPKAPK2	1.333447924	1.199388182	Positive
1.26664195	MARK1	1.397679844	1.135604047	Positive
1.26712201	CDC7	2.023614359	0.510629657	-
1.26799457	LOC390777	1.853547194	0.682441953	-
1.26814682	TIE	1.616006798	0.920286851	-
1.26854707	ZAK	2.262395592	0.274698545	-
1.26910958	DAPK2	1.668442581	0.869776581	-
1.27182035	DYRK3	1.353872028	1.189768672	Positive
1.27182469	HIPK1	1.786867125	0.756782249	-
1.27395687	MAPK11	1.395254548	1.152659197	Positive
1.27424773	SIK2	1.436687616	1.111807838	Positive
1.27546514	IPMK	1.67136974	0.87956055	-
1.2759303	MARK3	1.554322375	0.997538221	-
1.27686576	SPHK1	1.332641096	1.221090428	Positive
1.27877961	CLK3	1.771024674	0.786534555	-
1.2795754	PKLR	1.406691241	1.152459554	Positive
1.27970836	CDKL2	1.588895806	0.970520919	-
1.28169975	PLK1	2.260125018	0.303274483	-
1.2829319	CALM3	1.558452113	1.007411689	Positive
1.28441271	HSMDPKIN	1.838807532	0.730017892	-
1.28445287	TYK2	1.548911198	1.01999455	Positive
1.28484379	CDK9	1.58999223	0.979695343	-
1.28491173	GK	1.42587368	1.143949785	Positive
1.28527868	STK19	1.612947362	0.957609996	-
1.2886789	STK32B	1.899215439	0.678142352	-
1.28888346	PDK4	1.647536212	0.930230702	-
1.28927656	MAPKAPK5	1.379427472	1.19912565	Positive
1.28972878	MAPK3	2.282243582	0.297213988	-
1.2902563	AKAP7	1.628189914	0.952322677	-
1.29105206	IHPK3	1.499080332	1.083023786	Positive
1.29108571	MAPK4	1.892323587	0.689847824	-
1.29112109	STK24	1.565839632	1.016402541	Positive
1.29139063	LOC390975	1.599591689	0.983189565	-
1.29346211	FLJ32685	1.549545844	1.03737837	Positive
1.29426086	MAGI1	2.828495226	-0.239973515	-
1.29452688	ACVR1C	1.563817262	1.025236502	Positive
1.29494362	PRKCG	1.357556111	1.232331129	Positive
1.29558506	MAPK12	1.719004174	0.87216595	-
1.29618865	MELK	1.461364244	1.131013059	Positive

1.29713625	FLJ16518	1.46653623	1.127736273	Positive
1.29760872	BUB1B	1.760442583	0.834774849	-
1.29782407	JAK1	1.77340433	0.822243816	-
1.29909566	ADK	1.485821818	1.112369502	Positive
1.30047691	CAMK2D	1.621862803	0.979091008	-
1.30104186	PRKCZ	1.559205415	1.042878308	Positive
1.30518291	FLJ34389	1.589573336	1.020792492	Positive
1.30631951	DGKI	1.474285259	1.138353755	Positive
1.30699945	CAMKK2	1.89731801	0.71668089	-
1.30809521	NME5	1.72335167	0.892838749	-
1.30878834	EPHA5	1.95566329	0.661913387	-
1.30932248	FRK	1.520752043	1.097892916	Positive
1.31275781	PLXNB2	1.830498265	0.795017362	-
1.31600446	PKMYT1	1.863133676	0.768875243	-
1.31610051	PIM3	1.485377761	1.14682326	Positive
1.31709068	LOC440451	2.087567534	0.546613829	-
1.31942061	SNF1LK	1.920477489	0.718363721	-
1.31963411	MAP3K12	2.253087919	0.386180306	-
1.31973773	PIP5KL1	1.568294134	1.071181316	Positive
1.32062369	TNNI3K	1.854348716	0.786898658	-
1.32141874	CDKL3	1.820909257	0.821928214	-
1.3218597	RPS6KB1	1.386658543	1.257060851	Positive
1.32192612	CHEK1	1.548114059	1.095738177	Positive
1.32193611	LOC442075	1.435979163	1.207893048	Positive
1.32205492	PRKR	2.000686978	0.643422859	-
1.3228598	LRRK2	1.419028278	1.226691317	Positive
1.32324166	LOC441787	1.425343448	1.221139875	Positive
1.32413395	FN3K	1.48275253	1.165515367	Positive
1.32559167	CARKL	1.979310106	0.671873243	-
1.32703377	FLJ25006	1.594834626	1.059232913	Positive
1.3317164	LATS1	1.708542802	0.954889995	-
1.33344388	LAK	1.416448986	1.250438775	Positive
1.33398299	MST1R	1.667996603	0.999969386	-
1.33421275	SLAMF6	1.709653026	0.958772465	-
1.33423558	STK11	1.772838892	0.895632266	-
1.33465634	C9orf96	1.528023516	1.141289158	Positive
1.33476678	RAGE	2.55096163	0.118571931	-
1.33905193	SBK1	1.617354724	1.060749139	Positive
1.34049924	PNCK	1.507097484	1.173900989	Positive
1.34242605	PDK1	1.732459146	0.952392956	-
1.34305881	LOC400301	1.398154597	1.287963018	Positive
1.34351495	LOC392347	1.668380628	1.018649262	Positive
1.34487651	PCM1	2.104498671	0.585254343	-
1.34516399	GUK1	1.444817187	1.245510799	Positive
1.34725706	XM_290793	1.691491695	1.003022425	Positive
1.34739985	MAP3K1	1.687209613	1.007590087	Positive
1.3515278	PIM2	1.991191084	0.71186452	-
1.35437533	OSRF	2.508060499	0.200690158	-
1.35469845	PRKCA	1.778885435	0.930511471	-

1.3559725	C19orf35	1.430694815	1.281250179	Positive
1.35611798	DOK1	2.104910705	0.607325256	-
1.35700794	GALK2	1.50857879	1.205437085	Positive
1.35911821	MAP2K5	1.428190892	1.290045533	Positive
1.36133241	XYLB	1.603591963	1.119072862	Positive
1.36172796	CIB4	1.845187078	0.878268837	-
1.36356048	GSK3A	1.721849833	1.005271117	Positive
1.36561907	TESK2	1.73396935	0.997268782	-
1.36880614	RET	1.87413963	0.863472654	-
1.37198638	EIF2AK3	1.667964935	1.076007828	Positive
1.37625829	PRKAA2	2.384848884	0.367667701	-
1.38016117	AURKB	1.698853194	1.06146915	Positive
1.38780078	PGK1	2.104726783	0.670874773	-
1.39727033	MAP2K1	1.575329555	1.219211098	Positive
1.40409933	PIK3AP1	1.78599107	1.022207593	Positive
1.41396849	CAMK1G	2.008639314	0.819297657	-
1.41472625	ITPKB	2.036831772	0.792620729	-
1.43063768	CKB	2.441421071	0.419854279	-
1.43247153	MAPK1	1.888739226	0.976203835	-
1.43285317	HIPK2	2.175545694	0.690160656	-
1.43496805	MAPKAPK3	2.604026027	0.265910077	-
1.44684582	CDK5	2.29618448	0.597507159	-
1.45181538	PFKP	2.308483531	0.59514722	-
1.46073518	PAPSS1	1.989363114	0.932107242	-
1.461663	STK38	2.038314066	0.88501193	-
1.46203177	TESK1	1.68079429	1.243269249	Positive
1.46212114	LOC390877	1.520546602	1.403695675	Positive
1.46922879	IRAK2	1.684382831	1.254074749	Positive
1.47704023	RPS6KA5	2.02950497	0.924575484	-
1.48087706	NRK	1.794053874	1.167700239	Positive
1.4952262	LOC441777	2.335971505	0.654480901	-
1.51685531	LATS2	2.649599266	0.38411136	-
1.51908697	MPP7	2.336502527	0.701671415	-
1.59799054	MAPK9	1.702702751	1.493278332	Positive
1.60001242	CERK	2.470479976	0.729544873	-
1.60657365	PCTK2	2.251622276	0.961525033	-
1.64410372	MAP3K7IP2	1.948527797	1.339679651	Positive

Appendix Table 2 Full results of the phosphatase screen presented in Figure 5.3. Death Index, upper and lower limits of the 95% confidence interval and statistical significance calculations are described in detail in section 2.2.10.3. Phosphatases with death indexes < 1 reduce RNAi activity and are presented in red. Phosphatases with death indexes > 1 increase RNAi activity and are presented in green.

Appendix Table 2

Death Index	Symbol	Upper limit	Lower limit	Statistical significance
		95% CI UL	95% CI LL	
0.803407399	PPA2	0.88298765	0.723827148	Positive
0.815793254	PPP4R1L	1.112320863	0.519265645	-
0.816851447	PTEN	0.898776497	0.734926396	Positive
0.823464326	SKIP	0.859888602	0.787040049	Positive
0.832725512	PPP3CC	0.869345413	0.796105611	Positive
0.836354741	LOC63928	1.011404566	0.661304916	-
0.836713385	NUDT5	0.910352798	0.763073972	Positive
0.841469277	IMPA2	0.874664058	0.808274496	Positive
0.844909275	FLJ20313	1.486677018	0.203141532	-
0.851401129	SYNJ1	0.893235532	0.809566726	Positive
0.856895277	PPM2C	0.980642394	0.733148159	Positive
0.861462578	TENS1	0.931962426	0.79096273	Positive
0.863323399	PDXP	0.918943073	0.807703725	Positive
0.863375378	DUSP12	0.935996764	0.790753991	Positive
0.863909944	INPP5B	0.954359083	0.773460805	Positive
0.864476679	INPPL1	0.912758023	0.816195334	Positive
0.865651405	PTPN14	1.161332264	0.569970545	-
0.867242898	MTMR9	0.943586369	0.790899427	Positive
0.86779013	DKFZP566K0524	1.283289206	0.452291055	-
0.868259702	LOC401823	0.914281802	0.822237602	Positive
0.868981874	OCRL	0.934429954	0.803533793	Positive
0.872139807	DUT	1.123467802	0.620811812	-
0.876460113	MTMR8	0.972911305	0.78000892	Positive
0.877616555	CIB3	1.036817898	0.718415212	-
0.884443315	PDP2	1.032952963	0.735933667	-
0.88575414	LOC442368	1.276150669	0.495357611	-
0.886256634	SSH1	1.025237574	0.747275694	-
0.890226783	TPTE2	0.936218364	0.844235203	Positive
0.893137582	PTPN9	0.99449439	0.791780774	Positive
0.893256465	MFN1	1.058745396	0.727767534	-
0.895067171	LOC441868	1.012213833	0.777920509	-
0.895736423	PPP3CA	0.95389264	0.837580206	Positive
0.895771716	NUDT3	0.984508423	0.807035008	Positive
0.896222769	TPTE	1.018927708	0.773517831	-
0.899505694	INPP1	0.922353927	0.876657462	Positive
0.899953288	ENTPD7	1.103247231	0.696659346	-
0.901760882	SET	1.014175468	0.789346295	-
0.902853321	PPEF2	0.920221569	0.885485073	Positive
0.903120375	ALPP	1.371999997	0.434240753	-
0.903828183	LOC442350	0.93181093	0.875845436	Positive
0.908491043	SBF1	0.961500124	0.855481962	Positive
0.9095179	ANP32E	0.956788274	0.862247525	Positive
0.910397334	DUSP23	1.096579526	0.724215141	-
0.91194304	INPP5A	0.928738841	0.89514724	Positive

0.912712433	CDC25A	1.047967873	0.777456994	-
0.914102563	TPTEps1	1.061326781	0.766878344	-
0.915287008	PPP2R5D	1.06897262	0.761601396	-
0.915771224	HINT1	1.068331403	0.763211046	-
0.915902578	ITPA	1.031278844	0.800526312	-
0.915918677	KIAA0274	1.1898718	0.641965553	-
0.918016515	PP	1.066222289	0.769810741	-
0.918670541	ANP32C	0.966379548	0.870961534	Positive
0.919212592	DUSP22	1.148568062	0.689857123	-
0.919479464	NAP1L2	1.031978865	0.806980063	-
0.919556268	PPAP2A	0.975561536	0.863551001	Positive
0.919700456	MTMR6	1.036901358	0.802499554	-
0.920897499	CDKN3	1.020929879	0.820865119	-
0.921119995	ACP2	0.954218921	0.888021068	Positive
0.921332649	LPPR4	1.271233852	0.571431445	-
0.923293841	FLJ23751	1.010393455	0.836194228	-
0.924720103	PPP1R3D	1.053551586	0.795888619	-
0.92578706	PPP3CB	0.99008389	0.86149023	Positive
0.92612736	EPM2A	1.114722198	0.737532522	-
0.927034701	ALPI	0.988468478	0.865600923	Positive
0.927282522	NAP1L5	0.986692819	0.867872225	Positive
0.930316783	LOC441567	1.007484284	0.853149281	-
0.931142006	LPPR2	1.028359366	0.833924647	-
0.93117153	HDHD2	1.245826922	0.616516138	-
0.931177222	LHPP	1.027492031	0.834862413	-
0.931197476	ENTPD2	1.217593584	0.644801368	-
0.931969236	PPP1R12B	1.036944111	0.826994362	-
0.932635693	SYNJ2	0.960126034	0.905145352	Positive
0.932985711	PPAPDC1A	1.124712948	0.741258474	-
0.933779275	PPP1R12C	0.972320174	0.895238376	Positive
0.933781807	PHACTR3	0.980686433	0.886877181	Positive
0.934582998	PTP4A2	1.088004444	0.781161552	-
0.935434653	FLJ11535	1.192799978	0.678069328	-
0.935560894	PR48	1.128575548	0.74254624	-
0.935687349	PPP2R2D	1.033465399	0.837909299	-
0.935836277	TNS	0.947274381	0.924398174	Positive
0.9363341	MTMR3	1.150589155	0.722079045	-
0.936917297	PIB5PA	1.053034437	0.820800157	-
0.938071663	ANP32F	0.996552595	0.879590731	Positive
0.939718704	PHACTR4	0.988054783	0.891382625	Positive
0.941267932	SSH2	1.035065723	0.847470141	-
0.941806871	ACP6	0.972985694	0.910628048	Positive
0.943299434	PIP3AP	0.964752275	0.921846594	Positive
0.944775263	PTPN1	1.112753131	0.776797396	-
0.945266883	ACYP2	1.072218657	0.81831511	-
0.946546092	ALPL	1.084851343	0.808240841	-
0.94843278	MTM1	1.031463101	0.865402459	-
0.948953778	UNQ2492	1.063145619	0.834761938	-
0.951597537	PPP1R3B	1.100638235	0.802556838	-

0.953475716	ENTPD8	1.183850191	0.72310124	-
0.953672689	ACPP	1.030142505	0.877202874	-
0.954024884	PPP2R3A	1.029985231	0.878064537	-
0.955993815	NAP1L4	1.082672946	0.829314685	-
0.956374356	TA-PP2C	1.096444858	0.816303854	-
0.956835918	MK-STYX	1.163932909	0.749738928	-
0.957742588	PPM1B	1.139878204	0.775606971	-
0.958183193	NUDT11	1.061632623	0.854733763	-
0.958895926	PPP1R3F	1.113753169	0.804038684	-
0.959943324	G6PC	1.051882953	0.868003696	-
0.961473504	FLJ20421	1.240851838	0.682095169	-
0.962308751	NAP1L1	1.044626301	0.879991202	-
0.966034683	PTPN13	1.11077535	0.821294015	-
0.966042547	CTDSPL	1.033297114	0.898787981	-
0.967454012	IMPA1	1.088314487	0.846593537	-
0.967814569	PPP1R3A	1.065796039	0.869833099	-
0.970816978	PTPN11	1.020258624	0.921375331	-
0.97206021	SACM1L	1.203057358	0.741063063	-
0.973204313	PTPN7	1.010920117	0.93548851	-
0.975101589	C11orf23	1.084965845	0.865237332	-
0.976650726	CRA	1.244678298	0.708623154	-
0.977299832	PPM1L	1.172899799	0.781699865	-
0.978092018	SGPP2	1.311503447	0.644680588	-
0.979119544	PRG-3	1.258465207	0.699773881	-
0.979346165	PPP1R14B	1.134200227	0.824492103	-
0.979395365	PALD	1.151082589	0.807708141	-
0.979623286	ALPPL2	1.120668519	0.838578052	-
0.979758147	PPP2R2C	1.283237521	0.676278773	-
0.980608447	LOC441215	1.104368821	0.856848074	-
0.980886935	FLJ22405	1.034139073	0.927634796	-
0.982047614	PPP5C	1.199107517	0.764987712	-
0.983712925	SGPP1	1.180896265	0.786529585	-
0.983758686	PPP2R1A	1.403074901	0.56444247	-
0.985013009	KIAA1115	1.036513666	0.933512352	-
0.98547822	PPP3R1	1.062529045	0.908427395	-
0.987238905	NUDT10	1.320005079	0.654472731	-
0.987246571	PTPRA	1.048656719	0.925836423	-
0.987681108	FHIT	1.290086549	0.685275666	-
0.989137526	PPP1R12A	1.071756143	0.906518909	-
0.99029984	PPM1G	1.155555105	0.825044575	-
0.990982194	MTMR1	1.18476222	0.797202168	-
0.993196976	CDC14A	1.781921202	0.204472749	-
0.993645381	PPM1H	1.084672565	0.902618197	-
0.99485286	PPP2R5B	1.032191512	0.957514209	-
0.994861959	CTDP1	1.119572569	0.870151349	-
0.995593729	PPP1R14D	1.0640666	0.927120859	-
0.996166389	PPP1CC	1.1101524	0.882180379	-
0.996469941	ACYP1	1.227040413	0.765899469	-
0.997005207	DUSP19	1.052933326	0.941077088	-

0.997211774	PTPN12	1.0933829	0.901040647	-
1.004750363	CHP	1.070771499	0.938729227	-
1.005045419	MGC1136	1.156799724	0.853291114	-
1.005945331	MINPP1	1.021158895	0.990731768	-
1.006686117	ANP32B	1.093755688	0.919616547	-
1.006987159	NUDT6	1.111220553	0.902753765	-
1.00795711	DUPD1	1.111744797	0.904169424	-
1.009543251	LOC163404	1.207958449	0.811128052	-
1.009805908	PPP1R2	1.066292479	0.953319337	-
1.012219862	FLJ32658	1.217390615	0.807049108	-
1.012491481	HDHD1A	1.099119082	0.92586388	-
1.013055477	KIAA0685	1.115042264	0.91106869	-
1.015012543	PTPN22	1.193984185	0.836040901	-
1.01552079	PTPN5	1.135392988	0.895648593	-
1.015768153	PPP2R5C	1.137484952	0.894051353	-
1.016596191	DUSP11	1.1709586	0.862233781	-
1.016761748	PPM1A	1.129540676	0.903982819	-
1.017421766	PPM1E	1.276879871	0.757963661	-
1.018511597	PPP1R7	1.05772389	0.979299303	-
1.018645711	ACP5	1.177802071	0.859489351	-
1.019644833	LOC389217	1.050477105	0.98881256	-
1.02113071	PPAP2B	1.058174926	0.984086495	-
1.023002823	RNGTT	1.171491171	0.874514476	-
1.02322244	PPEF1	1.122311762	0.924133119	-
1.023698811	LOC389168	1.084096026	0.963301596	-
1.023800216	LOC283871	1.352405827	0.695194605	-
1.025084506	PPP1R3C	1.134704183	0.915464829	-
1.026951165	PPP2R1B	1.128909509	0.92499282	-
1.027020455	ANP32A	1.12091087	0.933130041	-
1.027954021	FLJ25449	1.104397687	0.951510354	-
1.031226053	PPP2R5A	1.137634482	0.924817624	-
1.0337749	PPP2R4	1.220229444	0.847320357	-
1.033887664	CTDSP2	1.121593901	0.946181427	-
1.035666231	PPAP2C	1.158953273	0.912379189	-
1.03581041	CDC25C	1.126967192	0.944653628	-
1.037297597	CDC14B	1.100083748	0.974511447	-
1.037741985	FBP1	1.127782258	0.947701712	-
1.038511044	G6PC3	1.150667331	0.926354757	-
1.041093238	LOC440388	1.203701219	0.878485257	-
1.042288465	ACPT	1.155462955	0.929113976	-
1.042864611	INPP5D	1.197325267	0.888403955	-
1.044778795	ENTPD6	1.12641438	0.963143211	-
1.045641228	C9orf67	1.208441319	0.882841136	-
1.045990027	PTP4A1	1.273470617	0.818509437	-
1.046325798	FLJ16165	1.28813557	0.804516025	-
1.046547461	ACP1	1.183449833	0.909645089	-
1.047472776	MTMR2	1.247627255	0.847318296	-
1.048610739	LOC339819	1.205756281	0.891465198	-
1.049178285	DUSP3	1.14749344	0.95086313	-

1.050398556	ENTPD3	1.290590032	0.810207079	-
1.051165581	LOC441959	1.168458557	0.933872605	-
1.051292558	ENTPD5	1.141713146	0.96087197	-
1.051797624	FLJ32332	1.156772329	0.94682292	-
1.053388318	NUDT14	1.146491909	0.960284726	-
1.057417119	CTDSP1	1.171628315	0.943205923	-
1.057583034	PPP1R16A	1.086863016	1.028303052	Positive
1.057975754	NAP1L3	1.138485185	0.977466322	-
1.059917124	DUSP13	1.085404497	1.034429751	Positive
1.060335515	PTPMT1	1.329889893	0.790781137	-
1.061236781	LOC399969	1.411289343	0.71118422	-
1.061269241	PPP1R14A	1.321002954	0.801535528	-
1.064248606	C6orf56	1.154347467	0.974149745	-
1.065747554	PPP3R2	1.126718827	1.004776281	Positive
1.066239298	FBP2	1.137760728	0.994717867	-
1.068533699	MTMR7	1.378193771	0.758873628	-
1.070512214	MFN2	1.185930722	0.955093707	-
1.071935637	PTPN2	1.210415955	0.933455319	-
1.072007534	PFKFB1	1.129218098	1.01479697	Positive
1.073226231	PTP4A3	1.186388731	0.960063731	-
1.079006605	PPP1R14C	1.235743031	0.922270179	-
1.080796771	FLJ32786	1.169519976	0.992073566	-
1.081342474	PTPDC1	1.22227204	0.940412908	-
1.081604882	LOC400927	1.184608947	0.978600816	-
1.081982924	DOLPP1	1.300648048	0.8633178	-
1.082654892	PSPH	1.259660751	0.905649032	-
1.083311227	PTPN21	1.317996696	0.848625757	-
1.08424051	PPP1R16B	1.186603704	0.981877317	-
1.08531432	PPP1CB	1.288580939	0.882047701	-
1.085343818	NUDT4	1.385428697	0.78525894	-
1.085873226	PPP2R2B	1.263048445	0.908698007	-
1.087914718	PHACTR1	1.171553864	1.004275571	Positive
1.092685323	CMT4B2	1.213425649	0.971944997	-
1.095919691	LOC400708	1.198374313	0.993465068	-
1.096297184	NT5E	1.296579759	0.896014608	-
1.097450525	INPP5E	1.223972444	0.970928605	-
1.100288832	DKFZp761G058	1.265245655	0.93533201	-
1.101339357	ENTPD1	1.299719837	0.902958876	-
1.105810622	PTPN3	1.287550928	0.924070315	-
1.109976352	LOC401954	1.38481288	0.835139824	-
1.111674832	MTMR4	1.436201934	0.787147729	-
1.11250537	NT5C2	1.33982447	0.88518627	-
1.118428243	MGC26484	1.397820099	0.839036387	-
1.12044975	PTPRE	1.665358163	0.575541338	-
1.122891602	FLJ40125	1.244842272	1.000940932	Positive
1.124194256	ENTPD4	1.412353075	0.836035438	-
1.129244507	PFKFB3	1.16911789	1.089371124	Positive
1.129812093	PFKFB2	1.396542933	0.863081254	-
1.130037012	PPP4R1	1.286130002	0.973944023	-

1.133106302	PPM1F	1.24767392	1.018538683	Positive
1.135145769	HTPAP	1.285521429	0.984770108	-
1.136300064	PTPN18	1.255825535	1.016774592	Positive
1.142189869	INPP5F	1.417964569	0.86641517	-
1.142252738	SSH3	1.579510404	0.704995071	-
1.143271538	PPP2R2A	1.668519095	0.61802398	-
1.143719336	LOC442731	1.197368366	1.090070307	Positive
1.146425084	HINT2	1.402583166	0.890267001	-
1.150654502	ILKAP	1.351284544	0.950024461	-
1.151457142	MGC45386	2.083333723	0.219580562	-
1.155874176	NUDT8	1.367060478	0.944687874	-
1.171788908	PTPN6	1.289111636	1.054466181	Positive
1.17220025	LOC441511	1.69627789	0.64812261	-
1.176548022	LOC403313	1.545287713	0.807808331	-
1.181302478	PTPN23	2.133716298	0.228888658	-
1.195209034	MGC19531	1.522900086	0.867517982	-
1.199400795	G6PC2	1.389816615	1.008984975	Positive
1.208991448	PPP1CA	1.536780333	0.881202563	-
1.210797621	PPP2R5E	1.545131005	0.876464237	-
1.222617113	PPM1D	1.621990117	0.82324411	-
1.245912637	CDC25B	1.795513203	0.696312071	-
1.257100006	PFKFB4	1.414709202	1.099490809	Positive
1.294502012	ANP32D	1.390174233	1.198829792	Positive
1.309676474	CIB2	2.026833809	0.592519139	-
1.389924357	LOC390760	1.544373863	1.235474851	Positive

Appendix Figure 1. EGF, TNFα and insulin treatment inhibit RNAi activity. HEK293T cells were transiently transfected with the plasmids pBFP-N1; dsGFP-Slicer or dsGFP-NonSlicer; ±siRNA. Twenty-four hours post-transfection, the cells were treated with or without EGF, TNFα or insulin. Endonuclease-dependent and -independent silencing activities of Ago2 were measured 24h after treatment by assaying GFP expression from dsGFP-Slicer and dsGFP-NonSlicer plasmids. **A)** Cells were treated with 100 µg/mL EGF. **B)** Cells were treated with 10 ng/mL TNF. **C)** Cells were treated with 1, 3 or 10 insulin units per milliliter. The bar graphs represent the relative silencing of dsGFP-Slicer or dsGFP-NonSlicer in ligand- or mock-treated cells. Paired student's two-tailed t-test was used to compare the relative silencing, *** $p < 0.001$; **** $p < 0.0001$. Error bars indicate Standard Error of the mean.

Appendix Figure 1